N° Order ……/Faculté/UMBB/2016

الديمقراطيةالجزائريةالجمهوريةالشعبية

REPUBLIQUE ALGERIENNE DEMOCRATIQUE ET POPULAIRE

MINISTERE DE L'ENSEIGNEMENT SUPERIEUR ET DE LA RECHERCHE SCIENTIFIQUE

Université M'Hamed Bougara de Boumerdès

Faculté des Sciences

Thèse de Doctorat

Présentée par :

GUESMIA Abdelkader

Discipline : Sciences physiques

Unité de Recherche : Matériaux, Procédés et Environnement (URMPE) de l'UMBB

Contribution à l'étude des grandeurs physiques fondamentales (pouvoir d'arrêt, potentiel d'ionisation et straggling en énergie) régissant le ralentissement des ions lourds dans des cibles solides

Devant le jury :

Benmounah Abdelbaki	**Professeur**	**UMBB**	**Président**
Abaidia Seddik El Hak	**Professeur**	**UMBB**	**Examinateur**
Idiri Zahir	**Directeur de recherche**	**CRNA**	**Examinateur**
Tobbeche Said	**Professeur**	**U. Batna**	**Examinateur**
Ammi Hakim	**Directeur de recherche**	**CRNA**	**Encadreur**
Hedibel Mohamed	**MCA**	**UMBB**	**Co- Encadreur**
Carlos Pineda-Vargas	**Professeur**	**iThemba LABS**	**Invité**

N° Order ……/Faculté/UMBB/2016

الديمقراطيةالجزائريةالجمهوريةالشعبية

REPUBLIQUE ALGERIENNE DEMOCRATIQUE ET POPULAIRE

MINISTERE DE L'ENSEIGNEMENT SUPERIEUR ET DE LA RECHERCHE SCIENTIFIQUE

Université M'Hamed Bougara de Boumerdès

Faculty of Sciences

PhD Thesis

Submitted by:

GUESMIA Abdelkader

Discipline: Physical Science
Research Unit: Materials, Processes and Environment (URMPE) of UMBB

Contribution to the study of the fundamental physical parameters (stopping power, ionization potential and energy straggling) describing the slowing down of heavy ions in solid material.

Members of the jury:

Benmounah Abdelbaki	**Professor**	**UMBB**	**President**
Abaidia Seddik El Hak	**Professor**	**UMBB**	**Member**
Idiri Zahir	**Research Director**	**CRNA**	**Member**
Tobbeche Said	**Professor**	**U. Batna**	**Member**
Ammi Hakim	**Research Director**	**CRNA**	**Supervisor**
Hedibel Mohamed	**MCA**	**UMBB**	**Co-Supervisor**
Carlos Pineda-Vargas	**Professor**	**iThemba LABS**	**Guest**

Dedication

To the fond memory of my dear Father**, MESSAOUD BENKOUIDER,** who was keen to see this dissertation in print**,** May our God accept his soul in His Paradise.

And My dear Mom, **FATNAT BENT MAAMAR**, May Allah give her a long life.

Abstract

Title: Contribution to the study of the fundamental physical parameters (stopping power, ionization potential and energy straggling) describing the slowing down of heavy ions in solid material.

Conceptually the complex phenomenon of the slowing down of energetic charged particles through matter is described by two physical fundamental parameters, the stopping power and the energy straggling. The average energy loss of an ion per unit path length when it is crossing the matter is called the stopping power. At the same time the energy transfer during the collision between the ions and the target atoms follows a statistical behavior which gives rise to fluctuations in energy loss,the average square fluctuation (standard deviation) of the energy loss distribution is commonly called the energy straggling. Multitude contemporary applications of ion beam such as ion beam analysis, ion material modification, nuclear physics, radiology etc., requires a precise determination of the stopping power of heavy ions in a matter as well as an accurate measurement of the energy straggling. These two fundamental parameters have been studied experimentally and theoretically since the beginning of the 20th century. Whereas experimental and theoretical data are readily available for Helium and proton ions, the data are much scarcer for heavy ions and significant discrepancies are reported by different authors especially at low energies.

In the basis of Lindhard, Scharff and Schiott (LSS) formula and by inserting the effective charge a new semi empirical expression has been proposed and tested for better stopping power calculations of heavy ions in various solid targets at low energy range (0.1-1MeV/n).This new proposed expression exhibits a good agreement with H. Paul's electronic stopping power database.

Within the framework of this thesis we adopted a nuclear technique based on measurement of the flight time of the recoil ions produced by the interaction of ions beam (^{84}Kr, ^{63}Cu) of energy of 26 MeV, with a primary target for the measurement of the energy loss of heavy ions ($3 \leq Z1 \leq 14$) in a thin layer to deduce the stopping force and the energy straggling. The obtained values of stopping force are compared with the predicted values obtained from the Stopping and Range of Ions in Matter program SRIM-2013, Lindhard-Scharff-Schiott (LSS) formula, available experimental data from the literature and the new proposed semi empirical formula.

The energy straggling values are compared with theoretical prediction of the Bohr straggling, straggling deduced from the Bohr stopping power model, and the corrected Lindhard–Scharff formula by introducing the bunching effect according to the Besenbacher approach. The aim of such comparison is to check the reliability and accuracy of the existing energy loss straggling formulations, in the light of the present experimental results. The experimental results of energy loss straggling of all ions are found to be greater than those predicted by the Bohr stopping model or Lindhard–Scharff prediction model. The introduction of the bunching effect improves the comparison and gives an estimation of other effects such as charge exchange effect.

Keywords: Stopping power, Straggling, LSS theory, Firsov theory, Bunching effect

Résumé

Thème : Contribution à l'étude des grandeurs physiques fondamentales (pouvoir d'arrêt, potentiel d'ionisation et straggling en énergie) régissant le ralentissement des ions lourds dans des cibles solides.

Conceptuellement le complexe phénomène du ralentissement des particules chargées lourdes dans la matière est décrit par deux grandeurs physiques fondamentales, le pouvoir d'arrêt et le straggling en énergie. La perte d'énergie moyenne d'un ion par unité de longueur quand il se déplace dans la matière est nommé pouvoir d'arrêt. Naturellement le transfert d'énergie entre l'ion incident et la cible solide est accompagné d'une fluctuation dans la perte d'énergie caractérisé par sa déviation standard nommé straggling en énergie. La connaissance avec précision du pouvoir d'arrêt et du straggling en énergie est essentielle pour de nombreuses applications du faisceau d'ions tels que l'implantation ionique, radiothérapie, les techniques d'analyse par faisceau d'ions etc. Ces deux paramètres ont été extensivement étudiés expérimentalement et théoriquement depuis le début du $20^{ème}$ siècle pour l'hélium et le proton. En revanche l'étude du ralentissement des ions lourds est un problème complexe pour lequel il n'existe que très peu de données expérimentales en plus les données reportées par différent auteurs présentent des déviations jusqu'à 20%.

En se basant sur la théorie de de Lindhard-Scharff-Schiott (LSS) en introduisant le concept de charge effective une nouvelle formule semi empirique décrivant le pouvoir d'arrêt à basse énergie a été introduite. Les pouvoir d'arrêts fourni par la base des données de H. Paul présentent un accord satisfaisant avec la nouvelle formule proposée.

Dans le cadre de ce travail de thèse nous avons adopté une technique nucléaire basée sur la mesure du temps de vol des ions de recul produits par l'interaction d'un faisceau d'ions (^{84}Kr, ^{63}Cu) d'énergie de 26 MeV, avec une cible primaire, pour la mesure de la perte d'énergie des ions lourds ($3 \leq Z_1 \leq 14$) dans une couche mince. Les nouvelles données du pouvoir d'arrêt ont été étudiées et comparé avec les données disponibles dans la littérature, le programme SRIM-2013, la théorie Lindhard-Scharff -Schiott (LSS) ainsi que la nouvelle formule semi empirique.

Les données expérimentales du straggling en énergie ont été comparées avec les prédictions théoriques telles que le straggling de Bohr, le straggling déduit du modèle du pouvoir d'arrêt de Bohr, la théorie de Lindhard–Scharff corrigé par l'introduction du «bunchingeffect»suivant l'approche de Besenbacher. Le but de cette comparaison est de vérifier la fiabilité et la précision des formulations existantes du straggling en énergie, à la lumière des présents résultats expérimentaux. Nous avons trouvé que les résultats expérimentaux du straggling en énergie sont nettement supérieurs à ceux généré par les modèles théoriques tels que Bohr, Lindhard–Scharff, Bethe-Livigston et la formule de Yang. L'introduction du «bunching effect» dans le straggling en énergie améliore la comparaison et donne une estimation des autres effets comme le straggling du à l'effet d'échange de charge.

Mots-clés: Pouvoir d'arrêt, Etalement d'énergie, Théorie LSS, Théorie de Firsov, Bunching effect

ملخص

العنوان: مساهمة في دراسة المقادير الفيزيائية الأساسية (قدرة الايقاف، جهد التأين وتطوح الطاقة) التي تصف تباطؤ الأيونات الثقيلة في المواد الصلبة

من الناحية النظرية توصف الظاهرة المعقدة لتباطؤ الجسيمات المشحونة في المادة من خلال مقدارين فيزيائين أساسين هما قدرة الايقاف وتطوح الطاقة. قدرة الايقاف (Stopping Power) تعرف على انها مقدار الطاقة التي يفقدها الجسيم في كل وحدة طول من مساره خلال الوسط الموقف. في الوقت نفسه نقل الطاقة خلال تصادم بين أيونات وذرات الهدف يتبع سلوك إحصائي الذي يؤدي إلى تقلبات في فقدان الطاقة، فإن متوسط التذبذب مربع (الانحراف المعياري) للتوزيع فقدان الطاقة يطلق عليه عادة اسم تطوح الطاقة **(energy straggling)**. ان دقة تعيين هذه المقادير تعد موضوعا مهما ليس فقط في مجال الفيزياء وانما في مجالات تطبقية واسعة كأستخدام الاشعاع لقتل الاورام وكذلك استخدامها في الصناعة الأجهزه الالكترونية وغيرها من الاستخدامات المهمة. لقد تمت دراسة هذه الثوابت الأساسية نظريا وتجريبيا منذ بداية القرن العشرين. فبينما المعطيات التجريبية والنظرية متوفرة لالهليوم والبروتون ، فإن المعطيات الخاصة بالأيونات الثقيلة هي ندرة كثيرا وحتى ان وجدت فهنالك اختلافات كبيرة من قبل المؤلفين خصوصا في الطاقات المنخفضة.

بناء على صيغة Lindhard, Scharff and Schiott (LSS) وعن طريق إدراج مفهوم الشحنة الفعالة قد اقترحت واختبرت صيغة شبه تجريبية جديدة لمقدار قدرة الايقاف الأيونات الثقيلة في مختلف أهداف المواد الصلبةعند الطافات المنخفظة (0.1-1MeV/n). هذه الصيغة الجديدة تظهر اتفاق جيد مع قاعدة بيانات قدرة الايقاف الإلكترونية لH. Paul.

وقد استخدمنا طريقة فعالة اعتمادا على الجمع بين تقنيتين تقنية زمن الطيران (ToF) وتقنية الارتداد المرن (ERDA) لاستنتاج قوة الايقاف وتطوح الطاقة. تمت مقارنة القيم التي تم الحصول عليها لقدرة الايقاف مع القيم المتوقع الحصول عليها من برنامج SRIM عام 2013، صيغة (LSS) والبيانات التجريبية المتاحة و الصيغة الشبه تجريبية المقترحة.

تمت مقارنة قيم تطوح الطاقة مع التنبؤ النظري لBohr، تطوح الطاقة المستنتج من نظرى بور لايقاف الطاقة ،نموذج Lindhard–Scharff المصحح من عامل تكوم الالكترونات(bunching effect) حول النواة وفقا لنهج Besenbacher.الهدف من هذه المقارنة هو التحقق من موثوقية ودقة النظريات المقترحة لتطوح الطاقة على ضوء النتائج التجريبية الحالية. جميع القيم التجريبية لتطوح الطاقة المحصل عليها أكبرمن القيم المستنبطة جميع النماذج المقترحة لتطوح الطاقة مثل :

Bohr, Lindhard–Scharff, Beth-Livigston and Yang formula.

بينت هذه الدراسة ان إدخال تأثير تكوم الالكترونات على تطوح الطاقة يحسن المقارنة ويعطي تقيما لتأثيرات الأخرى مثل تأثير تبادل الشحنات.

الكَلِمَةُ المِفْتاحُ : تطوح الطاقة ،قدرة الايقاف ، نظرية فيرسوف ، نظرية LSS ,الطاقة تطوح ,الايقاف قدرة

Acknowledgments

First of all, I would like to thank **Pr. Benmounah Abdelbaki**, Professorat the University M'hammed Bougara Boumerdes(UMBB) for having kindly chaired the Examining Jury.

I warmly thank **Pr. Abadia Seddik el Hak**, Professor at UMBB, **Pr. S. Tobbeche**, Professor at Batna University, and **Pr. Idiri Zahir**, Director of research at Nuclear Center of Research of Algiers(CRNA) for the interest they have shown in this thesis by agreeing to be a member of the Board of Examiners and to have taken advantage of their pertinent remarks.

I am grateful to Director of iThemba LABS, **Dr. Faiçal Azaiez**, as well as to Deputy Director, **Dr. Rudzani Nemutudi**, for the access to all necessary facilities including office space on Campus of iThemba LABS Gauteng and Cape Town.

I would like to heartily appreciate **Pr.** Benmounah Abdelbaki, Director of Urmpe and **Pr. Bezzazi Boudjema,** ex Director of Urmpe for their warm welcome that they reserved for me every time I went to the Urmpe and for their encouragements**.**

I am greatly indebted to **Dr. Ammi Hakim**, Director of research at CRNA for suggesting and supervising this work. He has always been extremely supportive, helpful and encouraging. I would also like to thank him for the warm welcome that he reserved for me every time I went to the CRNA. I associate him **Dr. Hedibel Mohamed**, my Co-supervisor for his assistance and availability.

I express my great gratitude to **Prof. Carlos Pineda-Vergas**, Head of Material Research Department a iThemba Labs laboratory, for having followed and directed me with his advices during my stay at iThemba LABS from October 2014 to June 2016 and for the critical reading of the manuscript which has considerably improved this thesis. I would also like to thank him for the warm welcome that he reserved for me every time I went to iThemba LABS laboratory. I associate to him **Dr. Mandla Msimanga**, researcher at iThemba LABS, who taught me with a lot of kindness and enthusiasm the principles of ToF-ERDA spectrometers and he has allowing me to use his personal library of data.

My thanks also go to **Prof. Craig Comrie**, **Dr. Morgan Madhuku, Dr. Mlungisi Nkosi**, **Dr. Christopher Mtshali** and **Dr. Phillip Sechogela,** for their availability and for the nice working atmosphere allows without them my experimental data could not have been collected.

I would like to express my most sincere appreciation to **Pr. Abaidia Seddik El Hak** and **Dr. Saadi Mohamed** for their kind assistance in all administrative matters related to my thesis and for their encouragements.

I particularly would like to thank Professor, **Benamar Mohamed El Amine**, Director of the FUNDAP laboratory, for introducing me to the CRNA and giving me the opportunity to pursue this research, and for all of the guidance that he provided over the years.

A special thanks to Mrs.**Roya Minnis-Ndimba**, Research Assistant, for his invaluable help and assistance during my staying at iThemba LABS, she has the pleasure of transmitting both her knowledge and her motivation. She gave me the opportunity to discover the different departments of the famous laboratory of iThemba LABS.

Thanks to the colleagues researchers for the relevant discussions and for the great lunch and coffee breaks. In connection with this work I want to mention **Dib Amel**, **Mammeri Ster**, **Beladel Brahim**, **Oulebsir Allaoua** and **Ishak Ahmed**.

I feel very lucky to have the support of my family, especially my parents, thanks to whom I am who I am, their unconditional love makes me want to be a better person every day.

Contents

Chapter V: Results and discussion

Chapter I
Introduction

Chapter I, begins by a short and simple description of the phenomenon of the slowing down of energetic ions in matter. In this chapter we present the motivation of studying of the slowing down of swift heavy ions at low energies and frame the work in its scientific context.

I.1. Slowing down of swift ions in matter

Whenever an energetic charged particle, passes through a matter, it loses a certain fraction of its energy by collision with atoms of the stopper material. This loss depends on the stopper material, nature and energy of the incident ions.At the same timethe energy transfer during the collision between the ions and the target atoms follows a statistical behavior which gives rise to fluctuationsin energy loss called the straggling phenomenon.

Basically, the study of the slowing down of energetic ions in matter attempts to describe how the projectile loses its energy and changes its original direction after travelling a distance Δx, which gives very important information about the depth of penetration of the projectile into the material, namely the range.

Conceptually, for a quantitative understanding, the slowing down of energetic ions in matter is described by two fundamental parameters. The first one is the energy loss per unit path length, of matter crossed, S, which is alternatively called **stopping force** or **stopping power** or **linear energy transfer** (LET). The second one is the standard deviation of the energy loss distribution commonly called straggling in energy loss or simply energy straggling. Note that the depth of penetration is closely related to the stopping force and energy straggling.

When the relative loss energy is between 10% and 50%, the distribution of the energy loss ΔE is approximately Gaussian with variance σ^2[SIM-1997]. The formulation of the fundamental parameters is explained inFig.I.1 as follow: when a beam of energy E with variance $(\sigma_2)^2$ of its Gaussian distribution cross a distance Δx in matter it loses a certain fraction ΔE of its energy (due to collision with atoms of the stopper material) and a spreading of the incident beam. The explicit definitions of the fundamental parameters are:

The stopping force is:

$$S = Lim_{\Delta x \to 0} \frac{\Delta E}{\Delta x} = \frac{dE}{dx} \tag{I.1}$$

The energy straggling is:

$$\sigma = \sqrt{\sigma_1^2 - \sigma_2^2} \tag{I.2}$$

where $\sigma_{2,1}$ the standard deviation of the ion beam before and after traversing the target respectively.

In the literature [Zie-2008, Zie-1985, Zie-1977, Sig-2006]), the stopping power is divided into nuclear stopping and electronic stopping terms. The nuclear stopping describes the energy loss process due to elastic collisions between the incident ion and the nuclei atoms of the stopper material. Its behavior as a function of incident ion energy has a maximum at about 1keV/nucleon for all ions [Schw-2003].The electronic stopping describes the energy loss process due to the interaction of the incident ion with electrons of the target atoms. Hence, the stopping power can be written as:

$$S = S_{Nuclear} + S_{Electronic} \tag{I.3}$$

The capital information of the distance R inside the medium where the ion stops is predictable from the stopping power data as follow:

$$R = \int_0^{E_0} \frac{dE}{S(E)} \tag{I.4}$$

where E_0 is the energy of the incident ion and *S(E)* is the stopping power at the energy E.

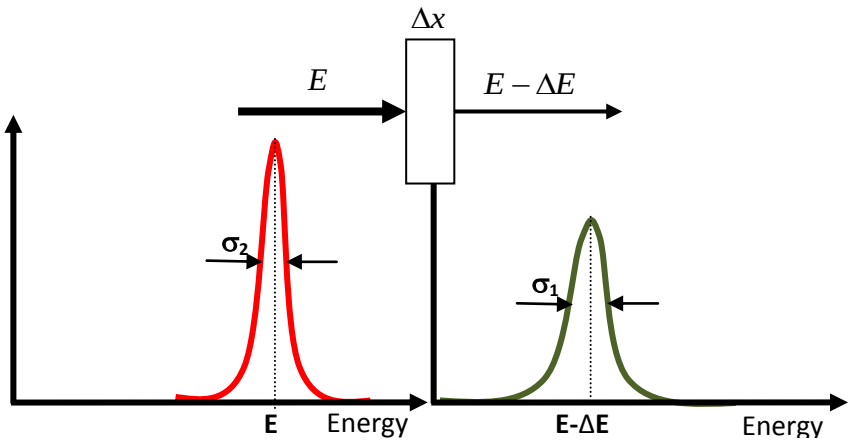

Fig. I.1: Sketch of principal of slowing down of swift ion of energy E traversing a target of thickness Δx. ΔE is the average of energy loss, σ_2 and σ_1 the standard deviation of the ion beam distribution before and after traversing the target respectively.

I.2. Motivation and problematic

Our interest in the investigation of the fundamental parameters describing the slowing down of heavy ions in matter stems from:

First: There is a need for accurate and precise value of fundamental parameters in wide areas of ion beam applications. A short overview of ion beam applications which requires precise values of fundamental parameters is reviewed in sub-section I.2.1.

Second: Data scarcity of fundamental parameters data for heavy ions and discrepancies between available data both at experimental and theoretical databases, especially at low energies. (See table 1.1 and Fig 1.2).The detailed explanation of this motivation is described in sub-sections I.2.2, I.2.3 and I.2.4.

I.2.1: Short overview of ion beam applications

- **Ion beam analysis**: Stopping power and energy straggling are indispensable and critical quantities in ion beam analytical techniques for surface and rear surface characterization. As an example, we will see in chapter IV the key role of the concepts of stopping **force** and energy straggling to develop the non destructive method of obtaining quantitative elemental depth profiling of surface sample material such as Rutherford Backscattering Spectrometry (RBS) and Elastic Recoil Detection Analysis (ERDA) techniques.
- **Nuclear physics:** For example the identification of fission fragments emitted in nuclear reaction by the ΔE-E telescope technique (using silicon Surface Barrier Detector) which needs a precise study of energy loss of heavy ions in silicon.
- **Radioprotection**: Accurate values of stopping force and energy straggling gives a precise response to critical question: What thickness and what type of material should be used to prevent the penetration of given particles with well defined energies in body tissues?
- **Microelectronic and nano-electronics***:* Exponential development in the microelectronic components industry has created a constant need for new specific materials. To obtain desired electronic properties certain impurities must be implanted into certain materials at an appropriate depth. Energetic ion beams can be used as a tool for adding these impurities. The accurate determination of the stopping force and energy straggling gives the exact necessary energy to put the specific impurity at the desired depth.
- **Tumor therapy with heavy charged particles**: To succeed in using heavy ion beams to treat, radio-resistant tumors during conventional therapy, there is a critical need for accurate values of stopping force in body tissues [Sch-2000], [Kra-1995].

In general, the great importance to determine fundamental parameters describing the slowing down of energetic ions in matter has been mentioned by several authors to introduce their papers or books **[Hel-2005,**kno-2000**]**.

I.2.2 Data scarcity of fundamental parameters for heavy ions

Stopping force and energy straggling have been studied experimentally and theoretically since the beginning of the 20th century [Zie-2008, And-1977, Nor-1963] but still deficient, especially at low energies as we can see in from the partial table I.1[Pau-2014]. At the present time, there is much less data known for the energy loss of the beam of heavy ions in matter.

Z_1 incident ion / Z_2 target	^{4}He	^{8}O	^{13}Al	^{23}V	^{28}Ni	^{40}Zr	^{45}Ph	^{55}Cs
^{1}H	0	2	0	0	0	0	0	0
^{6}C	5	21	9	1	4	1	1	1
^{18}Ar	1	4	1	0	1	0	0	0
^{13}Al	3	19	6	0	3	0	0	0
^{26}Fe	1	0	1	0	0	0	0	0
^{30}Zn	1	0	0	0	0	0	0	0
^{40}Zr	0	0	0	0	0	0	0	0
^{47}Ag	1	16	4	0	4	0	0	0
air	1	2	1	0	0	0	0	0
cell	0	0	0	0	0	0	0	0
PVC	1	0	0	0	0	0	0	0

Table I.1: The number of data files available in October, 2009, source [Pau-2014]

I.2.3 Discrepancy between available data

For heavy ions, even if the data of stopping power are available, an appreciable discrepancy up to 15%, in some cases, especially at low and intermediate energies was observed [Nee-2009]. For example in Fig. I.2 which shows the stopping power of the carbon in aluminum oxide measured by different laboratories marked by letters C(Accelerator Laboratory, Helsinki, Finland), D(iThemba LABS, South Africa) and E(University of Jyvaskyla, Finland), we can see the discrepancy between their measurements. For example at energy 0.25MeV/n we notice a relative discrepancy of about 16% between the laboratory C and laboratory E.

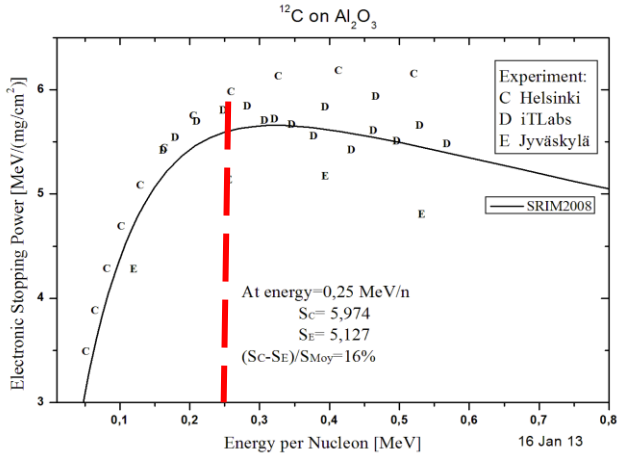

Fig. I.2: Electronic stopping power as a function of energy for ^{12}C ions in Al_2O_3, measured by research group three different laboratories. Source reference [Pau-2013]

I.2.4 The discrepancy between theory and experiment

I. 2.4.1 Stopping force

The theoretical study of the penetration of energetic heavy ions through matter is a complex many-body problem. In general the moving nucleus and its bound electrons interact with the nuclei and electrons of the stopping material. In the literature the theoretical treatment of the stopping force is performed by separating the incident ion velocity in three main regions: high velocity, intermediate velocity and low velocity (see Fig. I.3) [Schw-2003].

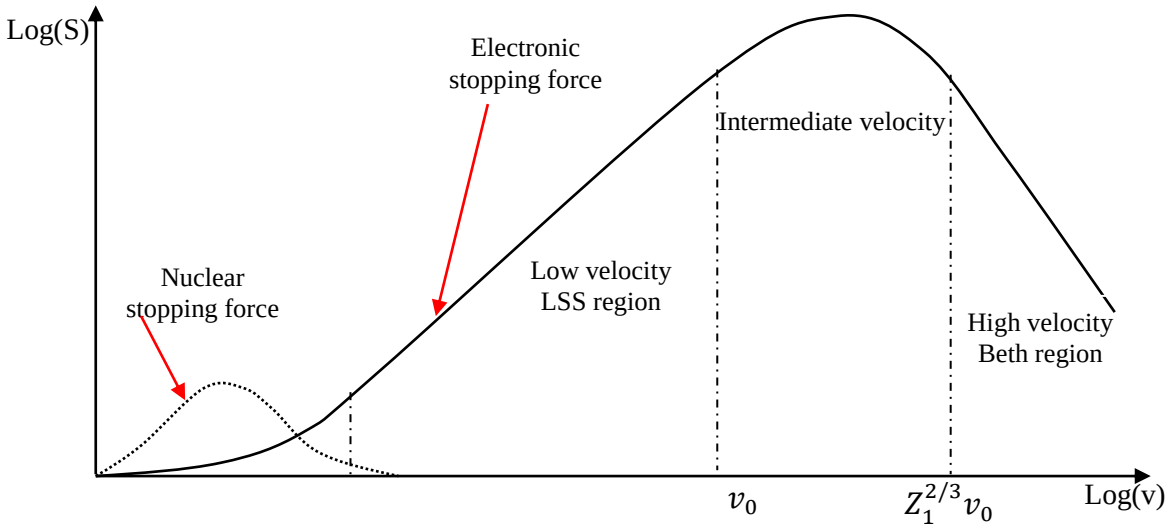

Fig. 1.3: Schematic behavior of the nuclear and electronic stopping force as a function of ion velocity.

Region of high velocity: $v > Z_1^{2/3} v_0$(the mean velocity of the electrons of a neutral atom with atomic number Z_1 deduced from the atomic Thomas-Fermi model, v_0 is the Bohr velocity)

In that case the ion loses all its electrons and then, is completely stripped of its electrons. In this region the classical Bohr Theory [Boh-1913] and the quantum theory of Bethe [Bet-1930] and Bloch [Blo-1933] both lead to an expression of the stopping force which is inversely proportional to the square of the ion velocity. This expression is relatively in good agreement with experimental values. Note that these theories require an empirical constant related to the electron binding in the stopper atoms. This velocity region is characterized by:

- The incident ion being fully stripped of its electrons
- The slowing down is due to the electronic collisions.

Region of intermediate velocity: $\boldsymbol{v_0 < v < Z_1^{2/3} v_0}$

As the velocity of the swift ions decreases and becomes comparable to the mean velocity of electrons in atoms $\boldsymbol{v_0 Z_1^{2/3}}$, several complications appears:

- Some bounded electrons remains attached to the ions; hence the ions are not fully striped of their electrons.

- Not all electrons contribute to the slowing down in particular the inner electrons (projectile or target).
- The incident ions are subject to charge exchange with the stopper material atoms.
- The energy loss still predominantly due to the inelastic encounters which excite or ionize the stopper atoms along its path.

This velocity region is the most difficult to describe theoretically, because all different contribution of energy loss are present in this domain of velocity such as: excitation and deexcitation of incident ions and target atoms, charge exchange (Ionisation of the target atoms and captures of electrons), moment exchange between ion and outer electrons of the stopper atoms, ionisation of the target atoms and probably collective effects. In this velocity region the existing theories of stopping power do not properly describe the experimental data and further theoretical research is required.

Region of Low velocity region: $v < v_0$

When the velocity of ions is slow some bounded electrons remain attached to the ions. In this velocity region the energetic ion still make inelastic collisions with the outer electrons of the stopper atoms along its path which leads to the excitation of the stopper atoms. The energy transfer is done via a momentum exchange between the energetic ions and the outer electrons of the stopper atoms. In this region, the charge exchange between ions and stopper atoms is probable. In this case the energy loss is mainly due to momentum exchange between the ion and outer electrons of atoms of the stopper matter and excitation (or de-excitation) of incident ions and stopper atoms.In this thesis, we are mainly interested in this low-velocity region.

The theoretical study of low velocity slowing down of heavy ion in matter was fundamentally investigated by Firsov [Fir-1959] and Lindhard, Scharff and Schiøtt (LSS) [Lin-1963] using the Thomas-Fermi statistical atomic model which gives a linear dependence of the stopping force on velocity. Surprisingly, the LSS approach gives satisfactory results for light incident ions. However, for heavy ions a discrepancy was observed between experimental data and calculated ones generated by LSS formula of up to 20% [Nee-2009].As an example for illustration, in Fig I.4 we compare the experimental [Pau-2013] stopping force of C in Au with the LSS theory.

On the other hand, the most accurate experimental method of direct transmission for determination of stopping force and straggling at low energy requires preparation of very thin foils, which present additional problems such as foil roughness and impurities [Cel-2013].

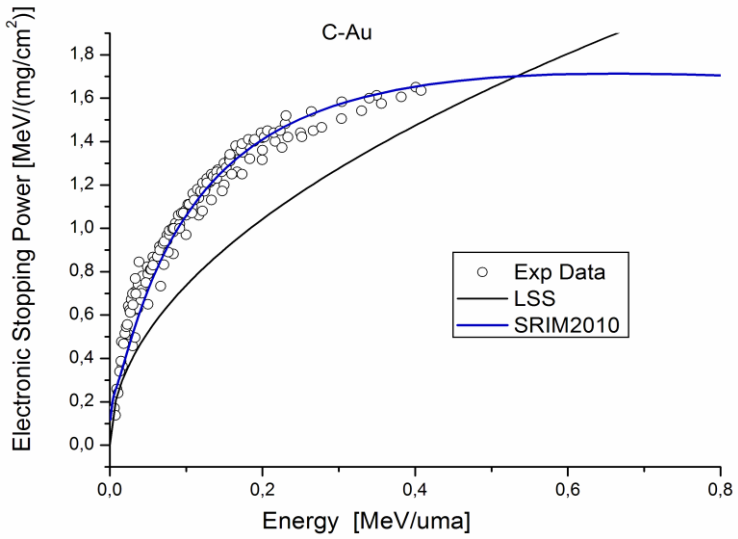

Fig. I.4: Electronic stopping power as a function of energy for C ions in Au, compared to LSS theory and SRIM 2010 simulation. The source of experimental data is the H. Paul data base. [Pau-2013].

It should be noted that in parallel to pure theoretical formulation of electronic stopping force some semi-empirical procedures have been proposed [Hub-1989, Nor-1970, Nee-2009] to generate formulas describing the stopping force for a wide range of energiesand all ion-target combinations. For example in 1970, Northcliffe and Schilling [Nor-1970] made a semi- empirical tabulation of electronic stopping power values for heavy ions in different targets. The Forter et al. [For-1976] measurement of Stopping power for ^{19}F, ^{24}Mg, ^{27}Al, ^{32}S and ^{35}Cl at energies ~0.2 to ~3.5 MeV/nucleon in several materials andthe Ziegler [Zie-1978] calculation of low energy He ion stopping forces show significant discrepancies with the values tabulated by Northcliffe and Schilling especially at low energy (<1 MeV/nucleon).

I.2.4.2 Energy straggling

Note that, in the literature stopping force has received more intensive attention in comparison to energy straggling.

At high velocity for nonrelativistic (energy less than 10 MeV/n) velocities, Bethe and Livingston [Liv-1937] developed an accurate quantum expression of energy straggling including binding of electrons by using a quantum mechanical perturbation treatment. Bohr in 1948 found a simple energy-independent formula proportional to the target thickness for energy straggling [Boh-1948]. For small energy losses the Bohr expression describes reasonably the energy straggling of ions in matter and is roughly in conformity with experimental available data [Gei-1983].

At very low energy theoretical investigations are complicated by the necessity of taking into account the scattering of ions by atoms (nuclear) which cannot be considered independent of the electronic collision [Hve-1971, Sig-2014].

However at low velocity less than $Z_1^{2/3} v_0$, both theoretical and experimental studies of energy straggling present several difficulties as the stopping power. At low beam energy, where the Bohr and Beth-Livingston approximation are not expected to be suitable, Lindhard and Scharff [Lin-1953] by considering independent excitations of an electron gas introduced a new expression of energy straggling without taking into account the charge exchange aspect and bunching effect. For heavy ions at low energy, the experimental values of straggling are in several cases unsatisfactory for all theories mentioned above, as discussed by Besenbacher et al. [Bes-1980], Geissel et al. [Gei-1983] and Kumar et al. [Kum-2015] indicate that the measured experimental values of energy straggling can fluctuate between 2 to 6 times the theoretical predicted values. The treatment of the stopper material as an electron gas ignores the fact that the electrons are bunching into atoms which cause an additional fluctuation in the number of encounters with atoms. This spatial correlation of bunching effect and charge exchange effect has been extensively discussed by Sigmund [Sig-1976, sig-1978, Sig-2006]. The introduction of these spatial correlations in energy straggling for the partially stripped heavy ions can explain the increase of energy straggling above the Bohr straggling.

I.3. Purpose and structure of the thesis

I.3.1 Purpose of the thesis

We had seen in previous sections, the slowing down of swift ions in matter present several difficulties both experimentally and theoretically especially for heavy ions at low velocity summarized as follows:

1. Scarcity of experimental data and dispersion of available data up to 15%
2. In the literature, there is no detailed information concerning the derivation of the LSS formula considered as the most suitable theory describing the slowing down of ions in matter at low energy [Bon-1978,].
3. Deviation of LSS theory with experimental data for heavy ions up to 20%.
4. Discrepancies between available data and theories of energy straggling up to 500%

From these facts, it becomes clear and necessary to investigate further the fundamental parameters governing the slowing down of energetic heavy ions in matter at low energy both experimentally and theoretically. The framework, objective and wide purpose of the present study is a contribution to improve the understanding of slowing down of heavy ions in matter at low energy as follow:

- In the aim to introduce a an improved semi-empirical expression describing the stopping force of heavy ions at low energy, we carried out an investigation about the Firsov and the Lindhard-Scharff-Schiott (LSS) stopping power models both based on the atomic statistical Thomas-Fermi (T-F) model. This leads us to check the insufficiency and application conditions of the T-F atomic model.

- On the basis of measuring simultaneously the velocity and energy of swift ion to determined the ion mass, a new experimental set up was developed at iThemba LABS, Faure, Cape Town, for Elastic Recoil Detection Analysis by using the Time of Flight Energy spectrometer (ERDA-ToF-E). This experimental set up was used to produce a new accurate data for stopping force and energy straggling. ERDA-TOF-E allowed the measurement of both the stopping force and energy straggling for a wide range of energies with one ion beam incident energy. In order to know the limitation and accuracy of the experimental method used, an investigation of physical principles of these experimental methods was made throughout this thesis. A new set of stopping force and energy straggling experimental values were obtained.
- Because the measure precision of the fundamental parameters are sensitive to the foil thickness uncertainty and the impurities, the thin foil thickness and the elemental characterization were verified by analysis with RBS using iterative simulation software code SIMNRA. A detailed description of RBS method is given throughout this thesis (Chapter IV).
- The obtained values of stopping force were compared with the predicted values obtained from the Stopping and Range of Ions in Matter program SRIM-2013 [Zie-2013]and Lindhard-Scharff-Schiott (LSS) formula [Lin-1963], as well as the available experimental data from the literature [Pau-2013,Mik-2015].
- The energy straggling values were compared with theoretical prediction of straggling Bohr model and Lindhard–Scharff formula corrected by introducing the bunching effect according to the Besenbacher approach [Bes-1980].
- Note that some stopping force and energy straggling data generated in this work for Formvar and Si_3N_4 are the first in the literature.

I.3.2: Content and outlines

The manuscript is organized in six chapters.

The current first chapter I, Introduction, presents the motivation of studying of the slowing down of swift heavy ions in matter especially at low energies and frames the work in its scientific context.

Chapter II, Review of theoretical stopping force, presents an overview of the underlying theories describing the electronic stopping force parameter; particular attention is given to the statistical model of the Lindhard-Scharff-Schiott (LSS) and Firsov model which was extensively used for low energy stopping force investigations. In this chapter we present also some modified expressions of LSS and Firsov theories proposed by several authors, as well as our proposed semi empirical formula based on LSS theory.

Chapter III, Energy straggling of heavy ions particles, presentssome widely used energy loss straggling formulations such as, Bohr [Boh-1948], Bethe-Livingston [Liv-1937] and Yang [Yan-1991]. This chapter is also devoted to describe the Bohr straggling deduced from the Bohr stopping power model and the different contributions to measured straggling for heavy ions at low energy such as: statistically independent excitation of an electron gas, Charge exchange, Bunching of electrons into atoms and Molecular correlation contribution.

Chapters IV, Experimental procedures, treat the concepts of different techniques used in this work. This chapter represents a baseline set of experiments to determine accurate values of fundamental parameters describing the slowing down of heavy ions in matter in range of energy. In this chapter, concepts of the Rutherford Backscattering Spectrometry (RBS), Elastic Recoil detection Analysis (ERDA) and Time of Flight Energy (ToE-E) spectrometry techniques are treated with describing the accuracy of the information obtained by these methods. In this chapter, a special attention was given to the combination of Heavy Ion Elastic Recoil detection Analysis (HI-ERDA) spectrometry and Time of Flight (ToF) telescope. This approach is extensively used in this dissertation.

Chapter V, Results and discussions, describes the main scientific contributions of the Thesis, including experimental results and comparison with theoretical models and available data.

Lastly, concluding remarks were presented.

Chapter II

Electronic stopping force theories

II.1. Collision of two charges

First we summarize the results of collision of two charges interacting with Coulombian force, considering the scattering of ion (m_1, Z_1) initially with velocity $\vec{v}$ by a free target particle(m_2, Z_2) at rest **(see Figs. II.1a and II.1b)**, the use of classical mechanics gives:

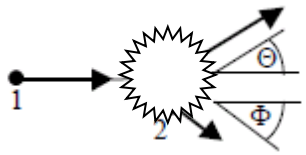

Fig.II.1a: Laboratory System (LS)

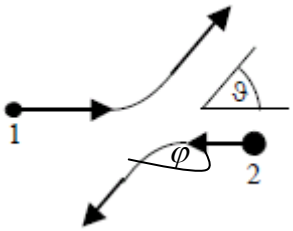

Fig.II.1b: Center-of-mass System (CMS)

The kinetic energy T transferred to the target for an impact parameter p (or diffusion angle θ in center of mass frame) is given:

$$T = T_{max} \sin^2 \frac{\theta}{2} \qquad \text{(II.1a)}$$

whereT_{max} denote the following expression : $T_{max} = \frac{4m_1m_2}{(m_1+m_2)^2} E$ (II.1b)

E is the kinetic energy of the incident particle. Other useful relations:

$$tan\frac{\theta}{2} = \frac{b}{2p}; \quad b = \frac{2Z_1Z_2e^2}{\mu v^2}, \quad \mu = \frac{m_1m_2}{m_1+m_2}, \quad T = T_{max}\frac{1}{1+\left(\frac{2p}{b}\right)^2}, \quad p^2 = \frac{b^2}{4}\left(\frac{T_{max}}{T} - 1\right) \qquad \text{(II.2)}$$

The cross section of energy transfer between T and T+dT corresponding to a collision with impact parameter between p and p+dp is:

$$d\sigma = 2\pi p dp = \frac{\pi b^2 T_{max}}{4T^2} dT \qquad \text{(II.3)}$$

We introduce some useful semi-classical picture of atomic collision for physical interpretation.

a) Recall that fortheoretical study of slowing down of ions in matter, we must firstly classified the velocity of the ions relatively to some special velocities such as: light velocity c, Bohr velocity v_0 reminding that in statistical atomic Thomas-Fermi model, the mean orbital velocity of an electron is about:

$$\langle v \rangle = Z^{2/3} v_0 \qquad \text{(II. 4)}$$

b) Conventionally, traditionally or acceptably the time of interaction (action) τ between an incident ion Z_1e of velocity $\vec{v}$with a fixed charge Q is estimated by a classical image like (see figure II.1):

$$\tau \sim \frac{2p}{v} \qquad \text{(II.5)}$$

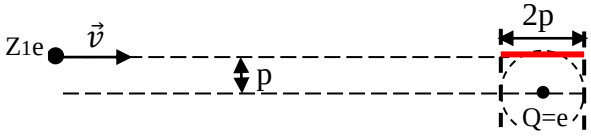

Fig. II.1c: Schema of classical collision between ion Z_1e and fixed charge Q

c) For an **isolate system** (Z_1e, Q) the variation of kinetic energy of the incident charge coming from ∞ with velocity $\vec{v}$when is at distance p from Q is:

$$\Delta E_C = \frac{1}{2}M_1 v_{atp}^2 - \frac{1}{2}M_1 v_{at\infty}^2 = -\Delta E_P = -\frac{Z_1 eQ}{p}$$

Then we can take approximately the energy exchange during the interaction in order:

$$\Delta E \sim \left|\frac{Z_1 eQ}{p}\right| \quad \text{(II.6)}$$

d) It is well known in quantum mechanics that, the perturbation of physical system is small if the following condition is realized:

$$\Delta E \tau \ll \hbar \quad \text{(II.7)}$$

For collision between Z_1e and Q=Z_2e (for electron interaction Z_2=1) this later condition writes:

$$v \gg 2Z_1 Z_2 \frac{e^2}{\hbar} = 2Z_1 Z_2 v_0 \quad \text{(II.8)}$$

II.2. Formal expression of energy loss in foil of thickness Δx

The target is considered as an ensemble of atoms distributed randomly in foil of thicknessΔx, with a density N (atoms/m^3). We consider that the thickness of the target is very small such as one incident ion in all likelihood made one collision. Note that the last consideration is not a restrictionbecause we can divide the thickness in small thickness.

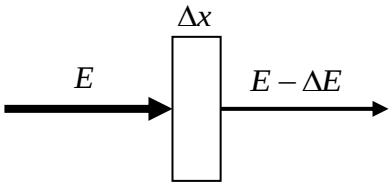

Fig.II.2 :Energy loss of projectile crossing target of Δx

Classically the cross section dσ of transfer of energy between T and T+dT, can be considired as an infinitesimal surface surround the target particle such as if the incident particle reach this section the transfer is realized. Then if the beam comes across a surface "S", the probability in order that the beam interact (transfer of energy T for an incident energy E) with the target is:

$$dP = \frac{Cross\ surface}{surface} = \frac{N\Delta x S d\sigma}{S} = N\Delta x d\sigma \quad \text{(II.9)}$$

The mean loss of energy in the target of thickness Δx, is:

$$\langle \Delta E \rangle = N\Delta x \int T d\sigma = N\Delta x S \quad \text{(II.10)}$$

$$S = \int T d\sigma \quad \text{(II.11)}$$

S is called the stopping parameter.

II.3. Electronic stopping power at high energy

II.3.1 Magic adiabatic criterion of Bohr

To give a physical estimation of E_{max} and E_{min} in the previous formal calculation where the target particles are considered free at the rest, Bohr proposes first his magic criterion for the condition to have exchange of energy between projectile and target.

Magic adiabatic criterion of Bohr

In reality, the atomic electrons are binding to the atoms and possess a velocity around the nucleus. The outer electron in atom can be considered as electron of hydrogenous atom (nuclear charge screened by Z_2-1 electrons) hence her velocity is about v_0 (Bohr velocity).

If $v \ll v_0$ (case of smooth playing without exchange like my kids when they playing together!): Bohr note that the interaction is slow and the outer electron have the time to readjust his trajectory and return to the initial trajectory. In this situation no energy T exchange between incident ion and outer electrons this idea is applicable for inner electrons because their velocities are greater than v_0. This interaction will not produce any exchange of energy it is called **adiabatic (no exchange of energy)**

Consider now, $\langle\omega_0\rangle$ as a mean angular velocity of atomic electrons (corresponding to the period T). $\langle\omega_0\rangle$: Resonance angular frequency

If $\tau \gg T \Leftrightarrow \frac{2p}{v} \gg \frac{2\pi}{\langle\omega_0\rangle} \Leftrightarrow p \gg p_0 = \pi\frac{v}{\langle\omega_0\rangle}$**(the same situation of $v \ll v_0$)**, the interaction is slow or commonly called adiabatic hence the loss of energy is negligible. Then p_0 represents an upper limit above them the transfer of energy is negligible. Less than p_0 ($v>v_0$) the approximation of free and at rest electrons seems to be justified. **Note that the parameter p_0 is related to the target by w_0 and to the incident ion v which have a dimension of impact parameter.** To have an approximate idea we take the following approximation for electrons:

$$\hbar\omega_0 \approx \frac{e^2}{a_0}, \text{ where } a_0 \text{ is the Bohr radius}$$

$$p_0 = \pi\frac{\hbar v}{e^2}a_0 = \pi\frac{v}{v_0}a_0$$

Then if $v \gg v_0$, we have $p_0 \gg a_0$, then to see the adiabatic cases we compare the impact parameter p with the characteristic parameter p_0 who is $\gg a_0$. In that case all collision who has red impact parameter participates in loss energy (see Fig.II.3), this leads to following conclusion (because the interatomic distance of solid state is of order a_0): one ion can interact with electrons of different atoms, we have a collective effect in solid state. For dilute gas **may be** the collective effect are negligible!

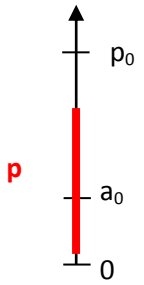

Fig. II.3: Representation of the impact parameter p in comparison with p_0 and a_0

With this image p_0 appear as a superior limit of impact parameter, above p_0 the energies transfer is negligible. Below this limit the approximation of free and at rest electrons appears justified.

II.3.2 Primarily Bohr approach

The conclusion of the magic adiabatic criterion of Bohr is that the electron collisions can be divided in two categories:

$p < p_0$ the collisions are sudden on the free at rest electron

$p > p_0$ the collisions are adiabatic and do not generate a transfer of energy.

We express the loss of electronic energy by the impact parameter p:

$$T = T_{max}\frac{1}{1+\left(\frac{2p}{b}\right)^2} = \frac{\left(\frac{b}{2}\right)^2 T_{max}}{\left(\frac{b}{2}\right)^2 + p^2}$$

$$\langle \Delta E \rangle = N\Delta x \int T d\sigma = N\Delta x \int_0^{p_0} \frac{\left(\frac{b}{2}\right)^2 T_{max}}{\left(\frac{b}{2}\right)^2 + p^2} 2\pi p dp$$

For Z_2 electrons we have:

$$\langle \Delta E \rangle_e = 2\pi N\Delta x \frac{Z_1^2 Z_2 e^4}{m_e v^2} \int_0^{p_0} \frac{2pdp}{p^2 + \left(\frac{b}{2}\right)^2} = 2\pi N\Delta x \frac{Z_1^2 Z_2 e^4}{m_e v^2} \ln\left(\frac{p_0^2 + \left(\frac{b}{2}\right)^2}{\left(\frac{b}{2}\right)^2}\right)$$

For $v >> v_0$, we have $p_0 >> b$ then

$$\langle \Delta E \rangle_e \approx 2 \times 2\pi N\Delta x \frac{Z_1^2 Z_2 e^4}{m_e v^2} \ln\left(\frac{2p_0}{b}\right)$$

We have $b = \frac{2Z_1 \times 1e^2}{m_e v^2}$ (electron collisionZ_2=1), and $\boldsymbol{p_0 = \pi \frac{v}{\langle \omega_0 \rangle}}$,

$$\langle \Delta E \rangle_e = 4\pi N\Delta x \frac{Z_1^2 Z_2 e^4}{m_e v^2} \ln\left(\frac{\pi m_e v^3}{Z_1 e^2 \langle \omega_0 \rangle}\right) \quad \text{(II.12)}$$

In conclusion Bohr [Boh-1913] considered the Z_2 electrons of the target as oscillators binding to their nucleus, the i-th electron have ω_i as angular frequency. His calculation leads to the following expression of electronic stopping force:

$$S_e = \frac{4\pi e^4 Z_1^2}{mv^2} N \sum_{i=1}^{i=Z_2} ln\left(\frac{1.23\ mv^2}{\hbar \omega_i Z_1} \frac{v}{v_0}\right) \quad \text{(II.13)}$$

where v is the projectile velocity, e is the electron charge, m is the electron mass and N atomic density of the stopper material.

In practice the expression (II.13) is often rewritten as a function of the mean angular frequency $\bar{\omega}$ determined experimentally and defined as follow:

$$\sum_{i=1}^{i=Z_2} ln\left(\frac{1}{\omega_i}\right) = Z_2 ln\left(\frac{1}{\bar{\omega}}\right) \quad \text{(II.14)}$$

Then the electronic stopping (II.13) power is rewritten:

$$S_e = \frac{4\pi e^4 Z_1^2 Z_2}{mv^2} N ln\left(\frac{1.23\ mv^2}{\hbar\bar{\omega} Z_1}\frac{v}{v_0}\right) \quad \text{(II.15)}$$

The expression (II.15)is identical to the expression II.12 and had been extensively used for high energy stopping force investigations.

II.3.3 Bethe theory

At high velocity ($v>Z_1v_0$), the quantum calculation of the stopping force was developed by Bethe [Bet-1930] by using the first order perturbation (Born approximation) to obtain the following expression:

$$S_e = \frac{4\pi e^4 Z_1^2 Z_2}{mv^2} N ln\left(\frac{2\ mv^2}{I}\right) \quad \text{(II.16)}$$

where I is the mean ionization potential.

II.4. Electronic stopping force at low energy

II.4.1. Theory of Firsov

Consider ion of low velocity v (5.10^6-10^8 cm/sec), energy E, charge Z_1, and mass m_1 colliding an atom of atomic number Z_2 and atomic mass m_2 at rest with impact parameter p_0. According to the Firsov's picture [Fir-1959] the transfer of energy, ΔE, from the ion to the atom is due to the passage of electrons from one particle to the other. The electrons transferred from the ion have the speed v of the ion; take place on the atom at higher energy levels. A consequence of this charge exchange is an excitation of the target atom by receiving fast electrons and giving up slow electrons to the ion. This leads to result in a change of the momentum of the ion after moving away from the atom. We can say that the picture of the energy lost in a single collision is a charge exchange between the ion and the target atom that appears in the form of target atom excitation resulting from the momentum charge exchange between the incident ion and the target atom. In this picture the treatment of the momentum exchange between the incident ion and the atom electrons is subject to the following perceptions and approximations (see Fig. II.4):

1. The motion and the distribution of electrons are according to the Thomas-Fermi model of the atom.
2. On the line joining the nuclei there is a minimum of the Thomas-Fermi potential (the superposition of the two T-F potential of the two atoms).
3. Introduction of a surface S 'Firsov surface' dividing the regions of action of the potentials of the first atom (ion) and the second atom. Recall that the electric field would be zero in a region of space that has the same potential throughout. Firsov take the surface S normal to the equipotential surfaces containing the minimum potential point. The normal component of the electric field vanishes everywhere at the surface S.
4. By using the Gauss theorem in case of a neutral quasimolecule (constitute by the two atoms: case treated by Firsov in his paper which consider the collision of two atoms not ion-atom),

Firsov [Fir-1959] found that at any instant the electronic charge present in one side of the S surface is equal to the charge of the corresponding nucleus. That is the reason why S divides the regions of the action of each atom during the collision.

We can say that the Firsov picture of the collision allow us the separation of the two teams (ion with its electrons and target atom with its electrons) during any instant of the collision.

5. The above charge distribution (based on the Gauss theorem) gives rise to a retarding force acting on the ion which changes the momentum of the ion.

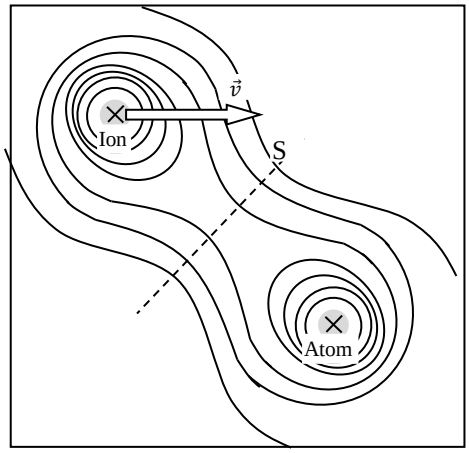

Fig. II.4 Sketch of the equipotential surfaces during the approaching of the ion and atom. Near the two nuclei the equipotential surfaces are spheres.

The random electron flux across a surface S in one direction at distance r from the atom centre is defined as:

$$\Gamma_S = \int d^3v\, f(\vec{v},\vec{r},t)\vec{v}.\vec{u} = \frac{n(r)\langle v_e(r)\rangle}{4} \qquad \text{(II.17)}$$

Where $\vec{u}$ is the unit vector normal to the surface S, f velocity distribution function which is considered Maxwellian, $\langle v_e(r)\rangle$ is the mean value of the electron velocity related to the electron density n(r) according to the Thomas-Fermi model by the following relation:

$$\langle v_e(r)\rangle = \frac{3}{4m}(3\pi^2)^{1/3}\hbar(n(r))^{1/3} \qquad \text{(II.18)}$$

where m is the electron mass.

The force acting on the ion will be given by the formula:

$$\vec{F} = m\frac{d\vec{R}}{dt}\int_S \frac{n(r)\langle v_e(r)\rangle}{4} dS \qquad \text{(II.19)}$$

where $\frac{d\vec{R}}{dt}$ the velocity of the ion relatively to the atom. Note that a similar force with opposite sign acts on the atom.

The total work of slowing down of the ion (i.e the electron excitation energy of the atom) is:

$$T = m \int \frac{d\vec{R}}{dt} d\vec{R} \left[\int_S \frac{n(r)\langle v_e(r) \rangle}{4} dS \right] \quad \text{(II.20)}$$

The use of Eq. II.18 gives:

$$T = \frac{3}{16} (3\pi^2)^{1/3} \hbar \int \frac{d\vec{R}}{dt} d\vec{R} \left[\int_S n(r)^{4/3} dS \right] \quad \text{(II.21)}$$

In the Thomas-Fermi model the relation between the potential ϕ and the electron density n is:

$$n = \frac{2^{3/2} (me\phi)^{3/2}}{3\pi^2 \hbar^3} \quad \text{(II.22)}$$

where e is the electric charge of the electron.

Using eq. II.22 in eq. II.21, we obtain:

$$T = \frac{m^2 e^2}{4\pi^2 \hbar^3} \int \frac{d\vec{R}}{dt} d\vec{R} \left[\int_S \phi^2 dS \right] \quad \text{(II.23)}$$

To perform the calculation of the energy lost in a single collision at impact parameter p, the following additional assumptions were made:

1- The velocity of the projectile does not change during the collision so the relative motion of collisions partners was taken as uniform (limit to small-angle scattering), then during the collision we have:

$$\left\| \frac{d\vec{R}}{dt} \right\| = v \quad \text{(II.24)}$$

2- The Firsov surface was considered as plane and placed at the midways between regions of action of the potentials of the ion and the atom (see Fig. II.5).

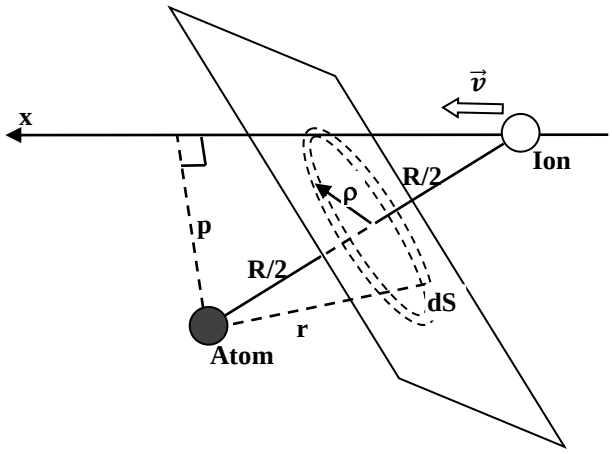

Fig.II.5: Geometry consideration in the Firsov's calculation

With these considerations we can write:

$$\frac{d\vec{R}}{dt} \cdot d\vec{R} = \frac{d\vec{R}}{dt} \cdot d\vec{R}_{//} = v dx \quad \text{(II.25)}$$

Substituting (II.25) in (II.23)

$$T = \frac{m^2 e^2}{4\pi^2 \hbar^3} v \int_{-\infty}^{+\infty} \left[\int_S \phi^2 dS \right] dx \quad \text{(II.26)}$$

In addition to all assumptions and considerations cited before, Firsov choose the potential ϕ(r) in the space between atoms as given by the expression of the interaction potential of atoms [Fir-1958-a]:

$$\phi(r) = \frac{Z_1 Z_2}{r}\chi(1.13(Z_1+Z_2)^{\frac{1}{3}}r/a_b) \quad \text{(II.27)}$$

Where χ is the universal Thomas-Fermi screening function where r is expressed in atomic unit (a_b=1 a.u.=0.529 Å).

From Figure II.5 we have the relations:

$$R^2 = p^2 + x^2 \quad \text{(II.28-a)}$$

$$r^2 = \frac{R^2}{4} + \rho^2 = \frac{p^2+x^2}{4} + \rho^2 \quad \text{(II.28-b)}$$

Finally, the electronic energy loss for one collision at the impact parameter p can be written

$$T = \frac{m^2e^2}{4\pi^2\hbar^3}v\int_{-\infty}^{+\infty}\int_0^{\infty}\left[\phi\left(\left(\frac{p^2+x^2}{4}+\rho^2\right)^{1/2}\right)\right]^2 2\pi\rho d\rho\, dx \quad \text{(II.29)}$$

The Firsov [Fir-1959] calculation of (2.29) using the expression (2.27) for the potential ϕ gives:

$$T = \frac{4{,}3\times10^{-8}(Z_1+Z_2)^{\frac{5}{3}}}{\left[1+3.1(Z_1+Z_2)^{\frac{1}{3}}10^7 p\right]^5}v \quad \text{(II.30)}$$

where v is expressed in cm/sec and p in centimetres.

Teplova et al. [Tep-1962] integrated the energy transferred in one collision (Eq. II.11) over the impact parameter p to obtain the stopping cross section for random media:

$$S_e = \int_0^{\infty} 2\pi p dp T(p)$$

To obtain the following stopping force:

$$S_e = 5{,}15.\,10^{-15}(Z_1+Z_2)\frac{v}{v_0} \text{ (eV.cm}^2\text{/atom)} \quad \text{(II.31)}$$

II.4.2 Theory of Linhard-Sharff-Schiott (LSS)

The derivation of the LSS [Lin-1963] expression was never published [Bon-1978]. The general trend of the LSS formula can be understand from the original model of Firsov [Fir-1957, Fir-1958-a, Fir-1958-b, Fir-1959] and the quasiclassical calculation of Tilinin [Til-1995].

The LSS theory is an extension of the theory of the slowing down of an ion passing through an electron gas in a similar way as an ion pass through stopper atoms described by Thomas-Fermi model. They achieved the expression of electronic stopping force for velocities below $Z_1^{2/3}v_0$[Lin-1963]:

$$S_e = \xi_e N\frac{8\pi e^2 a_0 Z_1 Z_2}{\left(Z_1^{2/3}+Z_2^{2/3}\right)^{3/2}}\frac{v}{v_0} \quad \text{(II.32)}$$

The factor ξ_e was added as fitting parameter independently to the Thomas-Fermi inter-atomic potential [Lin-1961] which is approximately equal to$Z_1^{1/6}$.

With all restricted considerations the equations (II.31) and (II.32) provide surprisingly a good estimation of the behavior of stopping force at low velocity. However a discrepancy between these later expressions and experimental results up to 20% was observed for heavy ions [Nee-2009].

II.4.3. Modified LSS formula

In this thesis a semi empirical formula based on LSS theory was proposed by considering the following assumptions (see Gue-2014):

a) Correlation factor ξ_e

The empirical factor ζ_e is chosen to be equal to Z_1^a, where a is a free parameter.

b) Effective charge

It is well known that at low velocity the incident ion is not completely stripped of its electrons. We propose to replace the charge Z_1 by the effective charge Z_1^* in the expression (II.32). We have adopted the expression given by Northcliffe and Schilling [Nor-1970] for effective charge evaluation.

$$Z_1^* = \left(1 - exp\left(\frac{v}{v_0 Z_1^{2/3}}\right)\right) Z_1 \qquad \text{(II.33)}$$

Based on the previous considerations, we propose through this work the following expression to evaluate the electronics stopping power (S_e) for heavy ions crossing solid targets at low energy regime (LSS domain):

$$S_e = Z_1^a N \frac{8\pi e^2 a_0 Z_1^* Z_2}{\left(Z_1^{\frac{2}{3}} + Z_2^{\frac{2}{3}}\right)^{\frac{3}{2}}} \frac{v}{v_0} f(E) \qquad \text{(II.34)}$$

where $f(E)$is a fitting exponential function expressed as:

$$f(E) = \frac{1}{1+\exp(bE)} \qquad \text{(II.35)}$$

where b is an adjustable parameter to give the best fit with the experimental stopping power.

Chapter III

Energy straggling theories

In this chapter we present some widely used energy loss straggling formulations such as, Bohr [Boh-1948], Bethe-Livingston [Liv-1937] and Yang [Yan-1991]. This chapter is also devoted to describe the Bohr straggling deduced from the Bohr stopping power model and the different contributions to measured straggling for heavy ions at low energy such as: statistically independent excitation of an electron gas, Charge exchange, Bunching of electrons into atoms and Molecular correlation contribution.

III.1. Introduction

In the literature stopping force has received more intensive attention in comparison to energy straggling.

At high nonrelativistic velocities (energies range 1-10 MeV/n), Bethe and Livingston [Liv-1937] developed an accurate quantum expression of energy straggling including binding of electrons by using a quantum mechanical perturbation treatment. Furthermore Bohr in 1913 found a simple energy-independent formula proportional to the target thickness for energy straggling [Boh-1948]. For small energy losses the Bohr expression describes reasonably well the energy straggling of ions in matter and is roughly in conformity with experimental available data [Gei-1983].

At very low energy theoretical investigations are complicated by the necessity of taking into account the scattering of ions by atoms (nuclear) which cannot be considered independent of the electronic collision [Hve-1971, Sig-2014].

However at low velocity less than $Z_1^{2/3} v_0$, both theoretical and experimental studies of energy straggling present several difficulties. At low beam energy, where the Bohr and Bethe-Livingston approximation are not expected to be suitable, Lindhard and Scharff [Lin-1953]by considering independent excitations of an electron gas introduced a new expression of energy straggling without taking into account the charge exchange aspect and bunching effect. For heavy ions at low energy, the experimental values of straggling are in several cases unsatisfactory for all theories mentioned above, as discussed by Besenbacher et al. [Bes-1980],Geissel et al. [Gei-1983]and Kumar et al. [Kum-2015]indicate that the measured experimental values of energy straggling can fluctuate between 2 to 6 times the theoretical predicted values. The treatment of the stopper material as an electron gas ignores the fact that the electrons are bunching into atoms which cause an additional fluctuation in the number of encounters with atoms. This spatial correlation of bunching effect and charge exchange effect has been extensively discussed by Sigmund [Sig-1976, sig-1978, Sig-2006]. The introduction of these spatial correlations in energy straggling for the partially stripped heavy ions can explain the increase of energy straggling above the Bohr straggling.

In all the following theories we consider an ion beam of velocity v, energy E, charge Z_1, and masse m_1 penetrate in target material of thickness Δx consisting of randomly distributed atoms with density N atoms per unit volume, atomic number Z_2 and atomic masse m_2.

Energy-Loss Straggling

Using the same notation parameters as in chapter II sub-section 2 the average square fluctuation over the thickness Δx (standard deviation Ω) of the energy loss distribution is given by **[Bohr-1948]:**

$$\Omega^2 = \langle(\Delta E - \langle\Delta E\rangle)^2\rangle = N\Delta x \int T^2 d\sigma(E,T) = N\Delta x W \quad \text{(III.1)}$$

$$W = \int T^2 d\sigma(E,T)$$

W is called straggling parameter.

III.2. Bohr Theory

III.2.1 Formal Bohr Theory:

At this stage, we must remember that the relations established in section 1 of chapter II, suppose that the target particle is free at rest and do not forget also that the incident ions must have a velocity much greater than $v_0 Z_1^{3/2}$ to be completely stripped to their electrons.

From Eq.II.1 for electron collision we have:

$$T_{max} = \frac{4m_1 m_e}{(m_1+m_e)^2} E \approx 2m_e v^2$$

$$b = \frac{2Z_1 Z_2 e^2}{\mu v^2} \approx \frac{2Z_1 \times 1e^2}{m_e v^2} \ (Z_2=1)$$

Then from eq. II.3:

$$d\sigma = 2\pi p dp = \frac{\pi b^2 T_{max}}{4T^2} dT = \frac{2\pi Z_1^2 \times (1)^2 e^4}{m_e v^2} \frac{1}{T^2} dT \quad \text{(III.2)}$$

Then from eq. II.10 the loss of Z_2 electrons is

$$\langle\Delta E\rangle_e = N\Delta x \int T d\sigma = \sum_1^{Z_2} \frac{2\pi Z_1^2 \times (1)^2 e^4}{m_e v^2} \int \frac{T dT}{T^2} = 2\pi N\Delta x \frac{Z_1^2 Z_2 e^4}{m_e v^2} \int \frac{dT}{T} = 2\pi N\Delta x \frac{Z_1^2 Z_2 e^4}{m_e v^2} \ln\left(\frac{T_{max}}{T_{min}}\right)_e \quad \text{(III.3)}$$

Similarly for the energy straggling from eq. III.1:

$$\Omega_e^2 = 2\pi N\Delta x \frac{Z_1^2 Z_2 e^4}{m_e v^2} \int dT = 2\pi N\Delta x \frac{Z_1^2 Z_2 e^4}{m_e v^2} (T_{max} - T_{min})_e \quad \text{(III.4-a)}$$

$T_{max} = \frac{4m_1 m_e}{(m_1+m_e)^2} E \approx 2m_e v^2$ ($m_1 >> m_e$)

If we consider $T_{max} >> T_{min}$ we obtain

$$\Omega_e^2 = 4\pi N\Delta x Z_1^2 Z_2 e^4 \quad \text{(III.4-b)}$$

Expression III.4-b is called Bohr straggling.

In conclusion**,** assuming that the target electrons contribute randomly to the energy loss, the velocity of the projectile is much greater than the orbital velocities of the electrons of the target atoms, and the energy loss of the ion per collision event with a target electron is very small as compared to the incident energy, Bohr [Boh-1948] found the expression III.4-b for electronic energy straggling.

Attempt to improve the Bohr straggling (III.4-b) when the velocity of the incident ion become comparable to the orbital velocity of the electrons in the stopper material, the Bohr formula can be modified by considering only the contribution of electron with velocity lower than v [Bes-1980]:

$$\frac{\Omega_{BB}^2}{\Omega_B^2} = 2\frac{v}{v_0}Z_2^{-2/3} \qquad \text{(III.5)}$$

In the same manner of the derivation of Eq. II.12 of electronic stopping force the energy straggling can be obtained as follow:

$$\Omega^2 = N\Delta x \int T^2 d\sigma(E,T) = N\Delta x \int_0^{p_0} \left[\frac{\left(\frac{b}{2}\right)^2 T_{max}}{\left(\frac{b}{2}\right)^2 + p^2}\right]^2 2\pi p dp$$

For one electron, ($T_{max} = 2m_e v^2$), $b = \frac{2Z_1 \times 1e^2}{m_e v^2}$

$$I = \int_0^{p_0} \left[\frac{\left(\frac{b}{2}\right)^2 T_{max}}{\left(\frac{b}{2}\right)^2 + p^2}\right]^2 2\pi p dp = \left[\left(\frac{b}{2}\right)^2 T_{max}\right]^2 \int_0^{p_0} \frac{2\pi p dp}{\left(\left(\frac{b}{2}\right)^2 + p^2\right)^2}$$

$$I = \left[\left(\frac{b}{2}\right)^2 T_{max}\right]^2 \pi \left[-\frac{1}{\left(\frac{b}{2}\right)^2 + p^2}\right]_0^{p_0} = \pi \left[\left(\frac{b}{2}\right)^2 T_{max}\right]^2 \left[\frac{1}{\left(\frac{b}{2}\right)^2} - \frac{1}{\left(\frac{b}{2}\right)^2 + p_0^2}\right]$$

For v>>v_0 , we have p_0>>b then, (zero order) we take $\boldsymbol{p_0} = \frac{\boldsymbol{v}}{\langle \boldsymbol{\omega_0} \rangle}$

$$I \approx \pi \left[\left(\frac{b}{2}\right)^2 T_{max}\right]^2 \left[\frac{1}{\left(\frac{b}{2}\right)^2} - \frac{1}{p_0^2}\right] = 4\pi Z_1^2 e^4 \times 1 - 4\pi Z_1^2 e^4 \times 1 \left(\frac{Z_1^2 e^4}{m_e^2 v^6} \langle \omega_0 \rangle^2\right)$$

Summation over Z_2 electron we obtain,

$$\Omega_e^2 = 4\pi Z_1^2 Z_2 e^4 N\Delta x \left(1 - \frac{Z_1^2 e^4}{m_e^2 v^6} \langle \omega_0 \rangle^2\right) = \Omega_B^2 \left(1 - \frac{Z_1^2 e^4}{m_e^2 v^6} \langle \omega_0 \rangle^2\right) \qquad \text{(III.6)}$$

III.2.2. Energy straggling deduced from Bohr stopping model

Until now, we have describe the slowing down of ions by considering the electron free and at rest or considering qualitatively the target's electrons have mean angular velocity of w_0. Now we describe the target's electron by an oscillators binding to their nucleus as considered by Bohr.

We use the approximation that the incident ion does not change his initial direction, which is the case of distant collision.

Let $\vec{r}$ and $\vec{\ell}$ represents the position relatively to the nucleus of the incident ion and target's electron respectively (see Fig.III.1).

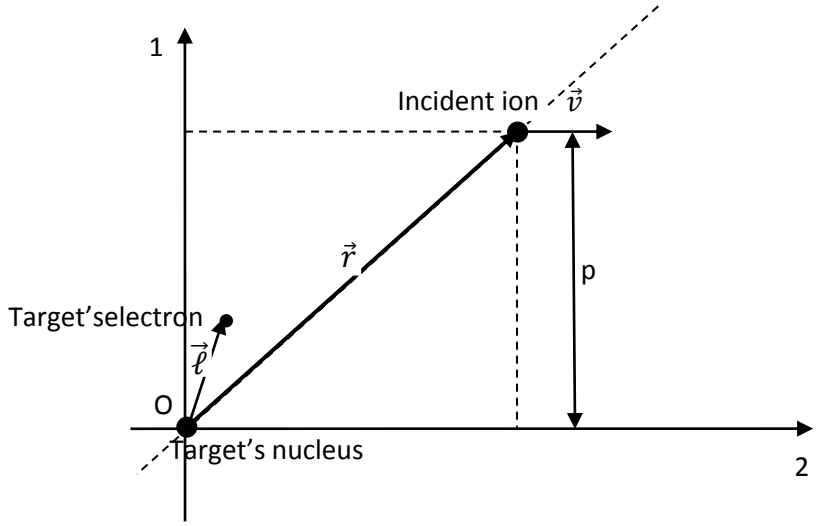

Fig. III.1: Schema of the position of the incident ion, target's nucleus and target's electron

The electric field creates by the incident ion on the vicinity of the nucleus is:

$$\overrightarrow{E(t)} = \frac{Z_1 e}{r^3}\vec{r} = \begin{Bmatrix} E_1(t) \\ E_2(t) \end{Bmatrix}$$

$$E_1(t) = \frac{Z_1 ep}{(p^2+v^2t^2)^{3/2}} \qquad \text{(III.7-a)}$$

$$E_2(t) = \frac{Z_1 evt}{(p^2+v^2t^2)^{3/2}} \qquad \text{(III.7-b)}$$

The energy transferred from the incident ion to the atom is described by $\int e\overrightarrow{E(t)} \cdot d\vec{\ell}$, then we interest on the movement parallel to $\overrightarrow{E(t)}$. Put $\vec{\ell} = \vec{\ell}_{//} + \vec{\ell}_{\perp}$ and not $\vec{\ell}_{//}$ by $\vec{x}$:

The parallel motion equation of the electron around the nucleus is:

$$m_e \frac{d^2x}{dt^2} = -kx - eE(t) - \mathrm{C}\frac{dx}{dt} \Rightarrow \frac{d^2x}{dt^2} = -\frac{k}{m_e}x - \frac{e}{m_e}E(t) - \frac{\mathrm{C}}{m_e}\frac{dx}{dt}$$

Put $\frac{k}{m_e} = \omega_0^2$ and $\frac{\mathrm{C}}{m_e} = \Gamma$ the motion equation is:

$$\frac{d^2x}{dt^2} = -\omega_0^2 x - \frac{e}{m_e}E(t) - \Gamma\frac{dx}{dt} \qquad \text{(III.8)}$$

The solution of equation (III.8) can be found by Fourier's decomposition:

$$x(t) = \frac{1}{\sqrt{2\pi}} \int_{-\infty}^{+\infty} e^{-it\omega} x(\omega)\, d\omega \qquad \text{(III.9-a)}$$

$$E(t) = \frac{1}{\sqrt{2\pi}} \int_{-\infty}^{+\infty} e^{-it\omega} E(\omega)\, d\omega \qquad \text{(III.9-b)}$$

$x(\omega)$and$E(\omega)$are the Fourier's components of x(t) and E(t) respectively. Note that x(t) and E(t) are reel, then $x^*(\omega) = x(-\omega)$ and $E^*(\omega) = E(-\omega)$.

Make eq.III.9-a and eq.III.9-b in eq.III.8 we obtain:

$$-\omega^2 x(\omega) - i\omega\Gamma x(\omega) + \omega_0^2 x(\omega) = -\frac{e}{m_e} E(\omega) \qquad \text{(III.10-a)}$$

Then

$$x(\omega) = -\frac{e}{m_e} \frac{1}{\omega_0^2 - \omega^2 - i\omega\Gamma} E(\omega) \qquad \text{(III.10-b)}$$

The transferred energy is

$$T = \int (-eE(t) dx = \int (-eE(t) \frac{dx}{dt} dt$$

$$T = \frac{ie}{2\pi} \int \int_{-\infty}^{+\infty} \int_{-\infty}^{+\infty} e^{-i\omega' t} E(\omega')(\omega) e^{-i\omega t} x(\omega)\, d\omega dt d\omega'$$

Note that

i- ω, ω' and t independents variables

ii- $\int_{-\infty}^{+\infty} e^{-i(\omega'+\omega)t} dt = 2\pi\delta((\omega' + \omega)$

This leads to:

$$T = ie \int_{-\infty}^{+\infty} E(-\omega)\omega x(\omega)\, d\omega$$

Then by use of Eq.III.10-b we obtain:

$$T = -\frac{ie^2}{m_e} \int_{-\infty}^{+\infty} \frac{E^*(\omega)E(\omega)\omega}{\omega_0^2 - \omega^2 - i\omega\Gamma} d\omega = -\frac{ie^2}{m_e} \int_{-\infty}^{+\infty} \frac{|E(\omega)|^2 \omega[\omega_0^2 - \omega^2 + i\omega\Gamma]}{(\omega_0^2 - \omega^2)^2 + (\omega\Gamma)^2} d\omega$$

The physical real part of energy transfer is

$$T = \frac{e^2}{m_e} \int_{-\infty}^{+\infty} \frac{|E(\omega)|^2 \omega^2 \Gamma}{\left(\omega_0^2 - \omega^2\right)^2 + (\omega\Gamma)^2} d\omega = \frac{e^2}{m_e} \int_{-\infty}^{+\infty} |E(\omega)|^2 \frac{\Gamma}{\left(\frac{\omega^2 - \omega_0^2}{\omega}\right)^2 + (\Gamma)^2} d\omega \qquad \text{(III.11)}$$

We remind the property of Dirac function:

$$\pi\delta(x) = \lim_{\Gamma \to 0} \left[\frac{\Gamma}{\Gamma^2 + x^2}\right] \qquad \text{(III.12)}$$

Then eq. III.11 becomes:

$$T = \frac{e^2\pi}{m_e}\int_{-\infty}^{+\infty}|E(\omega)|^2\delta\left(\frac{\omega^2-\omega_0^2}{\omega}\right)d\omega \qquad \text{(III.13)}$$

We remind also the property of Dirac function:

$$\delta[f(x)] = \sum_j \frac{\delta(x-x_j)}{f'(x)}, \text{ } x_j \text{ are the solution of equation f(x)=0} \qquad \text{(III.14)}$$

Then eq. III.13 become:

$$T = \frac{e^2\pi}{m_e}\int_{-\infty}^{+\infty}|E(\omega)|^2\left[\frac{\delta(\omega-\omega_0)}{2}+\frac{\delta(\omega+\omega_0)}{2}\right]d\omega = \frac{e^2\pi}{m_e}|E(\omega_0)|^2 \qquad \text{(III.15)}$$

Very important results which mean the energy transfer take place only at the frequency of electron oscillation.

Calculation of $|E(\omega_0)|^2$

$$|E(\omega_0)|^2 = |E_1(\omega_0)|^2 + |E_1(\omega_0)|^2$$

where (use the inverse of Fourier transformation eq. III.9-b):

$$E_1(\omega_0) = \frac{1}{\sqrt{2\pi}}\int_{-\infty}^{+\infty} e^{+i\omega_0 t}E_1(t)\,dt = \frac{1}{\sqrt{2\pi}}\int_{-\infty}^{+\infty} e^{+i\omega_0 t}\frac{Z_1 ep}{(p^2+v^2t^2)^{3/2}}dt$$

$$E_2(\omega_0) = \frac{1}{\sqrt{2\pi}}\int_{-\infty}^{+\infty} e^{+i\omega_0 t}E_2(t)\,dt = \frac{1}{\sqrt{2\pi}}\int_{-\infty}^{+\infty} e^{+i\omega_0 t}\frac{Z_1 evt}{(p^2+v^2t^2)^{3/2}}dt$$

changing the variable t to u: $u = \frac{vt}{p}$ we obtain

$$E_1(\omega_0) = \frac{Z_1 e}{pv\sqrt{2\pi}}\int_{-\infty}^{+\infty}\frac{e^{+i\omega_0\frac{pu}{v}}}{(1+u^2)^{3/2}}du \qquad \text{(III.16-a)}$$

$$E_2(\omega_0) = \frac{Z_1 e}{pv\sqrt{2\pi}}\int_{-\infty}^{+\infty}\frac{ue^{+i\omega_0\frac{pu}{v}}}{(1+u^2)^{3/2}}du \qquad \text{(III.16-b)}$$

From M. Abramovitz (formula 9.6.21 page 376)

$$K_0(x) = \int_0^{\infty}\frac{cosxt}{\sqrt{1+t^2}}dt \quad \text{x>0} \qquad \text{(III.17-a)}$$

In Eq. III.16.6, we need to calculate $I = \int_{-\infty}^{+\infty}\frac{ue^{+ixu}}{(1+u^2)^{3/2}}du$ with $x = \frac{p\omega_0}{v}$

$$\Re(iI) = -\int_{-\infty}^{+\infty}\frac{usin(xu)}{(1+u^2)^{3/2}}du$$

Put $f'(u) = \frac{u}{(1+u^2)^{3/2}}$ and $g(u) = sin(xu)$

Then $f(u) = -(1+u^2)^{-\frac{1}{2}}$ and $g'(u) = xcos(xu)$

$$\int_{-\infty}^{+\infty} \frac{ue^{+i\omega_0\frac{pu}{v}}}{(1+u^2)^{3/2}}du$$

$$\Re(iI) = -\left[\underbrace{-\int_{-\infty}^{+\infty} \frac{sin(xu)}{(1+u^2)^{1/2}}du}_{0} + \int_{-\infty}^{+\infty} \frac{xcos(xu)}{(1+u^2)^{1/2}}du\right] = -2xK_0(x)$$

Finally

$$\Re(iI) = -\int_{-\infty}^{+\infty} \frac{usin(xu)}{(1+u^2)^{3/2}}du == -2xK_0(x)$$

We can write in complex representation:$x = \frac{p\omega_0}{v}$

$$K_0(x) = \frac{i}{2x}\int_{-\infty}^{+\infty} \frac{ue^{+ixu}}{(1+u^2)^{3/2}}du$$

K_n is the Modified Bessel functions of 2nd kind.

$$E_2(\omega_0) = -\sqrt{\frac{2}{\pi}}\frac{Z_1 e\omega_0}{pv}\frac{p\omega_0}{v}K_0\left(\frac{p\omega_0}{v}\right) \quad \text{(III.18-a)}$$

In similar way we find:

$$E_1(\omega_0) = \sqrt{\frac{2}{\pi}}\frac{Z_1 e\omega_0}{pv}\frac{p\omega_0}{v}K_1\left(\frac{p\omega_0}{v}\right) \quad \text{(III.18-b)}$$

With Eq.III.15 the energy transfer becomes:

$$T = \frac{2Z_1^2e^4}{m_e p^2 v^2}x^2[K_0^2(x) + K_1^2(x)]x = \frac{p\omega_0}{v} \quad \text{(III.19)}$$

(Eq.III.19) is the expression of the energy transferred to an electron bounded to his nucleus from the passage of an ion of velocity v and charge Z_1.

Now the way is paved to calculate the energy straggling. The Bohr calculation of stopping force by considering the target's electron as an oscillator bound to its nucleus and using the approximation that the incident ion does not change its initial direction was extended for the energy straggling and was calculated by Sigmund**[Sig-2006]**:

$$\Omega_{BM}^2 = \Omega_B^2\left[\frac{1}{1+(b/2p_0)} + \frac{2}{y^2}\int_{x_0}^{\infty} x[K_0^2(x) + K_1^2(x)]^2\right]dx \quad \text{(III.20)}$$

where,$b = \frac{2Z_1 \times 1e^2}{m_e v^2}$, $y = \frac{mv^3}{Z_1 e^2 \omega_0}$, $x = \frac{p\omega_0}{v}$,$x_0 = \frac{p_0 \omega_0}{v}$, $I = \hbar\omega_0$, I is the mean excitation energy of the target atom, K_0 and K_1 are the modified Bessel functions of 2nd kind. The expression (III.20) is evaluated numerically.

III.3. Chu and Young straggling

Considering the electron binding in target atoms for lower ion energy E, Chu [Chu-1976] proposed the following semi- empirical formula:

$$\Omega_{Ch}^2 = H\left(\frac{E}{M_1}, Z_2\right)\Omega_B^2 \qquad \text{(III.21)}$$

where*H* is a correction factor tabulated for $100 \le E/M_1 \le 1000$ (keV/amu) by Szilágyi [Szi-1995].

The charge fluctuation state induced additional energy loss straggling given by Yang's et al. [Yan-1991]semi-empirical formula based on Chu's theory given by:

$$\frac{\Omega_{Yang}^2}{\Omega_B^2} = \frac{Z_1^{4/3}}{Z_2^{1/3}}\left(\frac{C_1\Gamma}{(\varepsilon - C_2)^2 + \Gamma^2}\right), \qquad \varepsilon = \frac{E}{\sqrt{Z_1^3 Z_2}}, \Gamma = C_3(1 - e^{-C_4\varepsilon}) \qquad \text{(III.22)}$$

where E is the energy in MeV/amu and $\mathbf{C_1}$, $\mathbf{C_2}$, $\mathbf{C_3}$, and C_4 are fitted constants.

The total energy straggling Ω_T^2 is then the sum of the Chu and Yang straggling components:

$$\frac{\Omega_T^2}{\Omega_B^2} = \gamma^2(Z_1, Z_2, v)\frac{\Omega_{Ch}^2}{\Omega_B^2} + \frac{\Omega_{yang}^2}{\Omega_B^2} \qquad \text{(III.23)}$$

where $\gamma(Z_1, Z_2, v)$is the effective charge for ions in matter.

III.4.Bethe and Livingston energy straggling

In the quantum theory of Bethe and Livingston [Liv-1937], the energy loss straggling is given by:

$$\Omega^2 = \Omega_{BL}^2 = 4\pi Z_1^2 Z_2 e^4 N\Delta x\left[Z_2' + \sum_i\left(k_i \frac{I_i Z_i}{m_e v^2}\ln\frac{2m_e v^2}{I_i}\right)\right], k_i = 4/3 \qquad \text{(III.24)}$$

where I_i the average excitation energy of the Z_i electrons in the ith atomic orbit, Z_2' is the total number of effective electrons. The summation extends over all shells for which $2m_e v^2 > I_i$ (m_e is the electron mass and v the incident particle velocity).

III.5.Lindhard and Sharff energy straggling

Also, Lindhard and Scharff[Lin-1953]make effort to improve the Bohr straggling expression at low velocity byconsidering the target atom as free electron gas and statistically independent excitations of electrons, find the following expression for energy loss straggling valid at low velocities ($v < \sqrt{3Z_2}v_0$):

$$\Omega_{LS}^2 = \frac{1}{2}\Omega_B^2\left[1.36\frac{v}{v_0}\frac{1}{\sqrt{Z_2}} - 0.016\left(\frac{v}{v_0}\right)^3\frac{1}{Z_2^{3/2}}\right] \qquad \text{(III.25)}$$

III.6. Bunching of electrons into atoms

Expression (III.25) ignores the fact that the target's electrons are bunching into atoms. This fact affect the fluctuation in the number of encounters with atoms, hence an additional straggling arises. This spatial correlation of bunching effect which is much less studied in the literature has been discussed by Sigmund **[Sig-1976**, **Sig-1978].**According Besenbacher et al, [Bes-1980]if we limit only to the spatial correlation due to the bunching effect for a monatomic gas the straggling is a combination of Lindhard-Scharff straggling and Firsov-Hvelplund expression [Hve-1971]:

$$\Omega^2 = \Omega_{\mathrm{LS}}^2 + \Omega_{\mathrm{A}}^2 \qquad \text{(III.26)}$$

where

$$\Omega_{\mathrm{A}}^2 = N\Delta x 8(Z_1 + Z_2)^{8/3} 10^{-15} \left(\frac{v}{v_0}\right)^2 eV^2cm^2/atom \qquad \text{(III.27)}$$

Chapter IV
Experimental procedures

The aim of this chapter is to describe the physics behind the various ion beam analytical techniques used in this thesis and the limitation of these methods. This will allow an accurate interpretation of the spectra obtained throughout this work. Section 1 describes the general principles of nuclear analytical techniques using MeV ion beams. The principles of RBS and experimental set up are described in section 2. Fundamental of Elastic Recoil Detection Analysis (ERDA) with the experimental procedure is given in section 3. In section 4 particular attentions is given to the combination of Heavy Ion Elastic Recoil detection Analysis (HI-ERDA) with Time of Flight (ToF) that was used throughout this thesis for energy loss determination. Finally, section 5 presents a powerful method for determination of stopping force by using the ERDA-TOF-E dispositive.

We will see throughout this chapter that, the accuracy of each analytical technique is mainly related to the precision with which cross-sections of the involved atomic and nuclear processes are known and the stopping force of the impinging ions in the sample and the out coming signal detected.

IV.1. General Principal of ion beam analysis:

Ion Beam Analysis (IBA) refers to a group of analytical techniques using ions beams. When a beam of particles (Proton,αparticles…) of MeV energy impinges on the sample to be analyzed, different atomic and nuclear processes (elastic and inelastic scattering, nuclear reactions and electromagnetic excitation) take place. In principle, the study of the radiation emitted or retransmitted back though the sample gives information about the sample composition. The interaction of the incident ion with the target atom can be either a collision between incident nucleus and target nucleus, or either an interaction between incident nucleus and the target electron cloud.

In the first case, the collision can be:

i. Elastic collision with scattering of the incident nucleus, this is the basis of the Rutherford Backscattering Spectrometry (RBS) technique.

ii. Elastic collision with fast recoils of the target nucleus, this is the basis of the Elastic Recoil Detection Analysis (ERDA) technique.

iii. When the incident ion beam energy exceeds a certain threshold value, inelastic collisions give rise to the formation of highly excited compound nuclei which is prone to disintegrate. Depending on the mass of the particle and target and the energy of the particle, a variety of final products may form; this is the basis of the Nuclear Reaction Analysis (NRA).NRA Technique is used to check the presence of light elements (Hydrogen, Carbon, Nitrogen, Oxygen, and Boron) in

thin samples. For example the content of hydrogen in a sample can be obtained by bombarding the sample with ^{15}N beam, knowing that at certain resonance energy E_{res} of the incident ^{15}N beam, the nuclei of H and ^{15}N form ^{16}O compound nucleus, which decays immediately to an alpha particle and an excited ^{12}C isotope. This latter nucleus of ^{12}Cin its turn emits a γ-ray with a well-defined energy of 4.43 MeV to reach its ground state $^{1}H(^{15}N,\alpha\gamma)^{12}C$.Particularly, ions of ~MeV energy especially the protons can penetrate the Coulomb repulsion barrier of certain light elements and the short range nuclear interaction come into play which can excite the target nuclei accompanied by a prompt de-excitation, leading toγ-rays emission characteristic of each elements (Proton Induced Gamma-ray Emission: PIGE).

In the second case, one will have excitation of the target atom translated by the displacement of the electrons from the deep electronic layer K or L to the upper electronic layers, followed by reorganization within electronic layers producing X rays (Particle-induced X-ray emission : PIXE).

The phenomena which appear during the collision between incident ion and target atom are sketched in Fig. IV.1. All these techniques need powerful machines capable of accelerating charged particles by means of a high voltage. Appendix A describes the accelerator facilities of iThemba LABS used in this work with brief description of their operational principles.

A thorough description of several IBA techniques and principles of the particle detection can be found in the textbooks of G. F. Knoll [kno-2000]R.Verma [Ver-2007] and T. Stefaan [Ste-2010].

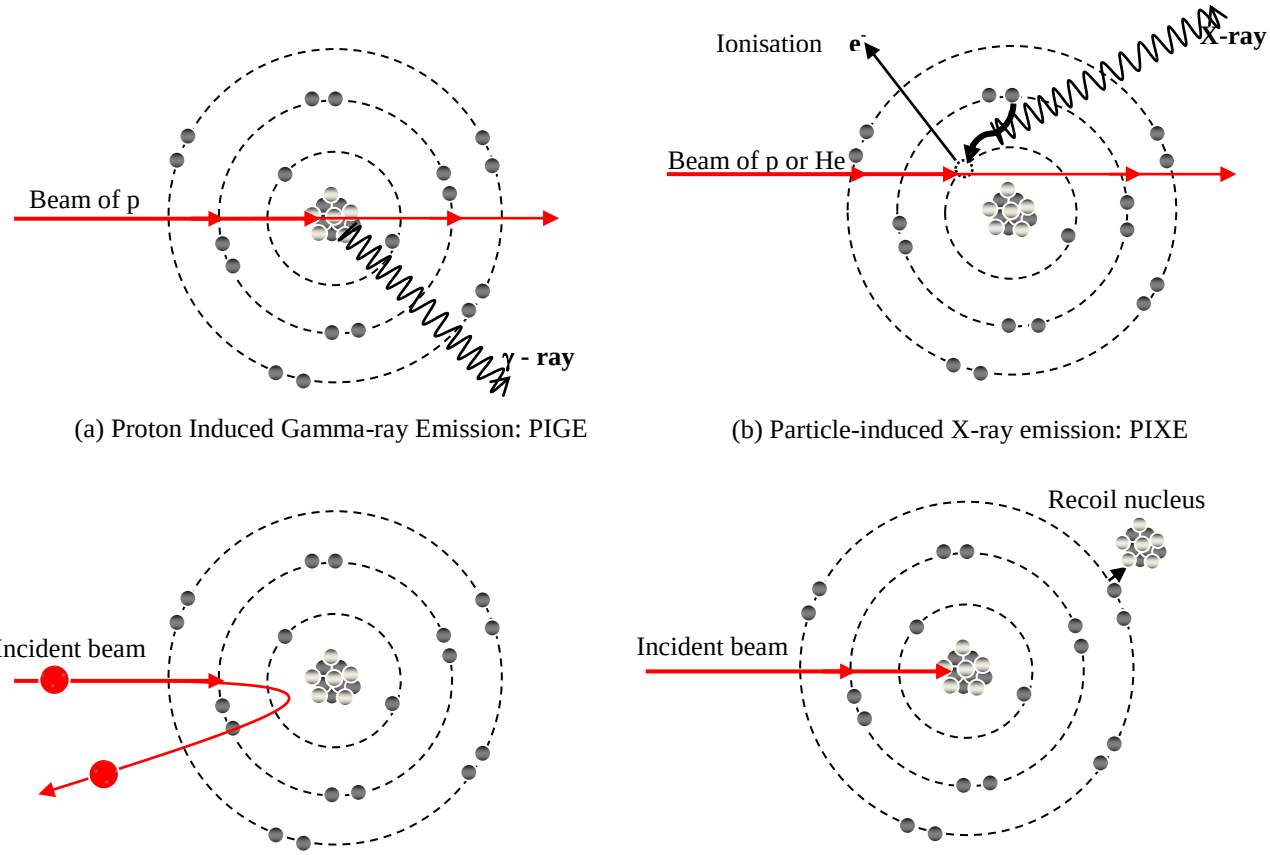

(a) Proton Induced Gamma-ray Emission: PIGE

(b) Particle-induced X-ray emission: PIXE

(c) Rutherford Backscattering spectrometry: RBS

(d) Elastic Recoil Detection Analysis: ERDA

Fig. IV.1: Sketch of physical principles of IBA

IV.2.Rutherford Backscattering Spectroscopy(RBS)

IV.2.1 Introduction

The Rutherford Backscattering Spectrometry (RBS) is a relatively nondestructive nuclear analytical method for elemental depth analysis of thin films, capable of providing a depth resolution of up 5nm for energy detector resolution of the order 10keV. With the RBS technique all the simple elements, excluding hydrogen, can be quantified, and provide also the depth information of elemental concentrations. The potential of RBS reaches up to sub-nanometer depth resolution by replacing the Silicon Surface Barrier Detector (SSBD) or Passivated Implanted Planar Silicon (PIPS) detectors with a focal plane detector spectrometer possessing an energy resolution about 1 keV [Kim-1994].

The origin of RBS dates back to the famous experiment of Rutherford in 1911 [Rut-1911] where the nucleus of an element was first detected and the introduction of scattering probability calculation by Geiger and Marsden in 1913 [Gei-1913].Note that the name RBS implicitly includes all cases of Particle Elastic scattering Spectrometry (PES), Scattering with non-Rutherford cross sections, back and forward scattering.

Figure IV.2 gives a schematic outline of the backscattering spectrometry setup. It primarily involves a collimated mono energetic beam of alpha (He^+)or proton (H^+)particles of energy E_0bombardinga sample surface and a system for registering the number of backscattered particles at different energies. The backscattered particles impinge on the detector volume, where they generate an electrical signal. The detector signal is magnified in the preamplifier and amplifier and processed by a multichannel analyzer. The multichannel analyzer as indicated by his name is constituted of a series of channels of equal increments. Each channel corresponds to a magnitude of the pulse signal. The multichannel analyzer allows the classification of the detected events by their magnitude. An event whose magnitude coincides within a particular channel (i) is recorded as event (count) for this specific channel. At the final stage of the experiment each channel (i) have recorded a certain number H_i of counts by channel, to gather the final output data in the form of a digitized spectrum $H_i = f(i)$.The energy 0.5-3 MeV range of beam $^4He^+$ or H^+ is usually used in the backscattering spectrometry.

The Rutherford Backscattering Spectrometry analytical technique is based on four basic physical concepts of particle-solid interaction. They are:

i. Process of energy transfer in the elastic collision between a charged particle projectile and a target nucleus at rest. The kinematics of this process leads to the concept of the **kinematic factor.**

ii. Probability of occurrence of such a two-body collision which is related to the concept of **scattering cross section**.

iii. The slowing down of swift ions in matter. As the ions projectile penetrates through the target material, they will undergo collisions with the target nuclei and electrons, losing an average energy$\bar{E}$. This Process leads to the concept of the average energy loss of fast ions in a matter by length unit traversed equivalent to the concept of **stopping cross section** (described in chapter II).

iv. The spreading of the energy of the penetrating ion along its path in the matter. It is well known that, the loss of energy of fast ions in matter is naturally accompanied by a statistical fluctuation in the energy loss called straggling phenomenon of energy loss. This process leads to the concept of **energy straggling**.

These four physical concepts allow us to translate the individual signals in the backscattering spectrum to depth distribution of atomic concentrations. In the next sections, we will present in brief the physical treatment of these processes; we give the fundamentals relationships governing these processes and explain how these processes enter into the backscattering experiment.

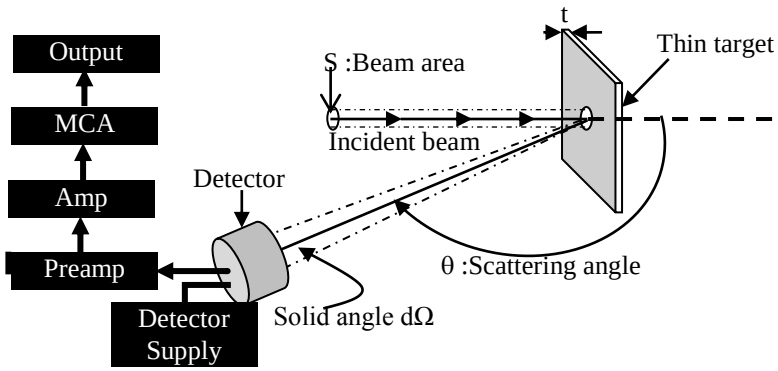

Fig. IV.2: Schematic diagram of the components of the backscattering scattering spectrometry system.

IV.2.2 Basic physical concepts of RBS

IV.2.2.1Kinematic factor

IV.2.2.1.1 Definition of Kinematic factor and mass resolution.

To begin let us consider the scenario where a particle with mass m_1 and kinetic energy $E_0=1/2m_1v_0^2$, where v_0 is its initial velocity, collides with a target particle of mass m_2 at rest (see Fig. IV.3).After collision, both particles movewith velocities $\overrightarrow{v_1}'$and$\overrightarrow{v_2}'$. The energy of the incident particle after collision is noted E_1. The application of the conservation principles of energy and momentum for elastic collision of two masses m_1 and $m_2$yield to the following relation [Nas-1996]:

$$E_1 = KE_0 \qquad \text{(IV.1)}$$

where K is called the kinematic factor of RBS or **scattering kinematic factor** given by:

$$K = \frac{E_1}{E_0} = \frac{\left[\frac{m_1}{m_2}cos\theta + \left(1 - \left(\frac{m_1}{m_2}\right)^2 sin^2\theta\right)^{1/2}\right]^2}{\left(1+\frac{m_1}{m_2}\right)^2} \quad \text{(IV.2)}$$

In the Fig. IV.4 we plot the kinematic factor K in a function of the scattering angle θ for ^{4}He incident particles on different target atoms. From Fig. IV.4 we can conclude that the sensitivity for small differences Δm_2 becomes a maximum for θ= 180°, then the best position of the detector is around 180° hence the term "back-scattering".

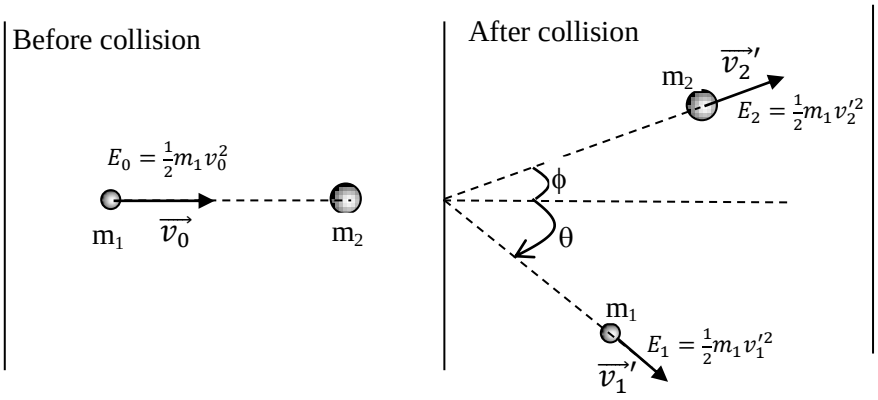

Figure IV.3: Schematic representation of collision of a particle of mass m_1 and velocity $\overrightarrow{v_0}$ with target particle of mass m_2 at rest.

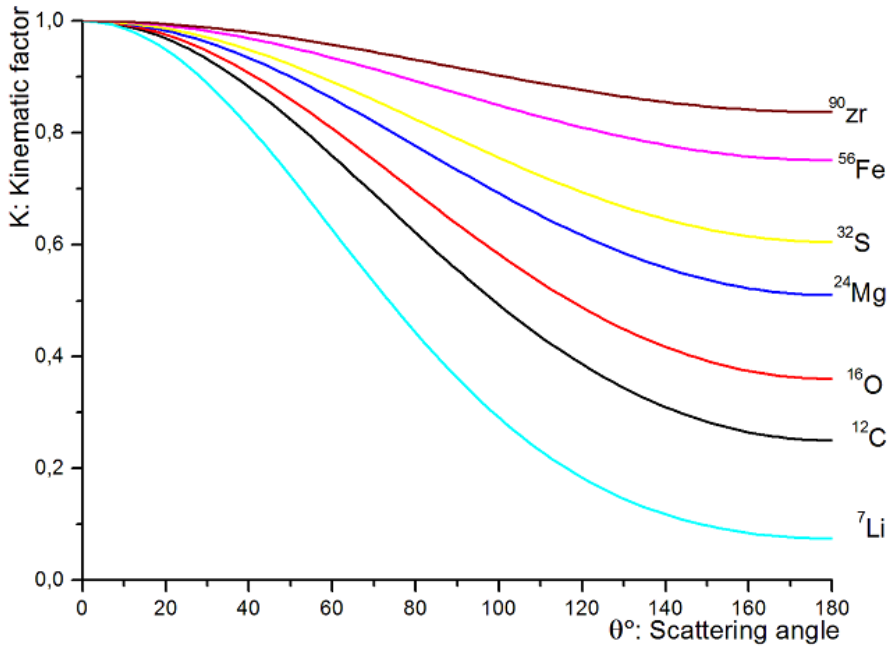

Fig. IV.4: Scattering kinematic factor as function of scattering angle for ^{4}He incident particle in different target atoms.

IV.2.2.1.2 Mass resolution

Suppose for example the target is a very thin layer containing two elements of massesm_2,and $m'_2 > m_2$, the mass resolution of the backscattering spectrometry system signifies the minimum difference between m_2 and m'_2($\Delta m_2 = |m_2 - m'_2|$)which can be separated in the spectra. Because the detection of m_2 and m'_2 is related to the backscattering energies, then, to

separate two masses m_2 and m'_2 their corresponding backscattering energies E_1 and E'_1 must be separable ($\Delta E_1 = |E_1 - E'_1| > Energie\ resolution$). The mass resolution in RBS is described by the following expression:

$$\delta m_2 = \frac{\delta E_1}{E_0}\left[\frac{dK}{dm_2}\right]^{-1} \quad \text{(IV.3.a)}$$

$$\left[\frac{dK}{dm_2}\right]^{-1} = \frac{1}{2}\left[\frac{(m_1+m_2)^2(m_2^2-m_1^2sin^2\theta)^{\frac{1}{2}}}{m_1m_2+m_1^2sin^2\theta-m_1cos\theta(m_2^2-m_1^2sin^2\theta)^{\frac{1}{2}}}\right]\times\left[\frac{m_1+m_2}{(m_2^2-m_1^2sin^2\theta)^{\frac{1}{2}}+m_1cos\theta}\right] \quad \text{(IV.3.b)}$$

FigureIV.5 presents a plot of $\left[\frac{dK}{dm_2}\right]^{-1}$ as a function of the scattering angle θ for He in O. This plot shows clearly that $\left[\frac{dK}{dm_2}\right]^{-1}$ become small for high θ angle which means a good mass resolution following Eq. IV.3.a. Then, for an optimal mass resolution, one chooses the recoil angle close to 180°.

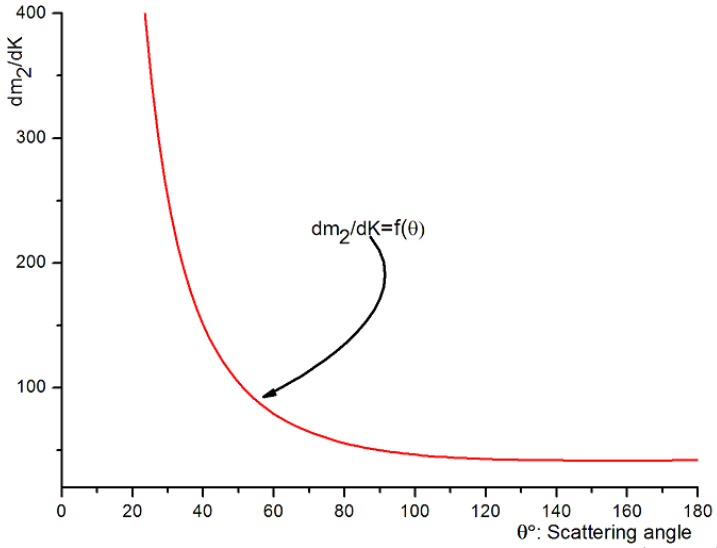

Fig. IV.5: Plot of dm_2/dK in function of scattering angle for ^4He in ^{16}O.

IV.2.2.1.3 Kinematic spread δE_θ

The uncertainty in the angle of scattering Δθ, leads to a spread, δE_θ, in the scattered energy E_1. This change is called the kinematic effect. The kinematic spread $\delta E_\theta \sim dK/d\theta$ is minimal for θ=180°. In conclusion the mass resolution of RBS system is improved if:

- First, the energy resolution of the detection system must be small,
- Second, the beam energy is chosen as high as possible as the short range interaction is negligible to expand the energy spectrum in order to reduce the overlap between the neighboring signal (see Figs. V.3a,b spectra of Si_3N_4 for 2 and 1.75 He MeV),
- Third, select the scattering angle near to 180°, (dm_2/dK is smallest at an angle of θ=180°)
- Fourth, use heavier ions to provide better kinematic separation.

Remark: we will see in the next section that the probability of scattering event occurring in the direction θ(scattering cross section) is smaller for backscattering angle (θ=180°), then the choice of backscattering angle in RBS have the disadvantage that the number of event is very small.

IV.2.2.2Scattering cross section.

IV.2.2.2.1 Definition of the scattering cross section.

The main parameters to be considered in the definition of differential scattering cross section were presented before in Fig. IV.2, with the followings considerations:

- The solid angle dΩ is so small that the scattering angle θis well defined
- The thickness t is so small that the energy loss of the particles in the target is negligible. Then the energy of the bombarding ions is virtually the same at any depth within the target.
- The thickness t is very small and the atoms of the target are randomly distributed in such a way that for every incident ions there is only one collision and the differential cross sections $d\sigma/d\Omega$ of the nuclei do not overlap.

if Q is the total number of particles that have hit the target with N atoms by volume unit and thickness t (Nt is the number of target atoms per unit area: areal density); the number dQ of particles recorded by the detector at the solid angle dΩ (10^{-2}sr or less for typical detection system with a surface barrier detector) is given by:

$$dQ = Q\,N\,t\,\frac{d\sigma}{d\Omega}\,d\Omega \qquad \text{(IV.4)}$$

$$\begin{bmatrix} number\ of\ detected \\ particles\ in\ d\Omega \end{bmatrix} = \begin{bmatrix} total\ number\ of \\ incident\ particles \end{bmatrix} \begin{bmatrix} number\ of\ target \\ atoms\ per\ unit\ area \end{bmatrix} \frac{d\sigma}{d\Omega}\,d\Omega$$

where the proportionality coefficient$\frac{d\sigma}{d\Omega}$ is called the differential scattering cross section.

We will see that that magnitude of $\frac{d\sigma}{d\Omega}$is a very small, then *Q* must be so large that the number of detected events (dQ) is significant.

If S is the surface area of the target bombarded uniformly by the beam, the total cross section of all particles exposed to the beam is S.N.t.dσ/dΩ. Dividing by the surface S exposed to the beam gives the probability (P) that the scattering event will be recorded by the detector.

The probability P that the scattering event will be recorded in the detector is:

$$\mathbf{P = N.t.d\sigma/d\Omega} \qquad \textbf{(IV.5)}$$

Therefore from Eq. IV.4, when we know the total number of incident particles, the number of detected particles in the solid angle dΩ; we can determine the number of atoms per unit area in the target, Nt.

IV.2.2.2.2 Rutherford cross section

The calculation of the differential cross section for elastic collision between two nuclei governed by the Coulomb repulsion force, with the assumption that the closed approach is large compared to the scope of nuclear force (absence of nuclear interaction) and less than the Bohr radius a_0 (the shielding effect of electrons is negligible) is given by the Rutherford formula [**Gol-1950**]:

$$\frac{d\sigma}{d\Omega} = \left(\frac{Z_1 Z_2 e^2}{4E}\right)^2 \frac{4}{sin^4\theta} \frac{\left[\left(1-\left(\frac{m_1}{m_2}sin\theta\right)^2\right)^{1/2}+cos\theta\right]^2}{\left[1-\left(\frac{m_1}{m_2}sin\theta\right)^2\right]^{1/2}} \quad \text{(IV.6)}$$

where Z_1 is the atomic number of the incident ion beam with mass m_l, Z_2 is the atomic number of the target atom with mass m_2, e is the electron charge and E is the energy of the incident projectile.

Remarks:

1. For small scattering angles $\theta \rightarrow 0^\circ$, the cross-sections Eq. IV.6 tend to infinity, which is in contradiction with the definition of finite cross section, but what does it means for small scattering angles?.Small scattering angles correspond to large flyby distances between the projectile and the target nuclei i.e., weak interaction in another word the impact parameter is large, this means that the projectile cross the target atom at distances greater than the radius of the innermost electron-shell of the target atom. At this distance the interaction potential between the projectile and the nuclei is not pure Coulomb's potential, then at small scattering angles the scattering cross section must be deduce from screened Coulomb's interaction.
2. At low energy it appears that the cross section tend to infinity but at over low energy the interaction of the ions with target atom is now screening by electrons then the potential is not Coulombian. In this situation then we must use a scattering cross section derived from a potential which take into account the screening effect.
3. When the ion incident energy is sufficiently high, the distance of closest approach between the incident ion and target nuclei becomes of the order of the dimensions of nuclear sizes, then in this case the short range nuclear forces contribute more to the scattering process, consequently the scattering cross section is deviated from Rutherford scattering cross section.

IV.2.2.2.3 Deviations from Rutherford cross-section

The Rutherford scattering cross section Eq. IV.6 is valid for the unscreened Coulomb'spotential and in the absence of short range interaction (high energy).

When the energy of the projectile is greater than coulomb barrier threshold value the short range interaction become appreciable and the cross section is **non-Rutherford cross section**. For example Huan-Sheng et al. [Hua-1991] shows that for ^{4}He energies greater than 3.0 and 3.5 MeV the backscattering cross-section for sodium and aluminum respectively become higher than the value predicted by the Rutherford cross-section.

When the energy E of the projectile is low i.e. the point of the closest approach is outside the bounds of the inner electron shells of the target atom. For low scattering angle as seen in previews remark the collision with nucleus of heavy atom is screened by the electron clouds of the projectile (ion) and the target atoms, hence the cross sections must be derived from potential which includes electrons screening. In this case the inter-atomic potential is written:

$$V(r) = \frac{Z_1 Z_2 e^2}{r}\phi(r/a) \quad \text{(IV.7)}$$

where$\varphi(r/a)$ is the screening function (Thomas-Fermi or Lenz-Jenssen screening function) and$a$ is the screening parameter given by :

$$a = a_0\left(Z_1^{2/3} + Z_2^{2/3}\right)^{-1/2}, \text{ with } a_0 \text{ Bohr radius} \quad \text{(IV.8)}$$

By introducing the inter-atomic potential (Eq. IV.7) in the scattering equations, the scattering cross-section become the product of Rutherford cross section Eq. IV.6 multiplied by a shielding factor $F(E, \theta)$.For scattering angle between 90° and 180°, L'Ecuyer et al. [Lec-1979] find the following expression for $F(E, \theta)$:

$$F(E,\theta) = 1 - \frac{Z_1 Z_2^{4/3}}{E_{CM}} \quad \text{(IV.9)}$$

where E_{CM} is the center of mass energy: $E_{CM} = \frac{1}{1+m_1/m_2}E$.

IV.2.2.3Energy loss and stopping cross section

We can see from the formula of Rutherford cross section (IV.6), that the scattering at large angle is less probable, and then the ions will have a tendency to penetrate the target. We know from chapter II that, as the ions penetrate the target its kinetic energy decrease, then in an experiment where the target have an appreciable thickness not all target atoms interact with the same incident energy E_0.In the approximation of continuous slowing down of ions in matter, **the stopping force** S(E) at energy E and for a specific target composition is defined as the energy loss by unit of length:

$$\lim_{\Delta x \to 0} \Delta E/\Delta x = S(E) = -\frac{dE}{dx}(E) \quad \text{(IV.10)}$$

In chapter 2, we have also defined the intrinsic parameter, stopping parameter ε as:

$$\varepsilon = \frac{1}{N}\frac{dE}{dx}[eVcm^2] \quad \text{(IV.11)}$$

where N is the target atomic density.

IV.2.2.4 Energy straggling

Implicitly, the measured RBS energy spectra are spread due to various contributions to the uncertainty of the measured spectrum which causes a limitation in the depth resolution. Among these contributions, we have the energy straggling δE_s which describe the statistical fluctuations in the energy loss of an atom moving through a dense medium. The energy straggling was studied in detail in chapter III. The others contributions such as detector resolution, geometrical straggling, and multiple scattering will be discussed in section **IV.**3.2.2 in this chapter. In general the distribution of energy loss was assumed to be Gaussian with the full width at half maximum (FWHM) δE_s. The same assumption is made for the other contributions with the total FWHM δE_O. Then the resolution in energy is limited by the total fluctuation δE:

$$\delta E = \sqrt{\delta E_O^2 + \delta E_s^2} \quad \text{(IV.12)}$$

IV.2.3 RBS spectra

IV.2.3.1RBS spectra of a mono-isotopic sample

In order to illustrate how the four physical concepts allow us to extract quantitative information of elemental depth of the sample, let's consider the simple case of RBS spectra of a mono-isotopic sample**.** The aim of this section is to determine the relation between the particle energy detected E^* and the depth d in the sample from where the particle was backscattered. For this purpose, we take the commonly used considerations:

1- The target material consists of a pure specie (high purity)

2- The beam travel in straight paths (**inward and outward paths**).

3- A continuous slowing down of ions in matter.

An ion beam, of energy E_0 hit a **mono-isotopic sample** at incident angle α between the normal to the sample and the incident beam, as shown in Fig. IV.7. some ions are scattered elastically from the surface with energy KE_0 at an angle βbetween the normal to the sample and the scattered particle. K is the kinematic factor given by Eq. IV.2, where m_1 and m_2 are the ion and thin mono-isotopic sample masses, respectively, and θ given by:

$$\theta = 180 - \alpha - \beta \qquad \text{(IV.13)}$$

The energy KE_0 is the edge of the backscattering spectrum and corresponds to the energy of particles scattered from atoms at the surface of the target. Some ions penetrate into the sample and arriveat the depth d with energy E, after losing some of its energy. At this depth some of the ions scatter at the angle βwith energy KE. These scattered ions again lose energy before exiting the layer with energy E^*. Fig. IV.7 gives the scattering geometry of the case considered and the expected RBS spectra.

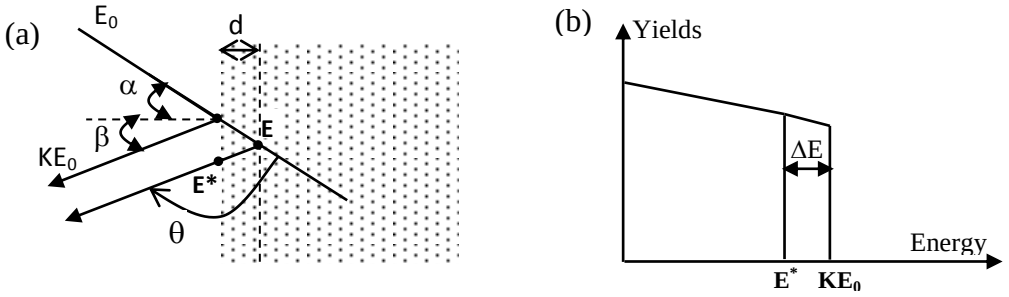

Fig. IV.7: (a) Scattering geometry from mono-isotopic sample.
(b) Expected RBS spectra for mono-isotopic sample.
α: Incident angle, β: exit angle, θ: scattering angle

The relationships between relevant quantities, E_0, E*, E, α andβentering on the scattering experiment are:

Energy loss along the inward path $$\Delta E_{in} = E_0 - E = \int_0^{\frac{d}{cos\alpha}} S(E(x))dx \qquad \text{(IV.14)}$$

Energy loss along the outward path $$\Delta E_{out} = KE - E^* = \int_0^{\frac{d}{cos\beta}} S(E(x))dx \qquad \text{(IV.15)}$$

From Eq.IV.14 and Eq. IV.15, we deduce the width of the backscattering spectrumKE_0-E^*:

$$\Delta E = KE_0 - E^* = K\int_0^{\frac{d}{cos\alpha}} S(E(x))dx + \int_0^{\frac{d}{cos\beta}} S(E(x))dx \quad \text{(IV.16)}$$

E(x) represents the energy of the projectile at depth x below the surface of a thin target into which ions penetrates with initial energy E_0. From Eq. IV.16 we can determine the depth d by an appropriate method if the energy E(x) is known at any depth x. Since the stopping force is generally given as function of energy E not as a function of x, we avoid E(x) in the following manner:

$$S(E) = \frac{dE}{dx} \Rightarrow dx = \frac{dE}{S(E)} \Rightarrow \frac{d}{cos\alpha} = \int_E^{E_0} \frac{dE}{S(E)} = f(E, E_0)\,(a) and \frac{d}{cos\beta} = \int_{E^*}^{KE} \frac{dE}{S(E)} = g(E, E^*)\,(b) \quad \text{(IV.17)}$$

Note that the Eq. IV.16 and Eq. IV.17 are general for any depth d.

A typical dependence of S(E) as a function of the kinetic energy and the deduced depth of penetration x as function of the energy E at the depth d are represented in Fig.IV.8 [Chu-1978].

As E_0 and E^* are known experimentally we can get d from the shaded areas but the only problem is that the energy E before scattering is not known. In the literature, three ways are proposed to overcome the problem of unknown value of E:

1- In the case were the values of $\frac{dE}{dx}$ are tabulated, by numerical integration we can find the correspond energy (E) to a particular depth (d).
2- In the case were $\frac{dE}{dx}$ have a well known analytical expression S(E), by matching the expression of d in function of E_0 and E from Eq. IV.17-a, and the expression of d in function of E and E^* from Eq. IV.17-b,we deduce E.
3- Make the approximation that $\frac{dE}{dx}$ is constant over each path (inward and outward). With this approximation Eq. IV.17 can be integrated and E eliminated (this approximation is valid for small d or considering a small layer within the target).

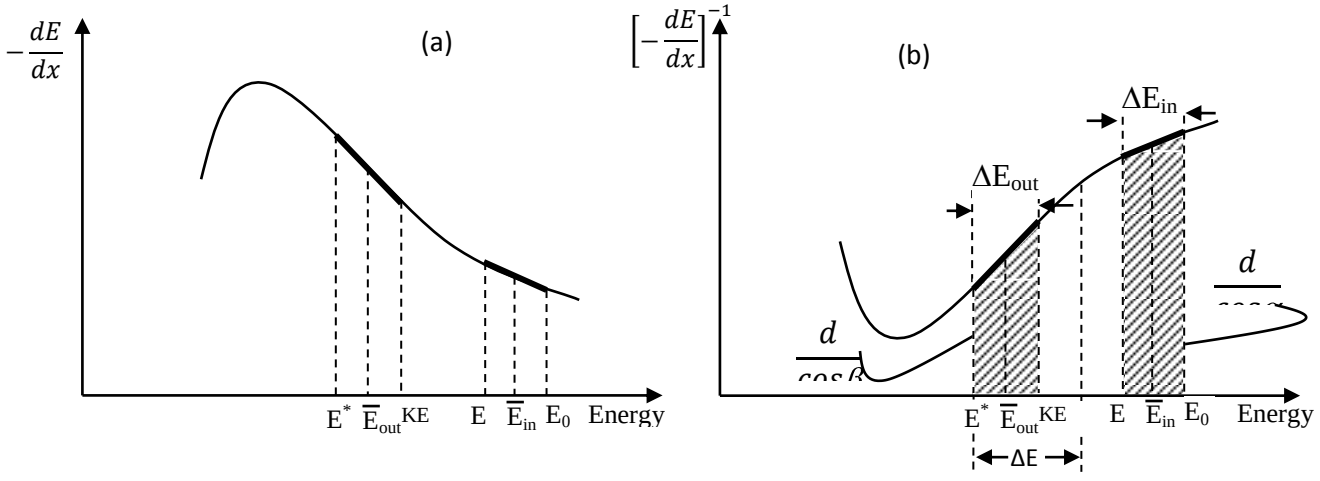

Figure IV.8: (a) Typical behavior of the stopping force dE/dx as a function of incident energy. (b) Deduced behavior of $[dE/dx]^{-1}$ as function of energy. Source [Chu-1978]

IV.2.3.2 Approximation of $\frac{dE}{dx}$ constant over each path (inward and outward path).

First of all, the assumption that the stopping power is constant over each path is valid only for extremely small depth d from the surface of the sample or within a small layer in the sample.

In this case the integrals in Eqs. IV.17 is reduced to:

$$\frac{d}{cos\alpha} = \frac{1}{S(E)|_{in}}(E_0 - E) \text{ (a)} \qquad \text{and} \qquad \frac{d}{cos\beta} = \frac{1}{S(E)|_{out}}(KE - E^*) \text{ (b)} \tag{IV.18}$$

By eliminating E from these last equations, we obtain

$$KE_0 - E^* = \left[\frac{K}{cos\alpha}S(E)|_{in} + \frac{1}{cos\beta}S(E)|_{out}\right]d \tag{IV.19}$$

We adopt the following notation:

$$\Delta E = KE_0 - E^* = [S]d \tag{IV.20-a}$$

where,
$$[S] = \left[\frac{K}{cos\alpha}S(E)|_{in} + \frac{1}{cos\beta}S(E)|_{out}\right] \tag{IV.20-b}$$

[S]is called the **energy loss factor**. By using the stopping cross sections:

$$\Delta E = KE_0 - E^* = [\varepsilon]Nd \tag{IV.21-a}$$

$$[\varepsilon] = \left[\frac{K}{cos\alpha}\varepsilon_{in} + \frac{1}{cos\beta}\varepsilon_{out}\right] \tag{IV.21-b}$$

$[\varepsilon]$ is called the **stopping cross section factor**.

$S(E)|_{in}$ and $S(E)|_{out}$ are determined by using surface energy approximation or mean energy approximation [Chu-1978].

IV.2.3.2.1 Surface Energy approximation

For small depth d the relative change along the incident path is small then we evaluate $S(E)|_{in}$ at E_0 and similarly by back projection argument $S(E)|_{out}$ is evaluate at KE_0. In this so called surface approximation the energy loss factor and the stopping cross section factor can be written:

$$[S_0] = \left[\frac{K_A}{cos\alpha}S(E)|_{E_0} + \frac{1}{cos\beta}S(E)|_{KE_0}\right] \tag{IV.22-a}$$

$$[\varepsilon_0] = \left[\frac{K_A}{cos\alpha}\varepsilon_{E_0} + \frac{1}{cos\beta}\varepsilon_{KE_0}\right] \tag{IV.22-b}$$

IV.2.3.2.2Mean Energy approximation

A better approximation is to choose the constant value of $\frac{dE}{dx}$ or ε at an intermediate energy $\bar{E}$of each track.

$$\left[\overline{S}\right] = \left[\frac{K}{cos\alpha}S(E)|_{\overline{E_{in}}} + \frac{1}{cos\beta}S(E)|_{\overline{E_{out}}}\right] \tag{IV.23-a}$$

$$[\overline{\varepsilon}] = \left[\frac{K}{cos\alpha}\varepsilon_{\overline{E_{in}}} + \frac{1}{cos\beta}\varepsilon_{\overline{E_{out}}}\right] \tag{IV.23-b}$$

$$\text{where } \overline{E_{in}} = \frac{1}{2}(E_0 + E) \text{ and } \overline{E_{out}} = \frac{1}{2}(KE + E^*) \tag{IV.23-c}$$

The value of E is unknown but it can be estimated using various methods. A priori we can accept as an approximation that the energy loss is **subdivided symmetrically** between inward and outward path [Chu-1978] (this is a good approximation especially when α≅β), then,

$$\overline{E_{in}} = E_0 - \frac{\Delta E}{4} \text{ (a)} \qquad \overline{E_{out}} = E^* + \frac{\Delta E}{4} \text{ (b)} \tag{IV.24}$$

Some methods to find the energy E before scattering are presented in appendix B.

IV.2.3.3 Height of energy spectrum for elemental sample.

In this sub-section we will present the relation between the height of the energy spectrum (ordinate of the energy spectrum) and the number of scattering centers per unit area of the target at the depth where backscattering occurs.

Our image of understanding of the spectra (see Fig.IV.9) is as follow: Each energy width $\delta = {}_iE^* - {}_{i-1}E^*$(same for all channel and is given by the detection system) at the position ${}_iE^*$of channel i in the multichannel analyzer represents the backscattered ions emanating from the slab i of thickness τ_I at the depth x_i. In another manner for any channel i of width δ (same width for all channel, I think this is defined by the multichannel analyzer) there exist a slab i of width τ_i.

From the definition of cross section (Eq. IV.4), the total number of particles detected in channel i is:

$$H_i = \sigma({}_iE)\Omega Q N \frac{\tau_i}{\cos\alpha} \qquad \text{(IV.25)}$$

Ω : solid angle subtended by the detector

σ(${}_i$E) is the differential cross section evaluated at the energy ${}_i$E of the projectile immediately before scattering at depth x_i averaged over the finite solid angle Ω.

Q: the total number of incident particles on the sample

N: the atomic density of the sample element at depth x_i.

Note: $N\tau_i$gives the number of the target atoms per unit of area perpendicular to the beam at normal incidence. The number of atoms per unit area as seen by the beam is therefore increased by 1/cosα for a general case.

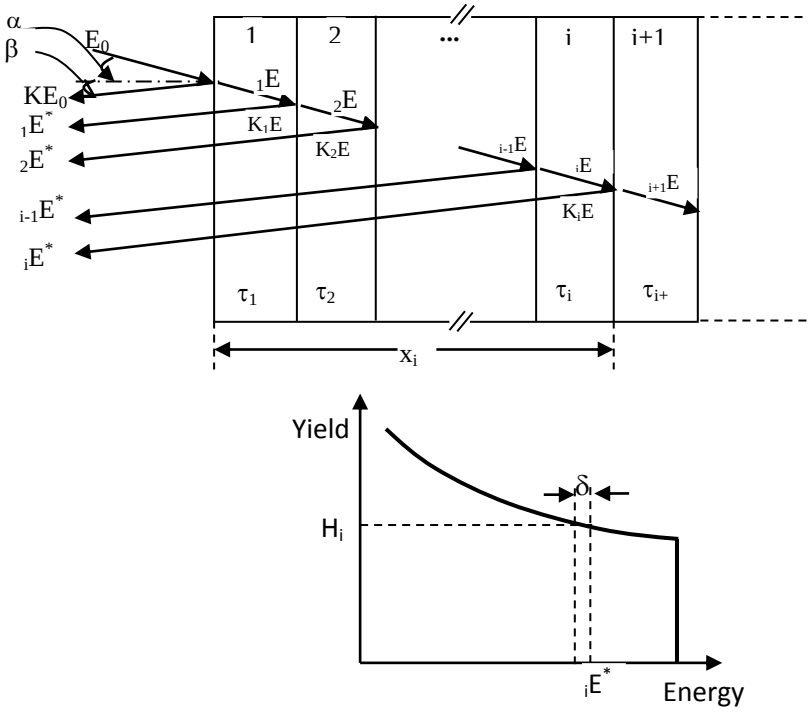

Fig. IV.9: Schema of channel i at the energy ${}_iE^*$ and its corresponding slab i at depth x_i from where the backscattering signal was emanate, for mono-isotopic sample. The width δ of every channel is the same however the width of slabs (τ_i) are not necessary equal.

IV.2.3.4Spectrum Height for scattering from the top surface layer

For thick sample the backscattering events at the surface or near the surface region where the energy before scattering can be taken as E_0(total number of particle detected in channel corresponding to E_0), can be written:

$$H_0 = \sigma(E_0)\Omega Q N \frac{\tau_0}{\cos\alpha} \qquad \text{(IV.26)}$$

The events H_0 are coming (scattering) from atoms within thickness $\tau_0$which is deduced from the energy width δ of a channel. Particles scattered from atoms within τ_0 will have energies (on the detector) between KE_0 and KE_0-δ. (see Fig. IV.10).

From Eq. IV.21-a

$$\Delta E = KE_0 - (KE_0 - \delta) = \delta = [\varepsilon_0]N\tau_0$$

Then, from Eq. IV.25:

$$H_0 = \sigma(E_0)\Omega Q \frac{\delta}{[\varepsilon_0]\cos\alpha} \qquad \text{Very important} \qquad \text{(IV.27)}$$

From Eq. IV.27 the height of the energy spectrum at the surface is proportional to σ, Ω, Q, and δ which is a natural evidence, and also proportionality to $[[\varepsilon_0]\cos\theta_1]^{-1}$.

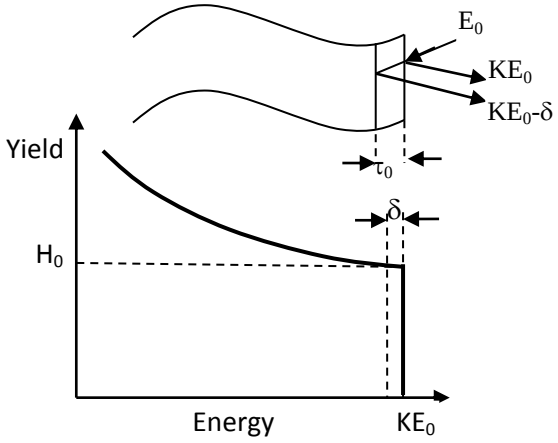

Fig.IV.10: Schema of expected RBS spectra at the surface region of a sample consisting of a mono-isotopic

IV.2.4 RBS set up at iThemba LABS

The layout of the 5.5 MV VDG accelerator at the Material Research Department, iThemba LABS, Cape Town is presented in section 4 of appendix A.

The RBS end station is located at about 5.0 m from the switching magnet and was designed and commissioned at the Material Research Department (MRD) in 1977. The RBS end station consists of:

- A main cylindrical chamber of ~50 cm diameter and ~50 cm height, with circular apertures windows to put the detectors.
- Goniometer for loading many samples into chamber and analyzing them sequentially,
- Vacuum system composed of conventional rotary pump (for primary vacuum) and turbo molecular pump to achieving high vacuum, up to 10^{-6}torr placed beneath the main chamber.

- A camera serves to display the position of the target via the goniometer.

A schematic diagram of scattering chamber and vacuum system is given in Fig. IV.11.

A standard target holder where we can mount eight samples is screwed to the goniometer that allows the sample to be positioned in the beam. The position of the samples with respect to the beam axis can be made manually or from a computer stepping motor. The silicon surface barrier (SBD) detector is placed in the apertures windows of the chamber at an angle $\theta=+165^{\circ}$ with respect to the incident He^{+} ion beam direction for detection of backscattered ions. The signal from the detector is then electronically processed and the data collected and recorded by the Maximum Integration Data Acquisition System (MIDAS).

Using the theory presented in sections 2.2 and 2.3, a program like SIMNRA or RUMP convert spectra into atomic density.

The results of the data analysis are presented in the chapter IV.

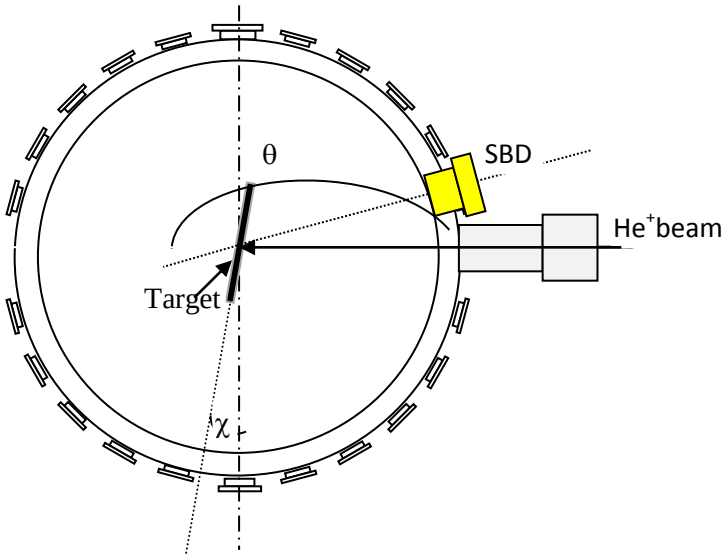

Fig. IV.11: Schematic of scattering chamber showing : Surface barrier detector, target,ion beam path from accelerator, scattering angle θ and tilting angle χ.

IV.3. Elastic recoil detection analysis (ERDA)

IV.3.1 Introduction

Elastic recoil detection analysis (ERDA) is similar to the standard RBS technique its basic physical principles are the same as RBS [Chu-1978]**.** In RBS the object of detection are the projectiles while in case of ERDA the object of detection are the ejected atoms from the target by energetic heavy ion beam. The recorded energy spectra of the recoiled atoms can be related to their concentration profiles; explicitly the yield of the recoil atoms of a certain element is proportional to the elemental number of atoms per unit area in the target. The experimental set-up of ERDA is

identical to the RBS set-up, the only difference is that the detector to detect recoiled particles is located forwards relatively to the beam direction (see Fig. IV.12).

In 1976L'Eculer et al. [Lec-1976]was the first using successfully the ERDA technique to detect the recoiled elements containing in the sample by using 25-40 MeV ^{35}Cl ion beam. RBS has a low sensitivity to light elements because the cross section is proportional to Z_2^2, where Z_2 is the atomic number of the target atom, in addition at low energy we have a high background produced from scattered projectiles coming from deeper in the sample from heavy atoms matrix. While ERDA is sensitive to light element in heavy atoms matrix, it becomes widely used for the detection of light elements (Z<10). RBS and ERDA are complimentary. In general ERDA use heavy ions beam like Cu, Ag, Au and Kr. The use of α particles in ERDA is restricted to the detection of hydrogen.In the literature, when the incident ion is much heavier than the recoil atoms we speak about Heavy Ion Elastic Recoil Detection Analysis (HI-ERDA).In this section we present a short introduction of the ERDA technique for determination of quantitative elemental depth profiling. An excellent review of various elastic recoil detection techniques was published by Tirira et al.[Tir-1996],we can also find a detailed description of ERDA technique in the chapter 5 of reference [Dol-2009].

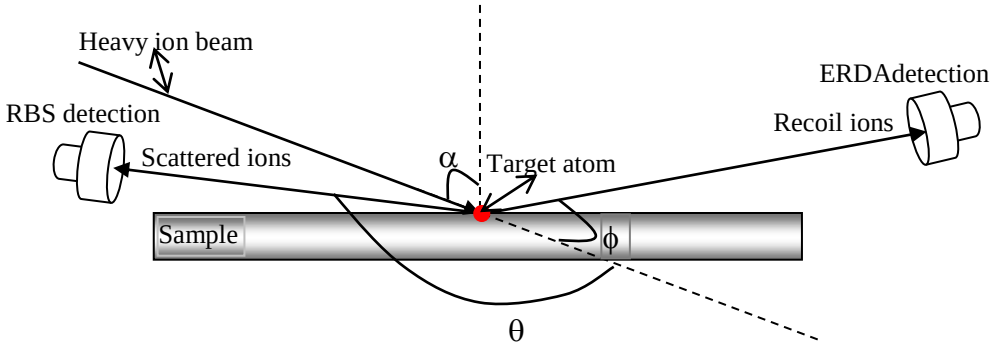

Figure IV.12: Geometry principal of ERDA and RBS

IV.3.2 Kinematic factor of ERD

The geometry and the notations of the recoiling experiment is given in Fig. IV.12. From the laws of conservation of energy and momentum, we can write the recoiled energy E_2 in function of the incident energy E_0 as follow:

$$E_2 = K'E_0 = 4E_0 \frac{m_1 m_2}{(m_1+m_2)^2} cos^2\phi \qquad \text{(IV.28)}$$

The parameter K' is called the kinematic factor of ERD or the recoil kinematic factor.

Fig. IV.13shows the recoil kinematic factor (K') as function of m_1/m_2 for fixed recoil angle. It shows that K' increases sharply with m_1/m_2up to a maximum value equal to $\cos^2\phi$ where the projectile and the target have the same mass. K' decreases gradually when the projectile becomes heavier than target.

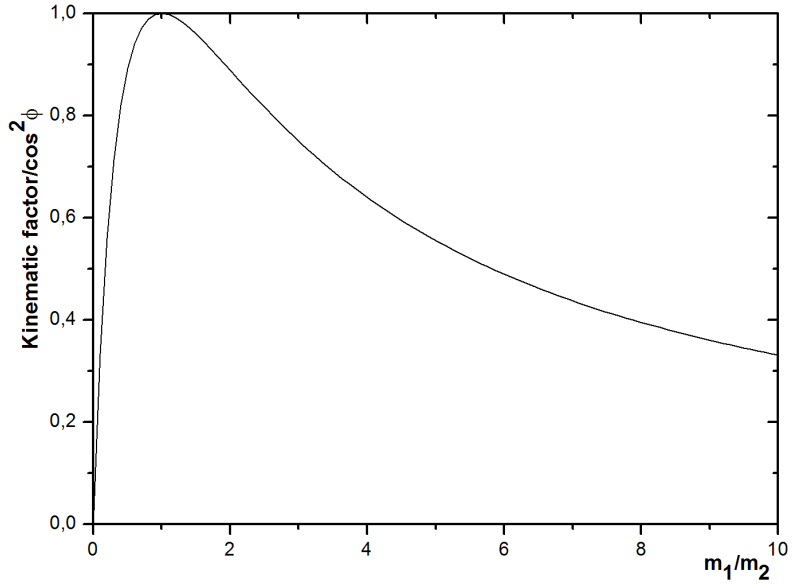

Fig.IV.13 : Recoil kinematic factor as function of m_1/m_2

Note that when the projectile is heavier than the target atom ($m_1>m_2$), the incident particle can't be scattered at angle $\theta>\theta_{Max}$, where

$$\theta_{Max} = arcsin\left(\frac{m_1}{m_2}\right) \quad \text{(IV.29)}$$

IV.3.2.1- Mass resolution

In the similar way to RBS (see section 2), the mass resolution in ERDA is the capability to separate two signals arising from two recoiladjacent mass elements (constituent of the target) in the recoiled energy spectrum. If two elemental masses containing in the sample differ by a quantity δm_2, their corresponding differences recoil energies is expressed by

$$\delta E_2 = \delta K' E_0 = 4E_0 \frac{m_1(m_1-m_2)}{(m_1+m_2)^3} cos^2\phi \delta m_2 = F(E_0, m_1, m_2, \phi)\delta m_2 \quad \text{(IV.30)}$$

If δE_2 is the energy resolution of the ERD system, then the mass resolution is defined usually by:

$$M_R = \frac{\delta E_2}{\delta m_2} = F(E_0, m_1, m_2, \phi) \quad \text{(IV.31)}$$

A best mass resolution is realized when **F takes high value**. According **Eq. IV.30**, when the value of the angle **ϕ decreases or** the incident energy increases the mass resolution becomes better.

To see what incident particle mass m_1 gives the best mass resolution, we study M_R versus m_1, which shows the optimum mass resolution is achieved when:

$$m_1 = 3.73 m_2 \quad \text{(IV.32)}$$

IV.3.2.2. Energy resolution

According to Eq. IV.28 each element containing at the target surface is recoiled at specific energy. Then in principle, the different elements recoiled from the sample could be identified in the experimental ERD spectra, this is true if system energy resolution is perfect. In practice multiple factors contribute to the uncertainty or spreading of the measured energy spectrum. It was accepted as a first approximation that these factors are independent (uncorrelated) and their distribution

contribution is Gaussian, then we adds quadratically these contributions to obtain the total energy spread as the full width at half maximum:

$$\delta E_t = \sqrt{(\delta E_0)^2 + (\delta E_d)^2 + \left(\delta E_g\right)^2 + (\delta E_s)^2 + (\delta E_{ms})^2}$$

where

δE_0: is the spread of incident beam

δE_d: is the energy resolution of the Si surface Barrier Detector

δE_g: is the geometrical straggling (or broadening) due to the finite beam spot size d on the target and the finite detector acceptance (detector aperture w).

δE_s: is the energy straggling in the target for both inward and outward path of particles

δE_{ms}: is the spreading due to the multiple-scattering for both inward and outward path of particles

In the following we discuss these limitation factors briefly.

IV.3.2.2.1 Spread of incident beam δE_0

The spread of incident beam δE_0 which depend to the type and performance of the accelerator used. For example for the 6 MV Tandem at iThemba LABS Cauteng theδE_0 amounts is about 0.2%of the beam energy.

IV.3.2.2.2 The energy resolution of the detection systemδE_d

In general the resolution of the detection system depends on the type of detector used and the range of energy detected. For the commonly used solid state surface barrier detector the energy resolution is about 10-15 keV proton or He, but the energy resolution become high for heavy ions for example for 20 MeV ^{16}O the energy resolution is about 130 keV [Mis-1995].

IV.3.2.2.3 Geometrical energy spread

The geometry of the ERDA is given in the Fig. IV.14.The incident angle α is considered to be fixed.

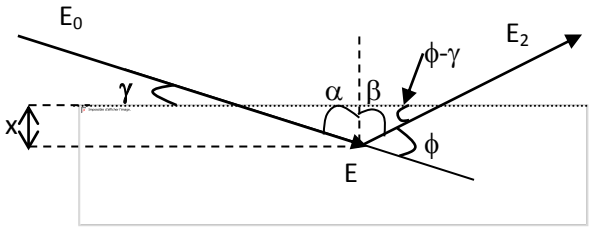

Fig.IV.14: Geometry of the experiment: Incident angle α, exit angleβand recoil angle ϕ. $\alpha + \beta + \phi = 180°$

Considering the stopping power constant in inward and outward directions, the recoil energy E_2 from the depth x is given:

$$E_2(x) = K'E_0 - S_1K'\frac{x}{sin\gamma} - S_2\frac{x}{\sin(\phi-\gamma)} \qquad \text{(IV.33-a)}$$

where$S_1$is the stopping force of the incident particles, and S_2 is the stopping force of the recoil particles.

The finite size of the incident beam and the finite size of the detector aperture lead to a distribution of recoils anglesϕ with uncertainty $\Delta\phi_g$, this means that the recoiled particles from the depth x reached the detector after traversing different path lengths in the material and therefore a spread of the recoiled energy called the geometrical energy spread or the geometrical straggling.*

The geometrical energy spread is given by [Nas-2014]:

$$\delta E_g(x) = \left[2K'E_0 tan\phi - \left[\frac{2K'S_1 tan\phi}{sin\gamma} + \frac{S_2 \cot(\phi-\gamma)}{sin(\phi-\gamma)}\right] x\right] \Delta\phi_g \qquad \text{(IV.33-b)}$$

The spread of the recoil angle γ is given by **[May-1997]**:

$$\Delta\phi_g = \frac{1}{L_D}\sqrt{w^2 + \frac{d^2 \sin^2(\phi-\gamma)}{sin^2\gamma}} \qquad \text{(IV.33-c)}$$

where L_D is the distance between the sample and the detector, w is the detector entrance width and d is the incident beam diameter.

IV.3.2.2.4. Multiple scattering

Until now we have considering that the trajectories of the incoming and outgoing particles are straight lines but in the physical reality when the particles penetrate in a matter, they undergo many small angle deflections (often referred as multiple scattering) and large angle deflections (often referred to as plural scattering) due to successive scattering with target atoms. This gives rise to spread $\Delta\phi_{scat}$ (multiple or plural), which is transformed into an energy spread via variation of Eq. IV.33-a. The probability that the small angle scattering event occur is large however the probability that the larger scattering angles event occur is small [Nas-2014].We interest to the multiple scattering.

Paszti et al. [Pas-1991]show an approximate expression of the full widths at half maximum of angular distributions from small-angle scattering of the incoming projectiles, $\Delta\phi_{in}$, and of the outgoing recoil ions, $\Delta\phi_{out}$, as follow:

$$\Delta\phi_{in} = 0.5\frac{2Z_1\widetilde{Z_2}}{4\pi\varepsilon_0 E_0}\frac{e^2}{a}\left[\pi a^2\left(\frac{1}{sin\gamma}\frac{x\rho(x)A_v}{A_2(x)}\right)\right]^{0.62} \qquad \text{(IV.34-a)}$$

$$\Delta\phi_{out} = 0.5\frac{2Z_{2i}\widetilde{Z_2}}{4\pi\varepsilon_0 E_{2i}}\frac{e^2}{a}\left[\pi a^2\left(\frac{1}{\sin(\phi-\gamma)}\frac{x\rho(x)A_v}{A_2(x)}\right)\right]^{0.62} \qquad \text{(IV.34-b)}$$

where $\widetilde{Z_2} = \sum_i n_i Z_{2i}$ represents the average value of the atomic numbers in sample, $a = \frac{0.885a_0}{\left(Z_1^{2/3}+\widetilde{Z_2}^{2/3}\right)^{1/2}}$ is the screening radius for the potential interaction, a_0 =0.529x10^{-10}m is the Bohr radius, Z_{2i} is the atomic number of the recoiled target atom of type i, Z_1 is the atomic number of the projectile, ρ(x) is the density of the layer at depth x (g/cm^3), $A_v$is Avogadro's number (A_v=6.629x10^{23}) and A_2(x) is the average atomic mass (g/mol).

IV.3.3 Recoil cross section

The Rutherford recoil cross section at a recoil angle ϕ [Dol-2009] is given by:

$$\left(\frac{d\sigma}{d\Omega}\right)_{Recoil} = \left(\frac{Z_1 Z_2 e^2}{2E_0}\right)^2 \left(1+\frac{m_1}{m_2}\right)^2 \frac{1}{cos^3\phi} \qquad \text{(IV.35)}$$

where E_0 is given in MeV, e^2=1.4398x10^{-13}MeV.cm, and dσ/dΩ in cm^2.

In the case of m_1>>$m_2$the recoil cross section is almost independent of Z_2 and m_2, in other words the cross section is fairly the same for all elements present in the sample which have m_1>>m_2.The comparison between the scattering cross section Eq. IV.6 and recoil cross section Eq. IV.35 leads that, they have the same dependence $1/E_0^2$.

Omitting all spreading phenomenon of the energy and considering very thin foil in the sense that the slowing down of the projectile is negligible, the yield Y_{m2} of recoils specific element m_2 measured by the detector is described by the following formula:

$$Y_{m_2} = NxQ\,\langle\left(\frac{d\sigma}{d\Omega}\right)_{Recoil}\rangle\,\Delta\Omega \qquad \text{(IV.36)}$$

where Q is the number of incident projectiles, ΔΩ is the solid angle of the detector, Nx is the number of the target atoms of element m_2 per unit area and $\langle\left(\frac{d\sigma}{d\Omega}\right)_{Recoil}\rangle$ is the differential cross-section given by Eq. IV.35 averaged over the surface of the detector.

3.4 Depth profile and recoil-scatter particle ambiguity

In general the energy corresponding to the peaks in ERDA spectra give the main elements present at and underneath the surface of the sample following Eq. IV.28, whereas the measured yield at certain energy gives the concentration of specific elements at certain depth (Eq. IV.36).

In ideal case where the energy loss of projectile and recoils ions in sample are negligible and the total energy resolution is perfect, the recording energy events of recoiled (eventually also the scattered ions) by ERDA technique are separate according to Eq. IV.1 and Eq. IV.28. This leads to the identification of all sample constituents. However in the real situation where the energy loss is not negligible and the limitation of the resolution system, ions of different elements coming from various depths can produce the same signal in the energy detector which gives rise to peaks overlap in the measured spectra. This is a serious difficulty of ambiguity of identification of all elements in the sample. In the remainder of this chapter we consider the case m_1>>$m_2$used in our work. One needs a second independent signal to separate the elemental information coming from the depth. In the following we will briefly discuss various methods that were used to solve the recoil-scatter particle ambiguity problem in ERDA.

i- Stopper foil

Due to the fact that heavier particles lose more energy per unit distance than lighter particles in a matter, even if the former have more or less kinetic energy than the latter, the separation between projectiles and recoils is easily achieved by placing a specific stopper foil in front of the

detector. This method referred to as conventional ERDA has the disadvantage of degradation of energy resolution due to the straggling via the foil and the inability to identify the various recoils elements when peaks overlap. Due to their thickness uniformity and durability,μm range foils of Mylar ($C_{10}H_8O_4$), Kapton ($C_{22}H_{10}N_2O_5$) and Aluminum are used in conventional ERDA experiment.

ii - ΔE-E telescope

This method consist of firstly of the measurement of the energy loss of a recoiled ion via foil of well-known thickness composing the ΔE detector and secondly the residual energy E of the ion by an energy detector placed directly behind the ΔE detector. The events corresponding to ΔE and E are recorded in coincidence by an electronic detection system. Adding the energy loss and the residual energy gives the total energy of the detected ions. The plot of the energy loss ΔE as a function of the total energy allows the identification of the elements of the recoil ion [Wan-2009], taking advantage of the knowledge of the stopping force S(E,m,Z).

iii-Time-of-Flight for EDRA

Another way to avoid this complication is to measure simultaneously of the time of flight and the energy of the recoiled ion; this method is called Time-of-Flight ERDA (ToF-ERDA). The mass m of recoiled/scattered ion is determined as follow:

1. The measurement of the time of flight t for a given distance of flight ℓ gives the velocity v of the particle (v=ℓ /t).
2. The measurement of its energy with silicon detector gives the energy E of the particle, then the mass of the recoil particle is determined by

$$m = \frac{2E}{v^2} = 2E\left(\frac{t}{\ell}\right)^2 \qquad \text{(IV.37)}$$

iv-Magnetic spectrometer

When recoiled ions with energy E, mass m and charge state q pass through a magnetic field $\vec{B}$, they will be deflected to a different radial position with radius r depends on m, q and E, according to the following relation:

$$r = \frac{\sqrt{2mE}}{q\|\vec{B}\|} \qquad \text{(IV.38)}$$

Experimentally a silicon detector is placed at different positions to measure the energies E of the recoiled particles corresponding to different q/m ratios.

In the case of ERDA, the recoiled atoms from the sample are identified by the detection system placed in the forward direction of the beam, the direction is chosen in the basis of:

1- Choice of the desired recoiled energies ($0<\phi<90°$)

2- Avoid the detection of the scattered ion used as projectile (in case of projectile heavier than the target atom) by chosen the recoil angle to be larger than θ_{Max},

3- Minimize as possible the spreading in recoiled energy due to the kinematic effect ($\phi<45°$).

4- Largest cross section i.e. ϕ near to 90°.

For all these conditions, generally the ERDA experiments are performed at recoil angles ϕ between 20° and 40°.

IV.4. Time detector

IV.4.1 Introduction

The time detector is built mainly by a carbon thin foil. When an ion crosses a carbon thin foil a small discharge of secondary electrons (electrical pulse) is emitted from the foil. These electrons are guided by an applied electric field between the carbon foil and a grid structure to the Micro-Channel Plates (MCP) multiplier. Electrons reaching the active area of the MCP are multiplied several times by the micro channels of the MCP and collected by the MCP anode to give a timing output signal. The carbon foil is used in various types of time-of-flight (TOF) mass spectrometers to produce start or stop pulses.

The emission of the electrons from the carbon thin foil occurs in both directions forward and backward. Allegrini et al[All-2003] show that the forward yield of emitted electrons depends strongly on the energy ion however the backward yield changes smoothly with ion energy (see Fig.IV.15). Thus, due to the wide energy range of the recoil/scatter ions which can worsen the quality of time resolution, it is preferable to use the backward electrons for timing detection.

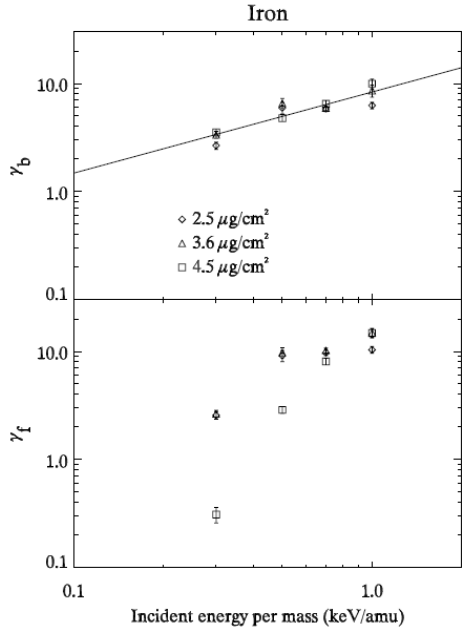

Fig. IV.15: Measured backward and forward yields of emitted electrons from carbon foil bombarded by iron for different energies. Source [All-2003]

The time detector carbon foil used in our work are produced by ACF® metals, have thickness of 9μg/cm^2 with density 2.01 g/cm^3 and size 25mmx70mm mounted on a steel frame with 96mm^2 rectangular apertures situated at the entrance of the detector. The foils are composed of the natural isotopic carbon with very small quantity of impurities such as^{1}H (2-5%). Figure IV.16shows the photo of the two timing detectors used in this work [Msi-2010].

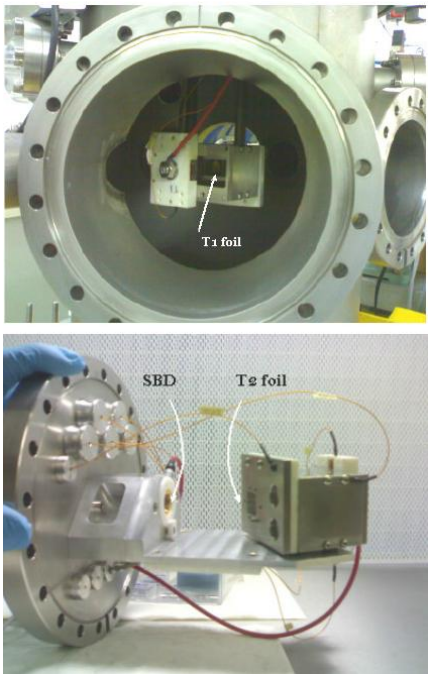

Figure IV.16: Photos of the two timing detectors; T1 inside the target chamber (top), and T2 on a flange mounted at the end of the flight tube (bottom). Source [Msi-2010]

IV.4.2 Multi-Channel Plate (MCP) multiplier

The micro-channel plate (MCP) is a compact electron multiplier of high gain incorporating 10^4-10^7 parallel channels of diameter about 10 μm made of glass (see Fig. IV.17). Channels axes are normal or tilted (~5-15°) to the MCP input surface. This angle of tilting is called channel bias angle. When an electron impinges in the inner of a channel it creates secondary electrons, throughout its path that in turn it creates more electrons. The MCP is intrinsically a very fast detector; the pulse transit time is of order ~0.1ns.

The assembly of two MCPs in Chevron configuration (V geometry) improves the gain. It is called "high gain Chevron configuration" [Wiz-1979] (see Fig IV.18).

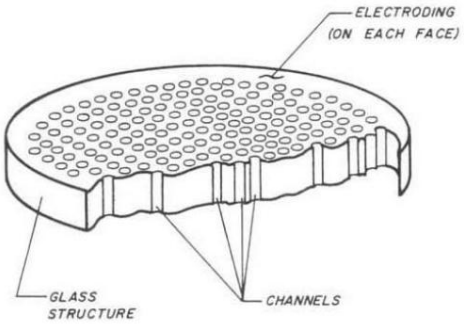

Fig. IV.17: The MCP structure [Wiz-1979]

IV.4.3. Electrons trajectory in the electric mirror time detector

Busch et al [Bus-1980] introduced a common configuration of time detector that employs electric field and electrostatic mirrors (see Fig. IV.18).This time detector contains three flatbed Grid sets

at specific homogeneous equipotential V_1, V_2 and V_3. The conception of a grid made of tungsten wires is in such manner that is transparent (~97%) to ions.

The path taken by the emitted electron in this type of time detector is explained in the Fig. IV.18. When the ion beam collide the carbon thin foil of the time detector the primary electrons knocked out backward are accelerate in the direction opposite to the electric field $\overrightarrow{E_a}$ between the carbon foil and the acceleration grid with the acceleration a_{ac} given by Eq. IV.39, travel to the electrostatic mirror where another electric field $\overrightarrow{E_m}$act to change their direction and are accelerate with the acceleration a_m given by Eq. IV.40 to the front of the MCP where they are multiplied and produce a large amplitude Start/Stop pulse at the anode (<1ns).

$$a_{ac} = \frac{e}{m_e}\frac{V_1 - V_2}{x_a} \qquad \text{(IV.39)}$$

Where e, m_e charge and mass of electron respectively, V_1 the potential of the carbon thin foil, V_2 the potential of accelerating grid, x_a the distance between grid accelerating and thin carbon foil.

$$a_m = \frac{e}{m_e}\frac{V_3 - V_4}{x_m} \qquad \text{(IV.40)}$$

where V_3-V_4 the potential difference between the two grids wall of the mirror and x_m is the distance between the two grids wall.

Note that the initial velocity of the electron is negligible relatively to the speed acquired by the acceleration a_{ac}.

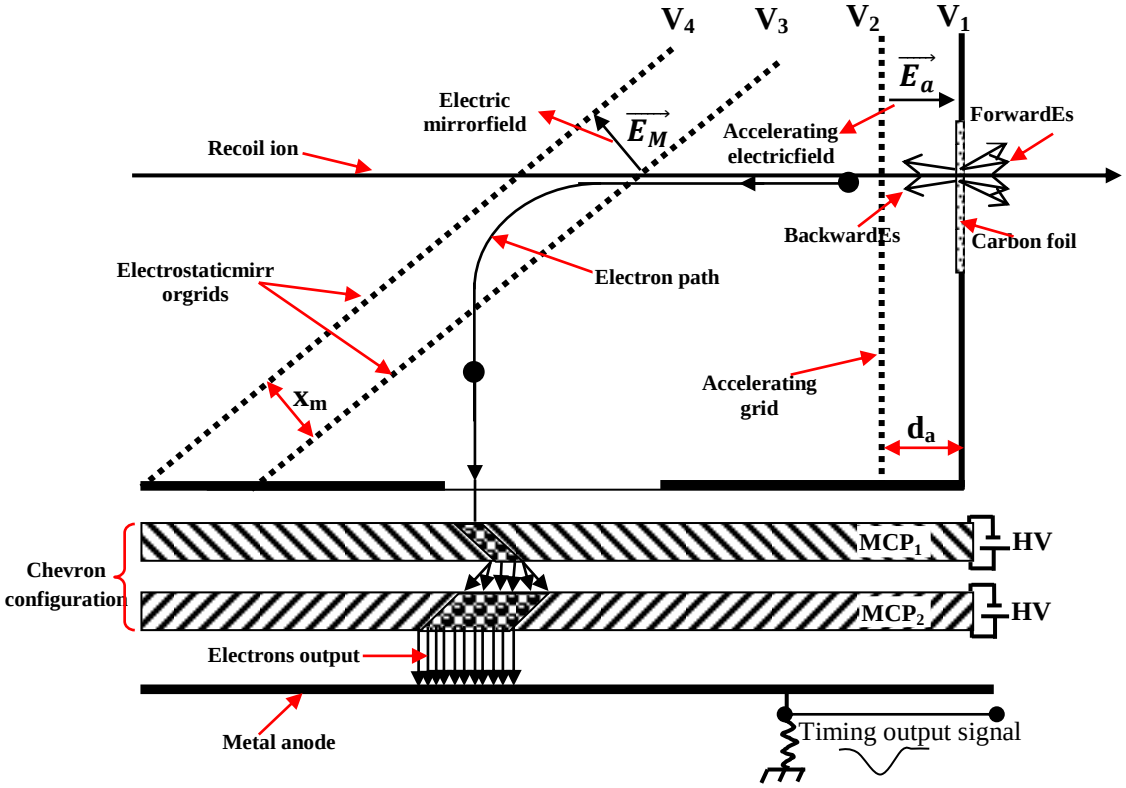

Fig. IV.18: Principle of the path taken by the emitted electrons in the time detector

IV.5. Time of Flight-Energy telescope (ToF-E)

IV.5.1 Introduction

We have pointed out in section3.4 of this chapter that ions of different elements coming from various depths can produce the same signal in the energy detector which complicate analyze of the energy spectra. One solution to overcome this ambiguity is the introduction of the ToF telescope in ERDA. To deduce the mass of heavy ions, with have a precise and known energy value, by measuring the time that these ions across a certain distance in vacuum, Hammer in 1911[Ham-1911] built the first ToF spectrometer. The ToF spectrometer reported was not commonly used at that time because of their poor time resolution until 1950 [Hak-1999]. The use of time of flight spectrometry for particle identification in nuclear physics (MeV energy range) required sub-nanosecond time resolution. The development of a suitable ToF detector was a big challenge. In 1970 Butler et al. [But-1970] built a detector with a time resolution of about 100ps. To identify the complex nuclei produced by nuclear reactions with heavy ions, Gelbke et al. **[Gel-1971]**constructed aToF spectrometer for heavy ions that consisted of an XP 1021 photomultiplier and a thin foil scintillator made of NE 102A . A time resolution of the order of 0.5 ns was been obtained.

The advantage of the ToF-E telescope is to distinguish single recoiling ions via simultaneous measurement of their flight time through a fixed distance and of their kinetic energy.

IV.5.2 Time of Flight resolution

Naturally the ToF measurement will be subject to certain uncertainties ΔT due first to the noise related to the dispersion of the secondary electrons in the MCP (electronic multiplication process) and to the cable length differences and electronic differences in the experimental set up, second to the energy straggling of incident ion in carbon thin foils. The first effect is intrinsic to the time detectors and to the experimental set up independently to the characteristic of the incident ion; the second effect is closely related to the type and energy of incident particle. Since these two effects are independent, we can write:

$$\Delta T = \sqrt{(\Delta T_n)^2 + (\Delta T_s)^2} \qquad \text{(IV.41)}$$

where ΔT_n and ΔT_s are the time of flight uncertainties due to the noise and straggling respectively.

The study makes by Gloeckler et al. [Glu-1979]of the timing uncertainty for different species of ions as a function of incident energy shows as expected that as the straggling becomes significant ΔT becomes important and an estimate value of ΔT_n~0.4 ns is founded in their experiment.

IV.6. Energy detector

The energy detector used in the ToF telescope is Si surface barrier detector (SBD). The SBD is located in the back flange of the second time detector. It was found by El Bouanani et al. [Bou-

1994] that the nonlinear response of the Si detector for Cu and heavier recoils in the energy range of 2-40MeV.

His energy resolution for 241Am 5.486 MeV α-particle is 15 keV Full width at half maximum. Studying the response of the SBD detector, Hinrichsen et al. [Hin-1990] found that, when the mass increases the resolution tends to deteriorate. In the recent study of resolution of the F series ORTEC SSB detector, which is specified as detector for heavy ion detection, Siketicet al. [Sik-2012] shows, ΔE=33-28 kev for E=2-5MeV ^{7}Li (lithium), ΔE=60-95 kev for E=2-10MeV ^{16}O (oxygen), ΔE=130-190 kev for E=2-14MeV ^{28}Si (silicon), ΔE=240-270 kev for E=4-14 MeV ^{35}Cl (chlorine).

IV.7. ERDA technique with Time of Flight-Energy telescope

The identification of particles (scatters or recoils) can be achieved by determining both the energy and ToF for each particles. This can be achieved by measuring the time interval that needs an ion to pass two very thin carbon foils, separated by some distance L=0.5-1m, followed by measuring their energy by using a semiconductor detector placed close to the second time detector.

The ERDA technique with heavy ions where simultaneously the Time of Flight (ToF) and recoiled energy E are measured in coincidence was developed in 1983 by two independent groups Thomas et al. [Tho-1983]from "Institut de Physique Nucléaire de Université Claude Bernard, Lyon I" and Groleau et al. [Gro-1983] from "University of Montreal". ToF-ERDA becomes a very powerful IBA method for quantitative elemental depth profiling.

At the end of 2009 a combined HI-ERDA and ToF spectrometer method was been developed and assembled for depth profiling analysis at iThemba Labs, Faure, Cape Town at line K1 of the 200MeV separated sector cyclotron (SSC) and now is operational at 30° beam line of the 6MV Tandem accelerator at iThemba LABS, Gauteng **[Msi-2010].**The ToF-E spectrometer consists of a Time of Flight detector, built from two timing detectors, T1 and T2, separate by a distance of flight L=0.600 m and a silicon surface barrier detector (SBD) positioned at about 6.5 cm behind the second time detector for energy measurement (see Fig. IV.19).The first detector T_1 is located inside the target chamber, close to the target at distance about 0.12m. A circular collimator of diameter 10 mm is inserted halfway between the second time detector and the SB detector limits the solid angle of the detector telescope to less than 0.15msr.In this experimental set up both the scattered projectiles and recoils particles are simultaneously detected.

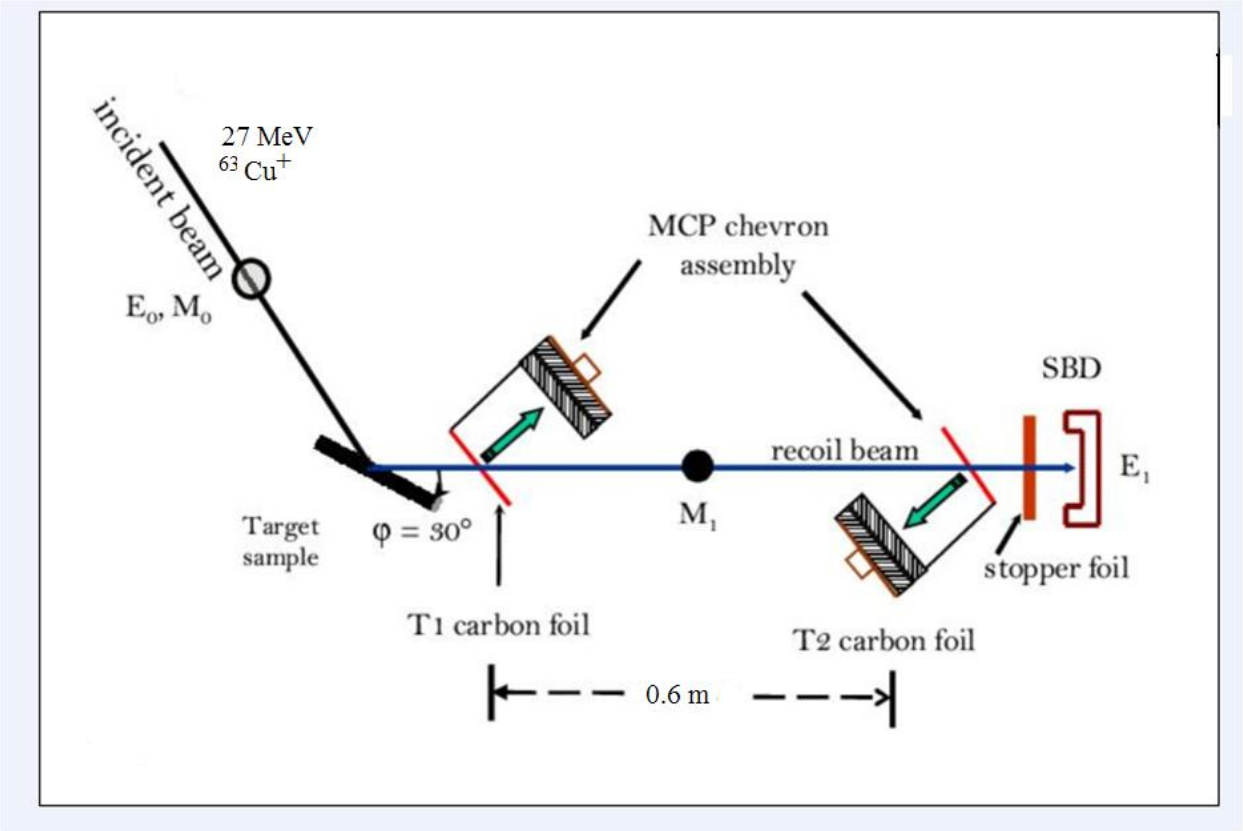

Fig. IV.19: Schematic setup of ERDA-ToF-E spectrometry

As discussed in sub section **3.2.2.3**, due to the detector's finite angular acceptance range and beam spot size the recoils/scatters particles reach the detectors with different angles ϕ in the scatter plan. This will lead to recoil kinematic energy spread and thus to a difference in the time of flight of recoils particles with same energy, due to the differences in flight path lengths. The last effect is called kinematic ToF spread. ϕ

Tilting time of flight detectors at an angle ϕ_t equal to recoil angle ϕ induces a first order kinematic correction, in fact at this detectors tilting, ions with same energy recoils cross the same distance between the two timing detectors[Dol-2009](see Fig. IV.20).

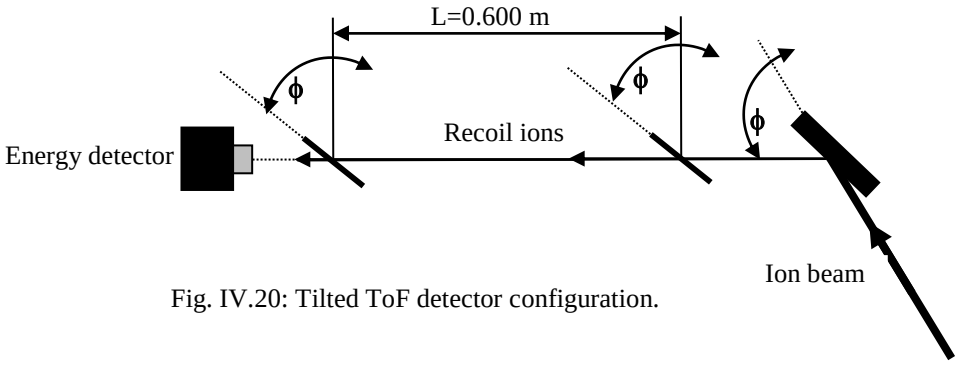

Fig. IV.20: Tilted ToF detector configuration.

The fundamental equation of ToF-E detector is given by

$$E = \frac{1}{2} m \left(\frac{L}{T}\right)^2 \qquad \text{(IV.42)}$$

where E is the recoil energy, m is the mass of ion, L is the flight distance, and T time of flight. Eq. IV.42 indicates that the measure of the kinetic energy of recoil/scatter ion as well as its time of flight allows us the identification of the ion via its mass m. According Eq. IV.42 the relative mass resolution of flight spectrometer is given by:

$$\frac{\Delta m}{m} = \sqrt{\left(\frac{\Delta E}{E}\right)^2 + \left(2\frac{\Delta T}{T}\right)^2 + \left(\frac{\Delta L}{L}\right)^2} \qquad \text{(IV.43)}$$

where ΔE, ΔT and ΔL are uncertainties in energy, time of flight and flight distance respectively.

The uncertainty ΔE is measured by the energy resolution of the Silicon Surface barrier Detector (SBD) which depends on the recoil's energy and mass as mentioned in section 6.When an ion with specific energy arrives to the carbon thin foil will be subject to the straggling phenomenon which gives rise to the uncertainty ΔT. The uncertainty ΔT is determined by the response of the time detectors, which is about 1 ns for the energy range and ions studied in this work. It is evident that the choice of larger L leads to a smaller relative uncertainty ΔT/T. $\frac{\Delta \ell}{\ell}$ is assumed to be negligible by choosing ℓ relatively high.

V.1. Determination of the thin foil thickness

For precise stopping force and energy straggling measurements, a precise knowledge of the foils thickness and their uniformity are required. The thickness verification and stoichiometry of thin foils were determined by analysis of their Rutherford backscattering spectroscopy (RBS) spectra, while the study of their surface roughness was achieved using Atomic Force Microscope (AFM).

V.1.1. RBS energy calibration

The energy calibration of the Si Surface Barrier Detector (SBD) was performed by fitting the energy edge of the channel energy spectrum of backscattered 2 MeV He^+ on a target with a Boltzmann sigmoidal model. The edge fitting gave the channel number corresponding to the energy of scatter He^+ from the surface by each atom present in the sample. The expression of the Boltzmann sigmoidal function is given by [Ori-2007]:

$$y = \frac{A_1 - A_2}{1 + e^{(x-x_0)/dx}} + A_2$$

where x_0 is the center, dx is the width, A_1 is the initial y value, and A_2 is the final y value. The y value at x_0 is half way between the two limiting values A_2 and A_2, y (x_0) = (A1+ A2) /2.

For channel-energy calibration we did use sequentially ^{78}Pt/Si, ^{46}Pd/Si, ^{22}Ti/Si and ^{14}Si thin foil as standard samples. As an example we present in figure V.1 the RBS spectra of Platinum target foil deposited on silicon and in figure V.2 the energy edge of the energy spectrum with its corresponding Boltzmann sigmoidal fit. Table 5.1 below summarizes the results of fitting for the four standard samples analyzed. The calibration equation was obtained by polynomial fitting.

$$E(keV) = Ax^2(Ch) + Bx(Ch) + C \quad \text{(V.1a)}$$

$$A = -6{,}51.10^{-4} \pm 1{,}20.10^{-4} \quad B = 2{,}88 \pm 0{,}15 \quad C = -269{,}32 \pm 45{,}30 \quad \text{(V.1b)}$$

Element	x_0[Channel]	Δx_0[Channel]	$E=KE_0$[keV]
Platinum : ^{78}Pt	927.50	0.05	1844.97
Palladium: ^{46}Pd	861.30	0.05	1724.93
Titanium : ^{22}Ti	710.17	0.12	1438.59
Silicon: ^{14}Si	553.90	0.13	1135.05
Nitrogen : ^{7}N	338.97	0.20	629.11

Table V.1: Backscattering energies at the surface with their corresponding channel for ^{78}Pt/Si, ^{46}Pd/Si, ^{22}Ti/Si and ^{14}Si thin foil.

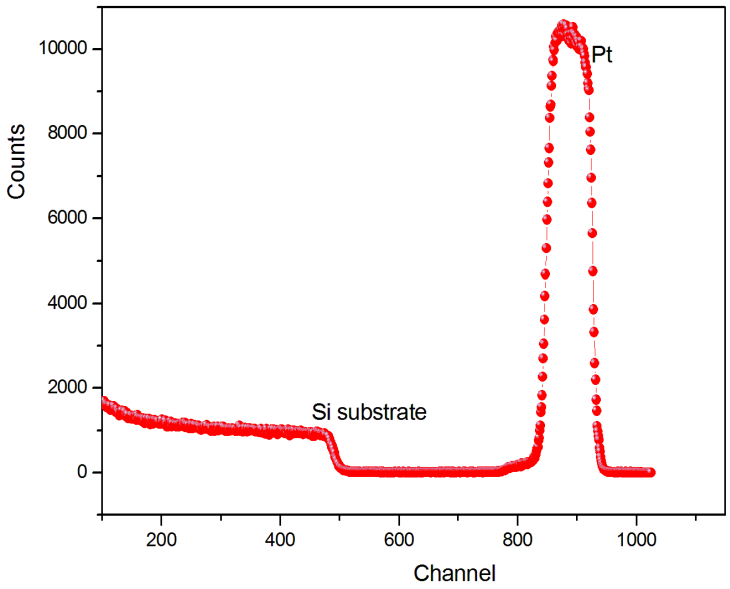

Fig. V.1: RBS spectra of the Pt/Si sample measured by 2 MeV He^{+} collected at a backscatter angle of 165°.

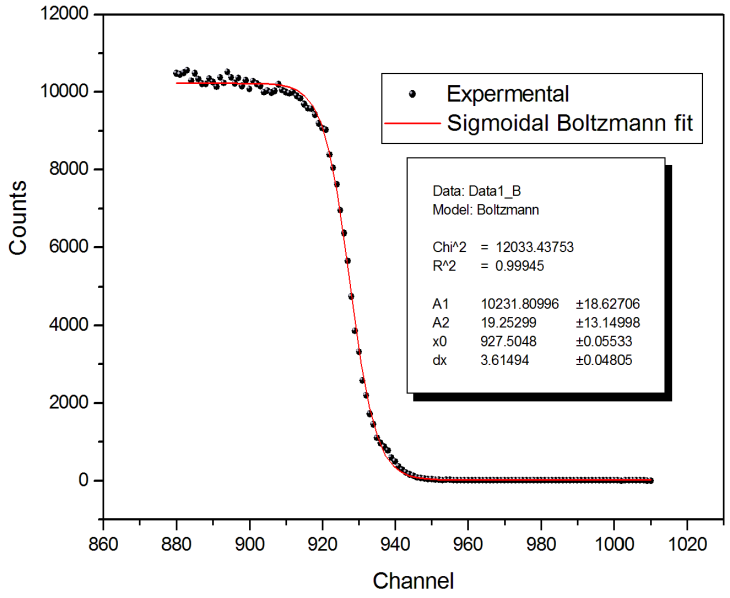

Fig. V.2: Boltzmann Sigmoïdal fitting of the edge spectra for $^{78}Pt/Si$

V.1.2. Thickness of the Silicon Nitrite (Si_3N_4) thin foil

Silicon nitride has good physical and chemical properties which allow it to be used in various applications. For example, because of its high mechanical resistance silicon nitride is used as chamber window in nuclear physics experiment [Van-1998]. Silicon nitride thin foil is also widely used in microelectronic devices [Mil-1971a, Mil-1971b].

The silicon nitride, Si_3N_4, foil used in our work was manufactured from ‘‘Silson Limited®”. The following characteristic of the Si_3N_4 foil was given by the manufacturer:

Thickness 500 nm, the uncertainties of the thickness was given 7-10%, the stoichiometry of the foil was ~0.75 Si/N.

In general the density of the manufactured thin foil is estimated from the bulk density (~3.1 g/cm^3) which can be relatively different from the real density value [Hus-2016].

From analysis of RBS spectra of Si_3N_4, using the SIMNRA code **[May-1997],** we found practically no deviation from the nominal stoichiometry with the following atomic ratios: Si (0.44) N (0.56) and thicknesses: 4650×10^{15}at.cm^{-2}(see Fig. V.3).

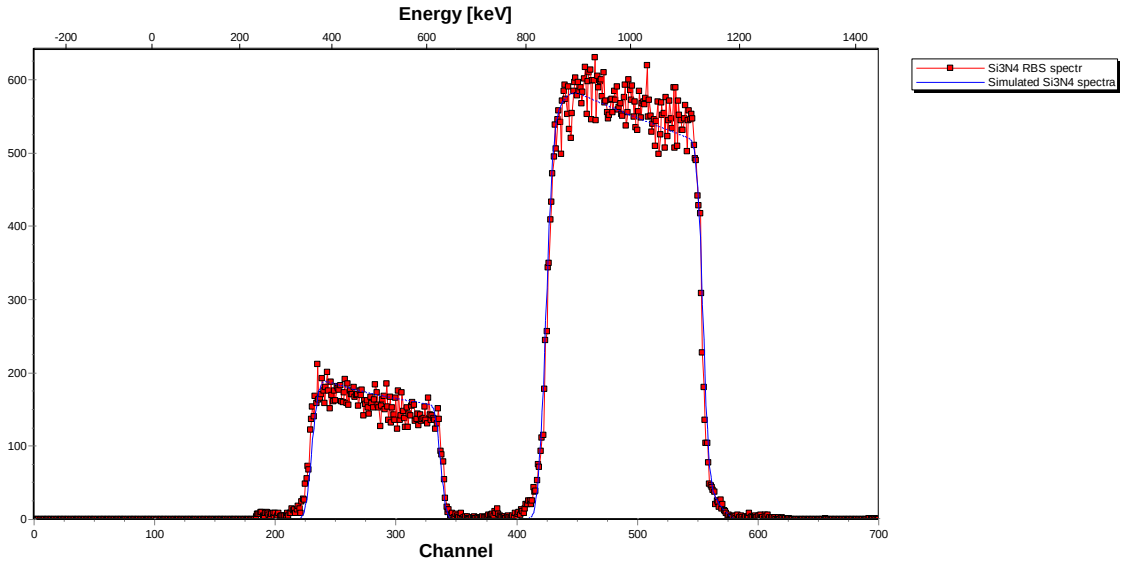

Fig. V.3a: RBS spectrum of the Si_3N_4 measured by 2 MeV He^+ collected at a backscatter angle of 165°. A fit using SIMNRA calculation is included.

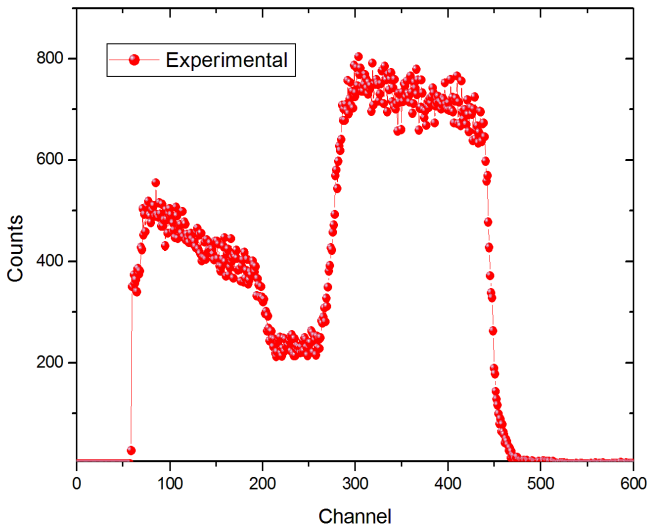

Fig. V.3b: RBS spectrum of the Si_3N_4measured by 1.75 MeV He^+ collected at a backscatter angle of 165°.

A typical AFM image (performed with the VECCO AFM at the MRD, iThemba LABS, Faure) in 3D of the Si_3N_4 from one scan area of 25μm^2 is shown in Fig. V.4.

The mean surface roughness of the scanned area was estimate to be σ=1.0 nm.

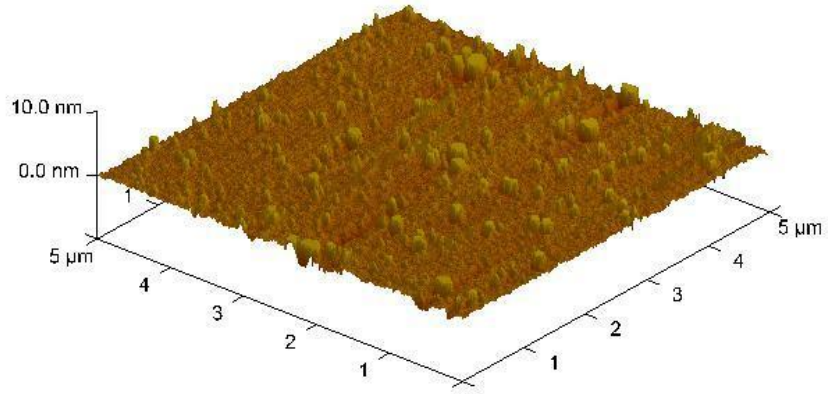

Fig. 2 Fig. V.4: AFM image of the surface of the silicon nitrate foil.

V.1.3. Thickness of the Formvar thin foil

The Formvar$C_5H_8O_2$ (poly vinyl Formal) foil with density 1.23g/cm^3 had a thickness x=0.4 μm which was determined by using the energy loss of 5.485 MeV alpha particles from an ^{241}Am radioactive source, passing through the Formvar foil [Amm-2006]. The surface roughness was analyzed within AFM treatment. The mean surface roughness (δ) value of the foil was estimated to be about ~10nm.Then the thickness uncertainty is Δx=20 nm.

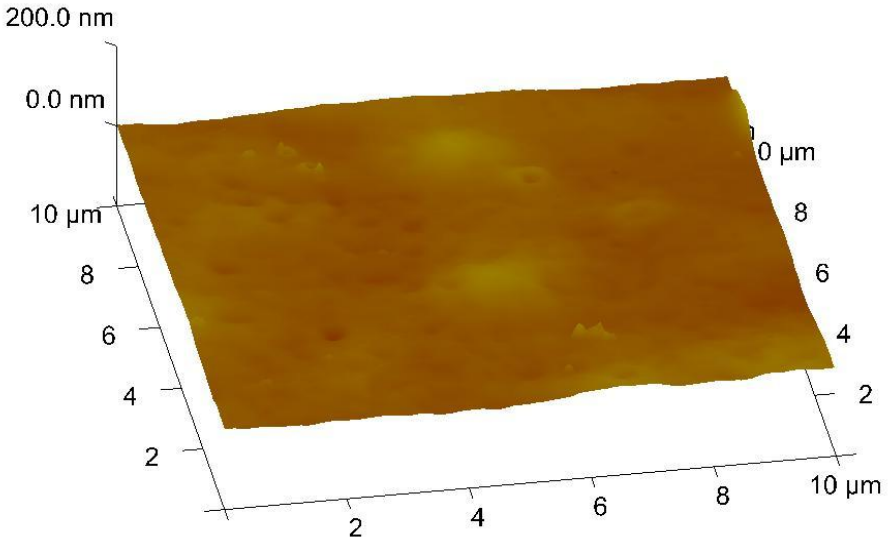

Fig. V.4: AFM image of the surface of the Formvar foil.

V.2- TOF-E Telescope Testing

This section presents testing results of the ToF-E telescope commissioned at iThemba LABS Gauteng. The whole TOF-E telescope diagram is shown in Fig. IV.5.

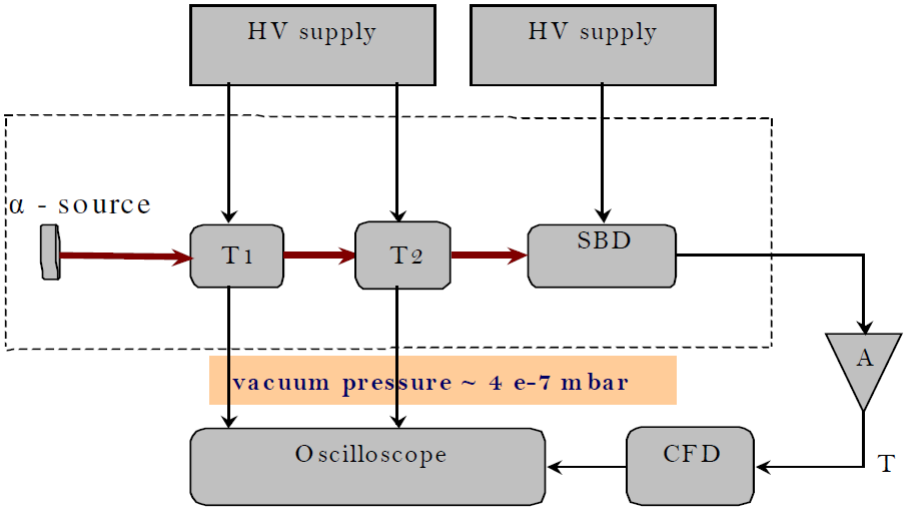

Figure V.5: Diagram of the ToF-E telescope set up for testing the MCPs in vacuum using radioactive sources. The SBD trigger signal is first amplified before being fed into a CFD to give out a fast timing output signal. Source [Man-2010]

The ToF-E telescope consists mainly of time start and stop detectors and an energy detector arranged in the start-to-stop geometry (start-to-stop arrangement) i.e. the time start signal was provided by the time detector (T1) while the time stop by the time detector(T2) triggered by the surface barrier detector (SBD).The pre-amplified (A) output signal (T) coming from the SBD goes into a constant fraction discriminator (CFD) which is an electronic signal processing device marking the arrival time of this same signal by a negative signal. The SBD plays two roles; first, it records the energy signal, and second it set the triggering coincidence between the two timing detectors and the recorded signal by the SBD. The fact of taking the SBD as timing trigger was based on the assumption that the detection efficiency is virtually 100% and the noise level is insignificant [Kno-2000]. The electronic line was designed for the direct time of flight measurement. During measurements, the pressure in the target chamber was in the order of 10^{-7} mbar.

The ToF-E telescope modules were first tested with the ^{252}Cf radioactive source.^{252}Cf is a fission foil source, and is an ideal candidate to be used for the ToF-E telescope testing because the fission products give the light and heavy groups. The light group has about 30% more energy than the heavy group. This energy difference is sufficient to easily separate the groups in the spectra. Another advantage to use this source was the wide energy range of the fission fragments 75-140 MeV [Van-1994]. Note that alpha particles of 6.12 MeV and 6.08 MeV are also emitted in the spontaneous fission of^{252}Cf.The energy range between 0.5MeV/amu and 1.5 MeV/amu emitted by

^{252}Cf is within the energies range of recoil ions in typical ToF-ERDA experiments [Man-2010, Gia-2008, Kim-1998]. The time needed to get a significant spectrum for ^{252}Cf was more than 24 hours due to the low source activity.

The measurement of time of flight and energy in coincidence (ToF-E telescope set up) was given by 2-D scatter plot where each point represents a coincidence event. The 2-D scatter plot generated by the ^{252}Cf source is shown in Fig. V.6.

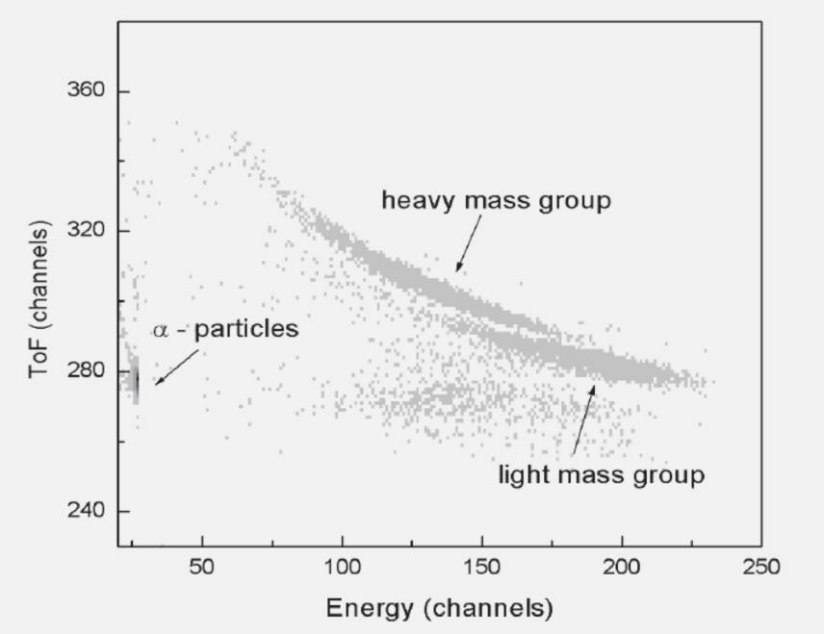

Figure V.6: time of flight and energy coincidence 2-D scatter plot of the decay products from a ^{252}Cf source.

The energy and ToF spectra were determined by selecting from the 2-D scatter plot a contour region and projecting it onto the energy and ToF axis respectively. The obtained spectra have a Gaussian shape. Consequently both the energy and ToF spectra were fitted by Gaussian functions to find the parameters list (peak position and its standard deviation in channels) of the energy and ToF at this specific region. The full width at half maximum (FWHM) of each Gaussian represent the timing resolution for the ToF spectrum and the energy resolution for the energy spectrum.

The energy of the ^{252}Cfα-particles was corrected from the energy loss via carbon thin foils of time detectors and within the thin entrance of energy detector. The evaluation of these energy losses was made with the help of SRIM 2013 code. The ToF spectrum fit parameters of 6.12 MeV alphas is represented in Fig. V.7.

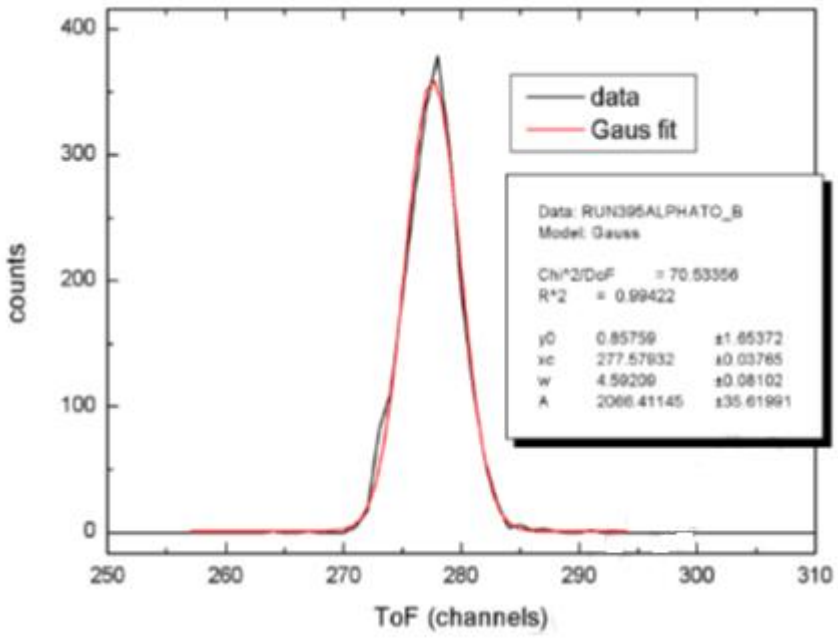

Figure V.7: Gaussian fit to the ToF spectrum of 6.12 MeV alphas

With calibration offset setting at 0,59 ns/channel the ToF spectrum of 6.12 MeV alphas fit parameters correspond to time of flight of about 27ns and the overall timing resolution of 3.2ns (full width at half maximum=4.59*1.17*0.59). For the light fission fragments the timing resolution was about 2.6ns.

The preliminary conclusion of the test using the ^{252}Cf source was that the spectra analysis proved the usability of the ToF-E telescope design for the elastic recoil detection analytical method.

V.3. Using of ERDA-ToF-E for real samples

V.3.1. 2D coincident E-TOF spectrum

The first ERDA-ToF-E measurements were carried out under the following conditions:

- 27.5 MeV Kr^{15+} incident beam
- Beam spot size viewed on a fluorescent wire mesh mounted on the target ladder together with the samples to be analyzed was about 2.5 mm in the lateral direction
- About 3.3 nA full beam current during the whole experiment
- Experimental geometry: incident beam angle 75°, exit recoil angle 75° with reference to the sample surface normal, ϕ=30° recoil angle
- 1 kV applied to the MCP detector
- 300 ns Time to Digital converter (TAC) full-scale time interval between the accepted input time impulses

The secondary ion beams were obtained by recoiled (sputtering) ions from known primary target samples bombarded by a 27 MeV Kr^{+7} beam. The measurement of the flight length was

determined by measuring the time of flight of 3.33 MeV He^{2+} scattered from a thin layer of gold deposited on silicon. The flight length was founded l=0.584 m with an uncertainty of 1.7%.

Fig.V.8 presents a typical 2D coincident E-TOF spectrum which contains events registered by the time and energy detectors in coincidence for MgO thick layer bombarded by 27 MeV $^{84}Kr^{+7}$beam.It shows clearly the separation of different masses of elements contained in the sample by separate curves called "banana curves". The scatter plot shows the major ion species from the sample^{16}O and ^{24}Mg.

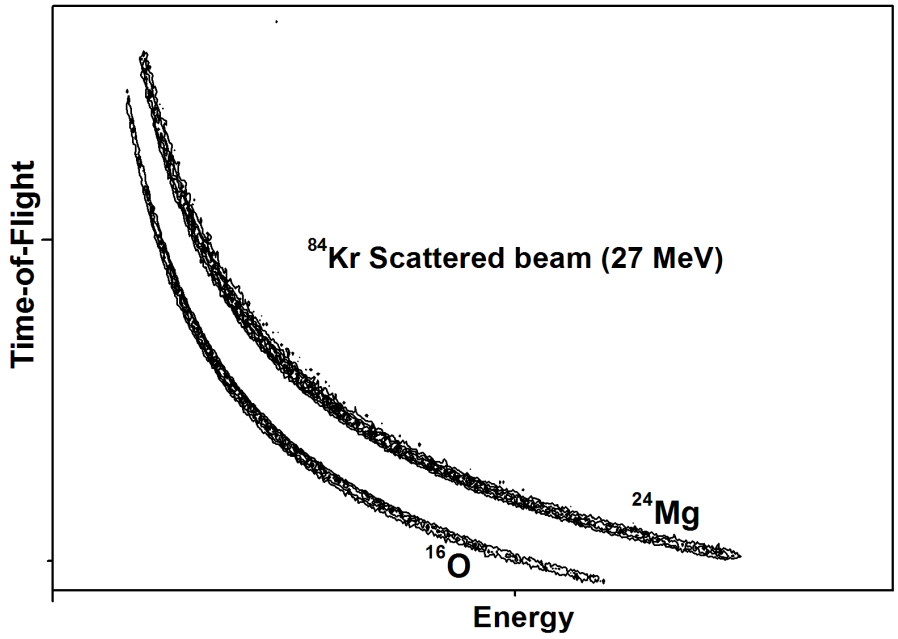

Fig.V.8: ToF-E histogram of MgO thick layer bombarding by 27.MeV $^{84}Kr^{+7}$.

V.3.2. Time calibration of the time of flight telescope

For the ToF detector calibration measurements of different recoils ion species from known target samples SiO2, Kapton and graphite bombarded by E_0=26 MeV $^{64}Cu^{+7}$ beam enter into the detection system. To calibrate the ToF telescope the H, C, O and Si mass contours in their corresponding 2D coincident E-TOF spectra were projected onto the ToF axis to get elemental time spectra. The short time (high energy) edge of the time spectrum of each identified recoil ion was then fitted using a Gaussian fit function using the graphing and analysis software ROOT as illustrated in the example in Fig. V.9.

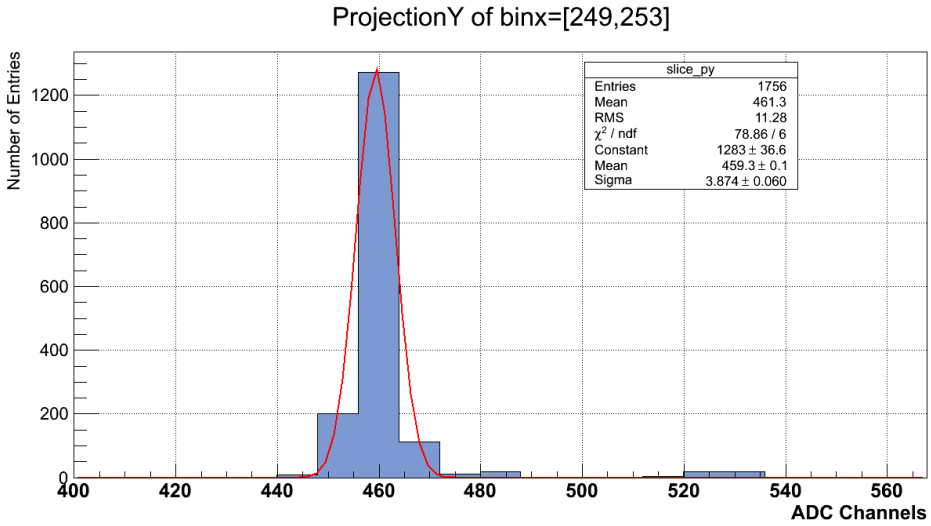

Fig.V.9: Gaussian fitting of the edge of the recoil graphite ion

The edge fit gave the channel number corresponding to the energy of recoils coming from the surface of the target sample after passing through the 0.025µm carbon foils of both timing detectors.The energy loss via carbon thin foils of time detectors was evaluated using SRIM 2013 code.

Table V.2 present the mean value of the ToF in channel for each ion (H, C, O, Si) recoiled from the surface of the sample included the theoretical calculated values in ns using the following expression:

$$t = \ell\sqrt{\frac{m}{2E_c}} \qquad \text{(V.2)}$$

where $\ell$the flight distance equal to 0.6m, m is the ion mass and E_C is the recoil energy of the ion of mass m from the surface (see Eq. IV.28) of the sample taking into account the energy loss ΔE_{T1} of through the T1 (see Fig. IV.19) carbon foil of thickness x=0.025µm. The calibration equation of the time of flight is represented in figure V.10.

Ion	A	ToF (ch)	$E_2=K'E_0$ (keV)	S_C (keV/µm)	ΔE_{T1} (keV)	$Ec=E_2-\Delta E_{T1}$ (keV)	$ToF(ns)=1366\sqrt{\frac{A}{E_c}}$
H	1	376	1210.11	45.89	1.15	1208.96	39.28
C	12	459	10491.17	1413.35	35.33	10455.84	46.27
O	16	482	12603.98	2129.56	53.24	12550.74	48.77
Si	28	560	16617.26	4491.37	112.28	16504,98	56.26

Table V.2.: Experimental times of flight in channel together their corresponding calculated in ns of different recoils ions from the surface of the samples. Sc is the stopping force of each ion in carbon taken from SRIM-2013 code.

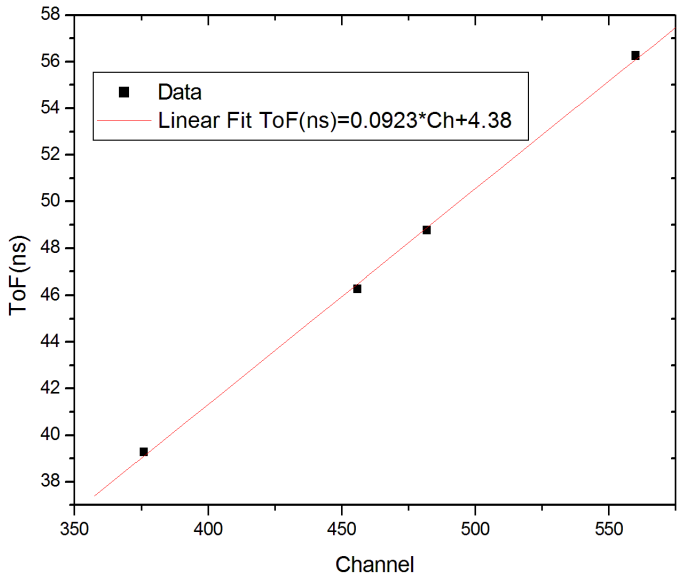

Fig.V.10: **Time calibration of the time of flight telescope**

V.3.3.Energy calibration of surface barrier detector

The response of the SBD to the charged particle is known to be mass (and energy) dependent [kno-2000]. The channel-energy calibration curve of the SBD over the mass range 12 – 84 u was non-linear [Man-2010]. On the other hand, we have seen in the sub-section 3.2 that the ToF calibration was quite linear then it was decided that to use the SB detector simply to tag events of certain energy and then the coincident ToF used to calculate the energy for each of the recoil masses.

V.4.Determinationof the stopping force and energy straggling

In order to explain the method of data analysis adopted in this work, the Carbon ion is given as illustration for the evaluation of its stopping force and energy straggling in Si_3N_4 foil. Fig. V.11 shows the raw ToF-E coincidence spectra of recoiled /scattered ions with and without foil placed in front of the SBD.In the first round (without Si_3N_4foil), one tagged energy E for the C ion by the SBD detector, corresponds to the energy E_2 of this recoil ion as recorded by the time of flight (Tof_2) between the timing detectors. In the second round (withSi_3N_4 foil) the same tagged value E corresponds to the energy E_1 of the recoil ion recorded by the ToF (Tof_1) between the timing detectors before traversing the foil.

V.4.1 Stopping power determination

We have (see Fig. V.11):

$$E = \frac{1}{2}m\left(\frac{L}{Tof_2}\right)^2 \text{and} E = \frac{1}{2}m\left(\frac{L}{Tof_1}\right)^2 - \Delta E \qquad \text{(V.3)}$$

whereΔE is the energy loss, m the mass of recoiled ion and L the distance of flight path between the two timing detectors. Therefore, the energy loss ΔE of recoil ion after passing through the stopper foil (Si_3N_4) is then given by:

$$\Delta E = E_1 - E_2 = \frac{1}{2}m\left(\frac{L}{Tof_1}\right)^2 - \frac{1}{2}m\left(\frac{L}{Tof_2}\right)^2 \quad \text{(V.4)}$$

We deduce the experimental stopping power S:

$$S\left(\bar{E} = \frac{E_1+E_2}{2}\right) = \frac{\Delta E}{\Delta x} \quad \text{(V.5)}$$

where Δx being the linear thickness of the foil.

V.4.2 Energy straggling determination

In this experiment the energy spectra of E_1 and E_2 have been found nearly Gaussian in shape with standard deviation Ω_1 and Ω_2 respectively (see Fig.V.11). The values of Ω_1 and Ω_2 are deduced from the ToF projection spectra by using the following formula:

$$\Omega_i = 2\frac{\Omega_{i(Tof)}}{Tof_i}E_i \qquad i=1,2 \quad \text{(V.6)}$$

where $\Omega_{i(Tof)}$ is the standard deviation of the ToF projection spectra.

The experimental total energy loss straggling δE is evaluated from:

$$\delta E_{exp} = 2.3548\sqrt{\Omega_1^2 - \Omega_2^2} \quad \text{(V.7)}$$

The last expression must be corrected from the extra straggling Ω_σ due to the texture and thickness variation of the target foil estimate by Besenbecher et al [Bes-1980] by:

$$\Omega_\sigma^2 = \left(\frac{\Delta E}{\Delta x}\right)^2 \sigma^2 \quad \text{(V.8)}$$

where σ is the standard deviation of the foil thickness and Δx is the mean value of the foil thickness. It has been shown by Szilagyi et al **[Szi-1995**] that, when the relative energy loss exceed 25%, the non-statistical component of energy loss straggling becomes significant, due to the energy-dependency of the electronic stopping power. Then the experimental corrected value of energy straggling considered for theoretical comparison, is writing as:

$$\left(\delta E_{exp}\right)_{corr} = 2.3548\sqrt{\left(\frac{S_2}{S_1}\right)^2(\Omega_1^2 - \Omega_2^2) - \left(\frac{\Delta E}{\Delta x}\right)^2\sigma^2} \quad \text{(V.9)}$$

where $S_{1,2}$ are the stopping forces at the front and at the back surface regions of the foil, respectively.

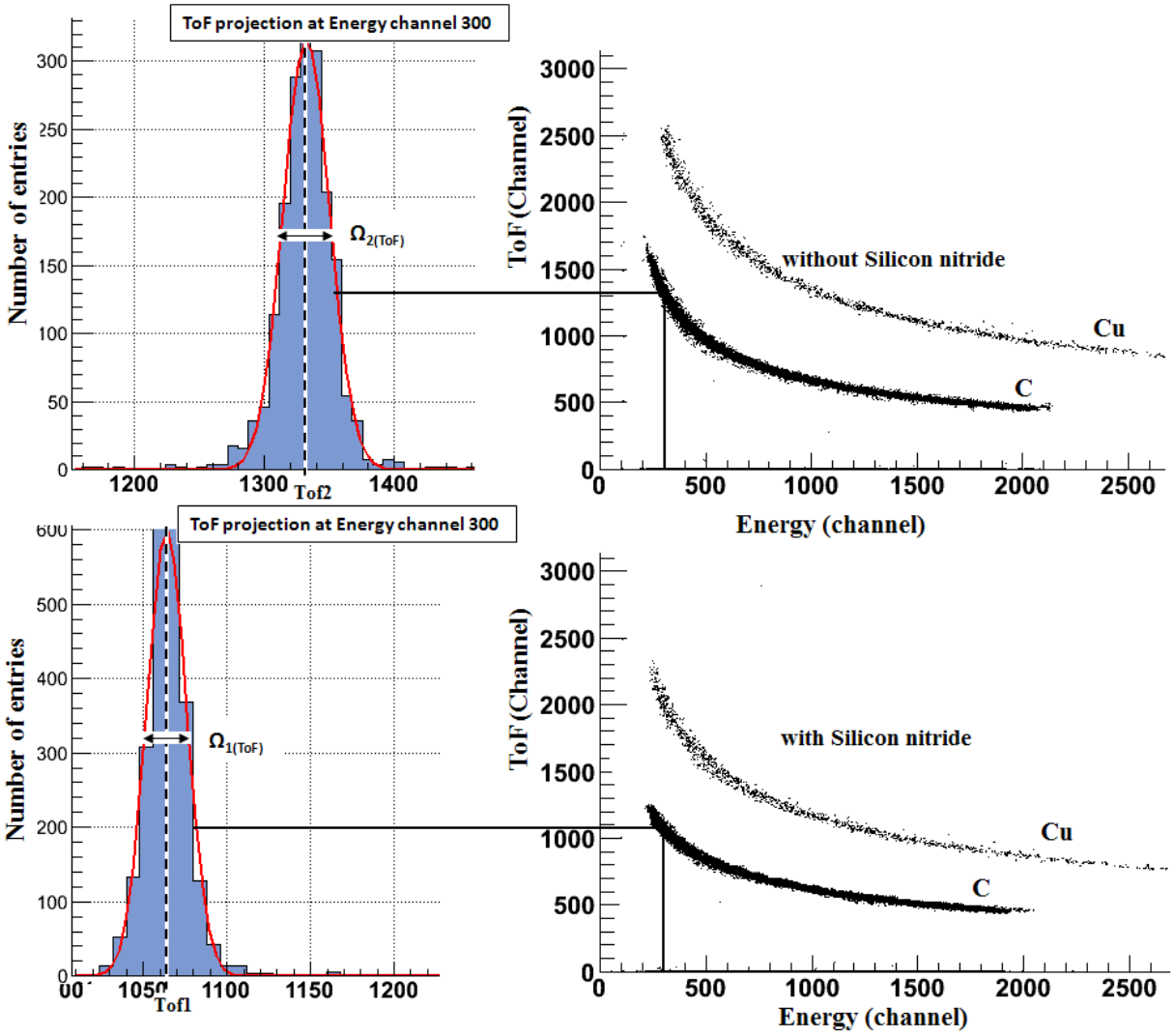

Fig. V.11: Two-dimensional Time of Flight-Energy projection maps of scattered ion (C) and recoiled ion (Cu) with and without thin silicon nitride as stopping foil.

V.5.Effective charge

The effective ion charge $Z^*_{Ion} = \gamma Z_{ion}$, where the effective charge fraction γ is defined by Northcliffe [Nor-1963]as:

$$\gamma^2 = \frac{1}{Z^2_{Ion}} \frac{S(Z_{Ion}, Z_{foil}, v)}{S(1, Z_{foil}, v)} \qquad (V.10)$$

where Z_{ion} is the atomic number of the incident ion, $S(Z_{Ion}, Z_{foil}, v)$ and $S(1, Z_{foil}, v)$ are the stopping cross-sections for the heavy ions and protons penetrating at a speed *v* through a foil with atomic number Z_{foil}. The effective charge formalism has become the basis for most semi-empirical expressionslike Northcliff and Schilling [Nor-1970], Betz[Bet-1972], Brown et al [Bro-1972], and Froster et al. [For-1976].

Several effective charge expressions are proposed by different authors. The effective charge expression given by Northcliffe & Schilling is as follow:

$$\gamma = \left(1 - e^{-\frac{v}{Z_{Ion}^{2/3} v_0}} \right) \qquad \text{(V.11)}$$

Montennegro et al.[Mon-1982] propose the following expression:

$$\gamma = \frac{1 - \exp(-\alpha\mu) - \frac{1}{6}\alpha\mu\exp(-2\alpha\mu)}{1 - \exp(-\mu) - \frac{1}{6}\mu\exp(-2\mu)} \qquad \text{(V.12)}$$

where $\mu = \frac{v}{v_0}$, $\alpha = Z_{ion}^{-2/3}$ and v_0 is the Bohr velocity. Expression (V.12) is valid for ion energies above 0.2 MeV/amu.

In order to verify the expression of the effective charge introduced in the modified LSS (see section II.3.2) formula we measured this effective charge and fit it by the following expression:

$$\gamma = 1 - Ce^{-\frac{v}{Z_{Ion}^{D} v_0}} \qquad \text{(V.13)}$$

where C and D are two fitting parameters.

To determine the experimental effective charges, the stopping force of the proton is deduced directly from the SRIM code [Zie-2013].

As an example we present in Fig. V.12 and Fig. V.13. the effective charge fraction of Mg and Si in Formvar as function per nucleon of energy of incident ion.

The fitting parameters C and D are founded to be $C \cong 1 \text{and} D \cong 2/3$, hence the Northcliffe & Schilling expression (V.11) is the best suitable expression of effective charge for the range and ions studied.

Further, we compared the measured effective charge with the Montennegro et al. formula (see figures V.12 and V.13), we found a good agreement for energies above 0.2 MeV/uma and a small discrepancies below 0.2 MeV/uma up to 10%. This discrepancy is predicted because the Montennegro effective charge is valid for ion energies above 0.2MeV/amu like mentioned above.

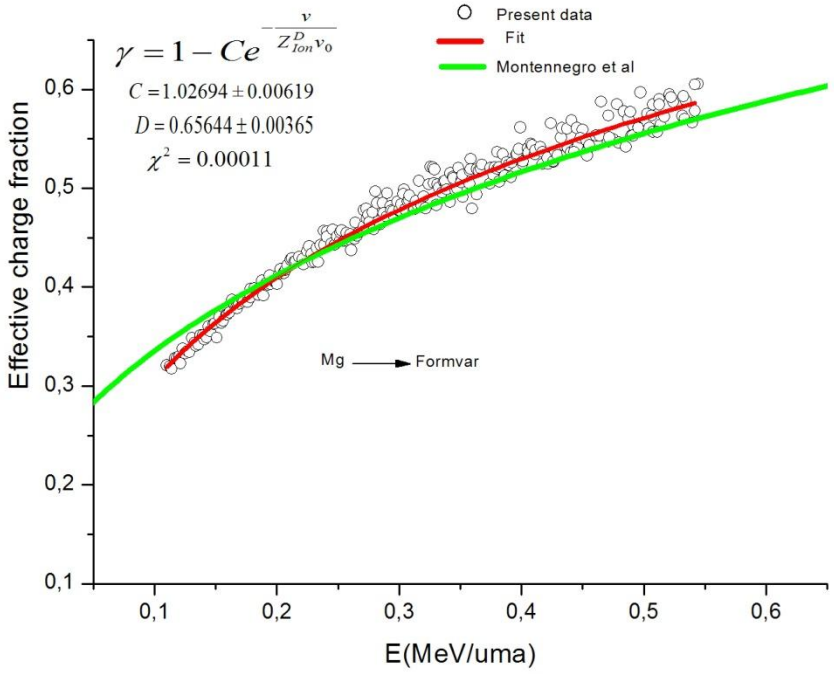

Fig.V.12 : Effective charge fraction of ^{24}Mg ion in Formvar as a function of the energy per nucleon of the projectile.

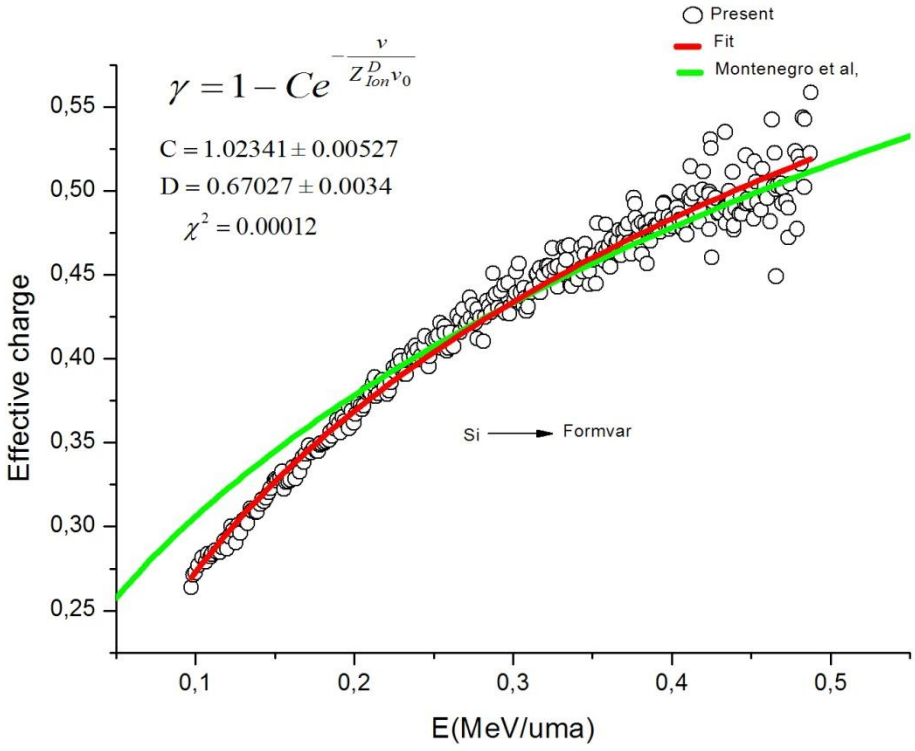

Fig. V.13: Effective charge fraction of ^{28}Si ion in Formvar as a function of the energy per nucleon of the projectile.

V.6.Stopping force

The resulting energy spectra of the systems (with and without stopper foil, see fig. V.11) have been found nearly Gaussian in shape, so that their peak positions have been considered to be a point of energy value.The statistical errors of S(E) in the presently obtained data are caused mainly by uncertainties in the localization of the peak position for the determination the mean energy-loss (<2%).

For material compounds, the calculation of S(E) with the LSS formula, and the modified LSS formula the Bragg's rule was considered to be strictly valid.

The present electronic stopping power data S_e are obtained by subtracting the SRIM nuclear stopping power values S_n from the experimental stopping powers S_{exp}, are shown in figures**.**

V.6.1. Applicability of the semi-empirical modified LSS formula

In order to check the reliability of the proposed semi-empirical formula of electronic stopping force (Eq. II.9), we have compared the calculated values of electronic stopping power generated by Eq. II.9 to those published by H. Paul [Pau-2013] for several selected couple of ions-targets in LSS low energy range.

Figures V.14 to V.17presentthe experimental stopping data [Pau-2013] of ^{12}C in ^{63}Cu, ^{12}C in ^{197}Au, ^{19}F in ^{63}Cu, ^{19}F in ^{107}Ag, ^{19}F in ^{197}Au, ^{27}Al in ^{12}C, ^{27}Al in ^{197}Au, ^{28}Si in ^{27}Al, ^{28}Si in ^{90}Zr, ^{28}Si in ^{107}Ag, and ^{28}Si in ^{197}Au, compared to the calculated stopping power values determined by equation II.9 and to those generated by LSS formula Eq. II.7.

It is apparent from Figures V.14 to V.17that the calculated stopping force values using the Eq. II.9 are in good agreement with H. Paul stopping force data in all studied examples, however a large discrepancy (up to 20%) has been observed with stopping force values calculated by LSS formula.

Table 3 summarize the values of adjustable parameters a and b (Eq. II.9) for the couples of ^{12}C in ^{63}Cu, ^{12}C in ^{197}Au, ^{19}F in ^{63}Cu, ^{19}F in ^{107}Ag, ^{19}F in ^{197}Au, ^{27}Al in ^{12}C, ^{27}Al in ^{197}Au, ^{28}Si in ^{27}Al, ^{28}Si in ^{90}Zr, ^{28}Si in ^{107}Ag, and ^{28}Si in ^{197}Au. We can see clearly that the value of the adjustable parameter "a" is close to1 and the parameter "b" is between1.5 and 4.6 for all couples presented in figures V.14 to V.17.

ion	target	a	b
C	Cu	1.1725±0.0901	4.4242±0.0312
	Au	1.3401±0.0100	4.6358±0.0416
F	Cu	1.0518±0.0904	3.4052±0.0203
	Ag	1.1396±0.0843	2.9598±0.0511
	Au	1.1230±0.0825	2.6340±0.0977
Al	C	1.2721±0.0301	2.5685±0.0635
	Au	0.9534±0.1118	1.5939±0.0913
Si	Al	0.8801±0.0092	2.2153±0.0622
	Zr	1.0216±0.0712	2.2075±0.0775
	Ag	0.9992±0.0511	1.8588±0.0214
	Au	0.9469±0.0481	1.5702±0.0955

Table 3:Fitting parameters a and b of eq. 2.9 for ions-targets couples ^{12}C in ^{63}Cu, ^{12}C in ^{197}Au, ^{19}F in ^{63}Cu, ^{19}F in ^{107}Ag, ^{19}F in ^{197}Au, ^{27}Al in ^{12}C, ^{27}Al in ^{197}Au, ^{28}Si in ^{27}Al, ^{28}Si in ^{90}Zr, ^{28}Si in ^{107}Ag, and ^{28}Si in ^{197}Auat low energy (0.06 – 0.65 MeV/nucleon).

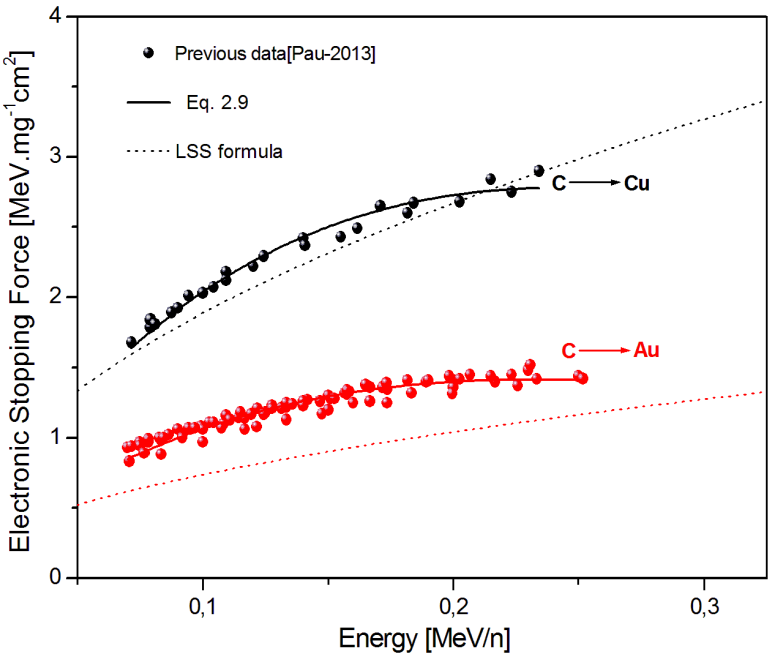

Fig. V.14: Comparison of previous stopping power data [Paul-2013] (circle) for ^{12}C in ^{63}Cu and ^{12}C in ^{197}Au together with LSS theory predictions (dashed lines), and, Eq. II.9 (solid lines).

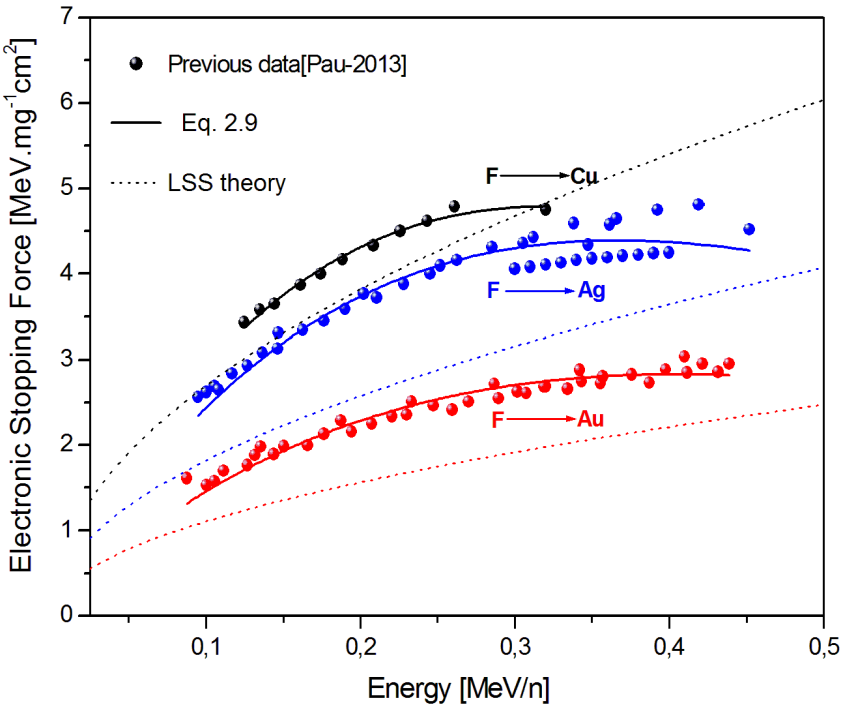

Fig. V.15: Same as in Fig. V.14but for ^{19}F in ^{63}Cu, ^{19}F in ^{107}Ag, and ^{19}F in ^{197}Au

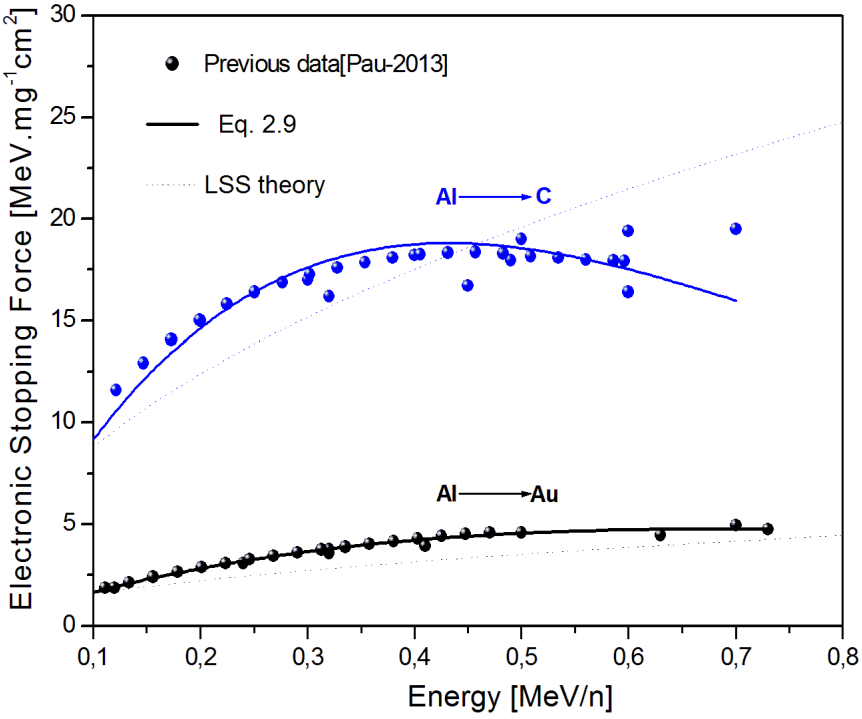

Fig V.16: Same as in Fig. V.14but for ^{27}Al in ^{12}C and^{27}Al in ^{197}Au

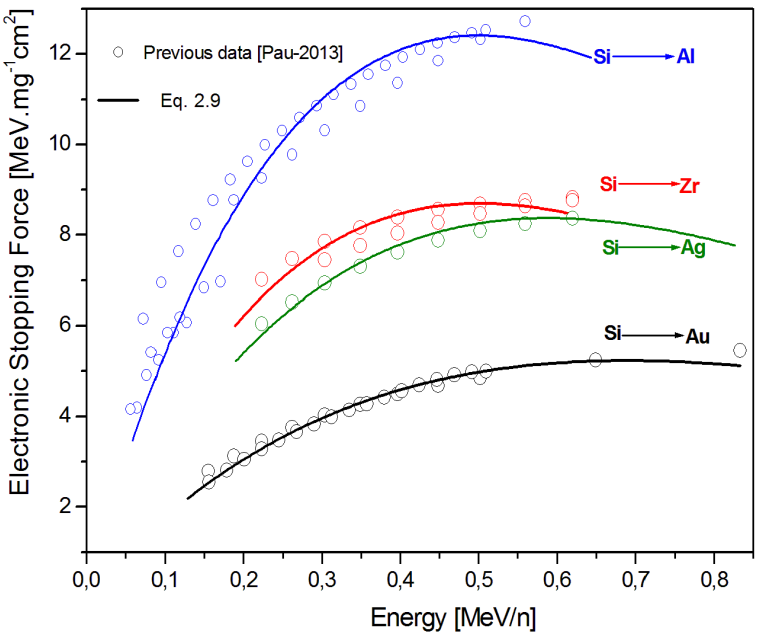

Fig. V.17:Comparison of previous stopping power data [Paul-2013] (circle) for ^{28}Si in ^{27}Al, ^{28}Si in ^{90}Zr, ^{28}Si in ^{107}Ag, and ^{28}Si in ^{197}Au together with Eq. II.9 (solid lines).

V.6.2. Stopping force of Formvar thin foil

First of all, the results presented in this dissertation are the first experimental study that has measured the stopping force of 0.10–0.6 MeV/nucleon ^{24}Mg, ^{27}Al and ^{28}Si ions in Formvar[Gue-2014]. Note also that in this energy range the nuclear stopping power can be neglected.

A survey of all measured stopping forces of Formvar for ^{24}Mg, ^{27}Al and ^{28}Si ions in the energy range 0.1- 0.5 MeV/uma are presented in Figs. V.18, V.19 and V.20 respectively for about 300 experimental points. The data have been compared with the LSS theory, the proposed modified LSS equation (Eq. II.9) and the well knows SRIM code [Zei-2013].

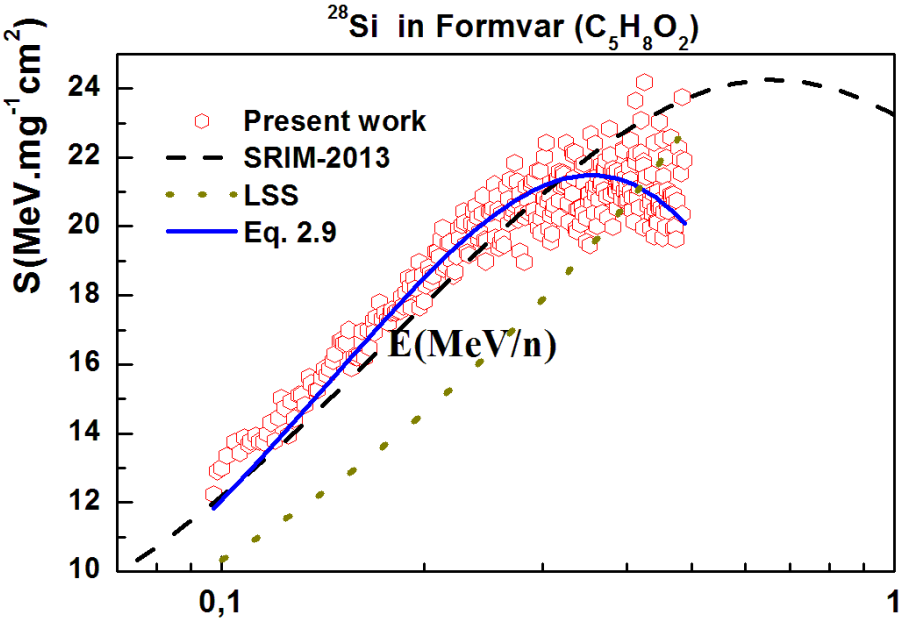

Fig V.18: Comparison of experimental stopping forces values for ^{28}Si ion (circle) in Formvar with data from Eq.II.9 (solid lines), SRIM-2013 predictions (dashed lines) and LSS theory (dot lines).

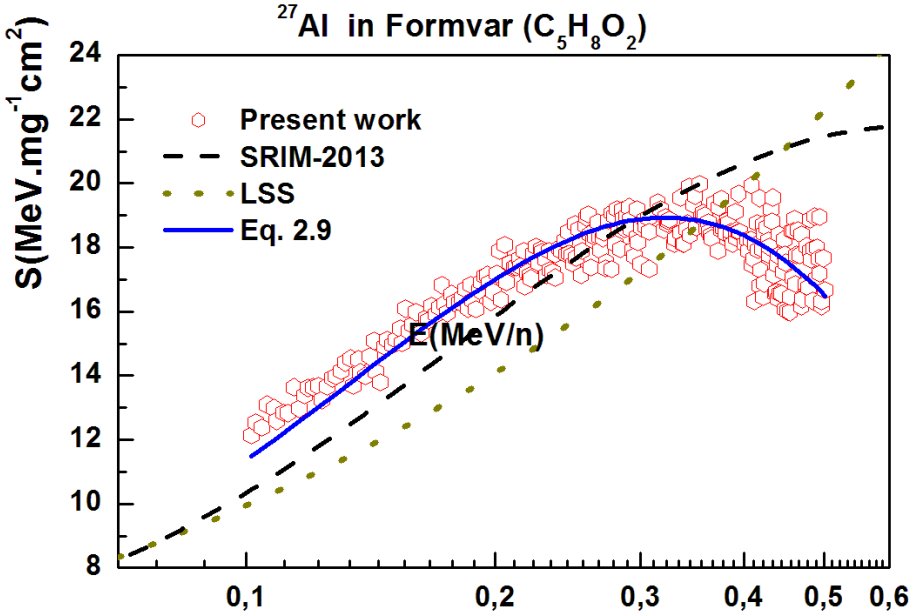

Fig V.19: Same as in Fig. V.18 but for ^{27}Al.

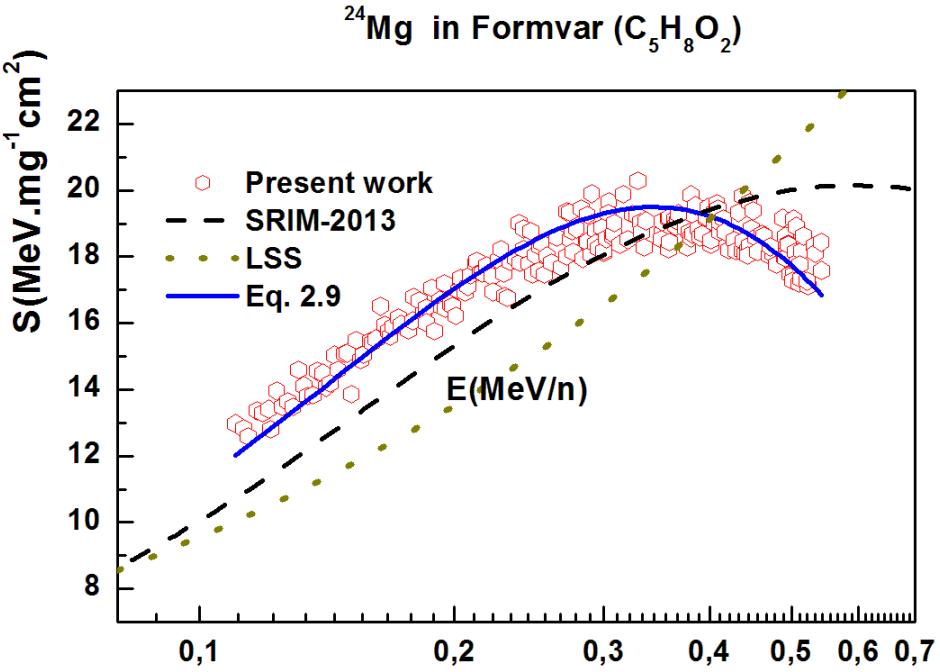

Fig V.20: Same as in Fig. 5.7 but for for ^{24}Mg.

From Figs. V.18, V.19 and V.20we can deduce that:

- The stopping forces predicted by SRIM are relatively in good agreement with the new obtained experimental data, with small discrepancies up to 10%. This discrepancy can be explained by the no availability of experimental data in this range of energy to incorporate in the SRIM fitting program.
- The measured stopping forces are in general greater than the LSS theory up to 20%except within the narrow region of 0.35-0.5 MeV/uma where the theoretical values are relatively in good agreement with our stopping force data (see Fig. V.18-V.20). This effect are noted by several authors [Nee-2009, Sha-2002]
- The calculated stopping force values based on our modified LSS expression (Eq. II.9) in the energy range 0.1-0.5 MeV/n provide excellent agreement with our experimental data and those calculated by the SRIM-2013 code.

V.6.3. Stopping force ofSi_3N_4 thin foil

We present here a brief discussion of the stopping force results. The results of measured stopping forces values of ^{12}C, ^{16}O, ^{28}Si and ^{63}Cu heavy ions traversing$Si_3N_4$are showed in figures V.21-V.24 respectively and compared to those generated by LSS formula, SRIM-2013 computer codeand available data from other authors. The statistical errors in the obtained data of stopping

force are caused mainly by uncertainties in the localization of the peak position for determination of the mean energy-loss (<5%).The obtained values are in good agreement with the predicted value from SRIM-2013 code over the measured energy range. The slight deviation of less than 4% for all ions can be related to experimental scatter and deviation from Bragg's additivity rule. However, a significant difference (up to 15%) was found between the values calculated by the LSS formula and those obtained experimentally, this discrepancy has been reported by several authors (see for exampleNee-2009, Sha-2002)**.**We observed in the case of ^{16}O discrepancy of up to 12%.

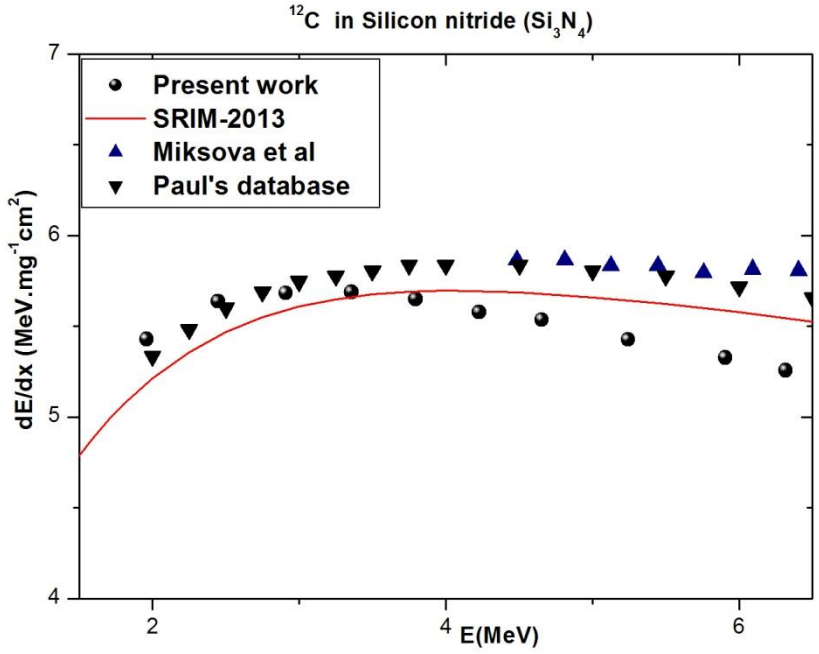

Fig V.21: Experimental stopping force values for ^{12}C ion in silicon nitridecompared to SRIM-2013 predictions (red line) and available data.

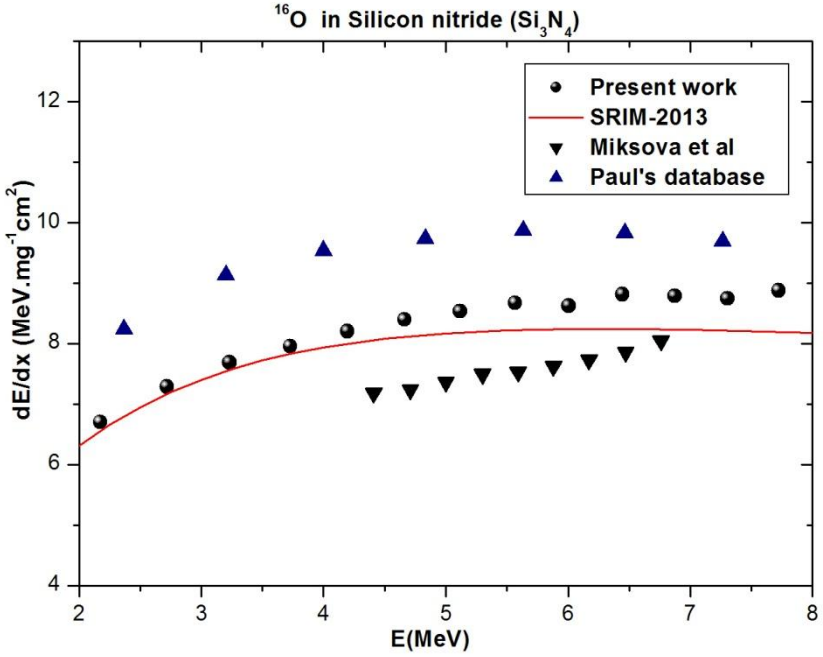

Fig V.22: Same as in Fig. V.21but for ^{16}O.

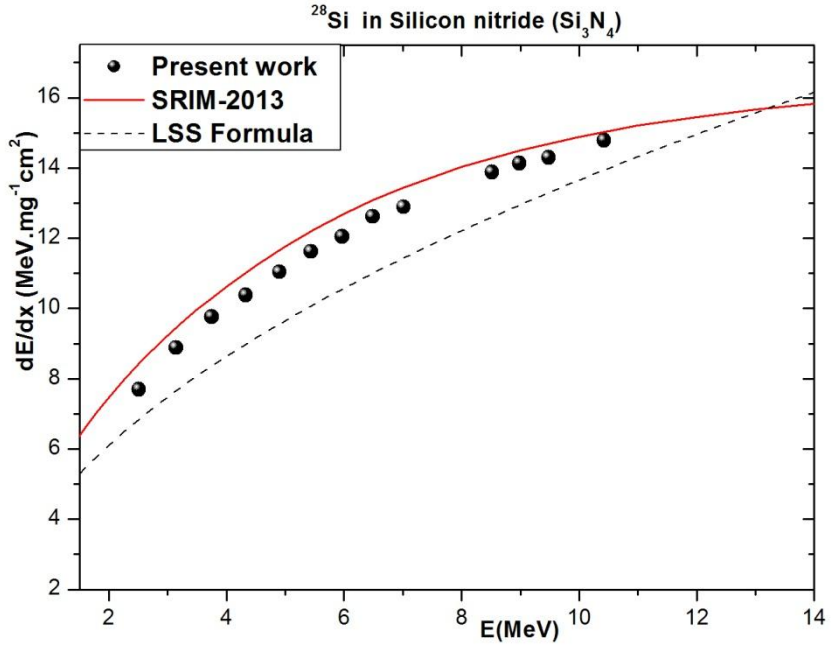

Fig V.23: Experimental stopping force values for ^{28}Si ion in silicon nitridecompared to SRIM-2013 predictions (red line) and LSS theory (dot line).

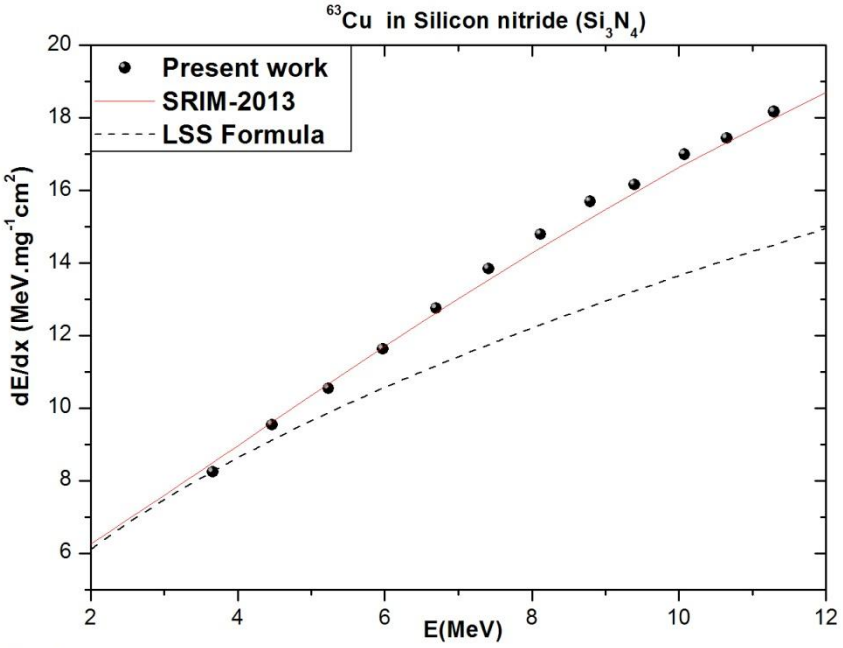

Fig V.24: Same as in Fig. V.23 but for ^{63}Cu

V.7. Energy straggling

V.7.1. Energy straggling in Formvar

A set of energy loss straggling data has been deduced from energy loss measurements of ^{28}Si, ^{27}Al, ^{24}Mg, ^{19}F, ^{16}O and ^{12}C heavy ions traversing Formvar thin foilover the energy range from 0.1 MeV/u to 0.6 MeV/u, as explain in section 4.2.The results of energy straggling and the associated uncertainties of studied ions are shown in figs V.25 to V.30. In these figures we included the calculated straggling values derived from Bohr's classical theory, Bethe-Livingston's quantum theory and Yang's empirical formula for comparison. The calculated straggling values derived from Chu's theory and Yang's empirical formulas were evaluated from the SIMNRA 6.04 code [May-2002].The absolute uncertainties associated to the measured energy loss straggling data were evaluated by considering the propagated errors originating from the different quantities in Eq. 4.7:

$$\Delta\Omega_{el} = \frac{1}{\Omega_{el}}\sqrt{\left(\Omega_1\Delta\Omega_1\right)^2 + \left(\Omega_2\Delta\Omega_2\right)^2 + \left[S\left(\Delta x\right)^2\Delta S\right]^2} \qquad \text{(V.14)}$$

Figures (V.25 to V.30) show the energy straggling as function of the energy of the incident ion. A general increasing trend of the energy straggling with increasing ions velocity was observed. It is also clearly shown that from these figures (V.25 to V.30), the electronic energy-loss straggling over the energy range from 0.1 MeV/u to 0.6 MeV/u where the ions are partially stripped ions was found to be significantly greater than predicted theories. These differences can be explained by the contributions of several effect sources of energy loss straggling (other than collisional electronic energy loss straggling) such as benching of the electrons on the atom, molecular effect and charge

exchange effect (loss and capture of the electrons of the projectile)[Efk-1975, Wei-2002]which are not taken into account in all theories subject of this comparison.

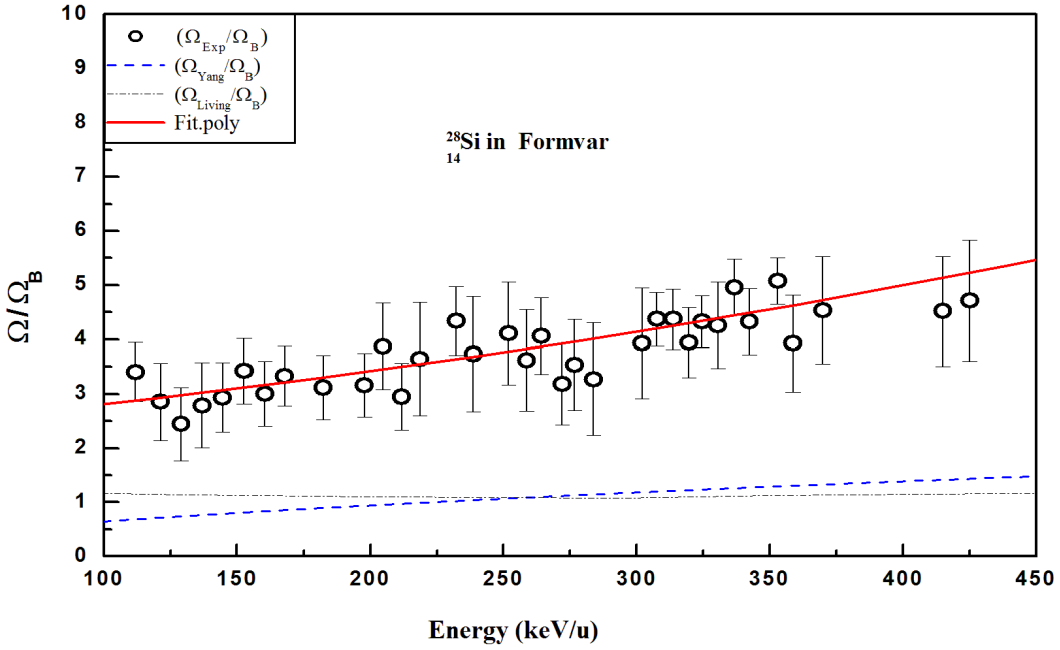

Fig V. 25: Comparison of experimental reduced electronic energy loss straggling of **^{28}Si** ions through Fromvar with predictions from Bohr's classical theory and Bethe-Livingston's quantum theory and Yang's empirical formula. The solid line is a second order polynomial fit to the experimental data.

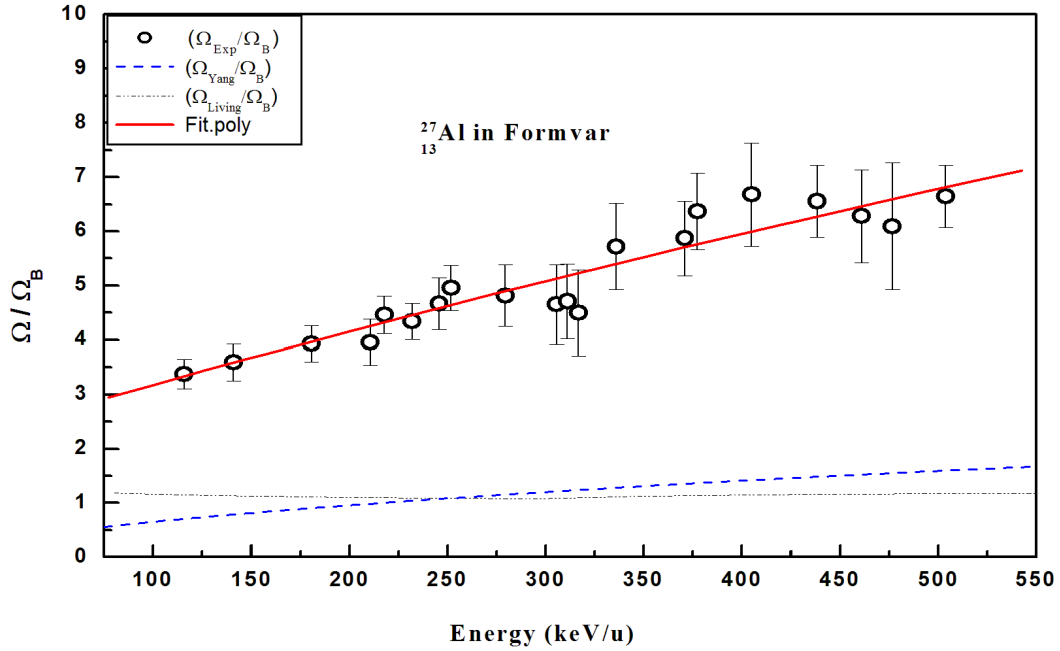

Fig V. 26: Same as in Fig. 5.14 but for ^{27}Al.

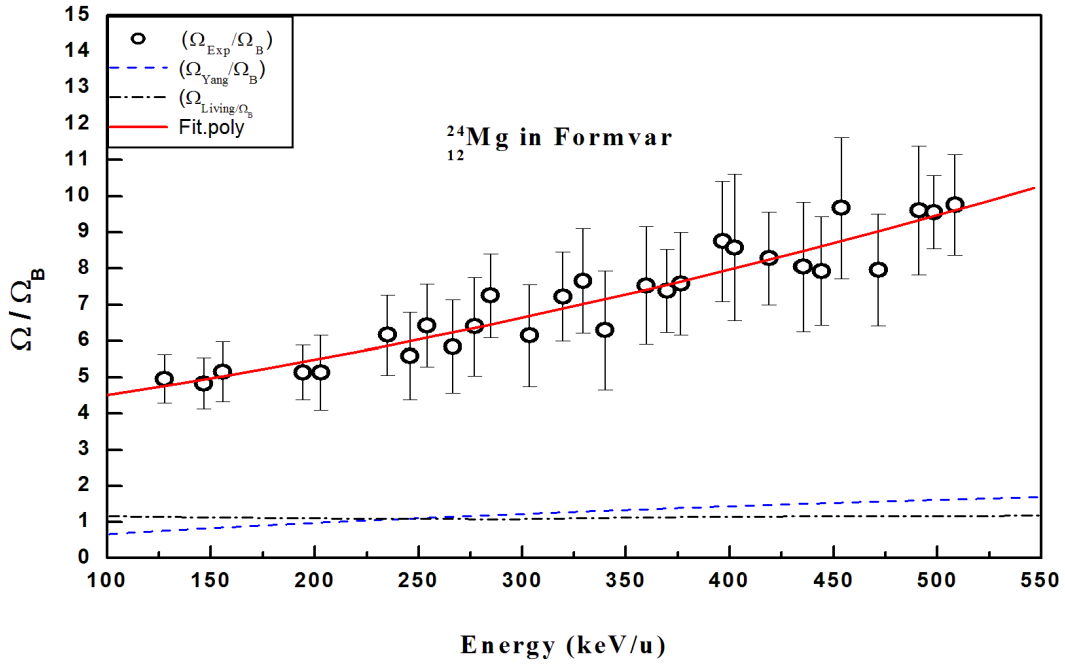

Fig V. 27: Same as in Fig. 5.14 but for ^{24}Mg.

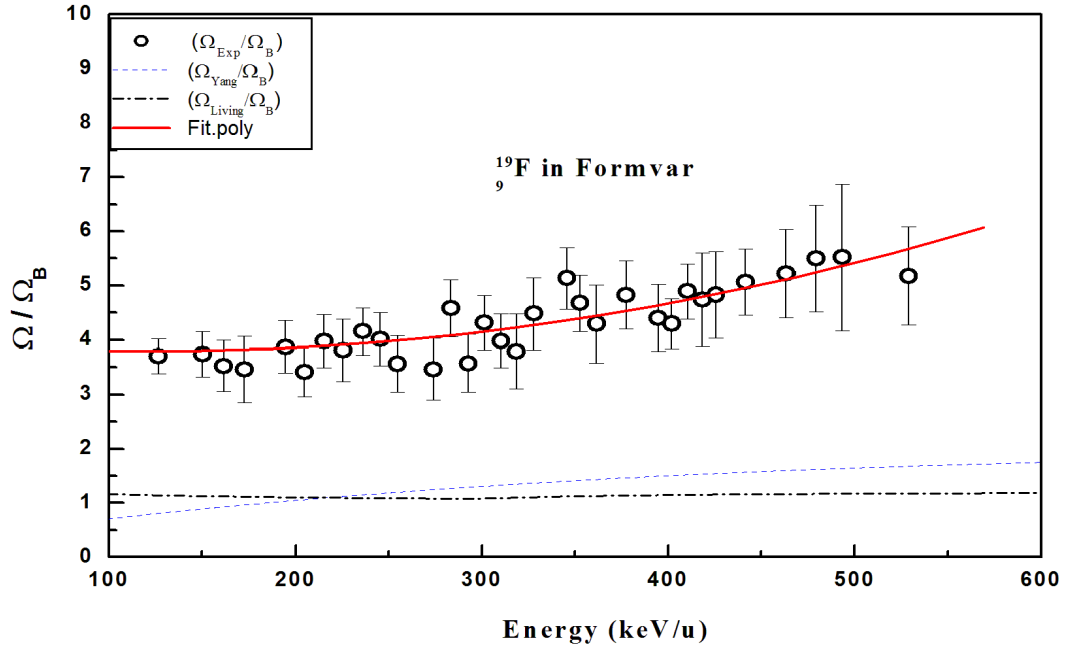

Fig V. 28: Same as in Fig. 5.14 but for ^{19}F.

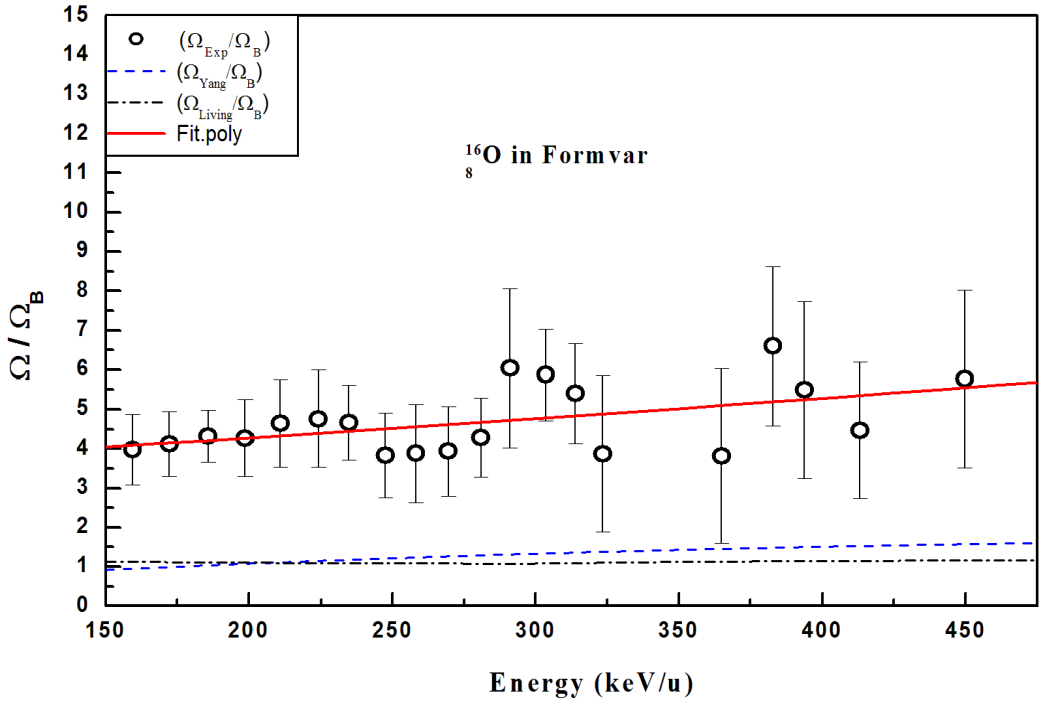

Fig V. 29: Same as in Fig. 5.14 but for ^{16}O.

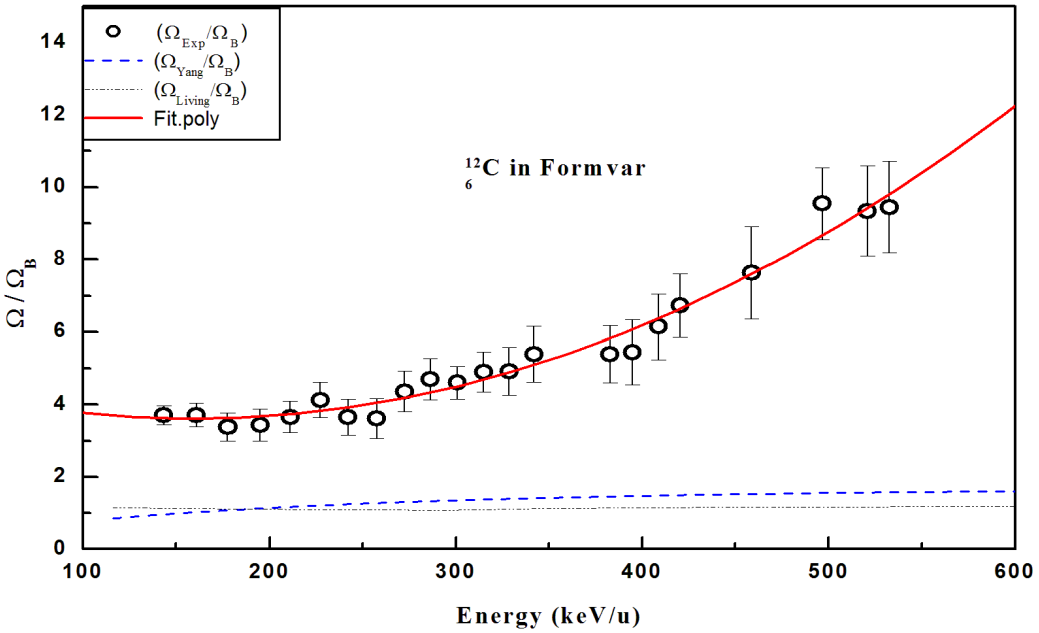

Fig V. 30: Same as in Fig. 5.14 but for ^{12}C.

V.7.2. Energy straggling in Si3N4

The data of measured energy straggling of C, O, Si, and Cu heavy ions in Si_3N_4overthe 2-11 MeV energy range are shown in Figures **V. 31**to **V. 34**respectively. Figs. **V. 31**to **V. 34**show also the comparison between the obtained energy straggling data and those derived from the more sophisticated straggling referred to as "Bohr model"[Sig-2006], the predicted value obtained by taken into account the bunching effect according to the Besenbacher approach (eq. 3.9) with the available data in the literature **[Mik-2015].**

Following our investigation there are not many experimental data on energy straggling especially for heavy ions. Miksova et al **[Mik-2015]** measured energy straggling of 4-7 MeV carbon and oxygen ions in $Si_3N_4$and obtained values of up to a factor of 1.5 above the Bohr values. These values are similar to ours within the limit of experimental uncertainty (see Figs V.31 and V.32).

It is clear from Figs. **V. 31**to **V. 34**that, the simple Bohr straggling as well as the more sophisticated straggling referred to as the "Bohr model", fail to predict the measured values of C, O, Si, and Cu heavy ions in Si_3N_4in the 2-11 MeV energy range. In all cases, the energy straggling is underestimated by a factor of 1.2-3 by the Bohr model. This large discrepancy between the Bohr model and the experimental data means that it is necessary to introduce other effects in straggling theory, such as the bunching effect and the charge exchange. In this work we have restricted our study to evaluate the bunching effect from the Hvelplund-Firsov formula [Hve-1971] following the Besenbacher approach (eq.III.26)**[Bes-1980].**

The energy straggling values given by eq. III.26 are reasonably comparable to the measured data. To make a clear comparison between calculations taking into account the bunching (Ω_{The}) and experimental data Ω_{Exp} we present in Fig. V.35 the ratio factor $\Omega_{Exp}/\ \Omega_{The}$. In the case of Carbon a minor discrepancy between calculations taking into account the bunching (Ω_{The}) effect and the experiment values, then, let us concluded that, the Hvelplund-Firsov formula exaggerate the straggling due to the bunching of electrons, or the straggling due to charge exchange is negligible in comparison with the bunching effect for carbon ions in the 2-8 MeV range of energy. For the oxygen ions the calculated energy straggling from eq. 3.9 underestimates slightly (<10% for 4-8 MeV) experimental data (see Fig.5.24).For Silicon and Copper there is a net underestimation of experimental data by eq.3.9 (up to Ω_{Exp}~$3\Omega_{Th}$ for energy less than 4 MeV for Copper).Finally, it is clear from Fig. 5.24 that the straggling due to charge exchange and molecular effect increase with atomic number Z of incident ion, obviously at this range of energy.

At all considered energies, the straggling resulting from the atomic (nuclear) collision is negligible for all studied ions except copper for energies 2-4MeV range (S_n/S_e~0.28-0.10). The appreciable value of nuclear stopping force relative to the electronic stopping force for the copper ions for energy less than 4 MeV can explain partially the rise of the energy straggling for energy less than 4MeV.

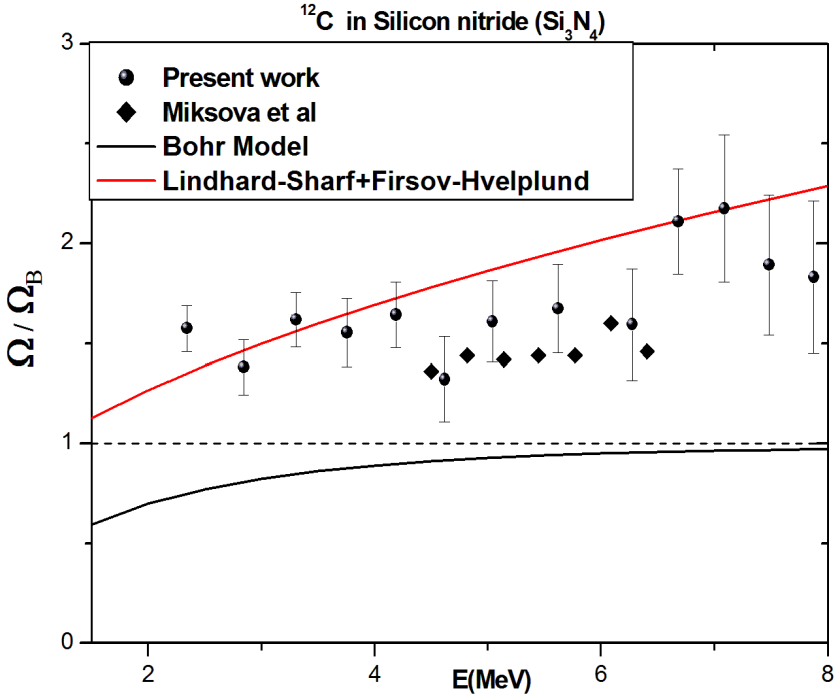

Fig.V.31: Experimental reduced energy loss straggling (Ω/Ω_B) of ^{12}C ions through silicon nitride foil compared to Bohr model, Lindhard-Scharff model including bunching effect and available data [Mik2015].

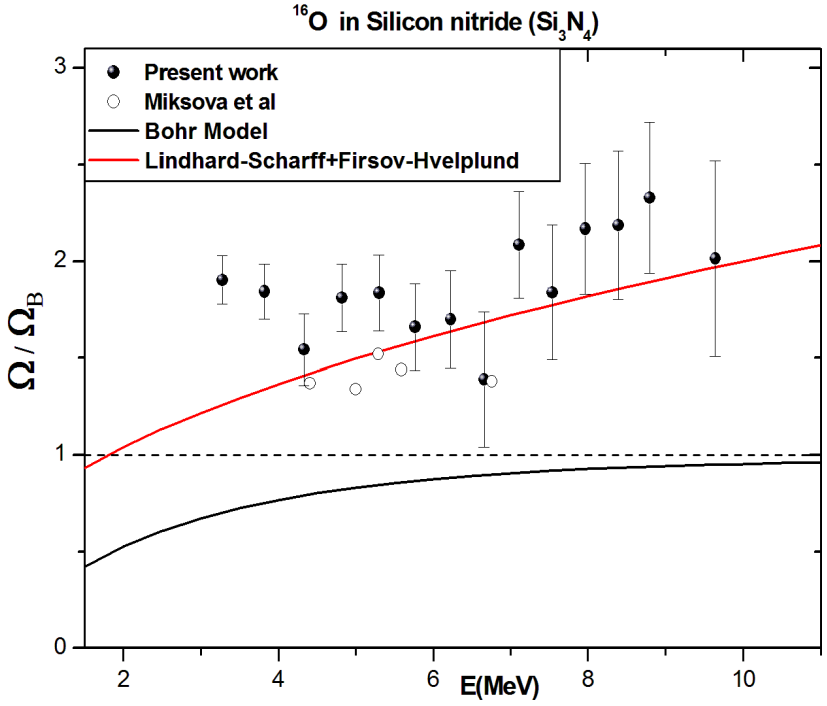

Fig. V.32: Same as in Fig. V.31but for ^{16}O.

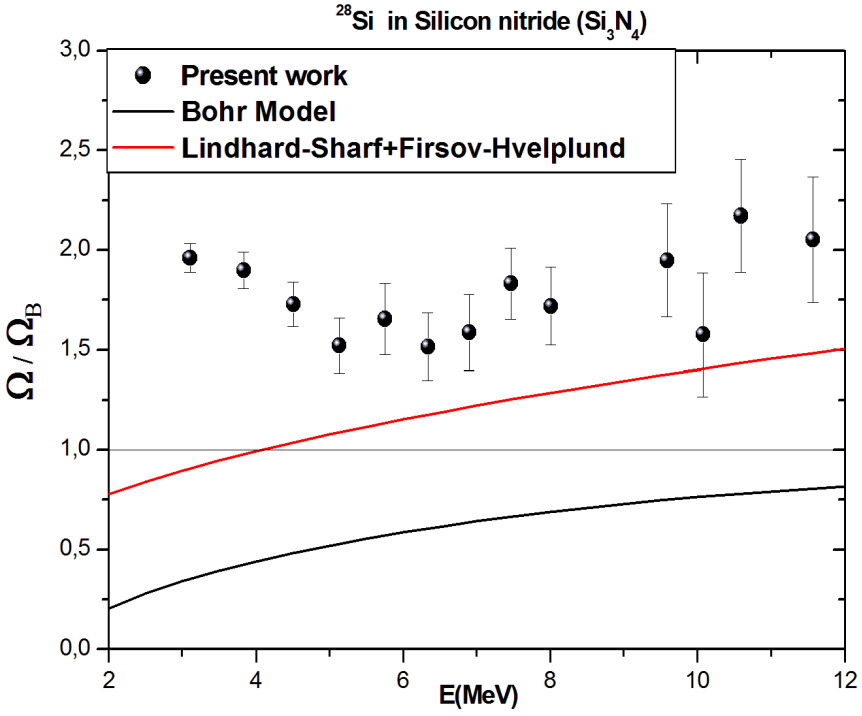

Fig. V.33: Experimental reduced energy loss straggling (Ω/Ω_B) of ^{28}Si ions through silicon nitride foil compared to Bohr model, Lindhard-Scharff model including bunching effect.

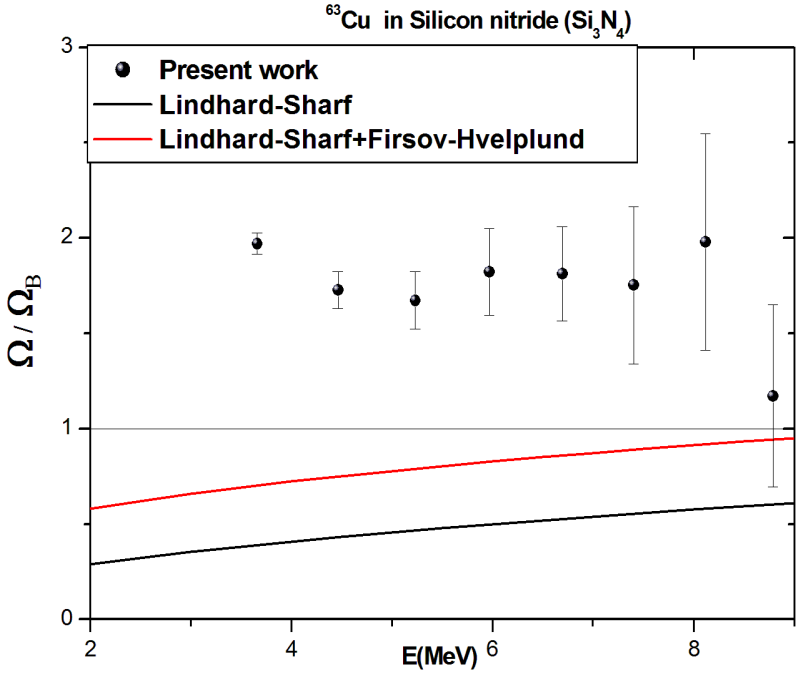

Fig. V.34: Experimental reduced energy loss straggling (Ω/Ω_B) of ^{63}Cu ions through silicon nitride foil compared to Lindhard-Scharff model and Lindhard-Scharff model including bunching effect.

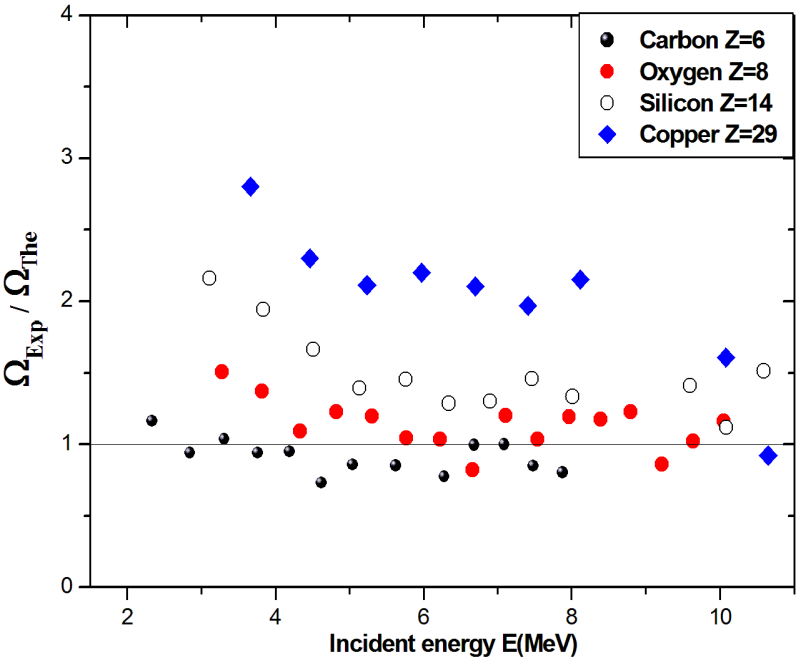

Fig. V.35: Plot showing the energy dependence of the ratio of experimental to eq. 2.9 energy straggling values of ^{12}C, ^{16}O, ^{16}Si and ^{63}Cu

Conclusions

In this thesis work we carried out the investigation on the fundamental parameters describing the slowing down of heavy ions in matter at low energy. We have successfully used an experimental set up for the measurement of energy loss, consisting of the combination of a Heavy Ion Elastic Recoiled Detection Analysis (HIERDA)with a Time of Flight Energy spectrometer (ToF-E).The original purpose of this set up was to do surface depth profiling in the analysis of light elements and transition metals in thin and thick foils materials at iThemba LABS as a complementary technique of traditional HI-ERDA. A detailed description of this set up and the method for evaluation of the energy loss and energy loss straggling of energetic heavy ions through thin foils were presented through this work. In comparison with direct transmission this method (HIERDA-ToF-E) has the advantage to give in one round of experiment (one monoenergetic beam) the values of fundamental parameters in a range of energies.Another advantage of the experimental method ToF-E is that the energy of the un-straggled and straggled projectile ions are simultaneously measured event-by-event, which leads to the cancelling of the possible fluctuations of the incident projectiles. The newly obtained data are studied in the light of available data and theoretical predictions.The new obtained stopping forces show good precision and accuracy and were in agreement with previously published values in the literature. The new data obtained in this work, agrees with the available data from other independent research work from the field of IBA, and gives a strong indication that the results and the methodology followed are valid.

The electronic stopping forces in Formvar thin foil have been determined for Si, Al, and Mg ions at low energy region (0.1- 0.5 MeV/n) in the energy region validity of the LSS domain. Following our investigation on experimental slowing down processes of charged particles crossing compound materials, this study gave a new set of stopping force data. The SRIM-2013 stopping force values are in good agreement with the experimental data presented in this work and with available data in the literature. However a large discrepancy has been observed with stopping force values calculated by LSS formula up to 20%. The same trend was observed for the new determined stopping force data of 2-11 MeV ^{12}C, ^{16}O, ^{28}Si and ^{63}Cu heavy ions through Si_3N_4.

In the present study, we have attempted to introduce a semi-empirical formula by taking into account the effective charge of moving ions concept and introducing the exponential fit function. In order to best describe the slowing down process which occurs at low energy region, we have proposed a new expression (eq.II.2.9) to evaluate the electronic stopping force at low energy in the LSS domain. The stopping forces values generated by the proposed semi-empirical formula have

been compared to those published by H. Paul for ions-targets couples ^{12}C in ^{63}Cu, ^{12}C in ^{197}Au, ^{19}F in ^{63}Cu, ^{19}F in ^{107}Ag, ^{19}F in ^{197}Au, ^{27}Al in ^{12}C, ^{27}Al in ^{197}Au, ^{28}Si in ^{27}Al, ^{28}Si in ^{90}Zr, ^{28}Si in ^{107}Ag, and ^{28}Si in ^{197}Au at low energy (0.06 – 0.65 MeV/nucleon),to our new obtained experimental stopping data for2-11 MeV ^{12}C, ^{16}O, ^{28}Si and ^{63}Cu heavy ions through $Si_3N_4$and for 0.10–0.6 MeV/nucleon ^{24}Mg, ^{27}Al and ^{28}Si ions in Formvar, to data generated by SRIM-2013 computer code and the LSS model. It is apparent from this comparison that the calculated stopping force values using the semi-empirical formula (eq. 2.9) are in good agreement with H. Paul stopping force data in all ions-targets considered and with the new obtained data; however a large discrepancy was observed with the LSS stopping powers values.

In this work we also studied the energy straggling of 2-11 MeV ^{12}C, ^{16}O, ^{28}Si and ^{63}Cu heavy ions through Si_3N_4as well as the energy region for 0.10–0.6 MeV/nucleon for ^{24}Mg, ^{27}Al and ^{28}Si ions in Formvar. The energy straggling values have been corrected from thickness variation and from the non-statistical component due to the energy dependency of stopping force. The discussion of obtained energy straggling is mainly based on the available data and the following theoretical and empirical predictions:

- Bohr straggling
- Bethe-Livingston's quantum theory
- Yang's empirical formula
- Straggling predicted by Bohr Stopping model
- Lindhard-Sharff model (free gas model and statistically independent excitations)
- Introduction of bunching effect by Firsov–Hvelplund expression according to the Besenbacher approach.

The comparison of our obtained energy straggling with theoretical predictions gives the following conclusions:

- The computed values of energy loss straggling based on the Bohr model or Lindhard-Scharff model or Bethe-Livingston model or Yang model underestimate considerably the obtained experimental data, proof of contribution of additional source of energy straggling in case of heavy ions at low energies.
- The discrepancy is attributed to the bunching of electrons into target atoms, charge exchange effect and molecular effect.
- The introduction of the bunching of electrons into target atoms gives an estimation of other effects such as charge exchange and molecular effect.
- The straggling due to charge exchange and molecular effect increases with atomic number Z of incident ion.

- The comparison of the new obtained data with the theoretical models serves as a reference for theoretical development on energy straggling, and then the theoretical and empirical prediction formulas are continually improved through the provision and analysis of experimental data.

Some basic tasks remain to be done in future with respect to the energy loss of heavy ions at low energy such as:

1. Production of new accurate data of fundamentals parameters describing the slowing down of heavy ions in matters for different couple ions-targets.

2. Correlation of the fitting parameters a and b (Eq.II.29) with atomic mass and atomic numbers of projectile and target element.

3. Calculation of charge exchange straggling by using empirical formulations or pure theoretical development.

References:

[All-2003] F. Allegrini, F. Robert, W. Schweingruber, P. Wurz, P. Bochsler, Nucl. Instr. and Meth. B 211 (2003) 487-494.

[Amm-2006] H. Ammi, R. Zemih, S. Mammeri, M. Allab, Rad. Effect. Defects Solids, 161(2006)339–346.

[And-1977] H.H. Andersen, J. F. Ziegler, the Stopping and Range of Ions in Matter, Vol. 3 (Pergamon, New York, 1977).

[Bes-1980]F. Besenbacher, J.U. Andersen, E. Bonderup, Nucl. Instr. Meth. 168 (1980)1–15.

[Bet-1930]H. A. Bethe, Ann. Physik. 397, 3, (1930) 325-400

[Bet-1972] H.D. Betz, Rev. Mod. Phys., vol.44, n°3 (1972) 465.

[Blo-1933] F. Bloch, Ann. Physik, 408, 3, (1933)285–320

[Boh-1913]N. Bohr, , Phil. Mag 25, (1913) 10

[Boh-1948] N. Bohr, K. Mat. Fys.Medd Dan. Vid. Selsk.18(8) (1948)1-144.

[Bon-1978] E. Bonderup, Penetration of charged particles through matter, lecture note, university of Aarhus Denemark (1978)

[Bou-1994] M. El Bouanani, M. Hult, L. Persson, E. Swietlicki, M. Andersson, M. Odstling, N. Lundberg, C. Zaring, D. D. Cohen, N. Dytlewski, P. N. Johnston, S. R. Walker, I. F. Bubb, H. J. Whitlow, Nucl. Instr. and Meth. B 94 (1994) 530-536

[Bro-1972]M.D. Brown, C.D. Moak, Phys. Rev. B6 (1972) 90.

[Bus-1980] F. Busch, W. Pfeffer, B. Kohlmeyer, D. Schüll, F. Pühlhoffer, Nucl. Instr. and Meth., 171 (1980) 71.

[But-1970] :G.W. Butler, A. M. Poskanzer , D.A. Landis, Nucl. Instr. and Meth. 89 (1970) 189

[Cel-2013] C.E. Celedón, E.D. Cantero, G.H. Lantschner, N.R. Arista, ,Nucl. Instr. Meth. B 315 (2013) 21–25.

[Chu-1975] W.K. Chu, J. F. Ziegler, J. *Appl. Phys.* 46 (1975)2768.

[Chu-1976] W. K. Chu, Phys. Rev. 13 (1976) 2057.

[Chu-1978] W.K. Chu, J. W. Mayer, M. A.Nicole, Backscattering spectrometry, Academic Press, New York (1978).

[Cur-1989] R. Curtis Bird , J. S. Williams, Ion Beams for Materials Analysis, Academic Press (1989)

[Dol-2009] G. Dollinger and A. Bergmaier in Handbook of Modern Ion Beam Materials Analysis, Editors Y. Wang and M. Nastasi, Materials Research Society (MRS), Warrendale, Pennsylvania(2009).

[Efk-1975] B. Efken, D. Hahn, D. Hilscher, G. Wüstenfeld, Nucl. Instr. andMeth. **129**(1975) 219.

[Fir-1957]O. B. Firsov, Sov. Phys. JETP, 5, N°6, (1957)1192-1196

[Fir-1958-a]O. B. Firsov, Sov. Phys. JETP, 6, N°3, (1958)534-537

[Fir-1958-b]O. B. Firsov, Sov. Phys. JETP, 34(7), N°2, (1958)308-311

[Fir-1959]O. B. Firsov, Sov. Phys. JETP, 36(9), N°5, (1959)1076-1080

[For-1976] J.S. Forster, D. Ward, H.R. Andrews, G.C. Ball, G.J. Costa, W.G. Davies et I.V. Mitchel, Nucl. Inst. Meth.136 (1976) 349.

[Gei-1983] H. Geissel, Y. Laichter, W. F. W. Schneider, P. Armbruster, Nucl. Instr.And Meth.215 (1983) 329-335

[Gel-1971] C. K. Gelbke, K. D. Hildenbrand, R. Bock, Nucl. Instr. and Meth. 95 (1971) 397-402.

[Gia-2008] S. Giangrandi, T. Sajavaara, K. Arstila, A. Vantomme, W. Vandervorst, Nucl. Instr. and Meth. B 266 (2008) 5144- 5150

[Glu-1979] G. Gloeckler, K.C. Hsieh, Nucl. Instr. and Meth. 165(1979) 537-544

[Gol-1950] H. Goldstein, C. Poole, J. Safko, Classical Mechanics, chapter 3, Addison-Wesley Publishing Company, Inc.(1980)first edition (1950)

[Gro-1983] R. Groleau, S. Gujrathi, J. Martin, Nucl. Instr. and Meth., 218 (1983) 11-15

[Gue-2014]A.Guesmia, H.Ammi, M.Msimanga, A.Dibb, S.Mammeri, C.A.Pineda-Vargas, M. Hedibel, Radiat. Phys. Chem. 96(2014)205–210.

[Gue-2014] A.Guesmia, H.Ammi, M.Msimanga, A.Dibb, S.Mammeri, C.A.Pineda-Vargas, M. Hedibel, Radiat. Phys. Chem. 96(2014)205–210.

[Guj-1996] S.C. Gujrathi, D. Poitras, J.E. Klemberg-Sapieha, L. Martinu, Nucl. Instr. and Meth. B 118 (1996) 560-565.

[Hak-1999] P. Hakansson, Brazilian Journal of Physics, vol. 29, no. 3, (1999)422-427

[Ham-1911] W. Hammer, ZeitschriftfürPhysik 12 (1911) 1077.

[Hel-2005], R. Hellborg, J. McKay , Particle Acceleration and Detection, Springer-Verlag Berlin Heidelberg (2005)

[Hin-1990]P. F. Hinrichsen, D. W. Hetherington, S. C. Gujrathi, L. Cliché, Nucl. Instr. and Meth.B 45 (1990) 275.

[Hin-2008] F. Hinterberger, Physics of particle accelerators and ion optics, Springer Vergla, Berlin (2008), Chapter 2. "Germany"

[Hua-1991] C. Huan-sheng, L. Xiang-yang, Y. Fujia, Nucl. Instrum. Methods in Phys. Res. B56–57(1991)749-752

[Hub-1989] F. Hubert, R. Bimbot, H. Gauvin, Semi-empirical formulae for heavy ion stopping powers in solids in the intermediate energy range, Nucl. Instr. and Meth. B 36, 4 (1989) 357-363

[Hus-2016] R. Huszank, L. Csedreki, Z. Kertesz, Z. Torok, Journal of Radioanalytical and Nuclear Chemistry 307(1) (2016)341-346

[Hve-1971] P. Hvelplund, Mat. Fys.Medd. Dan. Vid. Selsk, 38 (1971) no. 4.

[Jan-1988] C. Janicki, P.F. Hinrichsen, S.C. Gujrathi, J. Brebner, J.P. Martin, Nucl. Instr. and Meth.B 34 (1988) 484.

[Kim-1994] K. Kimura, K. Ohshima, M. Mannami, Applied Physics Letters 64 (1994) 2232.

[Kim-1998] J.K. Kim, Y.S. Kim, G.D. Kim, H.W. Choi, H.J. Woo, S.Y. Cho,C.N. Whang, Nucl. Instr. and Meth. B 140 (1998) 380-388.

[kno-2000] G. F. Knoll, Radiation Detection and Measurement, John Wiley & Sons, Inc, third edition (2000).

[Kra-1995] G. Kraft, U. Arndt a, W. Becher, D. Schardt, H. Stelzer, U. Weber, Th. Archinal, Nucl. Instr. and Meth. A 367 (1995) 66-70.pdf

[Kum-2015] S. Kumar, P.K. Diwan, Shyam Kumar, Radiat. Phys. Chem. 106 (2015) 21–25.

[Lec-1976] J. L'Ecuyer, C. Brassard, C. Cardinal, J. Chabbal, L. Deschêne, J.P. Labrie, B. Terrault, J. G. Martel, R. Jacques, J. Appl. Phys 47(1976)381-382.

[Lec-1979] J. L'Ecuyer, J.A. Davies, N. MatunamiNucl. Instrum. Methods 160(1979)337-346

[Lev-1976] R. F. Lever, proceedings of first Ion Beam Surface Layer Analysis, Edited by O. Meyer, G. Linker, F. Kappeler, 1(1976)111-123

[Lin-1953] J. Lindhard, M. Sharff, Mat. Fys.Medd. Dan. Vid. Selsk. 27 No. 15 (1953)

[Lin-1961]J. Lindhard and M. Scharff, Phys. Rev (1961)124-128.

[Lin-1963] J. Lindhard, M. Scharff, H.E. Schiott, Mat. Fys.Medd. Dan. Vid. Selsk. 33 (14), (1963) 1–42

[Liv-1937] M.S. Livingston, H.A. Bethe, Rev. Mod. Phys. 9 (1937) 245.

[May-1997] M. Mayer, SIMNRA User's Guide, Report IPP 9/113, Max-Planck-Institutfür Plasma physik, Garching, Germany, (1997)

[May-2002] M. Mayer, Nucl. Instr. Meth. B, 194 (2002) 177. http://www.simnra.com/.

[Mik-2015] R. Mikšová, V. Hnatowicz, A. Macková, P. Malinský, P. Slepička,Nucl. Instr. and Meth. B 354 (2015) 205-209.

[Mil-1971a] J.T. Milek, Silicon nitride for microelectronic applications, IFI Plenum, New York, (1971) Part1

[Mil-1971b] J.T. Milek, Silicon nitride for microelectronic applications, IFI Plenum, New York, (1971) Part2

[Mis-1995]P. Misaelides, Application of Particle and Laser Beams in Materials Technology, Springer Science (1995)

[Mon-1982] E.C. Montenegro, S.A. Cruz, and C. Vargas-Aburto, Phys. Lett. 92A, 195 (1982)

[Mon-1982] E.C. Montenegro, S.A. Cruz, and C. Vargas-Aburto, Phys. Lett. 92A, 195 (1982)

[Msi-2009] M. Msimanga, C.M. Comrie, C.A. Pineda-Vargas, S. Murray, R. Bark, G. Dollinger, Nucl. Instr. and Meth. B 267 (2009) 2671–2674.

[Msi-2010] M. Msimanga, Ph.D. Thesis, University of Cape Town (UCT), RSA, January 2010

[Nas-1996]:M. Nastasi, J. W. Mayer, J. K. Hirvonen, Ion-Solid Interactions: Fundamentals and applications, Cambridge University Press (1996)

[Nee-2009] Neetu, Pratibha, V. Sharma, P.K. Diwanand Shyam Kumar. Radiat, Meas. 44 (2009) 363-368

[Nor-1963] L.C.Northcliffe, Ann. Rev. Nucl. Sci. 13 (1963)67.

[Nor-1970] L.C. Northcliffe, R. F. Schilling, R.F., Range and stopping-power tables for heavy ions Nuclear Data Tables, 7, (1970) 233-463.

[Ori-2007] Origin 8 User Guide, OriginLab Corporation, Northampton, MA 01060 USA, (2007)

[Pas-1991] F. Pászti, E. Szilágyi, E. Kótai, Nucl. Instrum. Methods B54(1991)507-512

[Paul-2013]H. Paul, Stopping power for heavy, http://www.exphys.uni-linz.ac.at/stopping/

[Paul-2014] H. Paul, private communication (2014).

[Rut-1911] E. Rutherford, The scattering of α and β Particles by Matter and the structure of the Atom, Phil. Mag. 21 (1911) 669-688

[Sch-2000] M. Scholz, Nucl. Instr. and Meth.B 161-163 (2000) 76-82

[Schw-2003] K. Schwartz, C. Trautmann, R. Neumann, Nucl. Instr. and Meth. B 209 (2003) 73–84

[Sha-2002] A. Sharma, P.K Diwan, S. Kumar, S, K. Sharma, V.K. Mittal, S.V.S NageswaraRao, B. Sannakki, S. Ghosh, D. K. Avasthi, Nucl. Instr. and Meth.in Phys. Res. B 194 (2002) 7–14

[Sha-2002] A. Sharma, P.K Diwan, S. Kumar, S, K. Sharma, V.K. Mittal, S.V.S NageswaraRao, B. Sannakki, S. Ghosh, D. K. Avasthi, Nucl. Instr. and Meth.in Phys. Res. B 194 (2002) 7–14

[Sig-1976] P. Sigmund, Phys. Rev. A14 (1976) 996

[Sig-1978]P. Sigmund, Mat. Fys.Medd. Dan. Vid. Selsk. 40 (5) (1978).

[Sig-2006] P. Sigmund, Particle Penetration and Radiation Effects, Springer-Verlag Berlin Heidelberg (2006)

[Sig-2014] P. Sigmund, private communication

[Sik-2012] Z. Siketic, I. BogdanovicRadovic, Nucl. Instr. and Meth. B 296 (2013) 78–81.

[Ste-2010]T. Stefaan, Experimental Techniques in Nuclear and Particle Physics, Springer-Verlag Berlin Heidelberg (2010)

[Szi-1995] E. Szilágyi, F. Pászti and G. Amsel. Nucl. Instr. Meth. in Phys. Res. B 100 (1995) 103

[Tho-1983] J. Thomas, M. Fallavier, D. Ramdane, N. Chevarier, A. Chevarier, Nucl. Instr. and Meth. 218 (1983) 125-128.

[Til-1995] I. S. Tilinin, Phys. Rev. A 51 (1995) 3058.

[Tir-1996] J. Tirira, Y. Serruys, P. Trocellier, Forward Recoil Spectrometry: Application to Hydrogen Determination in Solids, Plenum Press, New York (1996).

[Tom-1983] J. Thomas, M. Fallavier, D. Ramdane, N. Chevarier, A. Chevarier, Nucl. Instr. and Meth., 218 (1983)125.

[Van-1960] R. J. Van-de-Graaff, Nucl. Instr. and Meth.8 (1960)195-202

[Van-1994] J. Van Aarle, W. Westmier, R. A. Esterlund, P. Patzelt, Nucl. Phys.A 578 (1994) 77.

[Van-1998] H. van Bebber, L. Borucki, K. Farzin, A.Z. Kiss, W.H. Schulte, Nucl. Instr.And Meth.136-138 (1998) 72-76.

[Ver-2007] H.R.Verma, Atomic and Nuclear Analytical Methods, Springer Berlin Heidelberg New York (2007)

[Wan-2009] Y. Wang, M. Nastasi, Handbook of Modern Ion Beam Materials Analysis 2nd Edition. Materials Research Society.**1** (2009)83-121.

[Wei-2002] H. Weick, A.H. Sørensen, H. Geissel, C. Scheidenberger, et al., Nucl. Instr. andMeth. **B 193**(2002)1.

[Wiz-1979] J. L. Wiza, Nucl. Instr. and Meth. 162(1979) 587-601.

[Yan-1991] Q. Yang, D.J. O'Connor, Z. Wang, Nucl. Instr. and Meth.B in Phys. Res. 61 (1991) 149.

[Zie-1977] J.F. Ziegler, Hydrogen Stopping Powers and Ranges in all Elements, vol.3, Pergamon, New York, 1977.

[Zie-1978] J. F. Ziegler, Nucl. Instr. and Meth.149 (1978) 129

[Zie-1985] J.F. Ziegler, J.P. Biersack and U. Littmark, The stopping and range of ions in solids, Pergamon, New York, 1985; TRIM/SRIM computer code, available at http://www.srim.org.

[Zie-2008]J. F. Ziegler, J. P. Biersack, and M. D.Ziegler, The Stopping and Range of Ions in Matter (Pergamon, New York, edition 2008).

[Zie-2013] J. F. Ziegler, The Stopping and Range of Ions in Matter (http://www.srim.org/, version SRIM-2013).

APPENDIX A

Description of the accelerator facilities

A.1- Accelerators at iThamba LABS

All applications or verification of the theoretical study of ion beam technique requires an accelerator device. "iThemba LABS" Laboratory for Accelerator Based Sciences provides three accelerator used for research and training in nuclear and accelerator physics, radiation biophysics, radiochemical and material sciences, radio nuclide production and radiotherapy:

i: Cyclotron able to produce up to 200 MeV of proton light and heavy ions.

ii: 5.5 MV Van-de-Graaff installed at Material Research department (see Fig.A.1). The Van de Graaff accelerator at iThemha LABS was manufactured by High Voltage Engineering Corporation, Burlington Massachusetts, U.S.A, and installed in 1962. In the aim of increasing the reliability of the beam, a major upgrade of whole facilities was started on 2002, a new console program was installed to display all the beam lines and their diagnostic components, focusing and steering elements visually.

iii: 6MV tandem accelerator (see Fig.A.2) hosting at iThemba LABS (Gauteng)able to produces a stable proton beam of up to 100 nA on target with the energy variable between 1.0 MeV and 12 MeV.

*Fig. A.1: Photo*general view*of the 6MV VDG at MRD iThemba LABS.*

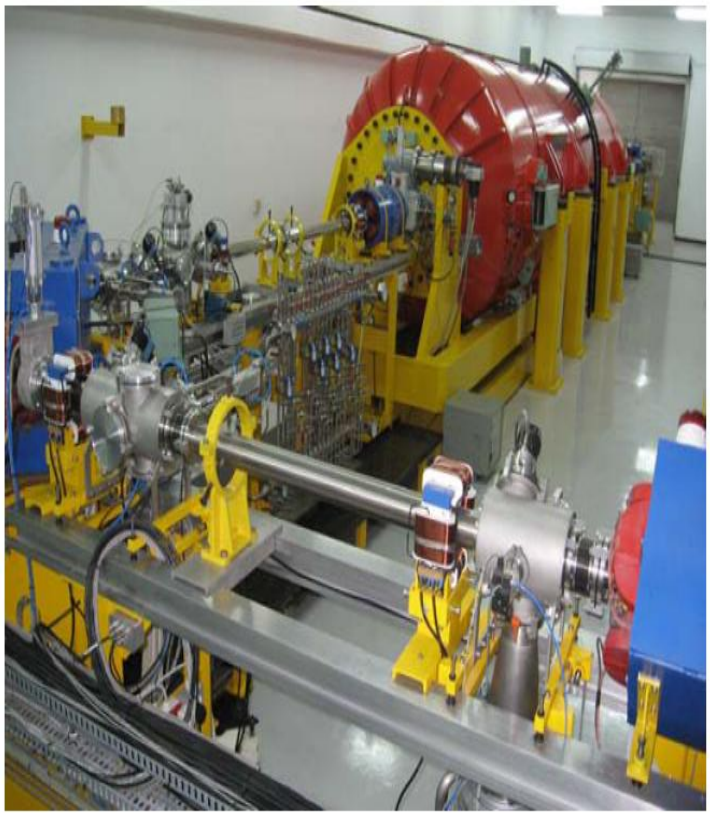

Fig. A.2: Photo of the EN Tandem accelerator of iThemba LABS where the HI-ERDA set up was installed around.

A.2- Description of the apparatus of Van De Graff generator

A.2.1 Physical principles

Van De Graff generator is an electrostatic generator capable producing high potential differences to be used for accelerate the charged particles. In 1931 Van De Graff [Gra-1931] was designed a voltage generator on the basis of the following three fundamental effects:

i-Triboelectricity effect: When two materials electrically neutral are in contact; there is a charge transfer which lead to obtaining two materials charged, one positively and another negatively. This transfer of electrical charges between different materials is called Triboelectricity phenomenon. For example when the molecule of vinyl (H_2C=C-H) is close enough to the molecule of glass it forms an electrochemical bond (new bigger molecule) by displacement of three electron from glass to vinyl, then the side of the vinyl molecule becomes negatively charged and the glass side positively charged. If one separates the molecules again the electrons don't go back again and then, the glass is positively charged and the vinyl is negatively charged.

ii- Corona Discharge phenomenon: A corona discharge occurs when a current is created between two electrodes at a high potential and separated by a neutral fluid, usually air, by ionizing that fluid. The discharge may be explained by the fact that when the electric field at a point of the fluid is sufficiently large, the fluid ionizes around this point and becomes a conductor. It should be noted that the intense electric field can be created at the points or corners of a charged object.

iii- At the equilibrium the electric charge of a charged conductor (Hollow or non-hollow) is distribute only on its outer surface.

A.2.2 The VDG components

The VDG consists of:

1- a large hollow sphere S mounted on insulated pillars T1 and T2

2- a flexible belt made of insulator like silk is make to run between two insulator pulleys P1 at the bottom and P2 at the top using an electric motor M.

3- C1 and C2 are two points conductors, C1 is a spray comb or brush connected to the earth ground voltage at the bottom, C2 is a collecting comb connected to the hollow sphere S at the top.

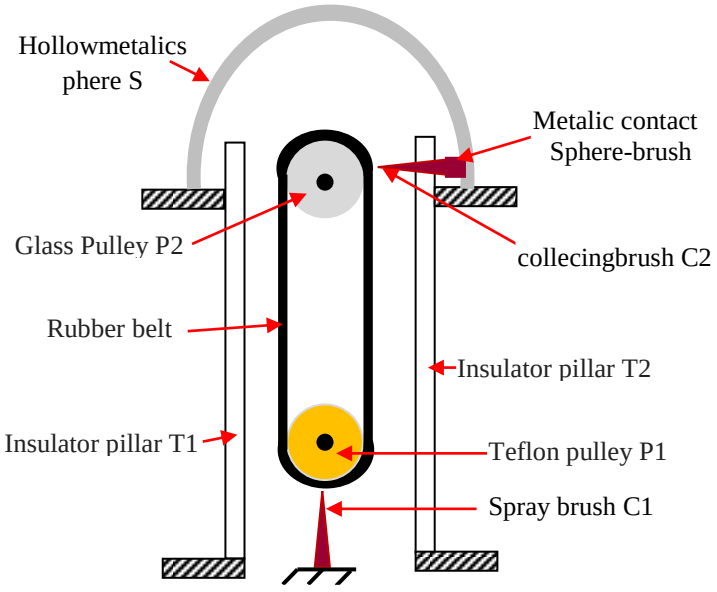

Fig. A.3: Schema of VDG

A.2.3. Operation of the VDG

First step:Charging the bottom roller by triboelectric effect (see Fig. A.4a):

When the motor is run the Teflon roller makes contact with the rubber belt and by triboelectric effect the belt become positively charged and the roller negatively charged.

Second step: Charging the outer surface of the belt (see Fig. A.4b): The negative charge on the Teflon pulley create an electric field who pushes the electrons on the spry brush to the earth ground and then a strong electric field arise between the sharp head of the spry brush and the pulley, the atoms of air in this strong field loss some electrons (one or more) who are going to the spry brush and after to the earth ground (Corona Discharge phenomenon). Then the air become positively ionized, eventually some ions arrive on the rear of the belt. In this second step the outer surface of the belt is charged positively by spry brush via corona effect.

Third step: interaction between the top pulley and the belt (see Fig. A.4c):

The second pulley is made of glass then it has tendency to loss electrons to the rubber belt, but inner of the rubber belt is positively charged then when the belt breaks contact with the pulley it takes some electrons make then the pulley charged positively.

Forth step: moving charge between the belt and the top brush (see Fig. A.4d)**:**

Now, outer the belt which is positively charged an electric field attract the electrons of the brush to the sharp head then the two charges create a strong field (corona effect) then the atoms of air like step 2 become ionized negatively (the electrons coming to the air because they are relatively free)

Fifth step: The metallic sphere which is in contact with the brush give up their free electron needed by the brush, then the sphere become charged positively at high potential V up to 55 million volts for the VDG of MRD at iThemba LABS.

If an ionized particle, with charge Ze, was introduced in the interior of VDG, it would move along the electric field generated by the large potential difference V.

The resulting particle had kinetic energy: E_0=ZeV

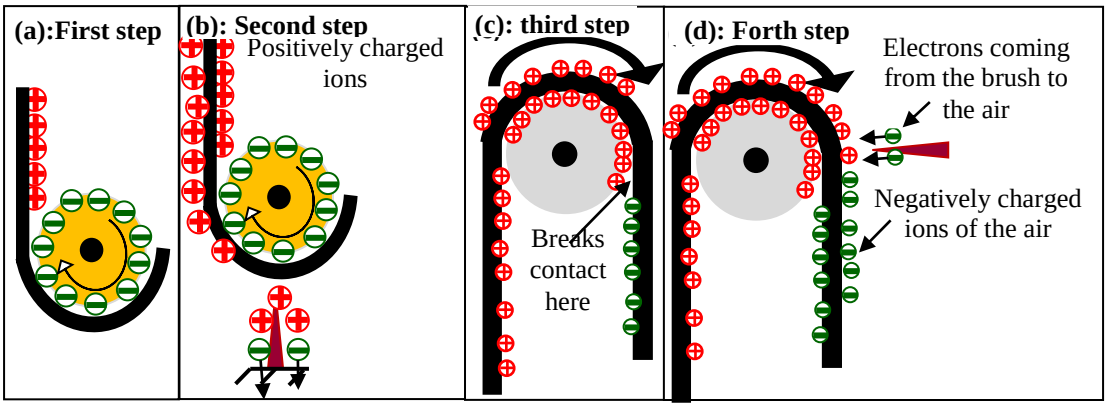

Fig. A.4: Operating principle of VDG

A.3.Tandem accelerator

In the following text a brief description of the operating principle of tandem accelerators used throughout our experimental work at iThemba LABS is presented.

The concept of the Tandem accelerator was invented in the aim to obtain beam energies of two or more times than that available in single acceleration [Van-1960]. Fig.A.5 shows the tandem accelerator including the basic elements of the high-voltage system. The tandem system is constructed of the following main components: ion sources, Mass analyzer magnet, focusing system at the entrance of the accelerator, tandem accelerator, focusing system at the exit of the tandem, switching magnet to direct the beam at different lines. Negative ions created by ion source (I) pass through the mass analyzer magnet (A) for isotopic separation. Selected ions are then accelerating in the first tube of the tandem from ground potential to a high positive voltage in the middle of the tandem terminal. In the middle of the accelerator a stripper system (very thin foil of carbon or nitrogen gas) hunting electrons from the negative ions and becomes positive ions. Then these positive charges accelerate a second time in the second tube straight to the ground potential, hence the name of tandem. Tandem accelerators can reliably produce continuous particle beams with currents up to 0.1 mA.

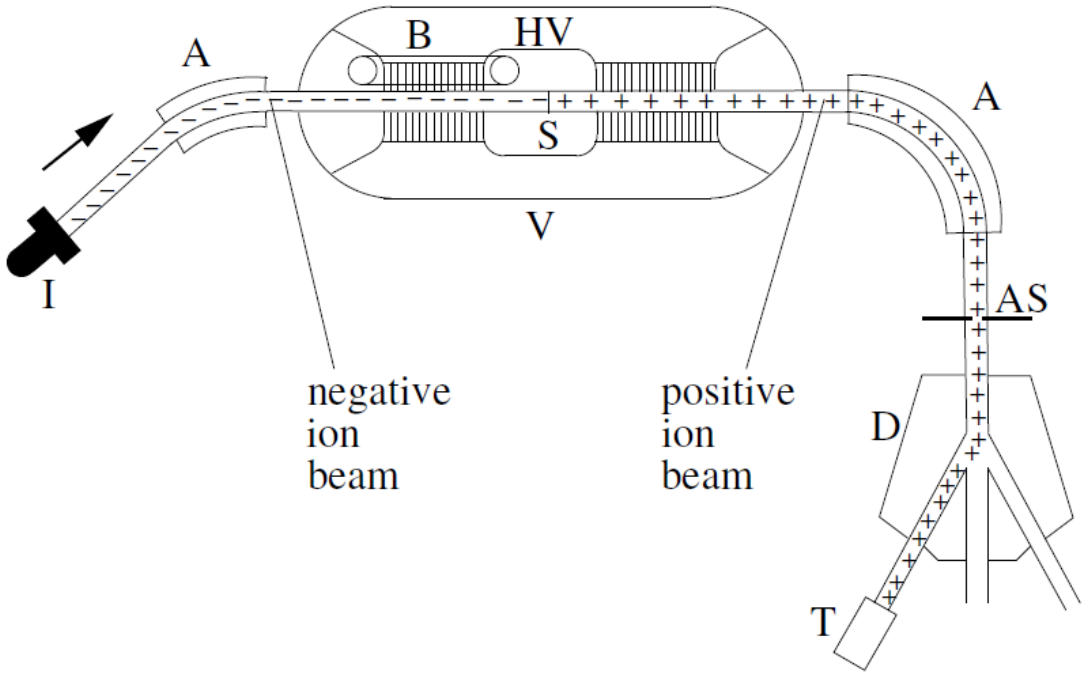

Fig. A.5: System arrangement of the tandem accelerator. I: ion sources, A: mass analyzer, V: vessel of the tandem, D: deflecting magnet, T: the HI-ERDA arrangement for example. Source [Hin-2008]

A.4.The layout of the 5.5 MeV accelerator at the MRD, iThemba LABS, Cape

Figure A.6 shows the layout of the 5.5 MeV accelerator at the Material Research Department, iThemba LABS, Cape Town, including all the beamlines used for Ion Beam Analysis. The 30° beamline B is devoted for normal RBS as well as in situ Real time RBS.

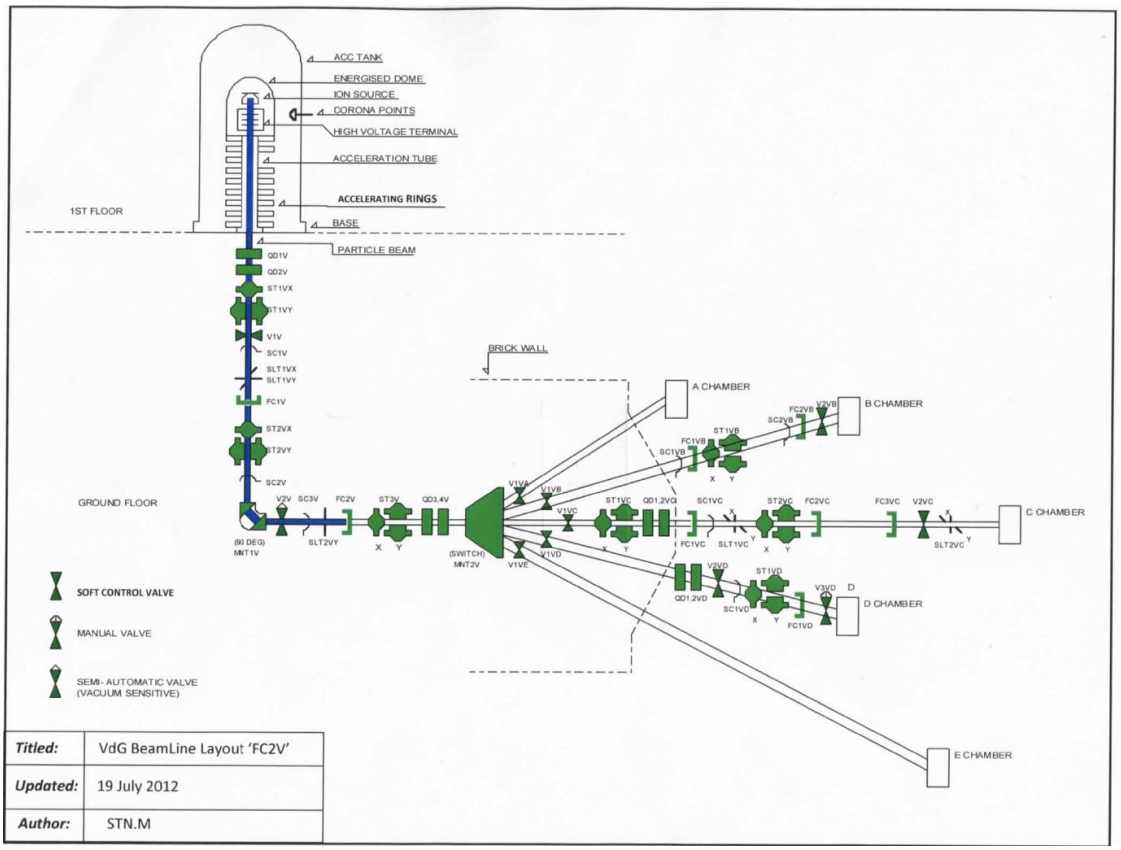

Fig. A.6: A plan view of the layout of the VDG accelerator beamlines at MRD

APPENDIX B

Energy E before scattering

In the chapter 4, we have seen the relation between the energy of the detected backscattered particle (abscissa of an energy spectrum) and the depth within the mono-isotopic sample where the backscattering events occurred.I n this appendix we enumerate some methods to find the energy E before scattering. The notations are the same as chapter 3. Note that we deal always in spirit of constancy of $\frac{dE}{dx}$ **over each path** and the value of $KE_0 - E^*$ is given experimentally.

F.1 Energy Loss Ratio Method

Lever et al [Lev-1976] assume that the ratio γ of the energy lost along the outward path ΔE_{out} to that lost along the inward track ΔE_{out} is independent of depth,

$$\gamma = \frac{\Delta E_{out}}{\Delta E_{in}} = \frac{KE - E^*}{E_0 - E} = const \quad \text{(F.1)}$$

$$\text{Then, } E = \frac{E^* + \gamma E_0}{K + \gamma} \quad \text{(F.2)}$$

We can use the surface energy approximation to find an approximate value of γ:

$\frac{E_0 - E}{d/cos\alpha} = S(E_0)$and $\frac{KE - E^*}{d/cos\beta} = S(KE_0)$, then

$$\gamma \cong \frac{S(KE_0)}{S(E_0)} \frac{cos\alpha}{cos\beta} \quad \text{(F.3)}$$

So, we have now an estimation of the energy E before scattering, which can used in the mean energy approximation Eq. IV.23-a-c.

F.2 Iterative Method for obtaining d by mean energy approximation

- **First step: surface energy approximation**

$\overline{E_{in}} \cong E_0\overline{E_{out}} \cong KE_0and\left[\overline{S}\right] = [S_0] = \left[\frac{K}{cos\theta_1} S(E)|_{E_0} + \frac{1}{cos\theta_2} S(E)|_{KE_0}\right]$

→ Obtain a zero-order depth d at which scattering appears by using Eq. IV.20-a

$$\Delta E = KE_0 - E^* = [S]d \quad \text{(IV.20-a)}$$

→then by use of Eq. IV.18-a :

$$\frac{d}{cos\alpha} = \frac{1}{S(E_0)|_{in}} (E_0 - E) \quad \text{(IV.18-a)}$$

to obtain a zero-order value of E=$_0$E

- **Second step:** by use of$_0$E in Eq. IV.23-c to obtain an improved value $_1\overline{E_{in}}$ and $_1\overline{E_{out}}$

$$\overline{E_{in}} = \frac{1}{2}(E_0 + E) \text{and} \overline{E_{out}} = \frac{1}{2}(KE + E^*) \quad \text{(IV.23-c)}$$

Then $_1\overline{E_{in}}$ and $_1\overline{E_{out}}$ define the first order $_1\left[\overline{S}\right]$ by Eq. IV.23-a

$$\left[\overline{S}\right] = \left[\frac{K}{\alpha} S(E)|_{\overline{E_{in}}} + \frac{1}{\beta} S(E)|_{\overline{E_{out}}}\right] \quad \text{(IV.23-a)}$$

And so on to obtain a better d, E and [S]. In principle this iterative process converges.

F.3 Analytical methods

This method was proposed by Chu and Ziegler [Chu-1975]:

$$\frac{E_0-E}{KE-E^*}=\frac{S(E)|_{in}}{S(E)|_{out}}\frac{cos\beta}{cos\alpha}=\frac{\varepsilon(\overline{E_{in}})}{\varepsilon(\overline{E_{out}})}\frac{cos\beta}{cos\alpha} \quad \text{(F.4)}$$

The Taylor expansion of ε gives:

$$\varepsilon(\overline{E_{in}})=\varepsilon(E_0)-\frac{1}{2}(E_0-E)\varepsilon'(E_0)+\cdots \quad \text{(F.5)}$$

$$\varepsilon(\overline{E_{out}})=\varepsilon(E^*)+\frac{1}{2}(KE-E^*)\varepsilon'(E^*)+\cdots \quad \text{(F.6)}$$

By substituting Eq. F.2 and Eq. F.3 in Eq. F.3, we obtain:

$$aE^2+bE+c=0 \quad \text{(F.7)}$$

where,

$$a=\frac{1}{2}K\left[\varepsilon'(E_0)\frac{cos\beta}{cos\alpha}+\varepsilon'(E^*)\right] \quad \text{(F.8)}$$

$$b=\left[K\varepsilon(E_0)\frac{cos\beta}{cos\alpha}+\varepsilon(E^*)\right]-\frac{1}{2}(KE_0+E^*)\left[\varepsilon'(E_0)\frac{cos\beta}{cos\alpha}+\varepsilon'(E^*)\right] \quad \text{(F.9)}$$

$$c=\frac{1}{2}E_0E^*\left[\varepsilon'(E_0)\frac{cos\beta}{cos\alpha}+\varepsilon'(E^*)\right]-E_0\varepsilon(E^*)-E^*\varepsilon(E_0)\frac{cos\beta}{cos\alpha} \quad \text{(F.10)}$$

The values of ε and ε' are tabulated or deduced from a semi-empirical formula.

F.4 Numerical method

In fact the assumption of constancy of $\frac{dE}{dx}$ over each path is a good approximation for very small depth d, when the depth is not very small then we divide it into many slabs of equal width Δx where we can consider $\frac{dE}{dx}$ constant over each path (see Fig. F.1).

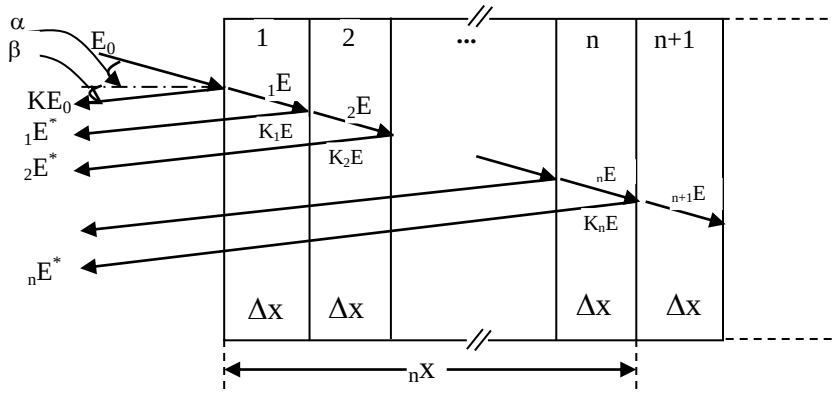

Fig. F.1: Schema of the subdivision of a layer into n sub-layer of width Δx, for calculation of the energy $E^*={}_nE^*$ before scattering at the depth $d=x_n$.

First step: **incoming path**: The calculation start from the first sub-layer of thickness Δx situated at the surface.

The energy ${}_{i+1}E$ of incoming beam at the entrance to the (i+2)th sub-layer is related to the incoming beam energy ${}_iE$ at the entrance to the (i+1)th sub-layer by:

$${}_{i+1}E={}_iE-\left.\frac{dE}{dx}\right|_{{}_iE}\left(\frac{\Delta x}{cos\alpha}\right) \quad \text{(F.11)}$$

Note that ${}_0E = E_0$; in this way we obtain the energy of the incident particles before scattering at each sub-layer. From the recursion relation Eq. F.11, we obtain the energy of the incident ions before scattering from any slab boundary i.

Second step: **outgoingpath**:

The energy lost in each tranche is equal to the production of the stopping power dE/dx (evaluated at this tranche surface approximation or mean energy in this tranche, we can choose one of them, I adopt the surface approximation) with effective path length $\frac{d}{cos\theta_2}$. We have:

$$ {}_1E^* = K\ {}_1E - \frac{\Delta x}{cos\beta}\frac{dE}{dx}\Big|_{K\ {}_1E} \tag{F.12-a} $$

$$ {}_{ret2}E^{out}_{2\to1} = K\ {}_2E - \frac{\Delta x}{cos\beta}\frac{dE}{dx}\Big|_{K\ {}_2E} \tag{F.12-i1} $$

$$ {}_2E^* = {}_{ret2}E^{out}_{2\to1} - \frac{\Delta x}{cos\beta}\frac{dE}{dx}\Big|_{{}_{ret2}E^{out}_{2\to1}} \tag{F.12-i2} $$

(F.12-i1)+(F.12-i2)→

$$ {}_2E^* = K\ {}_2E - \frac{\Delta x}{cos\beta}\frac{dE}{dx}\Big|_{K\ {}_2E} - \frac{\Delta x}{cos\beta}\frac{dE}{dx}\Big|_{{}_{ret2}E^{out}_{2\to1}} \tag{F.12-b} $$

$$ {}_{ret3}E^{out}_{3\to2} = K\ {}_3E - \frac{\Delta x}{cos\beta}\frac{dE}{dx}\Big|_{K\ {}_3E} \tag{F.9-ii1} $$

$$ {}_{ret3}E^{out}_{2\to1} = {}_{ret3}E^{out}_{3\to2} - \frac{\Delta x}{cos\beta}\frac{dE}{dx}\Big|_{{}_{ret3}E^{out}_{3\to2}} \tag{F.12-ii2} $$

$$ {}_3E^* = {}_{ret3}E^{out}_{2\to1} - \frac{\Delta x}{cos\beta}\frac{dE}{dx}\Big|_{{}_{ret3}E^{out}_{2\to1}} \tag{F.12-ii3} $$

(F.12-ii1)+(F.12-ii2)+(F.12-ii3)→

$$ {}_3E^* = K\ {}_3E - \frac{\Delta x}{cos\beta}\frac{dE}{dx}\Big|_{K\ {}_3E} - \frac{\Delta x}{cos\beta}\frac{dE}{dx}\Big|_{{}_{ret3}E^{out}_{3\to2}} - \frac{\Delta x}{cos\beta}\frac{dE}{dx}\Big|_{{}_{ret3}E^{out}_{2\to1}} \tag{F.12-c} $$

In the same manner we have:

$$ {}_{ret4}E^{out}_{4\to3} = K\ {}_4E - \frac{\Delta x}{cos\beta}\frac{dE}{dx}\Big|_{K\ {}_4E} \tag{F.12-iii1} $$

$$ {}_{ret4}E^{out}_{3\to2} = {}_{ret4}E^{out}_{4\to3} - \frac{\Delta x}{cos\beta}\frac{dE}{dx}\Big|_{{}_{ret4}E^{out}_{4\to3}} \tag{F.12-iii2} $$

$$ {}_{ret4}E^{out}_{2\to1} = {}_{ret4}E^{out}_{3\to2} - \frac{\Delta x}{cos\beta}\frac{dE}{dx}\Big|_{{}_{ret4}E^{out}_{3\to2}} \tag{F.12-iii3} $$

$$ {}_4E^* = {}_{ret4}E^{out}_{2\to1} - \frac{\Delta x}{cos\beta}\frac{dE}{dx}\Big|_{{}_{ret4}E^{out}_{2\to1}} \tag{F.12-iii4} $$

(F.12-iii1)+(F.12-iii2)+(F.12-iii3)+(F.12-iii4)→

$$ {}_4E^* = K\ {}_4E - \frac{\Delta x}{cos\beta}\frac{dE}{dx}\Big|_{K\ {}_4E} - \frac{\Delta x}{cos\beta}\frac{dE}{dx}\Big|_{{}_{ret4}E^{out}_{4\to3}} - \frac{\Delta x}{cos\beta}\frac{dE}{dx}\Big|_{{}_{ret4}E^{out}_{3\to2}} - \frac{\Delta x}{cos\beta}\frac{dE}{dx}\Big|_{{}_{ret4}E^{out}_{2\to1}} \tag{F.12-d} $$

And so on, we obtain $\mathbf{E^* \cong_n E^*}$.

Nuclear Instruments and Methods in Physics Research B 371 (2016) 69–75

Contents lists available at ScienceDirect

Nuclear Instruments and Methods in Physics Research B

journal homepage: www.elsevier.com/locate/nimb

Slowing down of 2–11 MeV ^{12}C, ^{16}O, ^{28}Si and ^{63}Cu heavy ions through Si_3N_4 thin foil by using Time-of-Flight spectrometry

A. Guesmia [a,c,f,*], M. Msimanga [b], C.A. Pineda-Vargas [a,d], H. Ammi [e], A. Dib [e], S. Mammeri [e]

[a] iThemba LABS, National Research Foundation, P.O. Box 722, Somerset West 7129, South Africa
[b] Physics Department, Tshwane University of Technology, P Bag X 680, Pretoria 0001, South Africa
[c] Departement de physique, Faculté des Sciences Université Saad Dahleb, B. P. 270, Route de Soumaa, Blida, Algeria
[d] Faculty of Health and Wellness Sciences, CPUT, P.O. Box 1906, Bellville 7535, South Africa
[e] Centre de Recherche Nucleaire d'Alger, 2 Bd. Frantz Fanon, B. P. 399, Alger-Gare, Algiers, Algeria
[f] Departement de physique, Faculté des Sciences Université M'hamedBougara, Boumerdes, Algeria

ARTICLE INFO

Article history:
Received 30 June 2015
Received in revised form 23 October 2015
Accepted 27 October 2015
Available online 23 November 2015

Keywords:
Electronic stopping power
Straggling
LSS theory
Time-of-Flight
HI-ERDA

ABSTRACT

The stopping force and the energy-loss straggling of ^{63}Cu, ^{28}Si, ^{16}O and ^{12}C partially stripped heavy ions crossing silicon nitride foil has been determined over a continuous range of energies 2–11 MeV, by using a method based on the Heavy Ion-Elastic Recoil Detection Analysis (HI-ERDA) technique using a Time of Flight (ToF) spectrometer. The obtained energy loss straggling values corrected for non-statistical straggling and the thickness variation using the Besenbacher's method have been analyzed and compared with the corresponding computed values. For computed electronic straggling we have used alternatively the widely used formulations such as, the universal Bohr straggling deduced from the Bohr stopping model, and the Lindhard–Scharff formula including the Bunching effect given by Hvelplund–Firsov formula according to the Besenbacher approach. The aim of such comparison is to check the reliability and accuracy of the existing energy loss straggling formulations, in the light of the present experimental results. The experimental results of energy loss straggling of all ions are found to be greater than those predicted by the Bohr stopping model or Lindhard–Scharff prediction model. The introduction of the bunching effect improves the comparison and gives an estimation of other effects such as charge exchange.

© 2015 Elsevier B.V. All rights reserved.

1. Introduction

Conceptually the complex phenomenon of the slowing down of energetic charged particles through matter is described by the average energy loss per path length (dE/dx) called stopping force and by the average square fluctuation (standard deviation Ω) of the energy loss distribution commonly called the energy straggling. Accurate information of these parameters is important for wide areas of ion beam applications, such as ion beam analysis, ion material modification, fundamental particle physics, nuclear physics, radiology etc. These two fundamental parameters are indispensable for any applications of ion beam and have been studied experimentally and theoretically since the beginning of the 20th century [1–3]. In the literature stopping force has received more intensive attention in comparison to energy straggling, especially at low energy where significant discrepancies are reported by different groups [4].

In the case of the Bethe stopping force region and for non-relativistic velocities, Bethe and Livingston [5] developed an accurate quantum expression of energy straggling including binding of electrons by using a quantum mechanical perturbation treatment. At high velocities much larger than the Bohr velocity v_0, all electrons are stripped from the incident ion and by considering the target as free electrons at rest, Bohr in 1948 found a simple energy-independent formula proportional to the target thickness for energy straggling [6] applicable for light ions. At high velocity and for small energy losses the Bohr expression describes reasonably the energy straggling of ions in matter and is roughly in conformity with experimental available data [7]. However at low velocity less than $v_0 Z_{ion}^{2/3}$, both theoretical and experimental studies of stopping force and energy straggling present several difficulties. At low energy theoretical investigations are complicated by the necessity of taking into account the scattering of ions by atoms (nuclear) which cannot be considered independent of the

* Corresponding author at: Departement de physique, Faculté des Sciences Université M'hamedBougara, Boumerdes, Algeria. Tel.: +213 773201773.
E-mail addresses: guesmia@tlabs.ac.za, guesssmia@hotmail.fr (A. Guesmia).

http://dx.doi.org/10.1016/j.nimb.2015.10.058
0168-583X/© 2015 Elsevier B.V. All rights reserved.

electronic collision [8] and the difficulties associated to the charge exchange effects [3,9]. On the other hand, the most accurate experimental method of direct transmission for determination of stopping force and straggling at low energy requires preparation of very thin foils, which present additional problems such as foil roughness [10]. At low beam energy, where the Bohr approximation is not expected to be suitable, Lindhard and Scharff [11] by considering independent excitations of an electron gas introduced a new expression of energy straggling without taking into account the charge exchange aspect and bunching effect. The experimental values of straggling are in several cases unsatisfactory for all theories mentioned above, as discussed by Besenbacher et al. [12]. Geissel et al. [7] and Kumar et al. [13] indicate that the measured experimental values of energy straggling can fluctuate between 2 to 6 times the theoretical predicted values. The treatment of the stopper material as an electron gas ignores the fact that the electrons are bunching into atoms which cause an additional fluctuation in the number of encounters with atoms. This spatial correlation of bunching effect and charge exchange effect has been extensively discussed by Sigmund [14–16]. The introduction of these spatial correlations in energy straggling for the partially stripped heavy ions can explain the increase of energy straggling above the Bohr straggling.

In the present work we investigated stopping force and energy straggling of ^{12}C, ^{16}O, ^{28}Si and ^{63}Cu heavy ions in silicon nitride (Si_3N_4) in the energy rang 2–11 MeV, within a relative energy loss 5–38%. We have used a powerful method based on the combination of Time-of-Flight (ToF) spectrometer and elastic recoil detection analysis (ERDA) to deduce the stopping force and the energy straggling. The new set of stopping force and energy straggling data of heavy ions in Si_3N_4 gives important information of the use of Si_3N_4 as an exit window for ion beams in air. The obtained values of stopping force are compared with the predicted values obtained from the Stopping and Range of Ions in Matter program SRIM-2013 [17] and Lindhard, Scharff and Schiott (LSS) formula [18], as well as the available experimental data from the literature [19,20]. The energy straggling values are compared with theoretical prediction of straggling Bohr model and Lindhard–Scharff formula corrected by introducing the bunching effect according to the Besenbacher approach [12].

2. Energy loss straggling formulations

Consider an ion beam of velocity v, energy E, charge Z_1, and mass M_1 penetratesa target material of thickness Δx consisting of randomly distributed atoms with density N atoms per unit volume, atomic number Z_2 and atomic mass M_2. As the ions move within the target material, they will undergo collisions with the target nuclei and electrons, losing an average energy $\overline{\Delta E}$ accompanied by a statistical fluctuation in the energy loss called straggling phenomenon of energy loss. We consider the most used situation where the distribution in energy loss is approximately a Gaussian, following Mayer [21], this situation is realized when the relative energy loss is between 10% and 50% $\left(10\% < \frac{\overline{\Delta E}}{E} < 50\%\right)$. For loss of energy characterized by individual transfer of energy T with differential cross section $d\sigma(E,T)$, the average square fluctuation on the thickness Δx (standard deviation Ω) of the energy loss distribution is given by [6]:

$$\Omega^2 = \langle(\Delta E - \langle\Delta E\rangle)^2\rangle = N\Delta x \int T^2 d\sigma(E,T) \tag{1}$$

The energy loss straggling δE is measured by the full width at half maximum (FWHM) of the energy loss distribution: $\delta E = 2\sqrt{2\ln 2}\Omega = 2.35482\Omega$.

For fast no relativistic ions, by using the Rutherford cross section which considers free electrons at rest, implicitly neglecting the binding energies of electrons and their orbital velocity, Bohr [6] found the electronic energy-loss straggling in an elemental target as:

$$\Omega^2_{elec} = \Omega^2_B = 4\pi Z_1^2 Z_2 e^4 N\Delta x \tag{2}$$

$$\Omega^2_B[\mathrm{keV}^2] = 0.26 Z_1^2 Z_2 \Delta x[10^{18}\ \mathrm{atoms/cm}^2]$$

where e is the charge of the electron. This expression is commonly called Bohr straggling.

In an attempt to improve the Bohr formula (Eq. (2)) when the velocity v of the incident ion becomes comparable to the orbital velocity of the electrons in the stopper material, the Bohr formula is modified by considering only the contribution of electron with velocity lower than v [12]:

$$\Omega^2_{BB} = \Omega^2_B 2\frac{v}{v_0} Z_2^{-2/3} \tag{3}$$

where v_0 is the Bohr velocity.

The real improvement of the Bohr formula is made by describing the target's electron as an oscillator binding to its nucleus and using the approximation that the incident ion does not change its initial direction to obtain the straggling predicted by the Bohr stopping model calculated by Sigmund [16]:

$$\Omega^2_{BM} = \Omega^2_B \left[\frac{1}{1+(b/2p_0)^2} + \frac{2}{y^2}\int_{x_0}^{\infty} x\left[K_0^2(x) + K_1^2(x)\right]^2\right] dx \tag{4}$$

where,

$$b = \frac{2Z_1 \times 1e^2}{m_e v^2},\ y = \frac{m v^3}{Z_1 e^2 \omega_0},\ x = \frac{p\omega_0}{v},\ x_0 = \frac{p_0\omega_0}{v},$$

$I = \hbar\omega_0$, I is the mean excitation energy of the target atom, K_0 and K_1 are the modified Bessel functions of 2nd kind.

The expression (Eq. (4)) is evaluated numerically [16].

Also, Lindhard and Scharff [11] made an effort to improve the Bohr straggling expression at low velocity by considering the target atom as free electron gas and statistically independent excitations of electrons, which gave rise to the following expression for energy loss straggling valid at low velocities ($v < \sqrt{3Z_2}v_0$):

$$\Omega^2_{LS} = \frac{1}{2}\Omega^2_B\left[1.36\frac{v}{v_0}\frac{1}{\sqrt{Z_2}} - 0.016\left(\frac{v}{v_0}\right)^3\frac{1}{Z_2^{3/2}}\right] \tag{5}$$

The previous formulas of energy straggling ignore the fact that the target's electrons are bunching into atoms. This fact affects the fluctuation in the number of encounters with atoms, in such a way that additional straggling arises. This spatial correlation of bunching effect which is much less studied in the literature has been extensively discussed by Sigmund [14–16]. After Besenbacher et al. [12] if we limit only to the spatial correlation due to the bunching effect for a monatomic gas the straggling is a combination of Lindhard–Scharff straggling and the Firsov–Hvelplund expression [8]:

$$\Omega^2_{The} = \Omega^2_{LS} + \Omega^2_A \tag{6}$$

where (for $v < v_0 Z_2^{2/3}$).

$$\Omega^2_A = N\Delta x 8(Z_1+Z_2)^{8/3}10^{-15}\left(\frac{v}{v_0}\right)^2\ \mathrm{eV^2\ cm^2/atom} \tag{7}$$

3. Experiment

3.1. Experimental set up

The measurements presented in this work were carried out at the 6MV EN Tandem accelerator based at iThemba LABS, Gauteng, South Africa. The experimental arrangement is illustrated schematically in Fig. 1. Since the detailed description of the experimental setup can be found in our previous publications [24–25], we give here a brief description and we focus on the determination method of the energy-loss straggling.

A 26 MeV heavy ion beam of ^{63}Cu coming from the Tandem, bombards alternatively a variety of thick samples of C (graphite) and SiO_2 at grazing incidence angle of 15°, to recoil ^{16}O, Si, and C ions. The recoiled ions and the scattered ions of copper pass through the Time of Flight Energy (ToF-E) detector system as illustrated in Fig. 1. The ToF-E spectrometer consists of a Time of Flight detector, built from two timing detectors, T_1 and T_2, separated by a flight distance of 0.6 m, and a silicon surface barrier detector (SBD) positioned at 6.5 cm behind the second time detector for energy measurement. The stopping foil of silicon nitride (Si_3N_4) is alternatively mounted between the second time detector T_2 and the SBD. The energy of individual ions (scattered or recoiled), before passing through the Si_3N_4 foil is recorded by ToF system. At each round of measurement, with or without Si_3N_4 foil, the ions, energies are tagged by the SBD detector. The SBD plays two roles, first is to record the energy signal, and second is to set the triggering coincidence between the two timing detectors and the recorded signal by the SBD.

3.2. Foil

The silicon nitride, Si_3N_4, foil used in our work was manufactured by "Silson Limited" without polymeric support. The foil has a circular form and mean thickness of 500 nm as declared by the manufacturer. The thickness was verified by RBS method using 2 MeV He^+ ion beam at several areas of the foil. From analysis of RBS spectra using the SIMNA code [21], we find practically no deviation from the nominal stoichiometry with the following atomic ratios: Si (0.44) N (0.56) and thicknesses: 4650×10^{15} at cm^{-2}. For precise stopping force and energy straggling measurements, a precise knowledge of the thickness uniformity of the target is required. Therefore topography of this foil was carried out using an Atomic Force Microscope (AFM), scanning on several regions of the foil. The mean surface roughness of the scanned area was estimate to be σ = 1.0 nm.

4. Data analysis and results

In order to explain the method of data analysis adopted in this work, the carbon ion is given as an illustration (see Fig. 2). In the first round (without foil), each tagged energy E by the SBD detector, corresponds to the energy E_2 of the recoil/scattered ions recorded by the time of flight ToF_2 between the timing detectors. In the second round (with foil) the same tagged value E corresponds to the energy E_1 of the recoil/scattered ions recorded by the ToF (ToF_1) between the timing detectors before traversing the foil.

Fig. 2 shows the overlaid raw ToF-E coincidence spectra of recoiled/scattered ions with and without foil placed in front of the SBD. We have (see Fig. 2):

$$E = \frac{1}{2}m\left(\frac{L}{ToF_2}\right)^2 \text{ and } E = \frac{1}{2}m\left(\frac{L}{ToF_1}\right)^2 - \Delta E \tag{8}$$

where ΔE is the energy loss, m the mass of recoiled/scattered ions and L the distance of flight between the two timing detectors. Therefore, the energy loss l of the recoil (or scatter) ion after passing through the stopper foil is then given by:

$$\Delta E = E_1 - E_2 = \frac{1}{2}m\left(\frac{L}{ToF_1}\right)^2 - \frac{1}{2}m\left(\frac{L}{ToF_2}\right)^2 \tag{9}$$

We deduce the experimental stopping force S:

$$S\left(\bar{E} = \frac{E_1 + E_2}{2}\right) = \frac{\Delta E}{\Delta x} \tag{10}$$

where Δx refers to the linear thickness of the Si_3N_4 foil.

In this experiment the energy spectra of E_1 and E_2 have been found nearly Gaussian in shape with standard deviation Ω_1 and Ω_2 respectively (see Fig. 2). The values of Ω_1 and Ω_2 are deduced from the ToF projection spectra (see Fig. 2) by using the following formula:

$$\Omega_i = 2\frac{\Omega_{i(ToF)}}{ToF_i}E_i \quad i = 1,2 \tag{11}$$

where $\Omega_{i(ToF)}$ is the standard deviation of the ToF projection spectra. The experimental total energy loss straggling δE is evaluated from the half widths of the two spectra:

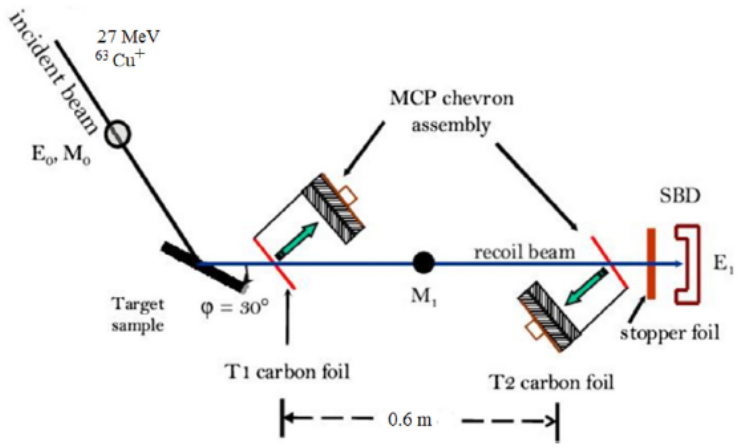

Fig. 1. Schematic setup of ToF–ERDA spectrometer at iThemba Labs.

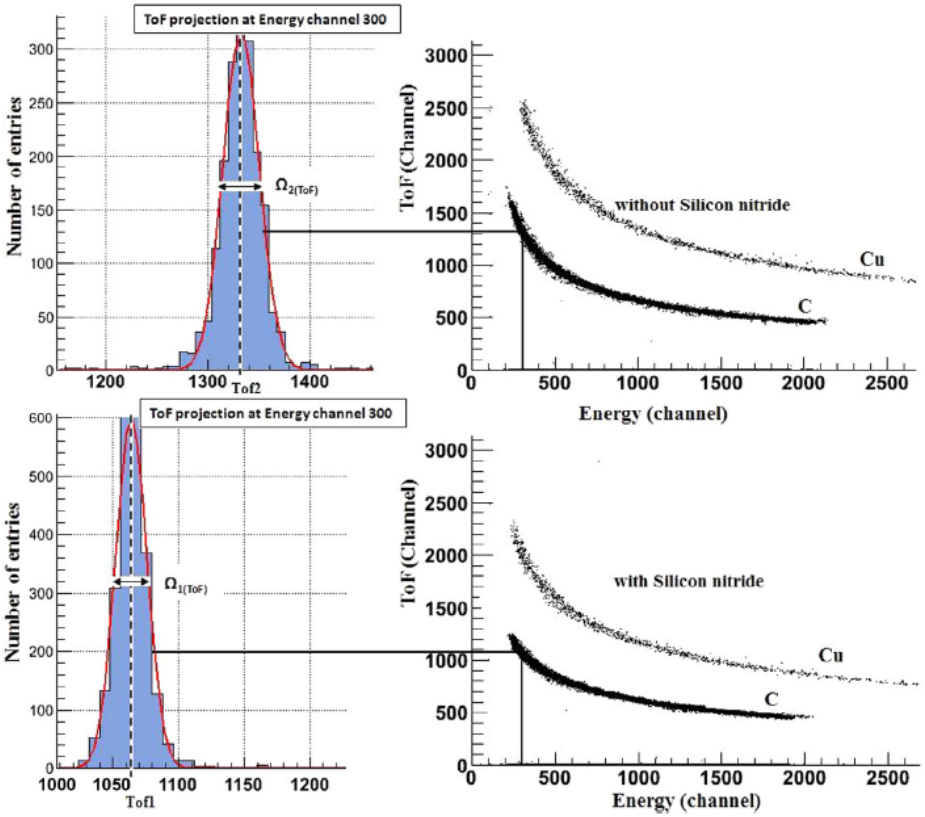

Fig. 2. Two-dimensional Time of Flight-Energy maps of scattered C ion and recoiled Cu ion with and without thin silicon nitride as stopping foil.

$$\delta E_{exp} = 2.3548\sqrt{\Omega_1^2 - \Omega_2^2} \tag{12}$$

The ToF and SBD energy resolution in our measurements is practically the same for any given pair of incident and exit beam energies. The last expression must be corrected from the extra straggling Ω_σ due to the texture and thickness variation of the target foil estimate by Besenbacher et al. by:

$$\Omega_\sigma^2 = \left(\frac{\Delta E}{\Delta x}\right)^2 \sigma^2 \tag{13}$$

where σ is the standard deviation of the foil thickness and Δx mean foil thickness. It has been shown by Szilagyi et al. [22] that, when the relative energy loss exceeded 25% the non-statistical component of energy loss straggling becomes significant, due to the energy-dependency of the electronic stopping force. As a consequence the experimental corrected value of energy straggling considered for theoretical comparison may be formulated as:

$$(\delta E_{exp})_{corr} = 2.3548\sqrt{\left(\frac{S_2}{S_1}\right)^2 (\Omega_1^2 - \Omega_2^2) - \left(\frac{\Delta E}{\Delta x}\right)^2 \sigma^2} \tag{14}$$

where S_1, S_2 are the stopping forces at the front and at the back surfaces regions of the foil, respectively.

For comparison of our obtained energy straggling with Bohr model, the mean excitation energy of silicon nitride $\langle I\rangle = \hbar\langle\omega_0\rangle$ is calculated according to the Bragg's rule as follows:

$$7\ln\langle I\rangle = 3\ln\langle I_{Si}\rangle + 4\ln\langle I_N\rangle \tag{15}$$

where $\langle I_{Si}\rangle = 171$ eV and $\langle I_N\rangle = 84.2$ eV (SRIM-2013). Then $\langle\omega_0\rangle = 17.335.10^{16}$ rd/s.

5. Results and discussion

First, for visual comparison with theoretical formulations we draw the Table 1 which presents some fractional energy losses ($\Delta E/E_1$) as a function of incident energy E_1 and the corresponding relative velocity (v/v_0), for studied ions.

5.1. Stopping force

We present here a brief discussion of the stopping force results. The results of measured stopping forces values of ^{12}C, ^{16}O, ^{8}Si and ^{63}Cu heavy ions crossing Si_3N_4 are summarized in Figs. 3–6 respectively and compared to those generated by LSS formula [18], SRIM-2013 computer code [17] and available data. The statistical errors in the obtained data of stopping force are caused mainly by uncertainties in the localization of the peak position for determining the mean energy-loss (<5%). The obtained values are in good agreement with the predicted value from SRIM-2013 code [17] over the measured energy range. The slight deviation of less than 4% for all ions can be related to experimental scatter and deviation from Bragg's additivity rule. However, a significant difference (up to 15%) is found between the values calculated by the LSS formula and those obtained experimentally, this discrepancy has been reported by several authors (see for example [23]). We observe

Table 1
The measured relative energy loss as a function of incident energy and the correspondent relative velocity (v/v_0) for different ions.

Carbon			Oxygen			Silicon			Copper		
E_1 (MeV)	$\Delta E/E$ (%)	v/v_0	E_1 (MeV)	$\Delta E/E$ (%)	v/v_0	E_1 (MeV)	$\Delta E/E$ (%)	v/v_0	E_1 (MeV)	$\Delta E/E$ (%)	v/v_0
2.34	32.49	2.79	3.81	31.19	3.09	3.10	38.36	2.11	3.66	34.87	1.53
3.30	27.77	3.08	4.82	26.36	3.48	4.5	33.59	2.54	5.23	31.20	1.82
4.62	18.88	3.74	6.22	21.59	3.95	6.34	28.42	3.01	7.41	28.93	2.17
5.62	13.51	4.34	7.53	18.05	4.35	8.01	24.94	3.39	8.79	27.66	2.37
7.09	10.23	4.87	8.79	15.54	4.70	10.58	20.92	3.89	10.07	26.13	2.54
8.27	8.56	5.26	10.04	13.76	5.02	11.57	19.81	4.07	11.29	24.90	2.68

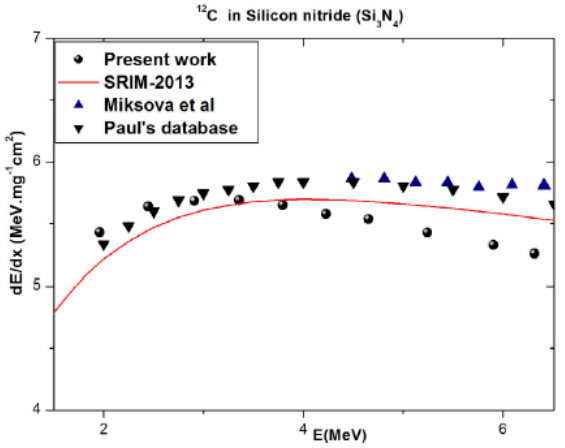

Fig. 3. Experimental stopping force values for ^{12}C ion in silicon nitride compared to SRIM-2013 predictions (red line) and available data [20]. (For interpretation of the references to color in this figure legend, the reader is referred to the web version of this article.)

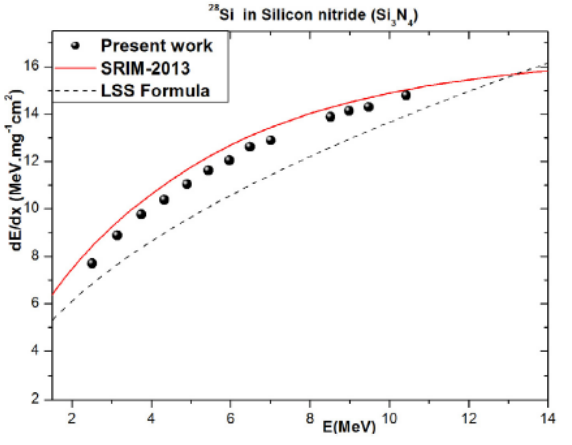

Fig. 5. Experimental stopping force values for ^{28}Si ion in silicon nitride compared to SRIM-2013 predictions (red line) and LSS theory (dot line). (For interpretation of the references to color in this figure legend, the reader is referred to the web version of this article.)

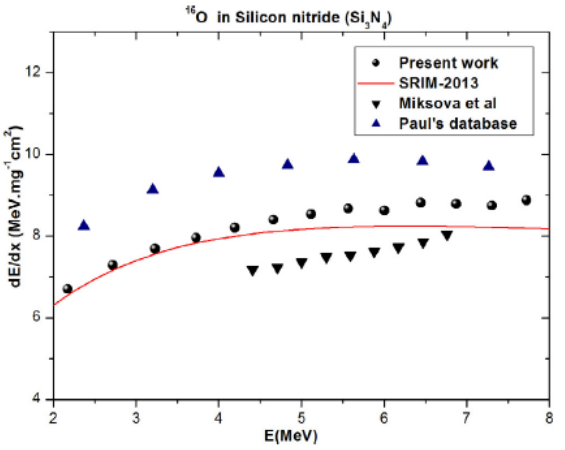

Fig. 4. Same as in Fig. 3 but for ^{16}O.

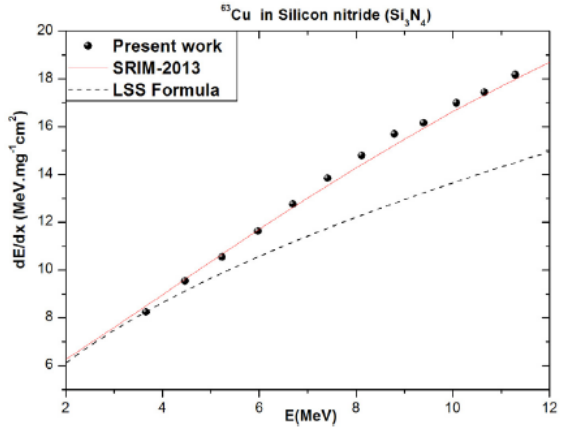

Fig. 6. Same as in Fig. 5 but for ^{63}Cu.

in case of ^{16}O discrepancies between different measurements up to 12%.

5.2. Energy straggling

The discussion of the obtained energy straggling is mainly based on the theoretical formulations discussed in paragraph 2. First, to remove all dependence on the foil thickness, the measured and calculated straggling values are normalized to Bohr's straggling (Eq. (2)). The data of measured energy straggling of C, O, Si, and Cu heavy ions in Si_3N_4 over the 2–11 MeV energy range are shown in Figs. 7–10 respectively. Figs. 7–10 show also the comparison between the obtained energy straggling data and those derived from the more sophisticated straggling referred to as "Bohr model", the predicted value obtained by taken into account the bunching effect according to the Besenbacher approach (Eq. (6)) with the available data in the literature [20].

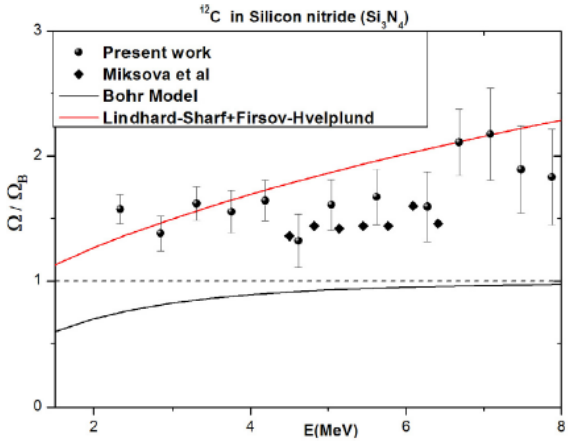

Fig. 7. Experimental reduced energy loss straggling (Ω/Ω_B) of ^{12}C ions through silicon nitride foil compared to Bohr model, Lindhard–Scharff model including bunching effect and available data [20].

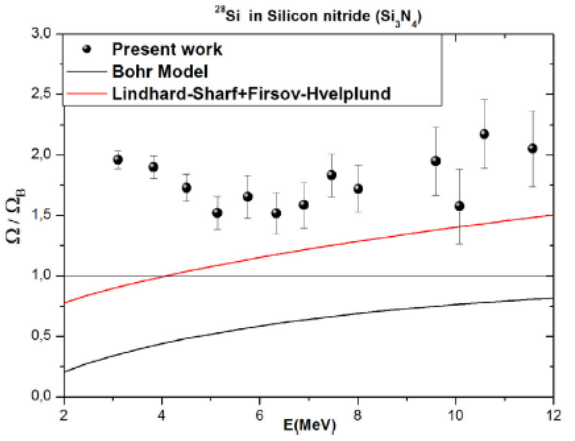

Fig. 9. Experimental reduced energy loss straggling (Ω/Ω_B) of ^{28}Si ions through silicon nitride foil compared to Bohr model, Lindhard–Scharff model including bunching effect.

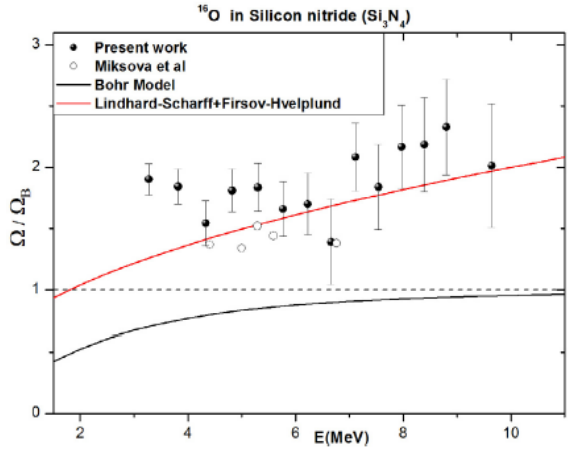

Fig. 8. Same as in Fig. 7 but for ^{16}O.

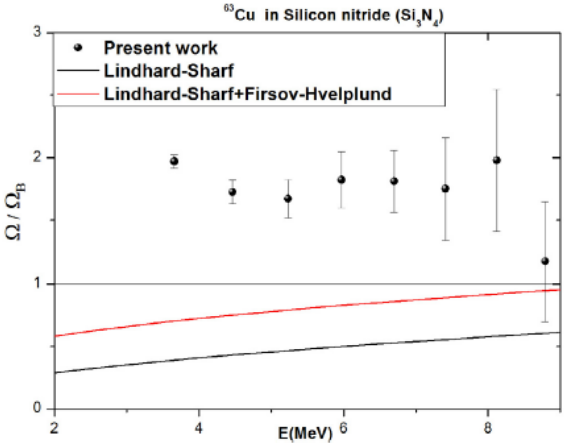

Fig. 10. Experimental reduced energy loss straggling (Ω/Ω_B) of ^{63}Cu ions through silicon nitride foil compared to Lindhard–Scharff model and Lindhard–Scharff model including bunching effect.

Following our investigation there are not many experimental data on energy straggling especially for heavy ions. Mikšová et al. [20] measured energy straggling of 4–7 MeV carbon and oxygen in Si_3N_4 and obtained values up to about a factor of 1.5 above the Bohr values. These values are similar to ours within the limit of experimental uncertainty (see Figs 7 and 8).

It is clear from Figs. 7–10 that, the simple Bohr straggling as well as the more sophisticated straggling referred to as the "Bohr model", fail to predict the measured values of C, O, Si, and Cu heavy ions in Si_3N_4 in the 2–11 MeV energy range. In all cases, the energy straggling is underestimated by a factor of 1.2–3 by the Bohr model. This large discrepancy between the Bohr model and the experimental data means that it is necessary to introduce other effects in straggling theory, such as the bunching effect and the charge exchange. In this work we have restricted our study to evaluate the bunching effect from the Hvelplund–Firsov formula [8] following the Besenbacher approach (Eq. (6)) [12].

The energy straggling values given by Eq. (6) are reasonably comparable to the measured data. To make a clear comparison between calculations taking into account the bunching (Ω_{The}) and experimental data Ω_{Exp} we present in Fig. 11 the ratio factor $\Omega_{Exp}/\Omega_{The}$. In the case of Carbon a minor discrepancy between calculations taking into account the bunching (Ω_{The}) effect and the experiment values, then, let us concluded that, the Hvelplund–Firsov formula exaggerate the straggling due to the bunching of electrons or the straggling due to charge exchange is negligible in comparison with the bunching effect for carbon ions in the 2–8 MeV range of energy. For the oxygen ions the calculated energy straggling from Eq. (6) underestimates slightly (<10% for 4–8 MeV) experimental data (see Fig. 11). For Silicon and Copper there is a net underestimation of experimental data by Eq. (6) (up to $\Omega_{Exp} \sim 3\Omega_{Th}$ for energy less than 4 MeV for Copper). Finally, it is clear from Fig. 11 that the straggling due to charge exchange and molecular effect increase with atomic number Z of incident ion, obviously at this range of energy.

At all considered energies, the straggling resulting from the atomic (nuclear) collision is negligible for all studied ions except copper for energies 2–4 MeV range ($S_n/S_e \sim 0.28$–0.10). The appreciable value of nuclear stopping force relative to the electronic stopping force for the copper ions for energy less than 4 MeV can

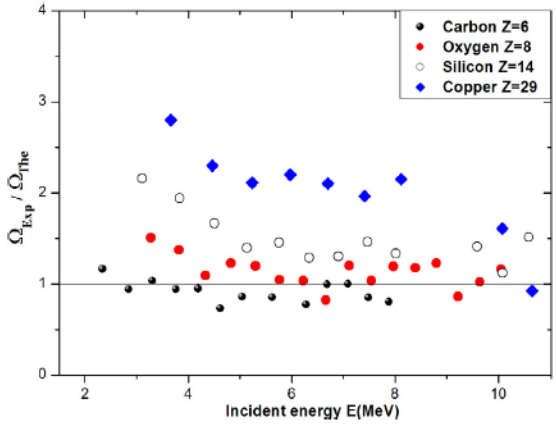

Fig. 11. Plot showing the energy dependence of the ratio of experimental to Eq. (6) energy straggling values of ^{12}C, ^{16}O, ^{16}Si and ^{63}Cu.

explain partially the rise of the energy straggling for energy less than 4 MeV.

6. Conclusion

We have presented a new data of stopping force and energy straggling of ^{12}C, ^{16}O, ^{28}Si and ^{63}Cu heavy ions crossing silicon nitride (Si_3N_4) thin foil, in a continuous range of energies (2–11 MeV).

The SRIM-2013 stopping force values are in good agreement with the experimental data presented in this work and with available data in the literature.

The computed values of energy loss straggling based on the Bohr model or Lindhard–Scharff model underestimate considerably the obtained experimental data, proof of contribution of additional effect on energy straggling. However the introduction of the bunching of electrons into target atoms on the Lindhard–Scharff model using the Besenbacher approach improves the comparison and gives an estimation of other effects such as charge exchange and molecular effect. The straggling due to charge exchange and molecular effect increases with atomic number Z of incident. The comparison of the new obtained data with the theoretical models serves as a reference for theoretical development on energy straggling.

Acknowledgment

The authors wish to acknowledge financial support from the National Research Foundation (NRF) of South Africa and the Ministry of Higher Education and Scientific Research of Algeria. We are much indebted to Profs P. Sigmund, H. Paul and O. Nemraoui for useful fundamental discussions. The authors appreciate the kind help of Mr Gerard Badenhorst, Mr Fritz Balzun and Mr Oleg Pekar with the operation of the tandem accelerator at iThemba LABS (Gauteng).

References

[1] J.F. Ziegler, J.P. Biersack, U. Littmark, The Stopping and Ranges of Ions in Solids, Pergamon, New York, 1985.
[2] J.F. Ziegler, Hydrogen Stopping Powers and Ranges in all Elements, vol. 3, Pergamon, New York, 1977.
[3] L. Northcliffe, Ann. Rev. Nucl. Sci. 13 (1963) 67.
[4] G. Konac, S. Kalbitzer, Ch. Klatt, D. Niemann, R. Stoll, Nucl. Instr. Meth. B 136–138 (1998) 159–165.
[5] M.S. Livingston, H.A. Bethe, Rev. Mod. Phys. 9 (1937) 245.
[6] N. Bohr, Mat. Fys. Medd. Dan. Vid. Selsk 18 (8) (1948).
[7] H. Geissel, Y. Laichter, W.F.W. Schneider, P. Armbruster, Nucl. Instr. Meth. 215 (1983) 329–335.
[8] P. Hvelplund, Mat. Fys. Medd. Dan. Vid. Selsk 38 (4) (1971).
[9] C.J. Sofield, N.E.B. Cowern, J.M. Freeman, Nucl. Instr. Meth. 191 (1981) 462–468.
[10] C.E. Celedón, E.D. Cantero, G.H. Lantschner, N.R. Arista, Nucl. Instr. Meth. B 315 (2013) 21–25.
[11] J. Lindhard, M. Scharff, Mat. Fys. Medd. Dan. Vid. Selsk. 27 (15) (1953).
[12] F. Besenbacher, J.U. Andersen, E. Bonderup, Nucl. Instr. Meth. 168 (1980) 1–15.
[13] Sunil Kumar, P.K. Diwan, Shyam Kumar, Radiat. Phys. Chem. 106 (2015) 21–25.
[14] P. Sigmund, Phys. Rev. A 14 (1976) 996.
[15] P. Sigmund, Mat. Fys. Medd. Dan. Vid. Selsk. 40 (5) (1978).
[16] P. Sigmund, Particle Penetration and Radiation Effects, Springer-Verlag, Berlin Heidelberg, 2006.
[17] J.F. Ziegler, The stopping and range of ions in matter, (<http://www.srim.org/, version SRIM-2013>).
[18] J. Lindhard, M. Scharff, H.E. Schiott, Mat. Fys. Medd. Dan. Vid. Selsk. 33 (14) (1963) 1–42.
[19] H. Paul, Stopping power for heavy, <http://www.exphys.uni-linz.ac.at/stopping/>.
[20] R. Mikšová, V. Hnatowicz, A. Macková, P. Malinský, P. Slepička, Nucl. Instr. Meth. B 354 (2015) 205–209.
[21] M. Mayer, SIMNRA User's Guide, Report IPP 9/113, Max-Planck-Institutfür Plasma physik, Garching, Germany, 1997.
[22] E. Szilàgyi, F. Pàszti, G. Amsel, Nucl. Instr. Meth. B 100 (1995) 103.
[23] Neetu Paratibha, V. Sharma, P.K. Diwan, Shyam Kumar, Radiat. Meas. 44 (2009) 363–368.
[24] M. Msimanga, C.M. Comrie, C.A. Pineda-Vargas, S. Murray, R. Bark, G. Dollinger, Nucl. Instr. Meth. B 267 (2009) 2671–2674.
[25] A. Guesmia, H. Ammi, M. Msimanga, A. Dibb, S. Mammeri, C.A. Pineda-Vargas, M. Hedibel, Radiat. Phys. Chem. 107 (2015) 189–194.

Radiation Physics and Chemistry 107 (2015) 189–194

Contents lists available at ScienceDirect

Radiation Physics and Chemistry

journal homepage: www.elsevier.com/locate/radphyschem

Energy loss straggling data of ^{28}Si, ^{27}Al, ^{24}Mg, ^{19}F, ^{16}O, and ^{12}C heavy ions in thin polymeric Formvar foil over a range of energies 0.1–0.6 MeV/u by time-of-flight spectrometry

A. Guesmia [a,f], H. Ammi [b,*], M. Msimanga [c], A. Dib [b], S. Mammeri [b], C.A. Pineda-Vargas [d,e], M. Hedibel [f]

[a] Département de physique, Faculté des Sciences Université Saâd Dahlab, B. P. 270, Route de Soumâa, Blida, Algeria
[b] Centre de Recherche Nucléaire d'Alger, 2 Bd. Frantz Fanon, B.P. 399, Alger-Gare, Algiers, Algeria
[c] iThemba Labs, National Research Foundation, P. Bag 11, WITS 2050, Johannesburg, South Africa
[d] iThemba Labs, National Research Foundation, P.O. Box 722, Somerset West 7129, South Africa
[e] Faculty of Health and Wellness Sciences, CPUT, P.O. Box 1906, Bellville 7535, South Africa
[f] Département de physique, Faculté des Sciences Université M'hamed Bougara, Boumerdes, Algeria

HIGHLIGHTS

- Measurement of energy loss straggling data of ^{28}Si, ^{27}Al, ^{24}Mg, ^{19}F, ^{16}O, and ^{12}C heavy ions in thin polymeric Formvar foil.
- The heavy ion elastic recoil detection analysis (HIERDA) technique coupled with time of flight (ToF) spectrometer was used.
- The aim of such a study is to check the reliability and accuracy of the existing energy loss straggling formulations.

ARTICLE INFO

Article history:
Received 4 December 2013
Received in revised form
4 November 2014
Accepted 6 November 2014
Available online 10 November 2014

Keywords:
Stopping power
Straggling
Time of Flight spectrometer

ABSTRACT

The energy-loss straggling of ^{28}Si, ^{27}Al, ^{24}Mg, ^{19}F, ^{16}O and ^{12}C partially stripped heavy ions has been determined in Formvar polymeric thin foil over a continuous range of energies 0.1–0.6 MeV/u, by using a powerful method based on the combination of Heavy Ion-Elastic Recoil Detection Analysis (HI-ERDA) technique and Time of Flight (ToF) spectrometer. The obtained energy loss straggling values have been analyzed and compared with the corresponding computed values adopting some widely used energy loss straggling formulations such as, Bohr, Bethe–Livingston and Yang formulas. The aim of such a comparison is to check the reliability and accuracy of the existing energy loss straggling formulations. The experimental results of energy loss straggling of all ions are found to be significantly greater than those predicted by the theories. These differences can be attributed to the charge exchange straggling. This effect has to be taken into account in order to explain the obtained results.

© 2014 Elsevier Ltd. All rights reserved.

1. Introduction

The study of energy straggling of ion in different materials is of fundamental importance for checking the reliability and accuracy of the existing energy loss straggling formulations, describing the passage of ions through matter, and their improvement. Following our investigation in this field (Ammi et al., 2002), this work will provide a new set of straggling data which will be useful for comparison with different straggling formulations. A large amount of experimental straggling data is available for a great variety of incident ions and target materials of different natures (Sofield et al., 1978; Herault et al., 1988; Yang et al., 1991; Ouichaoui et al., 2000; Ammi et al., 2002, 2004, 2006; Diwan et al., 2011; Mammeri et al., 2012). In particular, more experimental data has been added in recent years principally for light ions in thin polymeric foils (Ammi et al., 2002, 2004, 2006; Mammeri et al., 2012) by combining the Rutherford backscattering spectrometry and the transmission techniques. The straggling data measured this way were usually found to be in qualitative agreement with the available theoretical straggling models (Bohr, 1948; Livingston and Bethe, 1937; Titeica, 1939; Lindhard and Scharff, 1953; Chu, 1976) combining with the Bragg additivity rule (Bragg and Kleeman,

* Corresponding author. .
E-mail address: hakim_ammi@yahoo.fr (H. Ammi).

http://dx.doi.org/10.1016/j.radphyschem.2014.11.005
0969-806X/© 2014 Elsevier Ltd. All rights reserved.

1905) for compound materials. For heavy ions, the situation is quite different, although other improved experimental techniques have been successfully used (Msimanga et al., 2012), there are only few experimental straggling data permitting to assess the consistency of the theoretical predictions. Moreover, reliable energy straggling measurements for various ion-polymer combinations and incident energy ranges are still needed to enrich the existing database and test the predicting straggling model. Several theories dealing with different aspects of energy straggling process have been proposed in the past, starting with Bohr in 1948 (Bohr, 1948) who proposed a simple energy-independent formula proportional to the target thickness and valid in high energy region ($v > v_0 Z_1^{2/3}$ with v, $v_0 = c/137$ and c being the ion, Bohr and light velocities, respectively, and Z_1 the ion atomic number). Other theories and semi-empirical formulations have been also developed (e.g., (Livingston and Bethe, 1937; Lindhard and Scharff, 1953; Yang et al., 1991) and firstly applied to experimental straggling data of elemental targets, then extended in recent years to complex materials by using the Bragg additivity rule.

For partially stripped ions, it is expected that, besides the collisional (for fixed charge) effect of energy loss due to the fluctuation in ion charge an additional source of the energy-loss straggling arise (Sofield et al., 1980; Winterbon, 1977). The present study was devoted to present a new set of experimental straggling data and to compare it to the existing theories. For this, the energy loss straggling for ^{28}Si, ^{27}Al, ^{24}Mg, ^{19}F, ^{16}O and ^{12}C heavy ions at energies 0.1–0.6 MeV/u in Formvar thin polymeric foil has been determined. The experimental energy loss straggling data were deduced from Time of Flight (ToF) energy loss spectra analysis, obtained with the combined use of Heavy Ion Elastic Recoil Data Analysis (HI-ERDA) technique coupled and a ToF spectrometer. The experimentally determined straggling values have been compared with those calculated using Bohr and Bethe–Livingston classical theories or Yang et al.'s empirical formula.

2. Energy loss straggling theoretical formulations

Due to the statistical nature of atomic collisions, when a beam of mono-energetic (E) incident particles penetrates matter, the energy loss fluctuates around an average energy loss$\langle \Delta E \rangle$. This fluctuation of the energy loss ΔE is characterized by the so called energy loss straggling, which means the average square fluctuation in energy loss (Sigmund, 2006)

$$\Omega^2 = \left\langle (\Delta E - \langle \Delta E \rangle)^2 \right\rangle \tag{1}$$

where $\langle \Delta E \rangle$ is the mean energy loss over a traveled thickness x.

In Bohr's classical theory (Bohr, 1948), the following assumptions have been made: (**i**) the target electrons contribute randomly to the energy loss, (**ii**) the velocity of the projectile is much greater than the orbital velocities of the electrons of the target atoms, (**iii**) the energy loss of the ion per collision event with a target electron is very small as compared to the incident energy. Bohr's theory gives the energy-loss straggling in an elemental target as

$$\Omega_B^2 = 4\pi Z_1^2 Z_2 e^4 N x \tag{2}$$

where Z_1 and Z_2 are the beam and target atomic number respectively, x is the thickness of the foil, N the number of atoms per unit volume in the stopping material and e is the electronic charge. The assumptions of Bohr classical theory are valid only at high ion velocities but not in our case (low velocity regime).

As mentioned above, Bohr's straggling theory is valid in the limit of high ion velocities, for lower ion energies, Chu (1976) proposed a semi- empirical formula to correct Bohr straggling by taking into account the electron binding in target atoms

$$\Omega_{\mathrm{Chu}}^2 = H\left(\frac{E}{M_1}, Z_2\right)\Omega_B^2 \tag{3}$$

where M_1 is the atomic mass of the incident ion and H is a correction factor tabulated for $100 \le E/M_1 \le 1000$(keV/amu) by Szilágyi et al. (1995, 2000).

The Chu treatment neglects the charge state fluctuations. This fluctuation of charge state induces an additional energy loss straggling component given by Yang et al., (1991) semi-empirical formula based on Chu's theory given by

$$\frac{\Omega_{\mathrm{Yang}}^2}{\Omega_B^2} = \frac{Z_1^{4/3}}{Z_2^{1/3}}\left[\frac{C_1\Gamma}{(\varepsilon - C_2)^2 + \Gamma^2}\right],\ \Gamma = C_3[1 - e^{-C_4\varepsilon}],\ \varepsilon = \frac{E}{\sqrt{Z_1^3 Z_2}} \tag{4}$$

where E is the energy in MeV/amu and C_1–C_4 are fitted constants.

The total energy straggling $\Omega_T^2$is then the sum of the Chu and Yang straggling components

$$\Omega_T^2 = \gamma^2(Z_1, Z_2, v)\frac{\Omega_{\mathrm{Chu}}^2}{\Omega_B^2} + \frac{\Omega_{\mathrm{Yang}}^2}{\Omega_B^2} \tag{5}$$

with the effective charge fraction γ given by $\gamma = \left(1 - \exp\left(-\frac{v}{v_0 Z_1^{2/3}}\right)\right)$ where Z_1 is the atomic number of the ion, v is the ion velocity and v_0 is the Bohr velocity.

In the quantum theory of Bethe and Livingston (Livingston and Bethe, 1937), the energy loss straggling is given by

$$\Omega^2 = \Omega_{BL}^2 = 4\pi Z_1^2 Z_2 e^4 N x\left[Z_2^l + \sum_i\left(k_i\frac{I Z_i}{m_e v^2}\ln\frac{2m_e v^2}{I_i}\right)\right],\ k_i = 4/3 \tag{6}$$

Where I_i the average excitation energy of the Z_i electrons in the ith atomic orbit, Z_2^l is the total number of effective electrons. The summation extends over all shells for which $2m_e v^2 > I_i$(m_e is the electron mass and v the incident particle velocity). At low velocity (our case), only the electrons which are located at the inner shell contribute really to energy loss process, this assumption is not taking into account by Chu, Yang and Bethe–Livingston straggling formulations.

3. Experimental method

The set of energy loss straggling data has been deduced from energy loss measurements of ^{28}Si, ^{27}Al, ^{24}Mg, ^{19}F, ^{16}O and ^{12}C heavy ions traversing Formvar thin foil. A schematic diagram of the experimental Heavy Ions-Elastic Recoil Detection Analysis (HI-ERDA) technique coupled with a time of flight (ToF) spectrometer is illustrated in Fig. 1. The ToF-Energy spectrometer was partially mounted inside the flight flange at an angle of 30° to the incident beam direction. It consists of a ToF detector; built from two tilted timing detectors mounted in chevron configuration a flight distance of $L = 0.584$ m apart, and a silicon surface barrier detector (SBD) positioned about 6 cm behind the second time detector for energy measurement (Fig. 1). The first time detector T1 is located inside the target chamber, close to a primary target, and the second one T2 is towards the end of the flight flange. More details for the experimental set-up are given in Refs (Ammi et al., 2011; Msimanga et al., 2009, 2010). A variety of bulk samples and thick layer targets (Si, Al_2O_3, MgO, C and LiF) were bombarded by a primary 27.5 MeV Kr^{15+} ion beam at a grazing incidence angle of 15°, thereby creating different types of energetic recoil ions that pass through the T1 and T2 timing detectors and then through the Formvar absorber foil to reach finally the SBD detector. The signals from the timing detectors and the SBD were recorded in

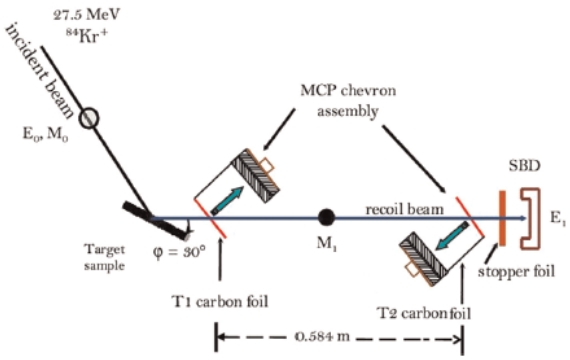

Fig. 1. Schematic setup of ToF-ERDA spectrometer at iThemba LABS, with additional foil for energy loss measurement.

coincidence. The energy E1 of the recoil/scattered species before passing through the target stopper foil is determined from the measured ToF (Tof_1) between the timing detectors T1 and T2. The exit energy E2 is tagged by the SBD detector, and is then determined from a coincident ToF (Tof_2) obtained in a second run without the stopper foil.

Finally, the Formvar $C_5H_8O_2$ (poly vinyl Formal) foil with density 1.23 g/cm^3 had a thickness x=0.4 μm which was determined by using the energy loss of 5.485 MeV alpha particles from a very thin ^{241}Am radioactive source passing through the Formvar foil (Ammi et al., 2006). The surface roughness was analyzed within AFM treatment. The mean surface roughness (δ) value of the foil was estimated to be about ~10 nm. Then the thickness uncertainty isΔx = 20 nm.

3.1. Data analysis

In order to illustrate the data analysis procedure adopted in this work, the C ion crossing thin Formvar foil is given as example (see Fig. 2). Tof1 and Tof2 are the measured flight times with and without the stopper foil respectively at the same energy channel. We note: $E_1 = \frac{1}{2}M\left(\frac{L}{Tof_1}\right)^2$ and $E_2 = \frac{1}{2}M\left(\frac{L}{Tof_2}\right)^2$.

For the same channel (coincidence) we have

$$E_1 = E_2 - \Delta E \tag{7}$$

The energy loss ΔE is then calculated from

$$\Delta E = E_2 - E_1 = \frac{M}{2}\left[\left(\frac{L}{Tof_2}\right)^2 - \left(\frac{L}{Tof_1}\right)^2\right] \tag{8}$$

Where, M in this instance is the mass of Carbon ion. In this experiment the energy spectra of E_1 and E_2 have been found nearly Gaussian in shape with standard deviation Ω_1 and Ω_2 respectively, so that their peak positions have been considered to be a point of energy value. The resulting relative energy losses measured varied from ~10% to ~20% of all incident energy considered in such case that Bohr's theory is valid (for energies losses of ~(10–25)%); we deduced stopping power $S\left(\bar{E} = \frac{E_1+E_2}{2}\right)$ value by dividing the energy loss by the target areal density ($S(\bar{E}) = -\Delta E/\rho x$, ρ and x being the mass density and the linear thickness of the studied foil). The statistical errors in the presently obtained data on $S(E)$ are caused mainly by uncertainties in the localization of the peak position for determining the mean energy-loss (< 5%).

The energy loss straggling has been determined by using the following relation:

$$\Omega_{exp} = \sqrt{(\Omega_2)^2 - (\Omega_1)^2} \tag{9}$$

where Ω_1 and Ω_2 are, respectively, the energy loss straggling with and without absorber foil. Note that in the energy domain (0.1–0.6 MeV/u) the nuclear energy loss straggling can be neglected. The last expression must be corrected from the correlation effect due to foil thickness uncertainty Δx by adopting the Besenbacher et al. (1980) approach. The statistical component of electronic energy loss straggling that was determined experimentally is then given by

$$\Omega_{el}^2 = (\Omega_2)^2 - (\Omega_1)^2 - S^2(\Delta x)^2 \tag{10}$$

where S is the measured average stopping power at mean energy $\frac{E_1+E_2}{2}$.

Finally, the absolute uncertainties associated to the measured energy loss straggling data are carefully evaluated by considering the propagated errors originating from the different quantities in

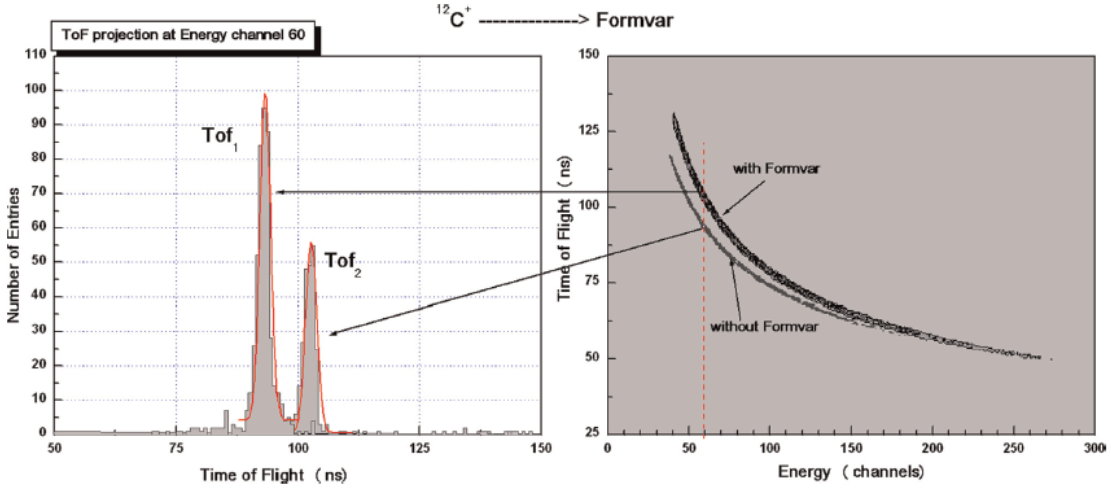

Fig. 2. A sample result of 2D ToF-Energy scatter plots obtained from measurements of ^{12}C recoils with and without Formvar stopper foil. The centroids of the ToF projections are used to calculate energy loss and the widths are used to evaluate the electronic energy loss straggling.

Eq. (10)

$$\Delta\Omega_{el} = \frac{1}{\Omega_{el}}\sqrt{(\Omega_1\Delta\Omega_1)^2 + (\Omega_2\Delta\Omega_2)^2 + \left[S(\Delta x)^2\Delta S\right]^2} \quad (11)$$

4. Results and discussion

The electronic energy loss straggling and the associated uncertainties, which has been experimentally determined for ^{28}Si, ^{27}Al, ^{24}Mg, ^{19}F, ^{16}O, and ^{12}C ions in Formvar foil over the energy range from 0.1 MeV/u to 0.6 MeV/u, is summarized in Figs. 3–8. The experimental electronic energy loss straggling data have been compared to the calculated ones deduced from Bohr and Bethe–Livingston theories and also to those generated by Yang's empirical formula. The calculated straggling values derived from Chu's theory and Yang's empirical formulas were evaluated using the SIMNRA 6.04 code (Mayer, 2002). In the energy domain of 0.1–0.6 MeV/u the velocities of ions are high enough, so the Bethe–Livingston theory is applicable. It should be noted that both the experimental straggling values and the calculated ones were normalized to the Bohr straggling value in order to remove the thickness dependence and display only the beam energy variation. No experimental data have been found in the literature to make any possible comparison to our obtained electronic energy loss straggling.

It is clearly shown that from these Figs. (3–8), the electronic energy-loss straggling was found to be significantly greater than predicted theories over the energy range from 0.1 MeV/u to 0.6 MeV/u where the ions are partially stripped and velocities high enough to meet the validity criterion of the Bethe–Livingston theory. Different reasons can explain the large discrepancy between experimental result and existing theories. Firstly, the assumption of the Bohr classical theory which is well applicable for light but not for heavy ions and as we know, the other existing theories are derived from the Bohr theory. Secondly, we think that the experimental method used is suitable for energy loss but not for energy loss straggling measurements. The third reason can be attributed to the charge exchange straggling (loss and capture of the electrons of the projectile) which occur in the investigated energy domain. This charge exchange straggling has to be taken into account by the used theories in order to explain the discrepancy which exist between experimental and calculated straggling values (Efken et al., 1975; Diwan et al., 2007). This effect

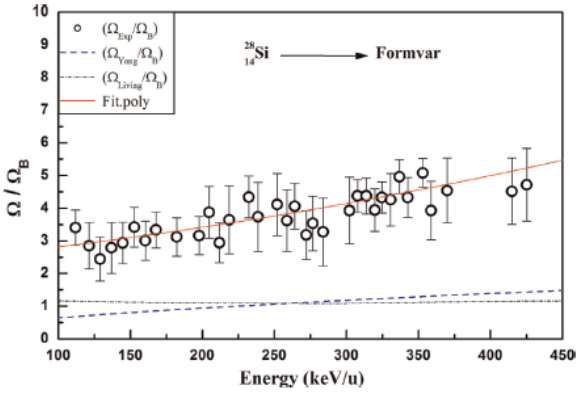

Fig. 3. Comparison of experimental reduced electronic energy loss straggling of ^{28}Si ions through Formvar foil and theoretical calculations of Bethe–Livingston's quantum theory and Yang's empirical formula. The solid line is a second order polynomial fit to the experimental data.

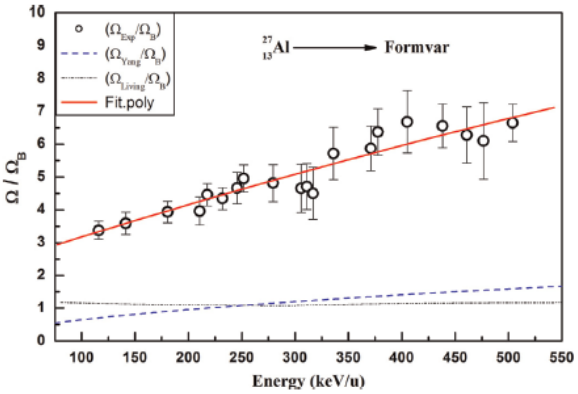

Fig. 4. Same as in Fig. 3 but for ^{27}Al.

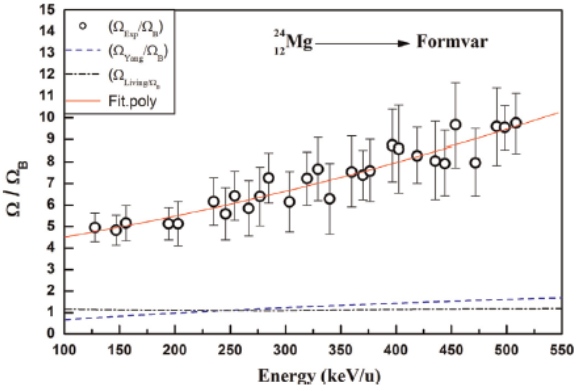

Fig. 5. Same as in Fig. 3 but for ^{24}Mg.

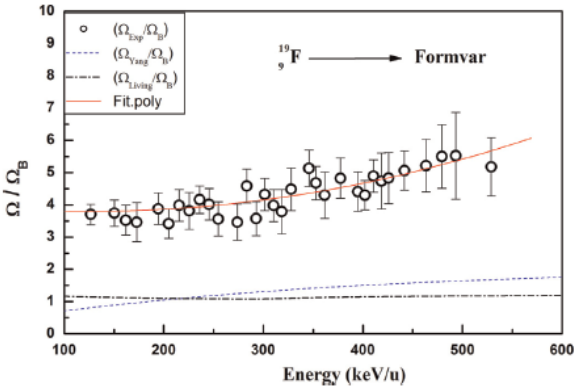

Fig. 6. Same as in Fig. 3 but for ^{19}F.

is not taken into account in this work because no charge change cross section data were available for the ion-target combinations and energies at which the experiments were performed.

The polynomial fit in each figure serves only to provide a means of reproducing current data for comparison with any other data set that may become available using;

$$\frac{\Omega}{\Omega_B} = a_0 + a_1E + a_2E^2 \quad (12)$$

where $a_0 - a_2$ are the fit constants, listed in Table 1, and E is the ion energy in MeV. The main observation made here is that Bohr,

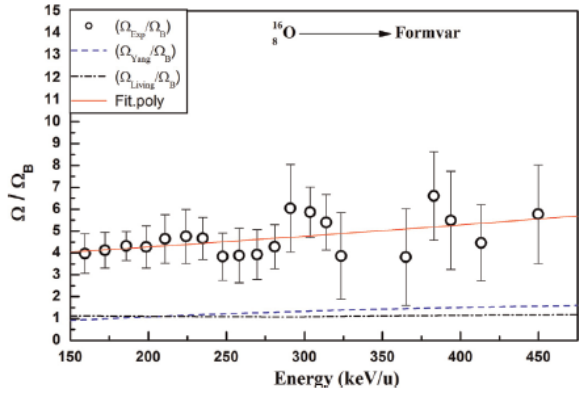

Fig. 7. Same as in Fig. 3 but for ^{16}O.

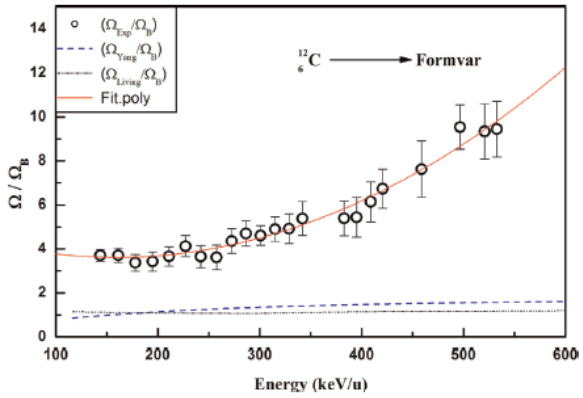

Fig. 8. Same as in Fig. 3 but for ^{12}C.

Table 1
Fit constants to the experimental straggling data presented in Figs. 3–8.

Ions	a_0	a_1	a_2
^{28}Si	2.35	0.007	$-2.51E^{-6}$
^{27}Al	3.24	0.003	$9.48E^{-6}$
^{24}Mg	3.71	0.007	$8.93E^{-6}$
^{19}F	4.58	−0.010	$2.63E^{-5}$
^{16}O	3.25	0.005	$2.96E^{-7}$
^{12}C	3.36	−0.003	$2.66E^{-5}$

Bethe–Livingston theories and Yang's formula greatly underestimate straggling for all the six ion species in the energy ranges concerned. The difference between Bohr, Bethe–Livingston prediction and Yang's formula is relatively much smaller in all six instances.

Foil thickness variation is almost assumed to be the dominant cause of discrepancy between experiment and theory in straggling measurements (Ammi et al., 2006). Besides, the experimental Ω_{Exp} values plotted in Figs. 3–8 have already been corrected for possible thickness variation effects on the measured straggling according to Eq. (10). This leads to the conclusion that the observed deviation is most likely due to other effects. In the limited data published on the measurement of straggling of heavy ions in solid foils, several authors explain the high experiment-theory discrepancy by charge exchange straggling (Ouichaoui et al., 2000; Msimanga et al., 2012; Sofield et al., 1978).

5. Conclusion

Electronic energy loss straggling in Formvar thin foil has been determined for ^{28}Si, ^{27}Al, ^{24}Mg, ^{19}F, ^{16}O, and ^{12}C ions at low energy region (0.1–0.6 MeV/u) by the Heavy Ions-Elastic Recoil Detection Analysis (HI-ERDA) technique coupled with a time of flight (ToF) spectrometer. This study gave a new set of electronic energy loss straggling data. The AFM scans of Formvar surface foil have been used to correct foil thickness uncertainty. Our obtained experimental electronic energy loss straggling data was found to be significantly greater than predicted theories (Bohr, Chu, Yang and Bethe–Livingston). The significant difference observed at the energy region of interest (0.1–0.6 MeV/u), may be due to the fact that in predicted theories it is assumed that heavy ion velocity is much larger than the velocity of electrons bound to target atoms. This feature is, however; only true at high ion velocities. Different reasons can explain the discrepancy between experimental result and existing theories as: the assumption of Bohr classical theory which is valid for light and not for heavy ions, the charge exchange effect which was not calculated in this study because no charge change cross section data were available for the ion-target combinations and energies at which the experiments were performed and finally, the inhomogeneity effect of the stopping foil in energy loss straggling measurements.

Acknowledgments

This work was carried at iThemba LABS (Cape Town, South Africa). The financial support by the NRF (South Africa) and by the COMENA (Algeria) is gratefully acknowledged. The authors would like to thank Professor M. Maaza for his precious assistance and Dr. L. Conradie for beam time at the Cyclotron accelerator of iThemba LABS, Cape Town.

References

Ammi, H., Mammeri, S., Chekirine, M., Bouzid, B., Allab, M., 2002. An experimental method for precise measurements of straggling in energy loss of ^{1}H and ^{2}H ions in composite materials: application to polymer foils. Nucl. Instr. Meth. B 198, 5–10.
Ammi, H., Mammeri, S., Allab, M., 2004. Energy loss straggling of energetic ^{1}H and ^{2}H ions crossing polypropylene foils. Nucl. Instr. Meth. B 213, 60–64.
Ammi, H., Zemih, R., Mammeri, S., Allab, M., 2006. Energy loss straggling measurements for helium ions in Mylar and polypropylene polymeric foils. Rad. Effect. Defects Solids, 161; , pp. 339–346.
Ammi, H., Pineda-Vargas, C.A., Mammeri, S., Msimanga, M., Ourabah, S., Dib, A., 2011. Stopping power measurements of heavy ions ($3 \leq Z1 \leq 14$) in Mylar foil by time-of-flight spectrometry. Nucl. Instr. and Meth. B 269, 386–391.
Besenbacher, F., Andersen, J.U., Bonderup, E., 1980. Straggling in energy loss of energetic hydrogen and helium ions. Nucl. Instr. and Meth 168, 1–15.
Bohr, N., 1948. The penetration of atomic particles through matter. Mat. Fys. Medd. Dan. Vid. Selsk 18 (8), 1–144.
Bragg, W.H., Kleeman, R., 1905. On the α particles of radium and their loss of range in passing through various atoms and molecules. Philos. Mag. 10, 318–340.
Chu, W.K., 1976. Calculation of energy straggling for protons and helium ions. Phys. Rev. 13, 2057–2060.
Diwan, P.K., Sharma, V., Kumar, S., Mittal, V.K., Khan, S.A., Avasthi, D.K., 2007. Energy loss and straggling of MeV heavy ions in polypropylene absorber foils. Nucl. Instr. Meth. Phys. Res. B 258, 293–298.
Diwan, P.K., Neetu, Gulati Pratibha, K., Kumar, S., Avasthi, D.K., 2011. Energy loss straggling in thick mylar polymeric foils for swift heavy ions in fractional energy loss limit $\Delta E/E \approx 5-80\%$. Nucl. Instr. Meth. Phys. Res. B 269, 1786–1791.
Efken, B., Hahn, D., Hilscher, D., Wüstenfeld, G., 1975. Energy loss and energy loss straggling of N, Ne, and Ar ions in thin targets. Nucl. Instr. Meth 129, 219–225.
Herault, J., Bimbot, R., Gauvin, H., Anne, R., Bastin, G., Hubert, F., 1988. Interaction of 20–100 MeV/u heavy ions with cold matterJ. Phys. C 7, 33–42.
Livingston, M.S., Bethe, H.A., 1937. Nuclear physics c. nuclear dynamics, experimental. Rev. Mod. Phys. 9, 245–390.
Lindhard, J., Scharff, M., 1953. Energy loss in matter by fast particles of low chargeMat. Fys. Medd. Dan. Vid. Selsk 27 (15), 1–31.
Mammeri, S., Ammi, H., Dib, A., Pineda-Vargas, C.A., Ourabah, S., Msimanga, M., Chekirine, M., Guesmia, A., 2012. Stopping power and energy loss straggling of

thin Formvar foil for 0.3–2.7 MeV protons and alpha particles. Radiat. Phys. Chym. 81, 1862–1866.
Mayer, M., 2002. Ion beam analysis of rough thin films. Nucl. Instr. Meth. B 194, 177–186.
Msimanga, M., Comrie, C.M., Pineda-Vargas, C.A., Murray, S., 2009. A time of Flight-Energy spectrometer for stopping power measurements in Heavy Ion-ERD analysis at iThemba LABS. Nucl. Instr. Meth. B 267, 2671–2674.
Msimanga, M., Comrie, C.M., Pineda-Vargas, C.A., Murray, S., 2010. Experimental stopping powers of Al, Mg, F and O ions in ZrO_2 in the 0.1–0.6 MeV/u energy range. Nucl. Instr. Meth. B 268, 1772–1775.
Msimanga, M., Comrie, C.M., Pineda-Vargas, C.A., Murray, S., 2012. Heavy ion energy loss straggling data force time of flight stopping force measurements. Nucl. Instr. Meth. B 273, 6–10.
Ouichaoui, S., Hourani, E., Rosier, L., Bimbot, R., Beaumevieille, H., Bouzid, B., Mammeri, S., 2000. Energy loss straggling of swift heavy ions in metals foils at E/A ~2 MeV/u. Nucl. Instr. Meth. Phys. Res. B 164-165, 259–267.
Sofield, C.J., Cowern, N.E.B., Petty, R.J., Freeman, J.M., Mason, J.P., 1978. Charge-exchange effects in the energy-loss straggling of O ions in Al. Phys. Rev. A 17, 859–867.
Sofield, C.J., Cowern, N.E.B., Freeman, J.M., 1980. Charge-exchange effects in energy-loss straggling. Nucl. Instr. Meth. 170, 221–225.
Sigmund, P., 2006. Particle Penetration and Radiation Effects. General Aspects and Stopping of Swift Point Particles, Springer Series in Solid State Sciences. Springer-Verlag, Berlin.
Szilágyi, E., Pászti, F., Amsel., G., 1995. Theoretical approximations for depth resolution calculations in IBA methods. Nucl. Instr. Meth. Phys. Res. B 100, 103–121.Szilágyi, E., 2000. Energy spread in ion beam analysis. Nucl. Instr. Meth. Phys. Res. B 161–163, 37–47.
Titeica, S., 1939. Sur les fluctuations de parcours des rayons corpusculaires. Bull. Soc. Rou. Phys 38, 81–100.
Winterbon, K.B., 1977. Electronic energy loss and charge-state fluctuations of swift ions. Nucl. Instr. and Meth. 144, 311–315.
Yang, Q., O'Connor, D.J., Wang, Z., 1991. Empirical formulae for energy loss straggling of ions in matter. Nucl. Instr. Meth. B Phys. Res 61, 149–155.

Radiation Physics and Chemistry 96 (2014) 205–210

Contents lists available at ScienceDirect

Radiation Physics and Chemistry

journal homepage: www.elsevier.com/locate/radphyschem

Semi empirical formula for electronic stopping power determination of ^{24}Mg, ^{27}Al and ^{28}Si ions crossing Formvar foil in the ion energy domain of LSS theory

A. Guesmia [a,f], H. Ammi [b,*], S. Mammeri [b], A. Dib [b], C.A. Pineda-Vargas [c,d], M. Msimanga [e], M. Hedibel [f]

[a] Département de physique, Faculté des Sciences Université Saâd Dahleb, B. P. 270, Route de Soumâa, Blida, Algeria
[b] Centre de Recherche Nucléaire d'Alger, 2 Bd. Frantz Fanon, B.P. 399, Alger-Gare, Algiers, Algeria
[c] iThemba Labs, National Research Foundation, PO Box 722, Somerset West 7129, South Africa
[d] Faculty of Health and Wellness Sciences, CPUT, PO Box 1906 Bellville 7535, South Africa
[e] iThemba Labs, National Research Foundation, P. Bag 11, WITS 2050, Johannesburg, South Africa
[f] Département de physique, Faculté des Sciences Université M'hamed Bougara, Boumerdes, Algeria

HIGHLIGHTS

- Experimental stopping data has been obtained by using Heavy Ions Elastic Recoil Detection Analysis technique with Time of Flight spectrometer.
- A new semi-empirical stopping formula based on LSS theory has been proposed for ^{28}Si, ^{27}Al and ^{24} Mg ions in Formvar foil.
- This expression well fit the experimental stopping data at low energy in LSS domain.

ARTICLE INFO

Article history:
Received 22 July 2013
Accepted 5 October 2013
Available online 25 October 2013

Keywords:
Electronic stopping power
LSS theory
Time-of-flight
HI-ERDA

ABSTRACT

We have determined continuous stopping power of heavy ions in thin Formvar foil for ^{28}Si, ^{27}Al and ^{24}Mg ions over an energy range of (0.1–0.5) MeV/nucleon. Heavy Ions Elastic Recoil Detection Analysis (HI-ERDA) technique coupled with time of flight (ToF) spectrometer has been used to measure energy loss of charged particles in this thin absorber. Lindhard, Scharff and Schiott (LSS) theory compared with the corresponding determined stopping values in Formvar, shows significantly large deviations. However, a novel semi empirical expression has been proposed here and tested for better stopping power calculations at low velocity in the ion energy domain of LSS theory for ^{28}Si, ^{27}Al and ^{24}Mg ions crossing thin Formvar foil. The results were compared to the obtained experimental stopping power data, predictions of LSS theory and also to those generated by SRIM-2010 computer code. The obtained results exhibit good agreement with experimental data.

© 2013 Elsevier Ltd. All rights reserved.

1. Introduction

Over several decades, a large number of theoretical and experimental works (Nastasi et al., 1996; Chu et al., 1977; Ziegler et al., 1980; Sigmund, 2006; Ziegler, 1980; Bardos and Gavrilenko, 1986; Oguri et al., 2007; Xiting et al., 2000) have been devoted to investigate the variation of stopping power as a function of ion kinetic energy for a great variety of materials of different natures. In particular, the energy loss of heavy ions in compound materials has received special attention recently (Diwan et al., 2008, 2010; Mizohata et al., 2012; Neetu et al., 2009) due to its widespread use in materials science and ion beam applications. With the increasing use of ion beam based analytical techniques, the energy loss phenomenon has gained importance. As energy loss is one of the main factors limiting depth resolution, accurate information on energy loss is important for the applications of Rutherford backscattering spectrometry (RBS), elastic recoil detection analysis (ERDA), nuclear reaction analysis (NRA) etc. in material analysis (Zhang and Weber. 2009; Strub et al., 2006; Zdravko et al., 2008). For this, different nuclear techniques have been improved for better energy loss measurements, as: ion transmission, RBS, HIERDA coupled with TOF spectrometer.

Following our investigation in slowing down phenomena of light and heavy energetic ions crossing polymeric foils (Ammi et al., 1997, 2000, 2002, 2004; Mammeri et al., 2012), we analyze in this paper our experimental stopping results obtained for ^{28}Si, ^{27}Al and ^{24}Mg through

* Corresponding author. Tel.: +21321434444; fax: +213 21 43 42 80.
E-mail address: hakim_ammi@yahoo.fr (H. Ammi).

0969-806X/$ - see front matter © 2013 Elsevier Ltd. All rights reserved.
http://dx.doi.org/10.1016/j.radphyschem.2013.10.003

thin foil of Formvar. The present study is the continuous work that we have started in 2011 (Ammi et al., 2011), concerning stopping power determination of heavy ions crossing polymeric foils by using HIERDA technique coupled with TOF spectrometer. This spectrometer, developed and assembled for HI-ERD analysis at iThemba Labs, is well used for energy loss measurements (Msimanga et al., 2012, 2013) for obtaining stopping power curves for several ions and absorber foils simultaneously over a continuous range of energies.

In the present work, we have determined electronic stopping power (S_e) values in Formvar foil for ^{28}Si, ^{27}Al and ^{24}Mg, ions at low energy (0.1–0.5 MeV/nucleon), and we would like through this work to describe our obtained stopping data by the well known theories developed for electronic stopping power at low ion energy. For this, we analyzed the theoretical model developed by Lindhard and Scharff (1961) for stopping power at low velocity. This model uses the Thomas–Fermi statistical model to describe the atomic structure and predict (S_e) values proportional to the projectile velocity. Lindhard et al. (1963) theory is found to provide reasonable descriptions of the main features of the electronic stopping phenomena at low projectile velocities. The obtained stopping data have been compared to the predicted values from SRIM-2010 code (Ziegler et al., 1985) and to the calculated ones generated by the well known model of electronic stopping power in the low velocity region, given by the so-called Lindhard, Scharff and Schiott (LSS) formula (Lindhard et al., 1963).

The Lindhard and Scharff theory has been used to make a comprehensive analysis of LSS formula through comparison with the corresponding experimental stopping data in the energy domain (0.1–0.5 MeV/nucleon). In this energy region the electronic stopping power is proportional to the ion velocity and for systems with different atomic numbers $Z_1 \neq Z_2$ (where Z_1 and Z_2 are the ion and the target atomic number, respectively) the LSS formula gives a fairly good average value of electronic stopping power. However, for given projectile–target combinations, a light discrepancy can be observed between experimental data and calculated ones generated by LSS formula. In our opinion, the discrepancy observed may be attributed to the fact that in LSS formula, some physical parameters are not taking into account for the evaluation of electronic stopping power, such as: charge state concept. Through the present work, we have suitably modified the LSS formula (Eq. (1)) of electronic stopping power that can be used in various projectile–target combinations at lower energies. For this and in order to give a best description of our obtained stopping data, we attempted to modify Eq. (1) by inserting in this equation the effective charge of incident ion Z_1^* and an exponential fit function $f(E)$. The validity and accuracy of this new approach is discussed in the light of new experimental data.

2. Theoretical approach

2.1. LSS formula

In general and in order to explain the slowing down of the projectile in matter, the statistical parameter S is defined as the probability that describes the energy dE lost by the particle through a thickness of material dX, S is given by the relation: $S = -(dE/dX)$.

Following the spirit of the Thomas–Fermi model (Fermi and Teller (1947)) of the atom, Lindhard, Scharff and Schiott proposed to evaluate the stopping cross section of an atom from the energy-loss function of a free-electron gas. The electronic stopping cross-section of low velocity ($v < v_0 Z_{ion}^{2/3}$) heavy ions can be calculated as follows:

$$\left(-\frac{dE}{dx}\right)_e = \zeta_e \times 8 \times \pi \times e^2 \times a_0 \times N \left\{\frac{Z_1 Z_2}{\left(Z_1^{2/3}+Z_2^{2/3}\right)^{3/2}}\right\}\left(\frac{v}{v_0}\right) \quad (1)$$

where ζ_e is a correction factor of order of $Z_1^{1/6}$; a_0 and N are Bohr atomic radius and atomic density, respectively; Z_2 and Z_1 are the atomic number of target material and incident ion. v and v_0 are the incident ion and Bohr velocity.

2.2. Semi empirical formula

Our proposed semi empirical approach is based on LSS theory (statistical model of atoms) and underlines the following points.

2.3. Correlation factor

ζ_e is approximated to be equal to $Z_1^{1/6}$ in LSS formula, in our proposed semi empirical formula, ζ_e is taken equal to Z_1^a, where a is a free parameter. We will see later that the value of a will be very close to 1 ($a \cong 1$).

2.4. Effective charge

The first physical parameter that we have taken into account in our approach is the effective charge Z_1^* of heavy ion penetrating solid matter. We know that at low velocity, when an ion penetrates matter, the projectile cannot be fully stripped of its electrons. Thus the projectile nucleus is accompanied by a cloud of electrons which partly screens the positive charge. The interactions between the ion and electrons of the target atom depend on the charge state of the projectile, so a proper treatment of the stopping power should take contributions from different charge states and charge-exchange effects into account. This effective-charge concept (Northcliffe., 1960; Bohr., 1941) has been widely accepted as a model to explain stopping data.

The charge variation of the ion due to electron capture and loss at low velocities is usually of minor concern for hydrogen and helium ions but dominates the behaviour of heavier ions. The various energy loss formulations employ empirical/semi-empirical relations to determine the effective charge and the accuracy to which stopping powers can be calculated mainly depends on the goodness of fit for the given effective charge expression. We have adopted the expression given by Northcliffe and Schilling (1970) for effective charge evaluation. Based on Bohr concept, Northcliffe and Schilling (1970) made a semi-empirical tabulation of electronic stopping power values for heavy ions in different targets. Northcliffe and Schilling proposed the following semi-empirical relation for determining the effective charge of heavy ions Z_1^*,

$$Z_1^* = \gamma Z_1 \quad (2)$$

where the effective charge fraction γ is defined by:

$$\gamma = \left(1 - \exp\left(-\frac{v}{v_0 Z_1^{2/3}}\right)\right) \quad (3)$$

So the effective charge of heavy ion is taken as:

$$Z_1^* = \left(1 - \exp\left(-\frac{v}{v_0 Z_1^{2/3}}\right)\right) Z_1 \quad (4)$$

where Z_1 the atomic number of the ion is, v is the ion velocity and v_0 is the Bohr velocity.

Based on the previous items, we propose through this work the following relation to evaluate the electronics stopping power (S_e) for heavy ions crossing solid targets at low energy regime (*LSS domain*). (S_e) is given as:

$$(S_e) = (S'_{LSS}) \times f(E) \quad (5)$$

where (S'_{LSS}) is the stopping power defined by LSS in Eq. (1) where Z_1 is replaced by Z_1^* given in Eq. (4) and $\zeta_e \cong Z_1^a$. So (S'_{LSS}) is given

by the following relation.

$$(S'_{LSS}) = Z_1^a \times 8 \times \pi \times e^2 \times a_0 \times N \left\{ \frac{Z_1^* Z_2}{\left(Z_1^{2/3} + Z_2^{2/3}\right)^{3/2}} \right\} \left(\frac{v}{v_0}\right) \quad (6)$$

and $f(E)$ is an exponential function expressed as:

$$f(E) = \frac{1}{1+\exp(bE)} \quad (7)$$

where b is a adjustable parameter. So the expression proposed to evaluate the stopping power at low energy for heavy ions is given by Eq. (8) as follow.

$$(S_e) = Z_1^a \times 8 \times \pi \times e^2 \times a_0 \times N \left\{ \frac{Z_1^* Z_2}{(Z_1^{2/3} + Z_2^{2/3})^{3/2}} \right\} \left(\frac{v}{v_0}\right) \times \left(\frac{1}{1+\exp bE}\right) \quad (8)$$

2.5. Experimental method

The set of stopping power data has been deduced from energy loss measurements of Si, Al and Mg ions traversing Formvar thin foil. The HI-ERDA setup at iThemba Labs (Cape Town) is installed on a beam line connected to a solid pole injector cyclotron (SPC2) equipped with ECR ion-source, where a range of low energy (≤ 0.34 MeV/nucleon) light and heavy ions is available.

The TOF–Energy spectrometer was partly mounted inside the flight flange at an angle of 30° to the incident beam direction. It consists of a TOF detector; built from two tilted timing detectors mounted in chevron configuration a flight distance of 0.584 m apart, and a silicon surface barrier detector (SBD) positioned about 6 cm behind the second time detector for energy measurement (Fig. 1). The first time detector T1 is located inside the target chamber, close to the target, and the second one T2 is towards the end of the flight flange. More details for experimental set-up are given in Ammi et al. (2011), Msimanga et al. (2012).

The essence of this method is to record both the energy and time of flight (ToF) of the ions while constantly alternating the measurements with and without the foil. Since the ToF, unlike the energy, is measured before the passage of the ion through the foil, we can match the events recorded with and without the foil even when the spread of energies of the initial ions is very large. In this way, ^{28}Si, ^{27}Al and ^{24}Mg ions over a continuous range of energies from 0.1 to 0.5 MeV/nucleon are produced for the energy loss measurements.

A 27.5 MeV ^{84}Kr projectile ion beam was used to recoil Si, Al and Mg ions from suitable target samples (SiO_2, Al_2O_3 and MgO) into the ToF telescope. The energy E1 of the recoil species before passing through the target stopper foil is determined from the measured ToF between the timing detectors T1 and T2, and the exit energy E2, tagged by the Si surface barrier detector (SBD) is determined from a coincident TOF obtained in a second run without the stopper foil.

3. Data analysis

In Fig. 2, T1 and T2 are the measured flight times with and without the stopper foil respectively and the impinging (E_1) and exit (E_2) energies in keV are given by:

$$E_1 = \frac{1}{2} M \times \left(\frac{L_{TOF}}{T_1(ns)}\right)^2 \quad (9)$$

$$E_2 = \frac{1}{2} M \times \left(\frac{L_{TOF}}{T_2(ns)}\right)^2 \quad (10)$$

The energy loss ΔE of recoil (or scattered) ion of mass m after passing through the stopper foil is then given by:

$$\Delta E = E_1 - E_2 = \frac{M}{2}\left[\left(\frac{L_{TOf}}{T_1(ns)}\right)^2 - \left(\frac{L_{TOf}}{T_2(ns)}\right)^2\right] \quad (11)$$

where, M in this instance is the mass of Silicon ion. The stopping power at the mean ion energy (E_{av}) in the foil was calculated by dividing the energy loss ΔE by the foil areal density ($\rho \Delta x$) (ρ represent mass density, $\Delta x$is the foil thickness, and $E_{av} = E_1 - (\Delta E/2)$, where E_1 is the incident energy (before crossing the Formvar foil). As a result, the stopping power $S = -(1/\rho)(dE/dx)$ (differential energy loss per unit path length), is taken as $\frac{\Delta E}{\rho \Delta x}$.

$$S = \frac{\Delta E}{\rho \Delta X} = \frac{M}{2\rho \Delta X}\left[\left(\frac{L_{TOf}}{T_1(ns)}\right)^2 - \left(\frac{L_{TOf}}{T_2(ns)}\right)^2\right] \quad (12)$$

The used Formvar foils were prepared as previously (Mammeri et al., 2012) from a polyvinyl formal powder of high purity (99.99%) purchased from SIGMA-Aldrich (South Africa) Company. It was diluted in chloroform at a concentration of 1.5% in solution. A drop of this solution was dropped on water surface and a thin foil was created. The thin foil was allowed to dry and then was scooped from the water and gently put in a clean aluminum holder. The film thickness was defined by normalizing the energy loss of alpha particles through the films over a wide energy region to the SRIM-2010 values, which result in 49.2 μg/cm^2 with uncertainty of less than 3%. The uncertainties resulted from the time calibration, the drift of the Si detector response due to the radiation damage, geometrical variation, recoil angle, and counting statistics, are too small. In addition to the foil thickness error

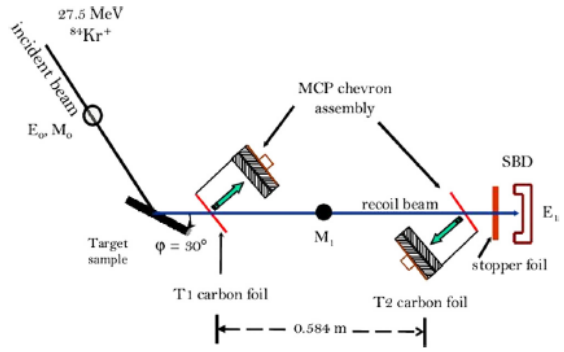

Fig. 1. Schematic setup of TOF-ERDA spectrometer at iThemba Labs, with additional foil for measurements of energy losses.

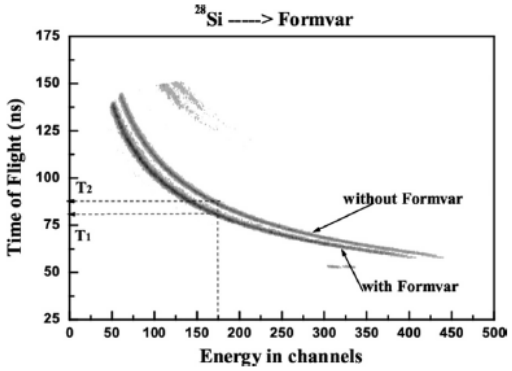

Fig. 2. Overlapped TOF-ERDA coincidence maps of scattered ^{28}Si with and without thin Formvar as stopping foil.

estimate, there is also an uncertainty associated with the energy loss measurement. Energy with (E_1) and without (E_2) the stopper foil is calculated from the measured TOFs (T_1) and (T_2), respectively. The time calibration procedure for TOF detector has been well described in our previously published work (Ammi et al., 2011). This approach takes advantage of continuous energy spectra to calibrate the Si detector using the TOF spectrometer for each channel over the whole measured energy region.

4. Results and discussion

The electronic stopping powers S of Formvar foil, which is experimentally determined for ^{28}Si, ^{27}Al and ^{24}Mg ions over the energy range from 0.1 MeV/nucleon to 0.5 MeV/nucleon, is summarized in Figs. 3–5. No experimental data have been found in the literature to make any possible comparison to our obtained stopping data for ^{28}Si, ^{27}Al and ^{24}Mg in thin Formvar foil.

In order to check the experimental validity of presently semi-empirical approach, the experimental stopping data are compared to the calculated stopping power values determined by Eq. (8), to those generated by LSS formula Eq. (1) and SRIM-2010 computer code, where the measurements were performed for the Formvar target thicknesses of 49.2 μg/cm^2. It is clearly shown that from theses Figs. 3–5, the calculated stopping power values based on our semi-empirical formula (Eq. (8)) in the energy range 0.1–0.5 MeV/n provide excellent agreement with experimental ones

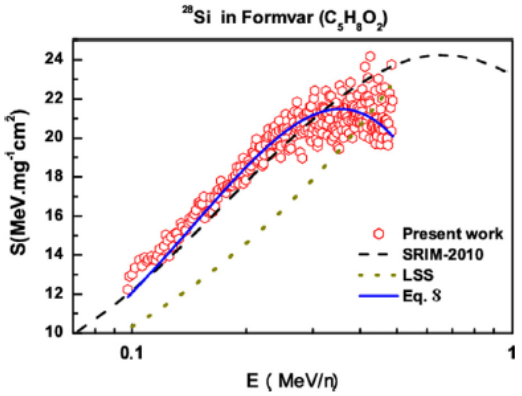

Fig. 3. Comparison of experimental stopping power values for ^{7}Si ion (star) in Formvar with data from Eq. (8) (solid lines), SRIM-2010 predictions (dashed lines) and LSS theory (dot lines).

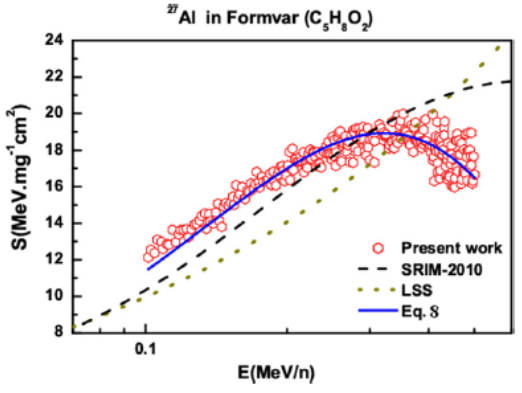

Fig. 4. Same as in Fig. 3 but for ^{27}Al.

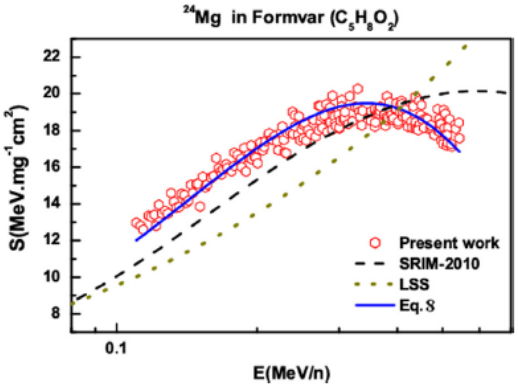

Fig. 5. Same as in Fig. 3 but for ^{24}Mg.

and those calculated by SRIM-2010 code. However, a significant discrepancy has been shown between the values calculated by the well known LSS formula and those obtained experimentally or given by Eq. (8) and SRIM-2010 code. In order to confirm the validity of our approach, we have compared the calculated values of electronic stopping power generated by our approach (Eq. (8)) to those published by Paul. (1999) for ^{28}Si in Ag foil, ^{27}Al in Mylar and ^{24}Mg in Ta foil, in LSS domain. It is apparent from Fig. 6a–c that the calculated stopping power values using the semi-empirical formula (Eq. (8)) are in good agreement with H. Paul stopping power data in all these solid targets (Mylar, Ag and Ta), however, a large discrepancy has been observed with stopping power values calculated by LSS formula.

From Table 1, we can see clearly that the values of the adjustable parameters are more or less constant ($a \approx 1$ and $b \approx 3$) for ^{28}Si, ^{27}Al and ^{24}Mg heavy ions crossing thin Formvar foil.

Further, it is interesting to note that for all the projectile–target combinations considered in the present study, the calculated stopping power values based on the present semi-empirical approach (Eq. (8)) are normally within acceptable limits with those obtained experimentally or calculated using SRIM-2010.

Energy loss measurements with HIERDA-TOF experimental set-up, is a powerful method for obtaining continuous stopping power curves and accurate stopping power determination. The high number of experimental points obtained during this work, allow us to provide a semi-empirical approach with accurate evaluation of the stopping powers values.

5. Conclusion

The electronic stopping powers in Formvar thin foil have been determined for Si, Al, and Mg ions at low energy region (0.1–0.5 MeV/n) in validity of LSS domain. Based on HIERDA-TOF spectrometry a continuous stopping power curves have been provided. Following our investigation on experimental slowing down processes of charged particles crossing compound materials, this study gave a new set of stopping data. In this present study, we have suitably attempted to introduce a semi-empirical formula by taking into account in our approach the effective charge of moving ions concept and exponential fit function. In order to best describe the slowing down process which occurs at low energy region, we have proposed a new expression (Eq. (8)) to evaluate the electronic stopping power at low energy in LSS domain. The stopping powers values generated by the proposed semi-empirical formula have been compared to our obtained experimental stopping data, to data calculated by SRIM-2010 computer code and LSS

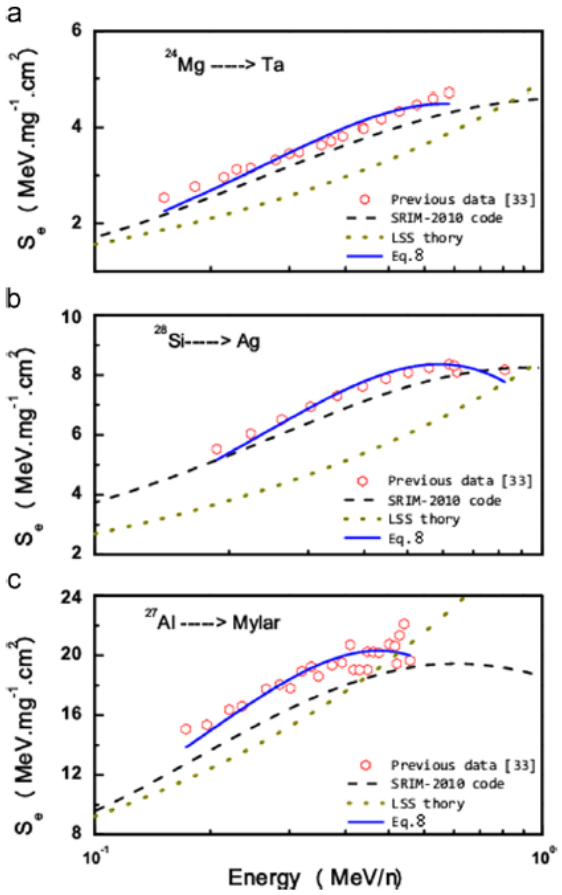

Fig. 6. Comparison of previous stopping power data (Paul, 1999) (star) for ^{28}Si in Ag foil (a), ^{27}Al in Mylar (b) and ^{24}Mg in Ta target (c), together with SRIM-2010 predictions (dashed lines), LSS theory (dot lines) and, Eq. (8) (solid lines).

Table 1
Free parameters obtained in our proposed semi-empirical formula (Eq. (8)) for stopping powers calculation of ^{28}Si, ^{27}Al and ^{24}Mg ions crossing Formvar foil in the energy range 0.1–0.5 MeV/n.

Free parameters	Ion		
	^{28}Si	^{27}Al	^{24}Mg
a	1.022 ± 0.002	$a = 1.027 \pm 0.002$	1.042 ± 0.006
b	3.211 ± 0.021	3.517 ± 0.024	3.258 ± 0.05

formula. Excellent agreement has been obtained between our semi-empirical formula stopping powers values and those obtained experimentally or determined by SRIM-2010 computer code, while a large discrepancy is observed with LSS formula stopping powers values. The same trend has been observed between stopping power values calculated by our proposed formula and those compiled by H. Paul.

It can be concluded that the new expression (Eq. (8)) can be employed for stopping power calculations for different target/projectile combinations in the energy domain validity of LSS theory.

In the present paper, we have given a set of fitting parameters used in our proposed semi-empirical formula, theses fitting parameters are more or less constant for ^{28}Si, ^{27}Al and ^{24}Mg heavy ions crossing thin Formvar foil over the energy range from 0.1 MeV/nucleon to 0.5 MeV/nucleon, and so if further experimental work proves our approach to be correct, the electronic stopping power for ions at low energy for different target/projectiles combinations can be calculated accurately.

Acknowledgements

This work was carried at iThemba LABS (Cape Town, South Africa). The financial support by the NRF (South Africa) and by the COMENA (Algeria) is gratefully acknowledged. The authors would like Professor M. Maaza for his precious assistance and Dr L. Conradie for beam time at the Cyclotron accelerator of iThemba LABS, Cape Town.

References

Ammi, H., Chekirine, M., Adjerad, A., 1997. Stopping power of 1.0–2.6 MeV protons in Mylar, Makrofol and Cellulose nitrate foils. Radiat. Meas. 28, 15–18.
Ammi, H., Chekirine, M., Allab, M., 2000. Slowing down of light ions in Makrofol KG solid nuclear track detector. Radiat. Meas. 32, 83–86.
Ammi, H., Mammeri, S., Chekirine, M., Bouzid, B., Allab, M., 2002. An experimental method for precise measurements of straggling in energy loss of ^{1}H and ^{2}H ions in composite materials: application to polymer foils. Nucl. Instrum. Methods Phys. Res., Sect. B 198, 5–10.
Ammi, H., Mammeri, S., Allab, M., 2004. Energy loss staggling of energetic ^{1}H and ^{2}H ions crossing polypropylene foils. Nucl. Instrum. Methods Phys. Res., Sect. B 213, 60–64.
Ammi, H., Pineda-Vargas, C.A., Mammeri, S., Msimanga, M., Ourabah, S., Dib, A., 2011. Stopping power measurements of heavy ions ($3 \leq Z_1 \leq 14$) in mylar foil by time-of-flight spectrometry. Nucl. Instrum. Methods Phys. Res., Sect. B 269, 386–391.
Bardos, G., Gavrilenko, G.M., 1986. Electronic stopping power formula for energetic ions. Acta Phys. Hung. 59, 393–399.
Bohr, N., 1941. Velocity-range relation for fission fragments. Phys. Rev. 59, 270–275.
Chu, W.K., 1977. Ion Beam Handbook for Material Analysis. In: Mayer, J.W., Rimini, E. (Eds.), Academic Press, New York.
Diwan, P.K., Sharma, V., Pratibha, Shyam Kumar, Khan, S.A., Avasthi, D.K., 2008. Stopping force of 0.5–3.5 MeV/u Cl ions in polymers. Nucl. Instrum. Methods Phys. Res., Sect. B 266, 4738–4741.
Diwan, P.K., Neetu, Gulati, Praitbha K., Kumar, S., Avasthi, D.K., 2010. Statistical variations in energy loss for Li, C and O ions in thick Kapton polymeric foils. Nucl. Instrum. Methods Phys. Res., Sect. B 268, 3523–3525.
Fermi, E., Teller, E., 1947. The capture of negative mesotrons in matter. Phys. Rev. 72, 399–404.
Lindhard, J., Scharff, M., 1961. Energy dissipation by ions in the keV region. Phys. Rev. 124, 128–130.
Lindhard, J., Scharff, M., Schiott, H.E., 1963. Range concepts and heavy ion ranges (notes on atomic collisions ii). Mat. Fys. Medd. Dans. Viden. Selskab. 33 (14), 1–40.
Lu, Xiting, Xia, Zonghuang, Zheng, Tao, Shen, Yixiong, 2000. Stopping power of C, Al, Ti, Cu, Nb and Ag for ^{16}O and ^{19}F ions. Nucl. Instrum. Methods Phys. Res., Sect. B 168, 287–293.
Mammeri, S., Ammi, H., Dib, A., Pineda-Vargas, C.A., Ourabah, S., Msimanga, M., Chekirine, M., Guesmia, A., 2012. Stopping power and energy loss straggling of thin Formvar foil for 0.3–2.7 MeV protons and alpha particles. Radiat. Phys. Chem. 81, 1862–1866.
Mizohata, K., Keinonen, J., Räisänen, J., 2012. Stopping force of polymide, vyns, Formvar and polysulfone for Cl, Br and I ions. Nucl. Instrum. Methods Phys. Res., Sect. B 280, 74–78.
Msimanga, M., Comrie, C.M., Pineda-Vargas, C.A., Murray, S., 2012. Heavy ion energy loss straggling data from Time of Flight stopping force measurements. Nucl. Instrum. Methods Phys. Res., Sect. B 273, 6–10.
Msimanga, M., Wamwangi, D., Comrie, C.M., Pineda-Vargas, C.A., Nkosi, M., Hlatshwayo, T., 2013. The new heavy ion ERDA set up at iThemba LABS Gauteng: multilayer thin film depth profiling using direct calculation and Monte Carlo simulation codes. Nucl. Instrum. Methods Phys. Res., Sect. B 296, 54–60.
Nastasi, M., Mayer, J.W., Hirvonen., J.K., 1996. Ion–Solid Interactions: Fundamentals and Applications. Cambridge University Press, Cambridge.
Neetu, Pratibha, Sharma, V., Diwan, P.K., Kumar., Shyam, 2009. Electronic stopping power of polymers for heavy ions in the ion energy domain of LSS theory. Radiat. Meas. 44, 363–368.
Northcliffe, L.C., 1960. Energy loss and effective charge of heavy ion in aluminum. Phys. Rev. 120, 1744–1757.
Northcliffe, L.C., Schilling, R.F., 1970. Range and stopping-power tables for heavy ions. Nucl. Data Tables 7, 233–463.
Oguri, Y., Niinou, T., Nishinomiya, Katagiri, S.K., Kaneko, j., Hasegawa, J., Ogawa, M., 2007.

Paul, H., 1999. Stopping Power for Light Ions; Collection of Graphs, Data and Comments. Available at ⟨http://www.uni-linz.ac.at/ fak/TNF/atomphys/STOPPING/welcome.htm⟩.
Sigmund, P., 2006. Particle Penetration and Radiation Effects. General Aspects and Stopping of Swift Point Particles, Springer Series in Solid State Sciences. Springer-Verlag, Berlin.
Strub, E., Bohne, W., Röhrich, J., 2006. Determination of the energy loss of various elements in metal foils with the TOF-ERDA setup at the ISL Berlin. Nucl. Instrum. Methods Phys. Res., Sect. B 249, 62–64.
Zdravko, Siketic´, Iva, Bogdanovic´ Radovic´, Milko, Jakšic´, 2008. Development of time-of-flight spectrometer at the Ruder Boskovic´ Institute in Zagreb. Nucl. Instrum. Methods Phys. Res., Sect. B 266, 1328–1332.
Ziegler, J.F., 1980. Handbook of Stopping Cross Section for Energetic Ions in all Elements. Pergaman Press, New York.
Ziegler, J.F., 1980. The stopping of energetic ions in solids. Nucl. Instrum. Methods Phys. Res., Sect. A 168, 17–24.
Zhang, Y., Weber, W.J., 2009. Response of materials to single ion events. Nucl. Instrum. Methods Phys. Res., Sect. B 267, 1705–1712.
Ziegler, J.F., Biersack, J.P., Littmark, U., 1985. The Stopping and Ranges of Ions in Solids. Pergamon, New York.

Nuclear Instruments and Methods in Physics Research B 363 (2015) 24–27

Contents lists available at ScienceDirect

Nuclear Instruments and Methods in Physics Research B

journal homepage: www.elsevier.com/locate/nimb

Energy loss measurements of ^{63}Cu, ^{28}Si and ^{27}Al heavy ions crossing thin Polyvinylchloride (PVC) foil

A. Dib [a], H. Ammi [a], A. Guesmia [b,c,f,*], M. Msimanga [d], S. Mammeri [a], M. Hedibel [c], B. Guedioura [e], C.A. Pineda-Vargas [f,g]

[a] Centre de Recherche Nucléaire d'Alger, 2 Bd. Frantz Fanon, B.P. 399, Alger-Gare, Algiers, Algeria
[b] Departement de physique, Faculté des Sciences, Université Saad Dahlab, B. P. 270, Route de Soumaa, Blida, Algeria
[c] Departement de physique, Faculté des Sciences, Université M'hamed Bougara, Boumerdes, Algeria
[d] Department of Physics, Arcadia Campus, Tshwane University of Technology, P. Bag X680, Pretoria, South Africa
[e] Centre de Recherche Nucléaire de Draria, B.P. 43, Sebala-Draria, Algiers, Algeria
[f] iThemba LABS, National Research Foundation, P.O. Box 722, Somerset West 7129, South Africa
[g] Faculty of Health and Wellness Sciences, CPUT, P.O. Box 1906, Bellville 7535, South Africa

ARTICLE INFO

Article history:
Received 5 March 2015
Received in revised form 11 August 2015
Accepted 11 August 2015
Available online 1 September 2015

Keywords:
Electronic stopping power
LSS theory
Time-of-Flight
HI-ERDA

ABSTRACT

Experimental stopping data of, ^{63}Cu, ^{28}Si and ^{27}Al heavy ions in thin Polyvinylchloride ($H_3C_2Cl_1$) foil have been obtained over the 0.045–0.50 MeV/nucleon energy range. The measured energy losses were carried out by Heavy Ion Elastic Recoil Detection Analysis (HI-ERDA) technique coupled with time of flight (ToF) spectrometer. A continuous stopping power data obtained in this work are well fitted by our proposed semi-empirical formula and the results are compared to those calculated by LSS formula or generated by SRIM-2013 and MSTAR predictions. Calculations using our formula agree well with the obtained experimental stopping powers, while the LSS formula underestimates the experimental data in the whole investigated energy range. In this work a simple expression for electronic stopping power of heavy ions at low energy in solid targets is introduced. This formula is based on the Firsov and Lindhard–Sharff stopping power models with a small modification made to the original expression, by incorporating the effective charge of moving ions concept and with exponential fit function.

© 2015 Elsevier B.V. All rights reserved.

1. Introduction

The penetration of energetic charged particles through matter is a complex phenomenon which can be measured in terms of stopping power. The stopping power has been studied experimentally and theoretically since the beginning of the 20th century because of its wide areas of application, such as: ion material modification, fundamental particle physics, nuclear physics and other applications. Scientists require reliable and precise values of the heavy ion energy loss rate. Therefore, the knowledge of stopping powers for heavy ions in various materials is of a great importance. Over several decades, a large number of theoretical and experimental studies have been devoted [1–9] to investigate the variation of stopping power as a function of ion kinetic energy. One of the famous theoretical approaches which provide reasonable descriptions of the main features of the electronic stopping phenomena at low projectile velocities is described by the well known Lindhard, Scharff and Schiott (LSS) formula [10].

As a continuation of our systematic study of heavy ion energy loss in foils, we provide a new set of experimental stopping data on Cu, Si and Al heavy ions, covering the energy range 0.045–0.500 MeV/nucleon, penetrating thin (PVC) foil. The experimental stopping power values have been obtained by applying HIERDA techniques coupled with ToF spectrometer method. This method has been well used by our group for energy loss measurements [11–16], it allows to obtain a continuous stopping power curves for several ions and absorber foils at low energy region. The obtained experimental stopping data have been firstly well fitted using our proposed semi empirical formula [16] and the result was compared to SRIM-2013 and MSTAR codes [17,18] and to the calculated ones generated by the so-called Lindhard, Scharff and Schiott (LSS) formula [10].

* Corresponding author at: Departement de physique, Faculté des Sciences, Université Saad Dahlab, B. P. 270, Route de Soumaa, Blida, Algeria. Tel.: +213 773201773/+27 822695604.
E-mail addresses: guesmia@tlabs.ac.za, guesssmia@hotmail.fr (A. Guesmia).

http://dx.doi.org/10.1016/j.nimb.2015.08.028
0168-583X/© 2015 Elsevier B.V. All rights reserved.

2. Experimental arrangement

The basic idea of this experiment is to produce heavy ions and to measure their energy before and after crossing thin foil. For this purpose, the Heavy Ion Elastic Recoil Detection Analysis (HIERDA) technique coupled with time of flight spectrometer (ToF) has been developed at iThemba LABS. A schematic diagram of the experimental arrangement is shown in Fig. 1. Only a brief description of the experimental method used for energy loss measurements will be given here. For detailed description see Ref. [15]. Energy loss measurements in PVC foil were carried out at the 6 MV Tandem accelerator at the iThemba LABS (Gauteng) in Johannesburg, using a 26.2 MeV Cu^{7+} beam for projectile ions at a grazing incidence angle of 15°. Silicon and aluminium ions were obtained as recoils from (SiO_2 and Al_2O_3) target samples, respectively. Copper ions on the PVC stopper foil were obtained by using a thick Au/Si layer to forward scatter the initial 26.2 MeV Cu^{+7} projectile beam into the spectrometer. The ToF-E spectrometer consists of a Time of Flight detector, built from two timing detectors, T_1 and T_2, separated by a flight distance of 0.6 m, and a silicon surface barrier detector (SBD) positioned at 6.5 cm behind the second time detector for energy measurement. The stopping foils are alternatively mounted between the second time detector and the SBD. The energy of individual ions before passage through the foil is determined from its ToF data; the exit energy after the stopping foil is essentially measured using the SB Detector, for which every channel has been calibrated using ToF data without the stopping foil.

The PVC thin foil of density $\rho = 1.68$ g/cm^3, has been prepared by using spin-coater for precise and uniform deposition of thin films and coatings. A two stage spin process allows dispensing at low speeds (Stage 1: 500–2500 rpm, 2–18 s) and homogenising the coating at high speed (Stage 2: 1000–8000 rpm, 3–60 s). The obtained film thickness of $\Delta x = 0.45$ μm with uncertainty of ~3 % has been tested by performing energy loss measurements of 5.485 MeV alpha particles from a very thin ^{241}Am radioactive source passing through the PVC foil.

3. Brief description of our theoretical approach

Based on the Thomas–Fermi atomic model, Lindhard, Scharff and Schiott (LSS) proposed to calculate the electronic stopping power at low velocity region ($v < v_0 Z_{ion}^{2/3}$ namely LSS domain) by the following formula [10,19]:

$$\left(-\frac{dE}{dx}\right)_e = \zeta_e . 8.\pi.e^2.a_0.N\left\{\frac{Z_{ion}Z_{foil}}{\left(Z_{ion}^{2/3}+Z_{foil}^{2/3}\right)^{3/2}}\right\}\left(\frac{v}{v_0}\right) \quad (1)$$

where ζ_e is a numerical factor of order of $Z_{ion}^{1/6}$; a_0 and N are the Bohr atomic radius and atomic density, respectively; Z_{foil} is the target atomic number, Z_{ion} and v are the atomic number and velocity of incident ion, respectively.

On the basis of the LSS theory and from the observed discrepancies between the LSS formula (Eq. (1)) and experimental stopping power data, we have proposed in our last paper [16] the following analytical expression to well describe the dependence on energy of the electronic stopping power $\left(-\frac{dE}{dx}\right)_e$ of heavy ions crossing solid materials in the LSS domain:

$$\left(-\frac{dE}{dx}\right)_e = Z_{ion}^{a}.8.\pi.e^2.a_0.N\left\{\frac{Z_{ion}\left(1-\exp\left(-\frac{v}{Z_{ion}^{2/3}v_0}\right)Z_{foil}\right)}{\left(Z_{ion}^{2/3}+Z_{foil}^{2/3}\right)^{3/2}}\right\} \times\left(\frac{v}{v_0}\right)\frac{1}{1+\exp bE} \quad (2)$$

the free parameters a and b, are determined by fitting (Eq. (2)) to the obtained experimental stopping power data.

In all theory, the target is assumed as an elemental material [20,21] which is the case of the formula (1) and (2). For compound targets, it is very common to use the famous Bragg and Kleeman additivity rule [22].

4. Data analysis and results

In order to illustrate the data analysis procedure adopted in this work, the Cu ion crossing thin PVC foil is given as example (see Fig. 2). T_1 and T_2 are the measured flight times given in (ns) with and without the stopper foil, respectively, for the same energy channel of the SBD. The electronic stopping power S_e of recoil (or scattered) ion of mass m after passing through the stopper foil is then given by:

$$S_e = \frac{(E_1 - E_2)}{\Delta x} = \frac{M}{2\Delta x}\left[\left(\frac{L_{Tof}}{T_1}\right)^2 - \left(\frac{L_{Tof}}{T_2}\right)^2\right] \quad (3)$$

where Δx is the foil thickness. For the measurements reported here the quantity $E_1 - E_2$ represents the energy loss through the foil.

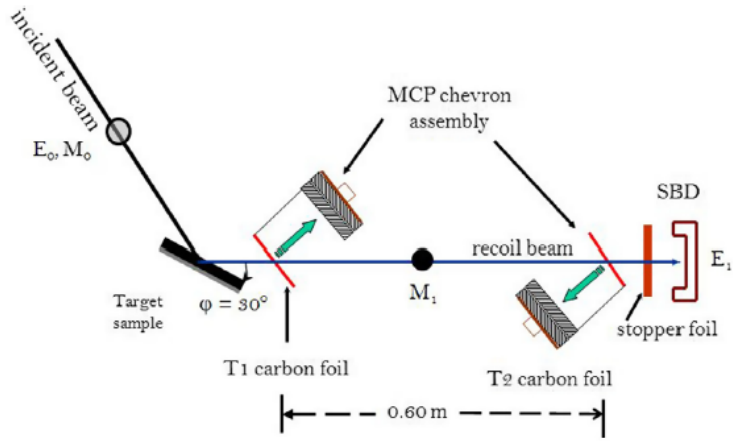

Fig. 1. The basic arrangement setup of TOF-ERDA spectrometer at iThemba Labs, with additional foil for measurements of energy losses.

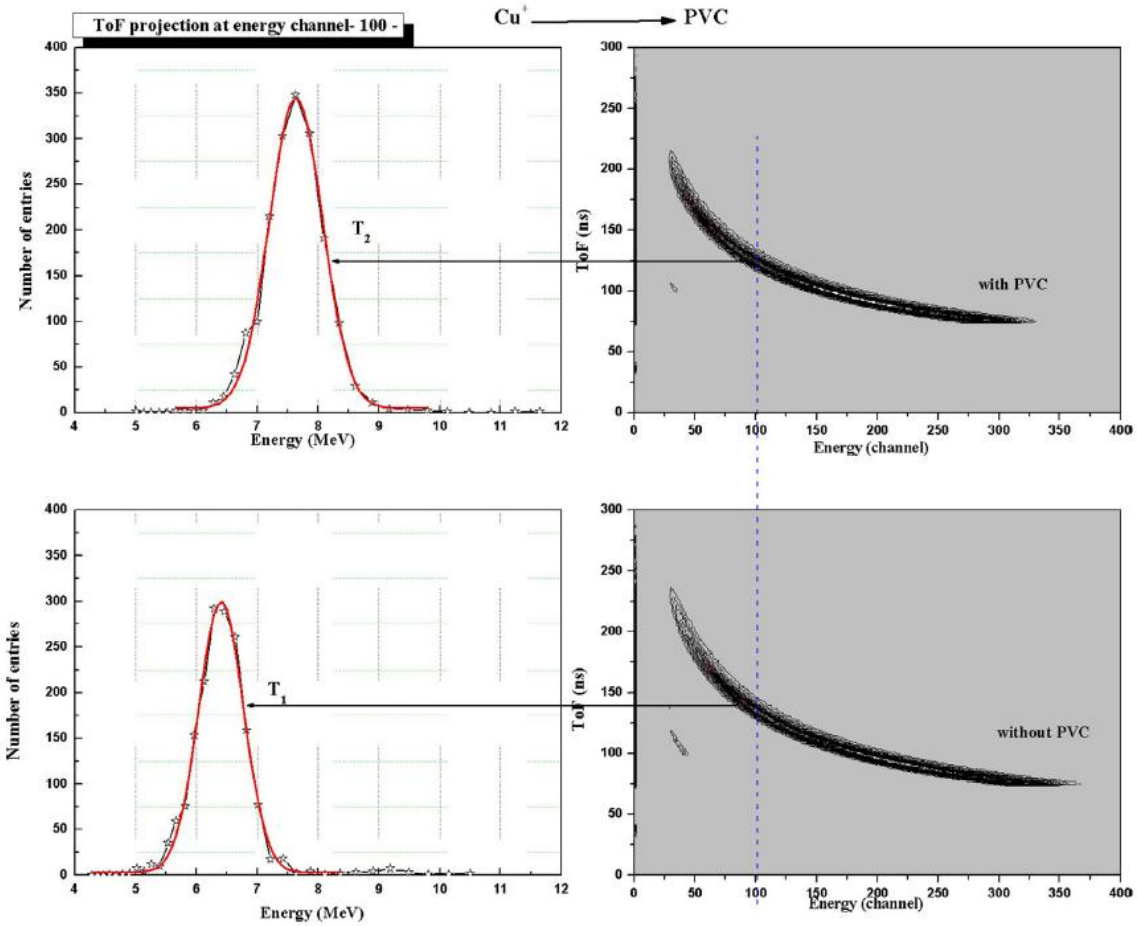

Fig. 2. A sample result of 2D ToF-Energy scatter plots obtained from measurements of ^{63}Cu ion with and without thin Polyvinylchloride (PVC) stopper foil. The centroids of the ToF projections are used to calculate energy loss.

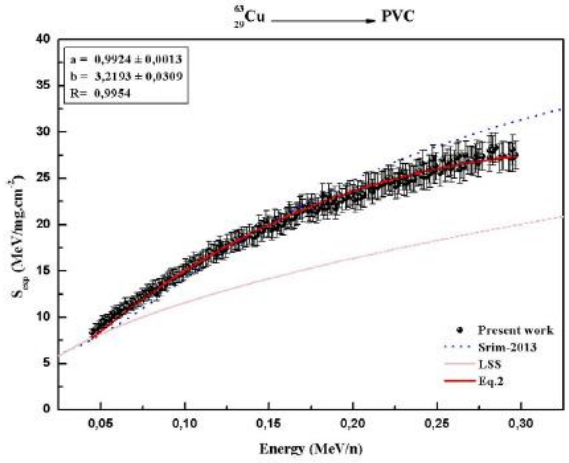

Fig. 3. Comparison of experimental stopping power values for ^{63}Cu ion (circle) in Polyvinylchloride (PVC) with data from Eq. (2) (solid lines), SRIM-2013 predictions (dashed lines) and LSS theory (dot lines).

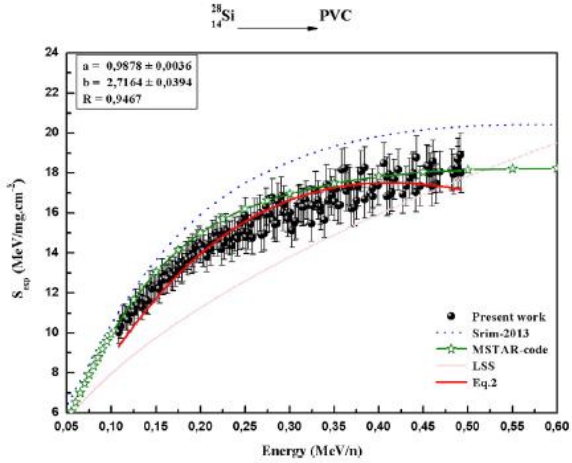

Fig. 4. Comparison of experimental stopping power values for ^{28}Si ion (circle) in Polyvinylchloride (PVC) with data from Eq. (2) (solid lines), SRIM-2013 predictions (dashed lines) and LSS theory (dot lines).

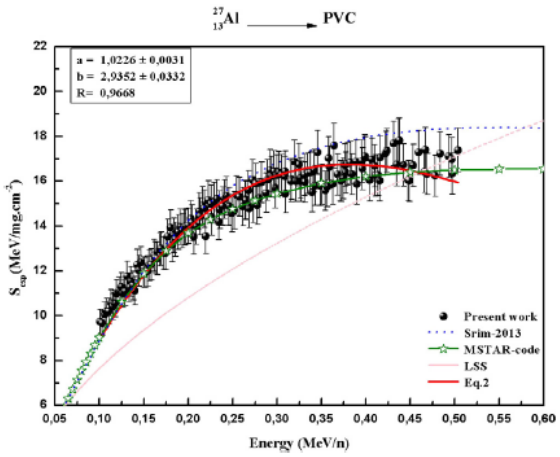

Fig. 5. Comparison of experimental stopping power values for ^{27}Al ion (circle) in Polyvinylchloride (PVC) with data from Eq. (2) (solid lines), SRIM-2013 predictions (dashed lines) and LSS theory (dot lines).

The resulting relative energy losses measured varied from ~10% to ~30 % of all incident energy considered. The measured stopping power S values of ^{63}Cu, ^{28}Si and ^{27}Al heavy ions crossing PVC foil, are presented in Figs. 3–5, no experimental data have been found in the literature to make any comparison. In addition to the foil thickness error estimate, there is also an uncertainty associated with the energy loss measurement. The time calibration procedure for ToF detector has been well described in our previously published work [15]. The time calibration procedure leads to ~3.4% uncertainty in each of E_1 and E_2. The overall uncertainty in the energy loss is then ~4.8% and if this is combined with the ~3% uncertainty in the foil thickness, one gets ~5.7% uncertainty in the calculated stopping powers.

As can be seen from these figures, we have produced experimental data to allow comparison with the data generated by different theoretical models. In Figs. 3–5, our obtained experimental stopping power values of ^{63}Cu, ^{28}Si and ^{27}Al ions in PVC are well fitted with our semi-empirical formula Eq. (2) in the energy range 0.045–0.5 MeV/n and provide a good agreement to those calculated by SRIM-2013 or MSTAR codes. However, stopping power data calculated with LSS formula underestimates the stopping power in the investigated energy range; this observation has been noted by several authors [23,24]. The free parameters a and b generated by matching the electronic stopping power formula (Eq. (2)), with our experimental data, are more or less constant ($a \sim 1$ and $b \sim 3$) for the used ions (Cu, Si and Al). It appears that our formula gives a better fit to the experimental stopping power data, at low energy region with just two free parameters. Hence it is possible to generate a semi empirical stopping power curves which fit the available data remarkably well. The analytical form of the relation proposed is expected to be valid for other pairs ion/target but more experimental data are needed to verify this assumption.

5. Conclusion

The electronic stopping powers in Polyvinylchloride (PVC) thin foil have been determined for Cu, Si and Al ions at low energy region (0.045–0.5 MeV/n) in the validity domain of LSS theory. Following our investigation on experimental slowing down processes of charged particles crossing compound materials, we have generated a new set of experimental stopping power data.

A simple expression based on the Firsov and Lindhard–Sharff stopping power models with a small modification made to the original expression, by incorporating the effective charge of moving ions concept and with exponential fit function, allows good fits of stopping power data of heavy ions at low energy, while a large discrepancy is observed for stopping powers values determined by LSS formula. More experimental data are needed in order to verify and to generalize the applicability of this formula.

Acknowledgements

This work was carried at iThemba LABS Gauteng (Johannesburg, South Africa). The financial support by the NRF (South Africa) and by the COMENA (Algeria) is gratefully acknowledged. The authors would like Dr. L. Conradie for his precious assistance and for beam time at the Tandem accelerator of iThemba LABS (Gauteng). We would like to thank also Dr. M. Nkosi for his precious assistance in targets elaboration and AFM analysis. Also the encouragement of Professor M. Maaza is gratefully acknowledged.

References

[1] J.F. Ziegler, J.P. Biersack, U. Littmark, The Stopping and Ranges of Ions in Solids, Pergamon, New York, 1985.
[2] J.F. Ziegler, Nucl. Instrum. Methods 149 (1978) 129.
[3] W.H. Bragg, R. Kleeman, Philos. Mag. 10 (1905) 318.
[4] H. Paul, A. Schinner, P. Sigmund, Nucl. Instr. Meth. B 164–165 (2000) 21.
[5] P. Sigmund, Stopping of heavy ions, Springer Tracts Mod. Phys. (Springer, Berlin) 204 (2004).
[6] A. Sharma, A. Fettouhi, A. Schinner, P. Sigmund, Nucl. Instr. Meth. B 218 (2004) 19.
[7] Paratibha Neetu, V. Sharma, P.K. Diwan, Shyam Kumar, Radiat. Meas. 44 (2009) 363–368.
[8] S. Mammeri, H. Ammi, A. Dib, C.A. Pineda-Vargas, S. Ourabah, M. Msimanga, M. Chekirine, A. Guesmia, Radiat. Phys. Chem. 81 (2012) 1862–1866.
[9] H. Ammi, M. Chekirine, M. Allab, Radiat. Meas. 32 (2000) 83.
[10] J. Lindhard, M. Scharff, H.E. Schiott, Mat. Fys. Medd. Dans. Viden. Selskab. 33 (1963) 14.
[11] M. Msimanga, C.M. Comrie, C.A. Pineda-Vargas, S. Murray, R. Bark, G. Dollinger, Nucl. Instr. Meth. B 267 (2009) 2671.
[12] M. Msimanga, C.M. Comrie, C.A. Pineda-Vargas, S. Murray, Nucl. Instr. Meth. B 268 (2010) 1772.
[13] M. Msimanga, C.A. Pineda-Vargas, C.M. Comrie, S. Murray, Nucl. Instr. Meth. B 273 (2012) 6.
[14] M. Msimanga, C.A. Pineda-Vargas, T. Hlatshwayo, C.M. Comrie, H. Ammi, S. Murray, Nucl. Instr. Meth. B 322 (2014) 54.
[15] H. Ammi, C.A. Pineda-Vargas, S. Mammeri, M. Msimanga, S. Ourabah, A. Dib, Nucl. Instr. Meth. B 269 (2011) 386.
[16] A. Guesmia, H. Ammi, S. Mammeri, A. Dib, C.A. Pineda-Vargas, M. Msimanga, M. Hedibel, Radiat. Phys. Chem. 96 (2014) 205–210.
[17] F. Ziegler, J.P. Biersack, U. Littmark, The Stopping and Ranges of Ions in Solids, Pergamon, New York, 1985. available from <http://www.srim.org>.
[18] H. Paul, A. Schinner, At. Data Nucl. Data Tables 85 (2003) 377. <http://www.exphys.uni-linz.ac.at/stopping/>.
[19] J. Lindhard, M. Scharff, Phys. Rev. 124 (1961) 128.
[20] H.A. Bethe, Ann. Phys. 5 (1930) 325.
[21] F. Bloch, Z. Phys. 81 (1933) 363.
[22] W.H. Bragg, R. Kleeman, Philos. Mag. 10 (1905) 318–340.
[23] A. Sharma, P.K. Diwan, S. Kumar, S.K. Sharma, V.K. Mittal, S.V.S. Nageswara Rao, B. Sannakki, S. Ghosh, D.K. Avasthi, Nucl. Instr. Meth. B 194 (2002) 7–14.
[24] Lu Zheng Tao, Zhai Yongjun Xiting, Xia Zonghuang, Shen Dingyu, Wang Xuemei, Zhao Qiang, Instr. Meth. B 135 (1989) 169–174.